Spring 1-1-2013

Granular Activated Carbon Adsorption of Organic Micropollutants: Scale-Up and Effect of Background Dissolved Organic Matter

Anthony Myers Kennedy
University of Colorado at Boulder, anthonymkennedy@gmail.com

Granular Activated Carbon Adsorption of Organic Micropollutants: Scale-Up and Effect of Background Dissolved Organic Matter

by

Anthony Myers Kennedy
B.S./M.S. Civil Engineering, University of Colorado at Boulder, 2013

A thesis submitted to the
Faculty of the Graduate School of the
University of Colorado in partial fulfillment
of the requirements for the degree of
Doctor of Philosophy
Department of Civil, Environmental, and Architectural Engineering
2013

This thesis entitled:
Granular Activated Carbon Adsorption of Organic Micropollutants: Scale-Up and Effect of Background Dissolved Organic Matter

written by Anthony M. Kennedy

has been approved for the
Department of Civil, Environmental, and Architectural Engineering

_____
R. Scott Summers (chair)

_____
Fernando L. Rosario-Ortiz

_____
Joann Silverstein

_____
Detlef Knappe

_____
Christopher Corwin

November 29th, 2013

The final copy of this thesis has been examined by the signatories, and we find that both the content and the form meet acceptable presentation standards of scholarly work in the above-mentioned discipline.

ABSTRACT

Kennedy, Anthony M. (Ph.D. Civil Engineering)

Granular Activated Carbon Adsorption of Organic Micropollutants: Scale-Up and Effect of Background Dissolved Organic Matter

Thesis directed by R. Scott Summers, Professor, Department of Civil, Environmental, and Architectural Engineering, University of Colorado at Boulder

Conventional drinking water treatment does not effectively reduce the concentrations of many common emerging trace organic contaminants or micropollutants (MPs), thus advanced treatment processes like granular activated carbon (GAC) are being evaluated for potential use in controlling MPs. However, adsorption by GAC is not selective for MPs as background dissolved organic matter (DOM), which is ubiquitous in all natural waters derived from both natural and anthropogenic sources, is also removed. Background DOM irreversibly reduces both adsorption capacity and kinetics for MPs, termed fouling, and varies in magnitude with GAC particle size thereby complicating valuable performance predictions. The objectives of this research are to (a) expand the database of MP breakthrough at environmentally relevant concentrations with full-scale and small-scale GAC media in several waters with different background DOM concentrations and types and (b) develop relationships that allow the breakthrough to be related to compound and system properties, and (c) better understand the effects of DOM type on MP breakthrough.

Adsorption of 30 environmentally relevant MPs using full- and small-scale GAC media was investigated using several different surface waters with different DOM, measured as dissolved organic carbon (DOC). For coagulated waters, MPs broke through earlier on average with increasing DOC and 52% later on average by doubling the EBCT based on the bed volumes

to 10% MP breakthrough. Several predictive relationships were presented for predicting the bed volumes to 10% MP breakthrough at the full-scale based influent DOC concentrations, MP pH-dependent octanol-water partition coefficients, MP polarizabilities, MP molar volumes, and bed volumes to 10% MP breakthrough using the proportional diffusivity design of the rapid small-scale column test (PD-RSSCT). On average, the PD-RSSCT over predicts MP adsorption capacity by a factor of 3.0±1.2. Relationships for adjusting the PD-RSSCT to predict full-scale MP breakthrough using a fouling factor were based on the ratios of the influent MP concentration to the influent DOC concentration, bed volumes to 10% MP breakthrough in the PD-RSSCT, and MP pH-dependent octanol-water partition coefficients. Smaller molecular weight DOM fouled GAC more than unfractionated and large molecular weight DOM, whereas large molecular weight slowed adsorption kinetics. Environmentally relevant background MP concentrations of about 3 μg/L had a small to negligible effect on target MP breakthrough.

DEDICATION

I dedicate this thesis to my mother and father for their never-ending love for their three children.

ACKNOWLEDGEMENTS

I am too indecisive to even approach something like this on my own; although I would say my decision-making abilities have greatly improved. Foremost I would like to thank my advisor, Scott Summers, who has a remarkable ability to build a student's confidence with constant enthusiasm and encouragement to challenge oneself. To have taught so many students both in the classroom and lab, each from scratch, shows true passion and dedication to the people and profession of engineering. The same applies to the other members of my committee, Fernando Rosario-Ortiz, Joann Silverstein, and Detlef Knappe, who I thank for their advice and passion for the protection of public and environmental health. I would also like to thank the last member of my committee, Chris Corwin, for sharing his wealth of knowledge and challenging me to succeed at the highest level.

Funding for this research came mainly from the Water Research Foundation Project No. 4235, but also from the Civil, Environmental, and Architectural Engineering Department's Dissertation Completion Fellowship. I would like to thank the City of Longmont and Bob Allen, George Talbott, and the Nelson Flanders Drinking Water Treatment Plant operations staff for their support in setting up a pilot column in their lab; the Orange Water and Sewer Authority, Allison Reinert, and Angela Mastropole for their parallel work in North Carolina; the Greater Cincinnati Water Works and Debbie Metz, Jeff Vogt, and Maria Meyer for their collaboration and support. So much of this thesis would not have been possible without the fantastic analytical work of Imma Ferrer and Mike Thurman.

I would like to thank the following current and past lab members for their help in developing my research and making the lab an enjoyable place work/learn/hang/complain/etc:

Dorothy Noble, Tom Zearley, Kyle Shimabuku, Janet Cardenas, Dave Kempisty, Julie Korak, Kate Dowdell, Ali Ling, Josh Kearns, Hyeongki Lee, Leigh Gilmore, and Eli Townsend.

I would also like to thank my friends and family for their support during the longest academic stretch a true Buff can make. Lastly I would like to thank my wonderful girlfriend Magda for her patience and love of the natural world.

TABLE OF CONTENTS

LIST OF TABLES

LIST OF FIGURES

Chapter 1
Introduction

1.1 Motivation

Recent advances in analytical techniques have led to a large number of trace organic contaminants or micropollutants (MPs) being detected in drinking water sources as well as finished drinking waters worldwide (Kolpin et al. 2002, Stackelberg et al. 2004, Batt et al. 2007, Donald et al. 2007, Kim et al. 2007, Barnes et al. 2008, Focazio et al. 2008, Benotti et al. 2009, Loos et al. 2009). MPs are typically present below low parts per billion (μg/L) levels, well below the maximum contaminant level (MCL), if one exists. Some of these compounds are known or suspected endocrine disrupting compounds (Snyder et al. 2003, Benotti et al. 2009) and pose potential risks to public health even at these trace levels. Thus, they are commonly referred to as contaminants of emerging concern.

At least for pharmaceuticals the risk from any single MP is most likely low as the ingestion from drinking water is orders of magnitude below common dosages or sub-therapeutic. The same can be said for personal care products such as sucralose or caffeine, which are consumed at much higher concentrations than those found in drinking water sources. However, toxicological research regarding a synergistic effect of chronic human exposure to these substances has not been thoroughly studied (Jones et al. 2005, Kuehn 2008, Schriks et al. 2010). Studies with fish and unicellular organisms have shown effects of MP mixtures with both synergistic and non-interacting modes of toxic action (Schwarzenbach et al. 2006). Pomati et al. (2006) observed embryonic kidney cell growth inhibition after exposure to a mixture of 13 environmentally relevant pharmaceuticals at a total concentration of approximately 3.7 μg/L.

Several of the MPs in this study have been regulated by the US Environmental Protection Agency (USEPA) because of potential health effects related to the kidney, liver, adrenal glands,

circulatory system, nervous system, and reproductive system (USEPA 1995a, USEPA 2009a). Considering the vast array of variables regarding toxicological effects, it may be more cost-effective and practical to simply target the removal of a wide range of MPs to ensure protection of public health. The USEPA has established MCLs for the following MPs in this study: 2,4-dichlorophenoxyacetic acid (2,4-D, herbicide, 0.07 mg/L), aldicarb (insecticide, 0.003 mg/L), atrazine (herbicide, 0.003 mg/L), and simazine (herbicide, 0.004 mg/L). The USEPA also has five MPs in this study on its unregulated Contaminant Candidate List 3 (CCL3, USEPA 2009b): acetochlor (herbicide), diuron (herbicide), erythromycin (antibiotic), metolachlor (herbicide), and molinate (herbicide), indicating the possibility of future regulations. Schriks et al. (2010) derived provisional drinking water guidelines for eight MPs in this study based on existing guidelines/regulations, tolerable daily intakes, acceptable daily intakes, and reference doses. In relation to this study, the lowest provisional drinking water guideline in Schriks et al. (2010) was for the anticonvulsant carbamazepine at 0.001 mg/L.

1.2 Granular Activated Carbon Adsorption of Micropollutants in Natural Waters

Conventional water treatment does not effectively reduce the concentrations of many common MPs (Ternes et al. 2002, Westerhoff et al. 2005, Stackelberg et al. 2007), thus advanced treatment processes like granular activated carbon (GAC) are being evaluated for potential use in controlling MPs. Many researchers have shown the efficacy of activated carbon for removing MPs in drinking water treatment settings (Ternes et al. 2002, Westerhoff et al. 2005, Snyder et al. 2007, Stackelberg et al. 2007, Rossner et al. 2009, Chowdhury et al. 2010, Cardenas 2011, Corwin and Summers 2012, Reinert 2013). Activated carbon is effective for the removal of many MPs because its large internal surface area (~1,000 m^2/g) provides for the nonspecific van der Waals forces that define physical adsorption (Crittenden et al. 2012). MP adsorption is thought to

occur mostly in the GAC micropores (pore diameter less than 20 Å), because of stronger adsorbate-adsorbent interactions (Summers et al. 2011).

Adsorption by GAC is not selective for MPs as background dissolved organic matter (DOM), which is ubiquitous in all natural waters derived from both natural and anthropogenic sources, is also removed. DOM covers a large range of molecular sizes, as it is comprised of humic substances, non-humic substances, wastewater effluent organic matter, and synthetic organic compounds. Along with MPs, DOM also adsorbs in the micropores but due to size exclusion (Summers and Roberts 1988b) some portions of DOM are limited to adsorption in the mesopores (pore diameter 20 to 500 Å) and macropores (pore diameter greater than 500 Å). Humic substances have been shown to be effectively irreversibly (non-displaceable) adsorbed due to both multi-segment attachment to the GAC surface and the constant presence of DOM in bulk solution which reduces the driving force for desorption (Summers and Roberts 1988a). Therefore background DOM permanently reduces both adsorption capacity and kinetics for MPs through direct site competition and pore blockage (Sontheimer et al. 1988, Hand et al. 1989, Carter et al. 1992, Li 2003, Li et al. 2003). The reduction in adsorption capacity and kinetics is termed fouling.

The mass transfer zone, or region of active adsorption for DOM, typically moves more quickly through the GAC bed compared the mass transfer zone of a MP because the adsorption kinetics of DOM are slower by 1 to 2 orders of magnitude relative to most MPs (Sontheimer et al. 1988). Therefore deeper in the GAC bed, DOM is adsorbed in the absence of MPs, further reducing the adsorption capacity and kinetics for MPs (Sontheimer et al. 1988, Summers et al. 2011). DOM adsorption prior to MP adsorption is termed preloading. Effects of preloading can be seen with increasing adsorber residence time or empty bed contact time (EBCT), where

longer EBCTs have shown less capacity for MPs on a normalized time or throughput basis (Hand et al. 1989, Knappe et al. 1997, Kim 2006, Corwin 2010, Corwin and Summers 2012).

A schematic showing typical MP breakthrough and mass transfer zone relative to DOM breakthrough, measured as dissolved organic carbon (DOC), is shown in Figure 1.1. Surface water DOC typically has a 10 to 20% nonadsorbable fraction and 10 to 20% biodegradable fraction, shown in Figure 1.1 at the bottom and top of the DOC breakthrough curve, respectively (Summers et al. 2011). Most MPs are fully adsorbable but have varying degrees of adsorption strength and biodegradability in drinking water filters (Zearley and Summers 2012).

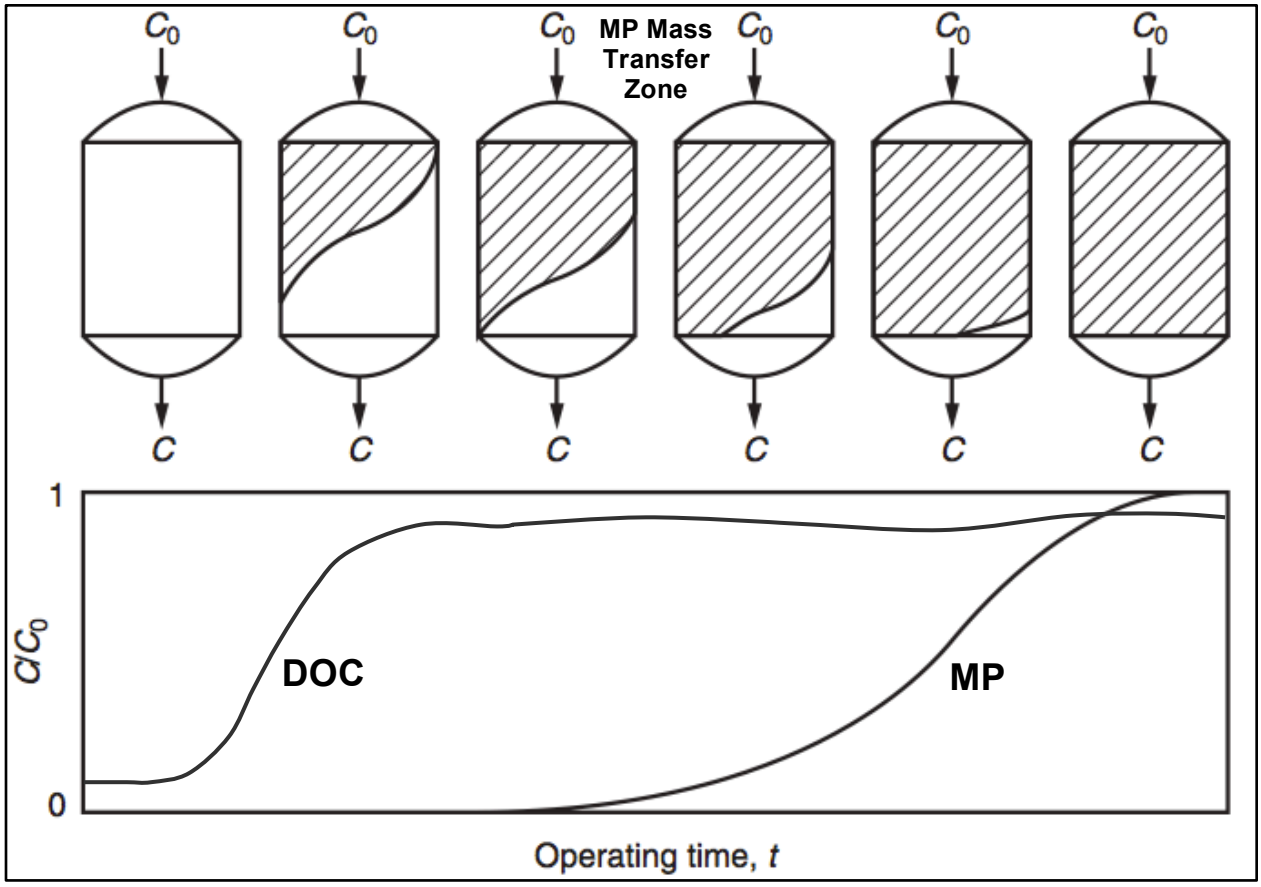

Figure 1.1. Schematic of MP breakthrough relative to DOC breakthrough with the mass transfer zone shown for the MP (adapted from Vermeulen 1958).

Despite the detrimental effects of fouling and preloading, GAC has been shown to exhibit economically efficient adsorption capacity for most MPs. However, predicting MP adsorption capacity and breakthrough has been difficult because of the amount of variability associated with background DOM. GAC adsorption predictions are also difficult because of adsorption kinetics. The process is at an unsteady state condition and mass transfer resistances, both external and internal to the GAC particle, need to be taken into account. External or film diffusion through the stagnant boundary layer on the outside of the GAC particles acts in series with internal or intraparticle diffusion. Intraparticle diffusion is surface and/or pore diffusion acting in parallel. Film diffusion is driven by a linear difference in MP concentration between the bulk flow and outside of the GAC particle. Intraparticle diffusion is driven by concentration gradients along the interior surface and pores. Actual adsorption of a MP to the surface of the GAC is assumed to be very fast and not rate limiting (Sontheimer et al. 1988). Consequently, any accumulation of DOM at the exterior and interior of a GAC particle would significantly affect these mass transfer mechanisms, complicating predictions with both models and bench-scale techniques.

1.3 Research Objectives and Hypotheses

The objectives of this research are to (a) expand the database of MP breakthrough at environmentally relevant concentrations with full- and small-scale GAC media in several waters with different background DOM concentrations and types and (b) develop relationships that allow the breakthrough to be related to compound and system properties, and (c) better understand the effects of DOM type on MP breakthrough. These outcomes will assist water providers in the design and operation of GAC adsorbers and are addressed by the following hypotheses:

Hypothesis 1: At the full-scale, the system characteristics of DOC concentration and EBCT affect GAC removal of a wide array of MPs. Increasing the DOC concentration causes earlier breakthrough of MPs on a normalized basis. Longer EBCTs yield lower carbon usage rates for high levels of MP removal. MP breakthrough can be predicted using properties of the MP and system.

Hypothesis 2: The rapid small-scale column test (RSSCT) can be used to predict full-scale removal of MPs by GAC. RSSCT results can be scaled using a fouling factor to predict full-scale GAC adsorption capacity and kinetics assuming intraparticle diffusivity decreases linearly with GAC particle size. MP molecular descriptors and system properties can be used to predict a fouling factor.

Hypothesis 3: The molecular size of DOM affects GAC adsorption of MPs. Low molecular weight fractions of DOM reduce GAC adsorption capacity for MPs. High molecular weight fractions of DOM slow MP adsorption kinetics. At a constant DOC concentration the type of background DOM, defined only by the presence or absence of MPs, has no impact on the breakthrough behavior of target MPs.

1.4 Scope

This research utilized both full- and small-scale techniques to produce GAC breakthrough. Many MPs were used and represented typical concentrations and types found in impacted surface waters in the United States. MPs represented a range of adsorbabilities and biodegradabilites. EBCTs of 4, 7, 7.5, 10, and 15 minutes were investigated. Nine source waters and DOM types were utilized including DOM fractionated by molecular size. Only bituminous-based GAC was investigated at two different full-scale particle sizes.

1.5 Thesis Organization

This thesis is divided into six chapters. Following this introduction, Chapter 2 outlines the methods and material used in detail. Following Chapter 2 there are three stand-alone chapters. Chapter 3 investigates field-scale adsorption of MPs and predicting their breakthrough to 10%. Chapter 4 investigates techniques for adjusting the results of the proportional diffusivity designed RSSCT to field-scale results. Chapter 5 investigates the effects of DOM molecular size and type. Chapter 6 summarizes the findings of this research and presents future research needs. Following Chapter 6 the Appendix shows relevant data, figures, and tables not included in the main parts of the thesis.

Chapter 2
Materials and Methods

Materials and methods are described separately in each chapter but are discussed here in more detail to better facilitate experimental replication.

2.1 Materials

2.1.1 Waters

2.1.1.1 Chapter 3 and Chapter 4

There are five different surface waters discussed in Chapter 3 and Chapter 4 (A, B, C, D, and E). Specific water quality parameters for Waters A, B, C, D, and E are presented in Chapter 3 and Chapter 4.

Waters A and B were made by spiking reverse osmosis (RO) membrane isolated DOM into pretreated tap water. City of Boulder, CO tap water was first passed through a 200 L high-density polyethylene (HDPE) barrel of bituminous-based GAC (Norit 1240) to remove chlorine, DOM, and disinfection by-products (DBPs) that may have interfered with MP adsorption. Periodic DBP samples taken throughout the entirety of the study confirmed no detectable DBPs in the effluent of the pretreatment GAC system. DBPs were analyzed using an Agilent 6890 Series gas chromatography (GC) system (Agilent Technologies, Santa Clara, CA) in accordance with EPA Methods 551.1 and 552.2 (USEPA 1995b).

The DOM was isolated using a low-pressure RO membrane (FILMTEC LE-4040, Dow Chemical Company, Midland, MI) from a high organic content and low alkalinity surface water source at Big Elk Meadows (BEM), CO after filtration through a 25 μm cartridge filter (DGD-7525-20, Pentek Inc., Upper Saddle River, NJ). The RO system, shown in Figure 2.1, was operated in batch mode (retentate flows back into the feed), discarding the permeate, until the

retentate had a conductivity of approximately 600 μS, which corresponded to a dissolved organic carbon (DOC) concentration of 76 mg/L. The RO feed was held constant at about 690 kPa and 45 L/min with the permeate flow rate at about 6 L/min. Concentrating BEM water was repeated several times throughout the course of the study after more water was collected from BEM. The conductivity of the RO permeate was measured during operation and consistently read 0 μS/cm. Minimal anthropogenic impacts were expected from the lake at BEM due to the very small population and mountain sources.

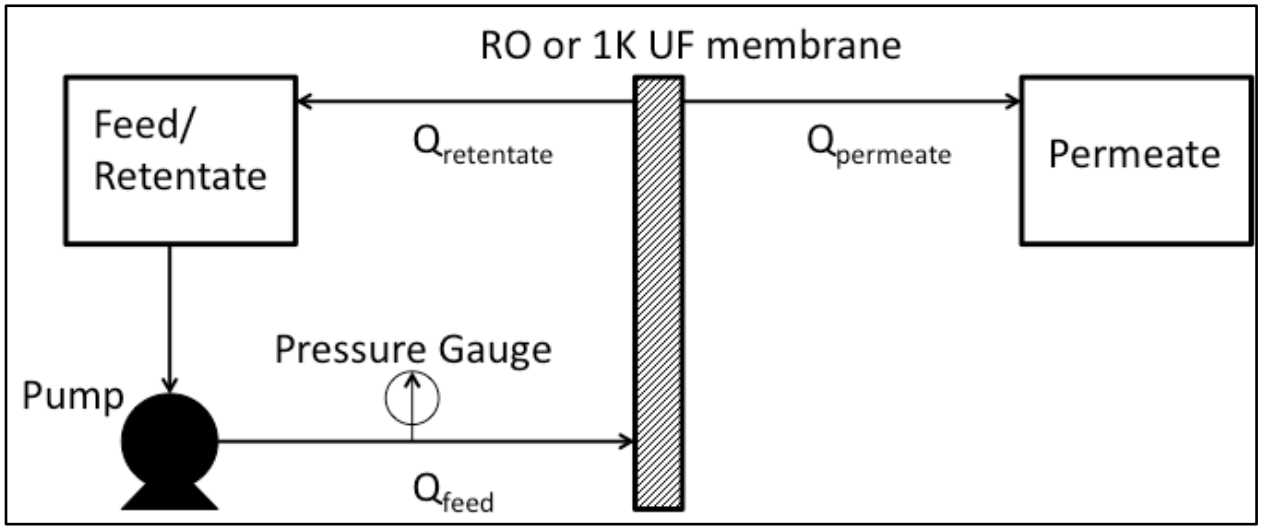

Figure 2.1. RO and UF membrane systems for obtaining DOM concentrates from BEM. Relevant for Waters A, B, <1K, BEM, >1K, CB, and CBMP. For RO operation the permeate was discarded.

Coagulation of the DOM extract using aluminum sulfate (~100 mg/L, Macron Fine Chemicals, Avantor Performance Materials, Center Valley, PA) removed about 10 to 20% of the DOC followed by filtration through a 0.45 μm cartridge filter (Memtrex MNY941CGS, General Electric Company, Fairfield, CT). Water A utilized this coagulated DOM extract, while Water B utilized ozonated DOM extract at a ratio of 1:1 mg O_3/mg DOC. The DOM extract was ozonated directly in a continuously mixed 20 L glass carboy using a fine bubble diffuser. The decrease in

UV absorbance was used as a measure of ozone dose. Ozonation was stopped when the DOM extract reached a predetermined ultraviolet absorbance at 254 nm (UVA_{254}). From small batch studies, a 60% reduction in UVA_{254} was obtained at the ratio of 1 mg O_3 to 1 mg DOC. Both DOM concentrates, coagulated and ozonated, were stored at 4°C before use.

Water C was coagulated, settled, and filtered (5 μm cartridge filter, WHCF-GD05, Whirlpool Corporation, Benton Harbor, MI) water from the Orange Water and Sewer Authority (OWASA, Carrboro, NC) and was derived from two North Carolina reservoir sources (Cane Creek Reservoir and University Lake). All of the primary data in this thesis concerning Water C is from Reinert (2013). Water D was conventionally treated combined filter effluent water from the City of Longmont (LM), CO, derived from the St. Vrain Creek and Colorado-Big Thompson Project sources.

In addition, data was also gathered from one adsorber in the full-scale GAC system at the Greater Cincinnati Water Works (GCWW) Richard Miller drinking water treatment plant from August 2011 to May 2012. GCWW uses full-scale GAC adsorbers to treat water from the Ohio River following alum coagulation, sedimentation, and filtration (biologically active). Water for the rapid small-scale test (RSSCT) was shipped to Boulder in May 2012. Water from the GCWW was termed Water E.

2.1.1.2 Chapter 5

There are five different surface waters discussed in Chapter 5 (<1K, BEM, >1K, CB, and CBMP). Specific water quality parameters for Waters <1K, BEM, >1K, CB and CBMP are presented in Chapter 5.

All waters were made by spiking RO membrane isolated DOM into RO-treated tap water. The DOM from BEM was isolated following the procedure outlined in Section 2.1.1.1. City of

Boulder, CO tap water was treated using a two-stage RO system (Merlin TLC-350 IND, General Electric Company) following pretreatment using sediment (Pentek P5), carbon (Pentek RFC-BB), and RO pre-filters (Merlin 1237460). The DOM extract was spiked into RO-treated tap water and was designated as BEM.

The same extract was used to create two DOM size fractions using an ultrafiltration (UF) membrane with a 1,000 Da nominal molecular weight cutoff. Nominal is emphasized here because the nature of DOM is complex. The value of 1,000 Da is calibrated with proteins and cannot be taken as a true MW cutoff for DOM (Newcombe et al. 1997, Matsui et al. 2002). The two DOM size fractions, less than 1,000 Da and greater than 1,000 Da, were spiked separately into RO-treated tap water and designated as <1K and >1K, respectively.

The same extract was also used to create a coagulated water. Coagulation of the DOM extract followed the procedure outlined in Section 2.1.1.1. The coagulated extract was spiked into RO-treated tap water. The coagulated water had two versions as well, one with only two MPs and one with 30 MPs (see Section 2.1.2.2), designated as CB and CBMP respectively. All DOM concentrates were stored at 4°C before use.

2.1.2 Adsorbates

2.1.2.1 Chapter 3 and Chapter 4

A total of 30 environmentally relevant MPs including pharmaceuticals, personal care products, herbicides, insecticides, a manufacturing additive, and the taste and odor compound 2-methylisoborneol (MIB) were chosen from occurrence studies of surface drinking water sources (Kolpin et al. 2002, Focazio et al. 2008). MPs are shown in Table 2.1 along with four other MPs discovered in Water E (bupropion, lamotrigine, metoprolol, and sucralose). MPs covered a wide range of hydrophobicities, ionic states, molecular weights, and biodegradabilities (Zearley and

Summers 2012). Target MP influent concentrations were based on the median concentrations from the same studies, detection limits, and a goal to be able to detect the onset of breakthrough at effluent concentrations that corresponded to 2.5 to 10% of the influent concentration. For Waters A, B, and D, one influent sample from each pilot column and RSSCT was measured for initial MP concentration estimation (C_0, n=6). The influent MP concentrations shown in Table 2.1 represent the average of these six samples and were assumed to be representative of the influent concentrations in Water C tests. The total MP concentration in the pilot and RSSCT influents averaged 8.1±2.7 μg/L for Waters A, B, C, and D, which was less than 0.5% of any influent DOC concentration.

For Water E, influent samples were analyzed for concentrations at each sampling event (n=4 for full-scale and n=6 for RSSCT). The average influent concentrations for buproprion, lamotrigine, metoprolol, and sucralose in Table 2.1 are from the RSSCT. The total measured MP concentration in the RSSCT influent for Water E averaged 4.6±2.1 μg/L (n=6, see Appendix Table A.14). The total measured MP concentration in the full-scale adsorber influent for Water E averaged 980±50 ng/L (n=4, see Appendix Table A.6). The total MP concentration in the RSSCT with Water E was greater because 29 of the MPs in Table 2.1 were also spiked into the influent (not MIB). Both of these total MP concentrations were less than 0.3% of the influent DOC concentrations, although there were likely more MPs that were not analyzed for by liquid chromatography-tandem mass spectrometry (LC/MS-MS).

All MPs were purchased from Sigma-Aldrich (St. Louis, MO), with three exceptions. 2,4-D was purchased from Acros Organics (New Jersey, US), iopromide was purchased from U.S. Pharmacopa (Rockvill, MD), and simazine was purchased from Alfa Aesar (Ward Hill,

MA). Again, bupropion, lamotrigine, metoprolol, and sucralose were not purchased but already present in Water E.

2.1.2.2 Chapter 5

Methyl ^{14}C radiolabeled MIB (ARC 1011-250 μCi) and ring ^{3}H radiolabeled warfarin (WFN, ART 1765-250 μCi) were purchased from American Radiolabeled Chemicals, Inc. (Saint Louis, MO). The properties of radiolabeled ^{14}C-MIB and ^{3}H-WFN are shown in Table 2.1. ^{14}C-MIB and ^{3}H-WFN influent concentrations over all tests (<1K, BEM, >1K, CB, and CBMP) averaged 107±3 and 100±6 ng/L, respectively. The total MP concentration in CBMP was estimated to average 3.0±0.9 μg/L (n=3), less than 0.1% of any influent DOC concentration. This concentration was estimated from a RSSCT that was run for the City of Aurora with the Chapter 3 and Chapter 4 MP cocktail, but during the time frame of the Chapter 5 tests. MPs in CBMP were ^{14}C-MIB and ^{3}H-WFN plus 27 MPs from Table 2.1 not from Water E. A table of the MPs and estimated concentrations in CBMP is shown in the Appendix (Table A.20). Ibuprofen was not spiked into CBMP because of its high biodegradability.

Table 2.1. MP influent concentrations and relevant properties. Where noted values were from SciFinder® (Chemical Abstracts Service, Columbus, OH).

Micropollutant	Type[a]	C_0[b] (ng/L)	MRL[c] (ng/L)	MW (Da)	pK_a[d]	log D[e]	D_L[f] ($x10^{-6}$ cm^2/s)	Biodegradation Rate[g]
2,4-D	Herb.	68±22	5	221	2.98(-)	-1.14	7.0	Fast
Acetaminophen	PPCP	404±183	5	151	9.86	0.47	7.9	Fast
Acetochlor	Herb.	392±160	10	270	1.29	3.05	5.2	Recalcitrant
Aldicarb	Insect.	450±90	10	190	13.81	0.92	6.3	Slow
Atrazine	Herb.	18±3	2	216	2.27	2.64	6.4	Recalcitrant
Bupropion[h]	PPCP	1±0.2	1	240	7.16(+)	1.94	5.5	N/A
Caffeine	PPCP	57±46	5	194	0.52	-0.63	7.4	Fast
Carbamazepine	PPCP	64±7	2	236	13.94	1.89	6.1	Recalcitrant
Carbaryl	Insect.	329±55	10	201	12.02	2.34	6.4	Recalcitrant
Clofibric acid	Herb.	231±40	5	215	3.18(-)	-1.06	6.4	Slow
Cotinine	PPCP	162±79	5	176	4.72	0.07	6.8	Slow
Diazinon	Insect.	3±2	1	304	1.21	3.77	5.0	Recalcitrant
Diclofenac	PPCP	118±52	10	296	4.18(-)	1.77	5.7	Slow
Dimethoate	Insect.	115±27	5	229	14.40	1.37	6.3	Fast
Diuron	Herb.	179±59	5	233	13.55	2.68	6.4	Recalcitrant
Erythromycin	PPCP	243±135	10	734	8.16(+)	0.81	3.0	Slow
Gemfibrozil	PPCP	66±24	5	250	4.75(-)	2.07	5.2	Fast
Ibuprofen	PPCP	173±140	10	206	4.41(-)	0.94	5.8	Very Fast
Iopromide	PPCP	2,951±1,074	25	791	10.62	-2.66	4.1	Recalcitrant
Lamotrigine[h]	PPCP	11±3	5	256	5.39	1.23	6.6	N/A
Malaoxon	Insect.	233±50	10	314	--	0.79	5.1	Slow
Methomyl	Insect.	309±78	5	162	13.27	0.60	7.3	Recalcitrant
Metolachlor	Herb.	117±63	1	284	1.45	3.03	5.0	Recalcitrant
Metoprolol[h]	PPCP	4±1	2	267	9.43(+)	-0.81	5.0	N/A
MIB[i]	T&O	105±39	1	168	15.43	2.93	6.3	Very Fast
Molinate	Herb.	216±68	10	187	-1.22	3.19	6.3	Fast
Naproxen	PPCP	176±29	10	230	4.84(-)	0.73	6.0	Fast
Prometon	Herb.	171±23	1	225	4.36	2.88	5.9	Recalcitrant
Simazine	Herb.	83±20	5	202	2.71	2.28	6.8	Recalcitrant
Sucralose[h]	PPCP	302±39	15	398	12.52	0.23	5.3	Recalcitrant
Sulfamethoxazole	PPCP	270±35	5	253	5.81(-)	-0.22	6.4	Recalcitrant
Tributyl phosphate	Plasticizer	259±95	5	266	--	3.83	4.9	Slow
Trimethoprim	PPCP	144±43	2	290	7.04(+)	0.27	5.4	Fast
Warfarin[i]	PPCP	74±27	5	308	4.50	0.67	5.3	Slow

[a]Herb-herbicide, T&O-taste and odor, PPCP-pharmaceutical/personal care product, Insect-insecticide. [b]Avg±SD, n=6 for each MP from Chapter 3 and Chapter 4. [c]Method reporting limit by LC/MS-MS. [d]Most relevant to pH 7 from SciFinder®, (+) or (-) represents dominant charge at pH 7. [e]pH-dependent log K_{ow} from SciFinder® at pH 7. [f]Calculated Hayduk and Laudie (1974) correlation at 20°C using molar volumes from SciFinder®. [g]Zearley and Summers (2012), except sucralose which is estimated from Scheurer et al. (2010); N/A – not in Zearley and Summers (2012). [h]Only existed in Water E. [i]Radiolabeled in Chapter 5, where MIB was at 107±3 ng/L and WFN was at 100±6.

2.1.3 Adsorbents

All of the pilot columns and RSSCTs were run with virgin bituminous-based GAC, which is common in drinking water treatment for controlling DOM and MPs (Summers et al. 2011). GAC in the pilot columns was either Norit 1240 (Cabot Norit Activated Carbon, Boston, MA) with a log-mean particle diameter of 0.92 mm (12x40 US standard mesh) and bed density of 450 kg/m^3, or Calgon F300 (Calgon Carbon Corporation, Pittsburgh, PA) with a log-mean particle diameter of 1.29 mm (8x30 US standard mesh) and bed density of 480 kg/m^3. The full-scale adsorber (Water E) utilized bituminous-based GAC that was freshly reactivated with a log-mean particle diameter of 0.92 mm (12x40 US standard mesh) and bed density of 490 kg/m^3. All RSSCTs were run with the corresponding ground GAC with a log-mean particle diameter of 0.11 mm (100x200 US standard mesh).

2.1.4 Pilot Column and Rapid Small-Scale Column Tests

All materials in the pilot columns and RSSCTs were either high-density polyethylene (HDPE), polyvinyl chloride (PVC), polytetrafluoroethylene (PTFE), stainless steel, or glass. Tubing was either 3/16” ID by 1/4" OD PTFE tubing (Nalgene 890 FEP, Thermo Fisher Scientific Inc., Waltham, MA) or 1/4" OD stainless steel. Water was fed to pilot columns and RSSCTs through PTFE or PVC tubing using a PTFE diaphragm pump (drive/controller 77521-50, head 7090-62, Cole-Parmer, Vernon Hills, IL) from a 200 L HDPE barrel or 20 L glass carboy, respectively. Stainless steel tubing, needle valves, ball valves, pressure relief valves, and fittings were all from Swagelok (Solon, OH). Pressure dampeners and gauges were also stainless steel. Pilot columns were 25 mm x 1200 mm glass chromatography columns and PTFE adapters from Ace Glass (Vineland, NJ). RSSCT columns were also 3/16” ID by 1/4" OD PTFE tubing.

2.2 Methods

2.2.1 Analytical Methods

2.2.1.1 Liquid Chromatography with Tandem Mass Spectrometry

Analysis of MPs shown in Table 2.1 (except MIB) was conducted by high performance LC/MS-MS at the Center for Mass Spectrometry at University of Colorado at Boulder (Ferrer et al. 2010). Solid-phase extractions were performed using an automated sample preparation system (GX-271 ASPEC, Gilson, Middleton, WI) fitted with a 25 mL syringe pump for dispensing the water samples through the sample extraction cartridges. Water samples were extracted with Oasis HLB cartridges (200 mg, 6 mL, Waters Corporation, Milford, MA). The cartridges were conditioned with 4 mL of methanol followed by 6 mL of HPLC-grade water at a flow rate of 1 mL/min. The water samples (100 mL) were then loaded at a flow rate of 10 mL/min. Elution of the analytes from the cartridge was carried out with 6 mL of methanol. The solvent was then evaporated to 0.5 mL with a stream of nitrogen at a temperature of 45ºC in a water bath using a Turbovap concentration workstation (Caliper Life Sciences, Mountain View, CA).

The samples were then transferred to vials and analyzed by LC/MS-MS. The mass spectrometry analyses allowed for the separation of the water extracts through use of an HPLC system (Agilent Series 1290), consisting of vacuum degasser, autosampler, and a binary pump, equipped with a reversed phase C18 analytical column of 50 mm x 2.1 mm and 1.8 μm particle size (Zorbax Eclipse Plus, Agilent Technologies). Column temperature was maintained at 25ºC. The injected sample volume was held constant at 15 μL. The optimized chromatographic method held the initial mobile phase composition constant for 1.7 min, followed by a linear gradient after 10 min. The flow rate used was 0.4 mL/min. A 4-minute post-run time was necessary after each run. The LC system connects to a triple quadrupole mass spectrometer Agilent 6460 that was equipped with electrospray Jet Stream technology, which can operate in positive and negative

ion mode.

Except for influent concentration estimations, for Waters A, B, C, and D the results from LC/MS-MS analysis were given as relative concentration (C/C_0) based on analyte area ratios from paired influent and effluent samples. Estimated influent and effluent concentrations in ng/L were given for Water E tests. Concentrations from LC/MS-MS analysis were estimated from an internal standard (carbamazepine, 100 ng/L). Samples for analysis were collected in muffled 250 mL amber glass bottles, stored at 4°C, and extracted within one week before quantification.

This study shows two pilot column data points in Water A in Chapter 3 for MIB that were obtained before analytical issues terminated MIB analysis. The GC/MS-MS procedure for the analysis of MIB in the aqueous-phase was developed by Yuncu (2010).

2.2.1.2 Liquid Scintillation

Radiolabeled ^{14}C-MIB and ^{3}H-WFN allowed for simultaneous quantification on a Packard Tri Carb 2300 liquid scintillation analyzer (PerkinElmer Inc., Waltham, MA) with a 20-minute counting time. Samples consisted of 4 mL of the water sample and 16 mL of Ultima Gold scintillation cocktail (Perkin Elmer Inc.) in 20 mL polyethylene vials. Standard curves ($R^2 \geq 0.94$) were run with concentrations of ^{14}C-MIB and ^{3}H-WFN ranging from 0 to 200 ng/L to obtain scintillation counting efficiencies (see Appendix Figure A.2). Method detection limits for ^{14}C-MIB and ^{3}H-WFN were 19 and 8 ng/L (based on counts from blanks), respectively. Standard deviations averaged ±1 ng/L from duplicate sample analyses.

Liquid scintillation analysis also revealed immediate GAC breakthrough of ^{3}H-WFN in the Chapter 5 tests, which was unexpected. From the LC/MS-MS analysis in Chapter 3 and Chapter 4 it was known WFN does not breakthrough immediately in GAC columns. The influents of the tests in Chapter 5 were slowly (~1 mL/min) run through solid-phase extraction

(SPE) cartridges (AccuBOND IIODS-C18 Cartridges 188-1356, Agilent Technologies) after conditioning the cartridges with 4 mL of methanol followed by 8 mL of deionized water (Barnstead Nanopure, Thermo Fisher Scientific Inc.). Liquid scintillation analysis of the effluent concentrations from the SPE cartridges showed about 1 ng/L of ^{14}C-MIB and 14 ng/L of ^{3}H-WFN on a consistent basis, from influent concentrations of about 100 and 125 ng/L, respectively. MIB at this concentration was considered negligible but because WFN does not immediately breakthrough in GAC, the 14 ng/L was thought to be tritiated water ($^{3}H_2O$) from a possible hydrogen exchange with ^{3}H-WFN.

Additional analysis of a several-month old cold WFN stock using LC/Time of Flight-MS (Agilent Model 6220) at the Center for Mass Spectrometry showed no WFN degradates from hydrolysis or biological oxidation. Therefore it was determined that some impurity existed in the stock from American Radiolabeled Chemicals, Inc., and was increasing with time.

Accordingly, for all tests in Chapter 5, each ^{3}H-WFN sample concentration was reduced by 14 ng/L (for $^{3}H_2O$) plus whatever concentration initially broke through from the respective GAC column (for stock impurity). After subtraction, ^{3}H-WFN results agreed well with those from LC/MS-MS analysis in Chapter 3 and Chapter 4 at the appropriate EBCT (see Appendix Figure A.9). Although radiolabeled MPs allow for many samples both quickly and easily, careful attention must be paid to what is being measured. If possible, radiolabeled stock concentrations should be confirmed using LC/MS-MS or GC/MS-MS analysis.

2.2.1.3 Dissolved Organic Carbon

DOC was measured with either a Sievers 800 TOC analyzer (General Electric Company) in accordance with Standard Method 5310C or a Shimadzu TOC-V CSH analyzer (Shimadzu Corporation, Kyoto, Japan) in accordance with Standard Method 5310B (APHA et al. 2005).

Potter and Wimsatt (2010) found relative standard deviations between DOC measurements using five different TOC analyzers was around 10% for DOC concentrations relevant to this study.

2.2.1.4 Ultraviolet Absorbance

UVA_{254} was analyzed at a wavelength of 253.7 nm using a Hach DR 4000 spectrophotometer (Hach Company, Loveland, CO) in accordance with Standard Method 5910 (APHA et al. 2005).

2.2.1.5 pH

pH was measured using a Denver Instrument pH meter (Model 220, Denver Instrument, Bohemia, NY) in accordance with Standard Method 4500-H^+ (APHA et al. 2005).

2.2.1.6 Conductivity

Conductivity was measured using a Hanna portable conductivity meter (HI 991300, Hanna Instruments, Woonsocket, RI) in accordance with Standard Method 2510B (APHA et a. 2005).

2.2.1.7 Alkalinity

Alkalinity was measured using a Hach Digital Titrator (16900-01) in accordance with Standard Method 2320 (APHA et a. 2005).

2.2.1.8 Size Exclusion Chromatography

Differences in molecular weight (MW) distributions for the waters in Chapter 5 were confirmed using high performance size exclusion chromatography (SEC). The SEC chromatograph for Waters <1K, BEM, >1K, CB, and CBMP from Chapter 5 is shown in the Appendix (Figure A.1). SEC was performed using an Agilent 1200 series with a Protein-Pak™ 125 7.8 x 300 mm column (Waters Corporation). The detector was an Agilent diode array that

monitored UVA_{254}. The mobile phase buffer consisted of 0.0024 M NaH_2PO_4, 0.0016 M Na_2HPO_4, and 0.025 M $NaSO_4$ at a flow rate of 0.7 mL/min. A calibration curve was generated using polystyrene sulfonates with MWs ranging from 210 to 17,000 Da and a linear relationship between the logarithm of MW and retention time was found (R^2=0.92, see Appendix Figure A.3). Weight averaged (MW_w) and number averaged (MW_n) MWs were determined using the absorbance and MW estimated from the calibration curve at the corresponding elution time.

2.2.2 Preparing Micropollutant Stocks

2.2.2.1 Cold Compound Stocks

Concentrated stocks for all MPs in Table 2.1 (except bupropion, lamotrigine, metoprolol, MIB, and sucralose) were created from dissolving the pure solid or liquid MP into methanol at concentrations ranging from 1 to 50 g/L. Methanol was used because it can be difficult to dissolve most MPs directly in water, except caffeine, which was held in a water stock. Limited degradation of MPs in methanol stocks was expected because water was not present to facilitate hydrolysis and they were stored at 4°C in muffled 20 mL glass vials.

Small volumes (~50 to 1,500 µL) of the methanol stocks were then pipetted into muffled 1 L amber glass bottles at no more than 2 mL of methanol per bottle. This resulted in 4 stock bottles. The amber bottles were manually rotated horizontally to cover the inside of the bottle with the added methanol stock, increasing evaporation potential. Stock bottles were allowed to sit overnight to allow methanol to completely evaporate. By spreading the methanol over the interior of the glass bottle, an amorphous solid of MPs could form, which dissolved easier in water compared to crystalline solids. After complete methanol evaporation 1 L of deionized water was added to each stock bottle. At this point caffeine was added to one of the bottles from

its respective water stock. Stock solutions were stirred on a heated stir plate for one hour then stored in at 4°C.

MP concentrations in the water stocks ranged from 0.1 to 5 mg/L, which allowed for simple calculations as to how much to spike in order to reach target influent concentrations (10 to 500 ng/L). MP methanol stocks were remade twice over the course of the study and MP water stocks were remade every 6 months. LC/MS-MS analysis was used as an indicator of whether the stocks should be remade or not. WFN was left out of the water stocks for Chapter 5 tests because ^{3}H-WFN was spiked from its radiolabeled stock.

2.2.2.2 Radiolabeled Compound Stocks

^{14}C-MIB was made into a pure stock in deionized water with a specific activity of 55 mCi/mmol. ^{3}H-WFN was made into a stock in deionized water, but diluted with cold warfarin to make a 0.8% (by mass) radiolabeled stock with a specific activity of 150 mCi/mmol. ^{14}C-MIB stocks were stored in muffled 20 mL amber glass vials and sealed with laboratory film to minimize volatilization. ^{3}H-WFN stocks were stored in muffled 250 mL amber glass bottles. ^{14}C-MIB and ^{3}H-WFN stocks were stored at 4°C.

2.2.3 Pilot Column and Rapid Small-Scale Column Tests

2.2.3.1 Pilot Column Design and Operation

A schematic of the pilot column setup is shown in Figure 2.2 for Water A, although all the pilot columns were essentially designed the same. Pilot columns were operated at a hydraulic loading rate (HLR) of 5 m/h, which resulted in a flow rate of 42 mL/min. A HLR of 5 m/h is at the lower end of typical rates, but was chosen to limit the amount of water required. In this range, intraparticle mass transfer still controls MP adsorption kinetics (Corwin 2010). The aspect ratios

for the columns were 27 (Norit 1240) and 19 (Calgon F300), which is greater than the 8 to 10 necessary to avoid wall effects on mass transfer (Knappe et al. 1999).

Water A was run at two the empty bed contact times (EBCT) of 7 and 15 minutes, which was accomplished with a 7 minute column followed by an 8 minute column. The 7 minute EBCT column was intended to simulate a filter adsorber and the 15 minute EBCT was intended to simulate a postfilter adsorber. These bed heights were 58 and 67 cm for the 7 and 8 minute columns, respectively. Water B was run at an EBCT of 7.5 minutes, which was a bed height of 63 cm. Waters C and D were run at EBCTs of 7 minutes, both with bed heights of 58 cm. Under each bed of GAC was 8 cm of 2 mm glass beads held in place by a stainless steel screen. Pilot columns and tubing were covered to prevent biological growth from exposure to light.

Influent water was spiked with MPs from the water stocks at initial concentrations ranging from 3 ng/L to 3 μg/L. MP-spiked water was fed to the columns from well-mixed 200 L HDPE barrels through PVC, PTFE, and stainless steel tubing using a PTFE diaphragm pump. For experiments with MIB, a volatilization trap was used by connecting the headspace of the influent container to the headspace of a 4 L glass carboy that was spiked with MIB at three times its initial concentration. Influent barrels were mixed with an agitator attached to an electric drill. Pilot column effluent water was treated in a secondary GAC barrel before being discharged to a drain. Prior to the start of pilot testing the GAC was backwashed with dechlorinated and organics-free water to remove carbon fines. Bed expansion was limited to about 20% to minimize the effects on particle size distribution (Hand et al. 1989).

Paired influent and effluent MP samples were collected immediately before and after the pilot column. A needle valve was used for flow control to maintain the desired EBCT during sampling. Pilot column influent and effluent DOC and UVA_{254} samples were taken biweekly at

the beginning of the run. After complete DOC breakthrough, UVA_{254} was used for measurements of DOM. Strong relationships were observed between DOC and UVA_{254} ($R^2 \geq 0.95$) for all waters.

At the full-scale Water E was sampled following biological filtration and from the effluent of the single adsorber with freshly reactivated GAC. The GAC adsorbers at GCWW are variable rate contactors and were designed for a HLR of 14 m/h and 15 minute EBCT but typically operate at a HLR of about 18 m/h and a 12-minute EBCT. A total of four paired influent and effluent samples were taken over the course of nine months from August 2011 to May 2012.

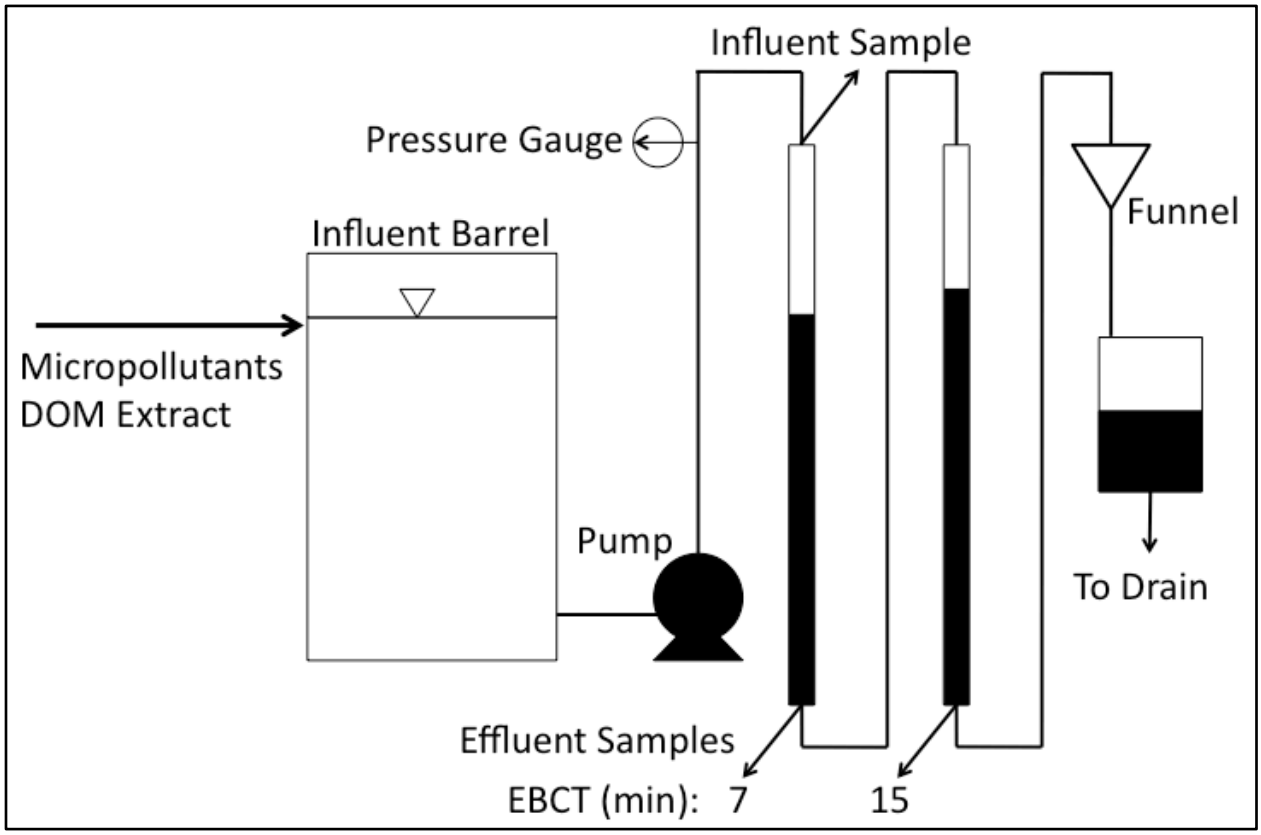

Figure 2.2. Schematic of pilot column setup for Water A (two EBCTs). Waters B, C, and D were only run at one EBCT. All materials were HDPE, PVC, PTFE, stainless steel, or glass (see Section 2.1.4).

The pilot columns were frequently backwashed using a peristaltic pump (drive 7553-70, head 7518-10, controller 7553-71, Cole-Parmer) to release air pockets in the columns and media, not to reduce head loss (pressure was always less than 10 psi). Air pockets were prevalent in the LM pilot column because the plant water temperature was about 5°C and the lab air temperature was about 20°C. This difference in temperature caused considerable dissolved air to come out of solution, forming air pockets in the column and media. Media was backwashed with deionized water or dechlorinated tap water because effluent water was not captured. Bed expansion was limited to about 20% to minimize the effects on particle size distribution (Hand et al. 1989). A thin stainless steel dowel was used to loosen the media. Such frequent backwashing caused pilot column bed heights to increase by about 10%. MP breakthrough plotted as specific throughput (volume treated divided by mass of GAC in bed), confirmed no difference from breakthrough plotted as bed volumes (volume treated divided by volume of GAC bed).

2.2.3.2 Rapid Small-Scale Column Test Design and Operation

All RSSCTs were designed according the proportional diffusivity (PD) design approach, because it has been successful for simulating full-scale DOM breakthrough (Crittenden et al. 1991, Summers et al. 1995, USEPA 1996) and because of success for MPs after scaling adjustments (Corwin and Summers 2010). PD-RSSCTs were designed to simulate full-scale EBCTs of 4, 7, 7.5, 10, and 15 minutes depending on the Chapter. Equation 2.1 and 2.2 determine the design of the PD-RSSCT,

$$EBCT_{SC} = EBCT_{LC}\left(\frac{d_{p,SC}}{d_{p,LC}}\right) \tag{2.1}$$

$$v_{f,SC} = v_{f,LC}\left(\frac{d_{p,LC}}{d_{p,SC}}\right)\left(\frac{\mathrm{Re}_{SC,\min}}{\mathrm{Re}_{LC}}\right) \tag{2.2}$$

where the subscripts SC and LC represent the small column and large column, respectively, d_p is the diameter of the GAC particle, v_f is the filter velocity or HLR, and Re is the Reynolds number for a fixed-bed reactor with granular media. These relationships originate from equating the dimensional numbers in the dispersed-flow pore and surface diffusion model (DFPSDM) between the large and small columns (Crittenden et al. 1986a, Crittenden et al. 1987). Equations for all the dimensionless numbers in the DFPSDM can be found in Crittenden et al. (1986a, 1986b), Crittenden et al. (1987), Sontheimer et al. (1988), and Crittenden et al. (2012). The dimensionless numbers in the DFPSDM are:

- Surface solute distribution parameter, Dg_s, which is a partitioning coefficient relating the mass of adsorbate in the solid phase to the mass of adsorbate in the liquid phase
- Pore solute distribution parameter, Dg_p, which is a partitioning coefficient relating the mass of adsorbate in the adsorbent pores to the mass of adsorbate in the liquid phase
- Surface diffusion modulus, Ed_s, which is the rate of adsorbate transport by surface diffusion relative to the rate of adsorbate transport by advection
- Pore diffusion modulus, Ed_p, which is the rate of adsorbate transport by pore diffusion relative to the rate of adsorbate transport by advection
- Peclet number, Pe, which is the rate of adsorbate transport by advection relative to the rate of adsorbate transport by axial dispersion

- Stanton number, St, which is the rate of adsorbate transport by film diffusion relative to the rate of adsorbate transport by advection

Other dimensionless parameters that are also important for fixed-bed adsorbers and RSSCT design are:

- Reynolds number, Re, which is a measure of water flow turbulence
- Schmidt number, Sc, which relates fluid viscosity to adsorbate bulk liquid diffusion coefficient
- Sherwood number, Sh, which relates adsorbate film mass transfer coefficient to the adsorbate bulk liquid diffusion coefficient

The minimum Reynolds number, $Re_{SC,min}$, was calculated by dividing the Schmidt number (for a fictitious small MP with molar volume~105 cm^3/mol) by 500 to ensure dispersion, measured by Peclet number, remains in the mechanical dispersion region and is less in the PD-RSSCT compared to the full-scale adsorber (Crittenden et al. 1987). A product of the Reynolds and Schmidt numbers equal to 500 also ensured the Gnielinski (1978) correlation for calculating film mass transfer coefficients, k_f, was valid. Axial dispersion in full-scale adsorbers is typically negligible, so choosing a flow rate for a PD-RSSCT is a matter of convenience (Crittenden et al. 1987). The PD-RSSCT flow rate was set at 2 mL/min to obtain a $Re_{SC}>Re_{SC,min}$.

The rate controlling mechanism that is responsible for the spread of the mass transfer zone, film or intraparticle diffusion, is determined by calculating the dimensionless Biot number (Bi), which is the ratio of the Stanton number to the surface or pore diffusion modulus. For MP adsorption in the presence of DOM at typical loading rates (5 to 25 m/h) intraparticle mass transfer, specifically pore diffusion, usually controls the adsorption rate and spreading of the

mass transfer zone (Hand et al. 1989, Carter and Weber 1994, Jarvie et al. 2005, Corwin 2010, Corwin and Summers 2011). The Biot number based on pore diffusion, Bi_p, is given by Equation 2.3,

$$Bi_p = \frac{St}{Ed_p} = \frac{k_f d_p \tau}{2 D_L \varepsilon_p} \tag{2.3}$$

where τ is the tortuosity or labyrinth factor, D_L is the liquid diffusion coefficient of the target MP, and ε_p is the GAC particle porosity. Tortuosity represents the increased diffusion path length from pore constriction in the GAC particle due to DOM adsorption. Pore diffusion control under typical adsorber operating conditions for MP removal corresponds to Biot numbers greater than 30 (Hand et al. 1984, Corwin 2010). If MP diffusivities are nonconstant with changing GAC particle size and intraparticle mass transfer controls the adsorption rate then the PD-RSSCT is more relevant than the constant diffusivity design (Crittenden et al. 1991). However, with the PD design the Stanton number will be greater in the PD-RSSCT compared to the full-scale and may underestimate the effect of film diffusion by up to 15% (Corwin 2010).

Because the PD-RSSCT works well for simulating full-scale DOM removal and is more relevant for large Biot numbers, only the PD design was evaluated. Relevant PD-RSSCT design parameters for Chapter 4 and Chapter 5 are shown in Table 2.2. There were no PD-RSSCTs in Chapter 3 experiments. For all PD-RSSCTs the log-mean GAC particle diameter was 0.11 mm. A schematic of the PD-RSSCT setup is shown in Figure 2.3 for Water A, although all the PD-RSSCTs were essentially designed the same.

Fresh bituminous GAC for the PD-RSSCTs was carefully ground using a mortar and pestle while minimizing the production of fines. The 100x200 mesh size fraction was obtained using US standard sieves and a sieve shaker (Cenco-Meinzer 18480, Central Scientific Company,

Inc., Chicago, IL). Prior to use the crushed GAC was rinsed with deionized water to remove fines, dried at 105°C, and stored in amber glass vials in a desiccator. Crushed GAC was then placed in 4.76 mm ID (3/16") PTFE columns based on a small-scale HLR of 6.7 m/h and flow rate of 2 mL/min. The aspect ratios for the columns were 43, which is greater than the 8 to 10 necessary to avoid wall effects on mass transfer (Knappe et al. 1999).

GAC beds in the PD-RSSCTs rested on 2 cm of glass wool. Glass wool was also used as a pre-filter to reduce head loss and was changed out weekly. Waters C, D, and E for the PD-RSSCTs were stored at 4°C before use. All other waters were made using the relevant DOM concentrate on a weekly basis. All PD-RSSCT tubing was covered to prevent biological growth from exposure to light.

Table 2.2. Full-scale and PD-RSSCT design parameters and relevant waters. For all PD-RSSCTs log-mean d_p=0.11 mm.

Relevant Water Chapter 4: A, B, C, D, E Chapter 5: <1K, BEM, >1K, CB, CBMP	Full-Scale			PD-RSSCT (HLR=6.7 m/h)		
	EBCT (min)	d_p[a] (mm)	HLR (m/h)	EBCT (min)	l_{bed}[b] (cm)	M_{GAC}[c] (g)
<1K, BEM, >1K, CB, CBMP	4	0.92	5	0.47	5.3	0.42
A, C, D, <1K, BEM, >1K, CB, CBMP	7	0.92	5	0.82	9.3	0.74
B	7.5	1.29	5	0.63	7.1	0.61
<1K, BEM, >1K, CB, CBMP	10	0.92	5	1.2	13.2	1.1
A	15	0.92	5	1.8	19.8	1.6
E	15	0.92	14	1.8	19.8	1.7

[a]Log-mean GAC particle diameter. [b]Bed length. [c]Mass of GAC in bed.

Spiked influent water was fed to the columns from well-mixed 20 L glass carboys through stainless steel and PTFE tubing using a PTFE diaphragm pump. For experiments with MIB, a volatilization trap was used following the same method as the pilot columns. Paired influent and effluent MP samples were collected from before the pump and after the columns. Biological MP removal in the lines from the pump to the column influent was not expected as

the glass wool pre-filter was changed weekly. Sampling before the pump also eliminated expansion of the GAC bed, which occurred when samples were initially taken directly above the column because of a sharp drop in line pressure. A needle valve was used for flow control to maintain the desired EBCT during sampling. Influent and effluent DOC and UVA_{254} samples were taken daily at the beginning of the run. After complete DOC breakthrough, UVA_{254} was used for measurements of DOM. Strong relationships were observed between DOC and UVA_{254} ($R^2 \geq 0.95$) for all waters.

PD-RSSCT run times were long resulting in high head loss through the columns. Therefore backwashing was required to loosen the media. Media was backwashed in PD-RSSCT effluent water in a 100 mL glass beaker using a glass dropper to mix the media. If necessary the glass wool base of the column was also replaced. Backwashing the column was able to bring pressures to about 10 to 20 psi, down from about 70 psi. Original bed heights were achieved after sufficient backwashing to break up clumps of GAC particles. Backwashing has been shown to have negligible effect on breakthrough curves using the PD-RSSCT (Corwin and Summers 2011). A significant amount of fines were not present during backwashing, indicating the high pressures were not crushing the GAC media.

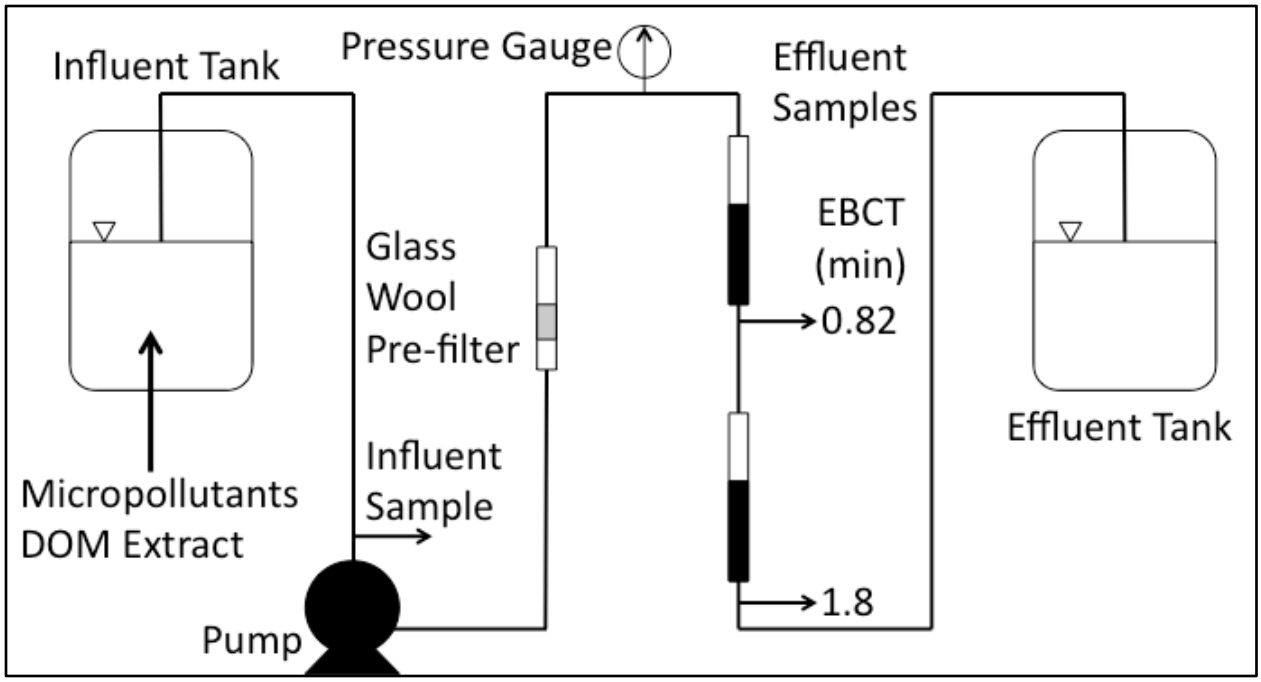

Figure 2.3. Schematic of PD-RSSCT setup for Water A (two EBCTs). Waters B, C, D, and E were only run at one EBCT. <1K, BEM, >1K, CB, and CBMP were run at three EBCTs. All materials were PTFE, stainless steel, or glass (see Section 2.1.4).

2.2.4 Ultrafiltration

Prior to use the UF membrane was cleaned according to the manufacturer's specifications. For Chapter 5, the <1,000 Da DOM size fraction (<1K concentrate) was obtained after running approximately 100 L of the DOM extract through a 1,000 Da nominal molecular weight cutoff UF membrane (0.1 m^2 Pellicon 2 Mini Ultrafiltration Module P2PLACC01, EMD Millipore, Darmstadt, Germany). Shown in Figure 2.1, the DOM extract was fed to the UF membrane in a tangential flow membrane holder (Pellicon 2 Mini filter holder XX42 PMI NI, EMD Millipore) using an external gear pump (Cole-Parmer drive 75211-22, Cole-Parmer controller 75211-21, Micropump GB-P25.JVS.A.B1) at a feed pressure of 415 kPa operated in batch mode (retentate flows back into the feed). Permeate flow (~25 mL/min) was about 2% of the retentate flow (~1.2 L/min). The 100 L of <1K concentrate was obtained in several batches. For each batch the

system was operated until the feed/retentate UVA_{254} was three times the initial UVA_{254} to avoid size-shift effects of increasing DOC concentration (Summers 1986). After the 100 L was obtained the <1K concentrate had a DOC concentration of 22 mg/L and the retentate had a concentration of 220 mg/L. There was about 10% mass loss in the UF membrane.

The >1,000 Da DOM size fraction (>1K concentrate) was obtained by cleaning the retentate (DOC of 220 mg/L). Cleaning was accomplished by using deionized water to dilute 10 L of the retentate up to a total volume of 40 L. The diluted 40 L was then recirculated through the UF membrane system to remove any remaining <1,000 Da DOM through the permeate until the feed/retentate was the original volume of 10 L. The final retentate (>1K concentrate) had a DOC concentration of 147 mg/L, indicating significant DOM had passed through the membrane during cleaning. However, a portion of DOM that could have potentially passed through the filter was likely retained in the >1K fraction.

At the beginning and end of each day of continued use 1 L of RO-treated tap water was run through the UF membrane. The UF membrane and holder were stored at 4°C each night during continued use. Before long-term storage, the UF membrane was cleaned by recirculating 4 L of RO-treated tap water at a pH of 12 (using sodium hydroxide) followed by 4 L of RO-treated tap water with a pH of 2 (using phosphoric acid) at the same feed pressure and flow rates as above. Each cleaning step was done for 30 minutes. The UF membrane was stored at 4°C in the RO-treated tap water with a pH of 2.

2.2.5 Adsorption Modeling

Adsorption capacity and kinetic information in the form of Freundlich adsorption capacity parameters (K) and diffusion coefficients (D) was obtained by curve fitting using the pore and surface diffusion model (PSDM using AdDesignS™ from Michigan Technological

University, Houghton, MI). Due to the presence of significant background DOM in all waters, the PSDM modeling approach followed that of Corwin and Summers (2011) where the following initial assumptions were made: (1) surface diffusion was negligible, (2) pore diffusion controlled mass transfer, (3) pore diffusion Biot numbers were high (>30), indicating film diffusion was not controlling, (4) film mass transfer coefficients were calculated using the correlation of Gnielinski (1978), and (5) isotherm behavior was linear, or the Freundlich adsorption intensity parameter, 1/n, was effectively equal to one. Freundlich K values from the PSDM were essentially the same as K^* values (equal to bed volumes at 50% breakthrough divided by the bed density), defined by Corwin and Summers (2011).

2.2.6 Statistical Analysis

All statistical analyses were done using Minitab 16 statistical software (Minitab Inc.) or Microsoft Excel 2011, following the methods presented in Montgomery (2013). Normality assumptions were checked using residual and normal probability plots, and confirmed in two ways: (1) residual plots showed random equal variance and (2) the Anderson-Darling test p-value was greater than 0.05 for normal probability plots.

Chapter 3
Full-Scale GAC Adsorption of Organic Micropollutants

3.1 Introduction

Recent advances in analytical techniques have led to a large number of trace organic contaminants or micropollutants (MPs) being detected in drinking water sources as well as finished drinking waters worldwide (Kolpin et al. 2002, Stackelberg et al. 2004, Batt et al. 2007, Donald et al. 2007, Kim et al. 2007, Barnes et al. 2008, Focazio et al. 2008, Benotti et al. 2009, Loos et al. 2009). MPs are typically present below low parts per billion (μg/L) levels, well below the maximum contaminant level (MCL), if one exists. Some of these compounds are known or suspected endocrine disrupting compounds (Snyder et al. 2003, Benotti et al. 2009) and pose potential risks to public health even at these trace levels (Pomati et al. 2006, Schwarzenbach et al. 2006). Thus, MPs are commonly referred to as contaminants of emerging concern.

Conventional water treatment is not effective at reducing the concentrations of many common MPs (Ternes et al. 2002, Westerhoff et al. 2005, Stackelberg et al. 2007), thus advanced treatment processes like granular activated carbon (GAC) are being evaluated for potential use in controlling MPs. Many researchers have shown the efficacy of activated carbon for removing MPs in drinking water treatment settings (Ternes et al. 2002, Westerhoff et al. 2005, Snyder et al. 2007, Stackelberg et al. 2007, Rossner et al. 2009, Chowdhury et al. 2010, Cardenas 2011, Corwin and Summers 2012, Reinert 2013), but full- or pilot-scale GAC data is limited. Bench-scale predictions using the rapid small-scale column test or isotherms typically overestimate GAC adsorption capacity (Speth and Miltner 1989, Summers et al. 1989, Crittenden et al. 1991, Knappe et al. 1997, Corwin and Summers 2010) due to particle size dependent fouling mechanisms and loading scenarios from background dissolved organic matter (DOM). Research is ongoing in this area to develop correction factors for scale-up (Corwin and Summers 2010,

Chapter 4). Therefore the most accurate predictions of full-scale GAC performance must still rely on pilot testing which utilizes the same GAC particle size as the full-scale. Full- or pilot-scale data is scarce because of the large investments of time and money that must be made. Accurate predictions for GAC performance are especially important because the technology is expensive and often over-designed.

The objectives of this chapter were to (a) expand the database of MP breakthrough at environmentally relevant concentrations with full-scale GAC media in five waters with different background DOM concentrations and types and (b) develop relationships that allow the breakthrough to be related to compound and system properties. These outcomes will assist water providers in the design and operation of GAC adsorbers. Bituminous-based GAC was evaluated at two empty bed contact times (EBCT) of 7 and 15 minutes.

3.2 Materials and Methods

3.2.1 Materials

3.2.1.1 Waters

The influent water quality for the four surface waters used to run GAC pilot columns (Waters A, B, C, and D) and a full-scale site (Water E) is shown in Table 3.1. Waters A and B were made by spiking reverse osmosis (RO) membrane isolated DOM into pretreated tap water. City of Boulder, CO tap water was first passed through a 200 L barrel of bituminous-based GAC (Norit 1240) to remove chlorine, DOM, and disinfection by-products (DBPs) that may have interfered with MP adsorption. Periodic DBP samples taken throughout the entirety of the study confirmed no detectable DBPs in the effluent of the pretreatment GAC system. DBPs were analyzed using an Agilent 6890 Series gas chromatography (GC) system in accordance with EPA Methods 551.1 and 552.2 (USEPA 1995b).

The DOM was isolated using a low-pressure RO system (Dow FILMTEC LE-4040) from a high organic content and low alkalinity surface water source at Big Elk Meadows (BEM), CO. Alum coagulation (~100 mg/L) of the BEM-DOM extract removed about 10 to 20% of the dissolved organic carbon (DOC) followed by filtration through a 0.45 μm cartridge filter (Memtrex MNY941CGS). Water A utilized this coagulated DOM extract, while Water B utilized ozonated BEM-DOM at a ratio of 1:1 mg O_3/mg DOC. Pilot studies for Waters A and B were run in the lab at the University of Colorado where the influent batches were prepared approximately every three days.

Water C was coagulated, settled, and filtered (5 μm filter cartridge, Whirlpool WHCF-GD05) water from the Orange Water and Sewer Authority (OWASA, Carrboro, NC) and was derived from two North Carolina reservoir sources (Cane Creek Reservoir and University Lake). Water D was conventionally treated combined filter effluent water from the City of Longmont (LM), CO, derived from the St. Vrain Creek and Colorado-Big Thompson Project sources. Pilot studies for Waters C and D were run at their respective treatment plants.

In addition, data was also gathered from the full-scale GAC system at the Greater Cincinnati Water Works (GCWW) Richard Miller drinking water treatment plant. GCWW uses full-scale GAC adsorbers to treat water from the Ohio River following alum coagulation, sedimentation, and filtration (biologically active) and was termed Water E.

Table 3.1. Average influent surface water quality and operational parameters.

Water	Source	pH	DOC (mg/L)	UVA_{254} (cm^{-1})	EBCT (min)
A	Coagulated BEM	7.0	3.9±0.4	0.098±0.012	7 & 15
B	Ozonated BEM	7.7	2.8±0.3	0.044±0.007	7.5
C	OWASA	6.0	2.1±0.4	0.027±0.005	7
D	LM	6.2	1.7±0.3	0.024±0.006	7
E	GCWW	7.8	1.9±0.3	0.043±0.012	15

3.2.1.2 Adsorbents

All of the pilot columns were run with virgin bituminous-based GAC, which is common in drinking water treatment for controlling DOM and MPs (Summers et al. 2011). GAC in the pilot columns run with Waters A, C, and D was Norit 1240 with a log-mean particle diameter of 0.92 mm (12x40 US standard mesh) and bed density of 450 kg/m^3. GAC in the pilot column run with Water B was Calgon F300 with a log-mean particle diameter of 1.29 mm (8x30 US standard mesh) and bed density of 480 kg/m^3. The full-scale adsorbers treating Water E utilized mesh bituminous-based GAC that was freshly reactivated with a log-mean particle diameter of 0.92 mm (12x40 US standard mesh) and bed density of 490 kg/m^3.

3.2.1.3 Adsorbates

A total of 30 environmentally relevant MPs including pharmaceuticals, personal care products, herbicides, insecticides, a manufacturing additive, and the taste and odor compound 2-methylisoborneol (MIB) were chosen from occurrence studies of surface drinking water sources (Kolpin et al. 2002, Focazio et al. 2008). The chosen MPs covered a wide range of hydrophobicities, ionic states, molecular weights, and biodegradabilities (Zearley and Summers 2012). Target MP influent concentrations were based on the median concentrations from the same studies, detection limits, and a goal to be able to detect the onset of breakthrough at effluent concentrations that corresponded to 2.5 to 10% of the influent concentration. All MPs

(except those found in Water E) were purchased from Sigma-Aldrich (St. Louis, MO), with three exceptions. 2,4-D was purchased from Acros Organics (New Jersey, US), iopromide was purchased from U.S. Pharmacopa (Rockvill, MD), and simazine was purchased from Alfa Aesar (Ward Hill, MA).

3.2.2 Methods

3.2.2.1 Analytical Methods

3.2.2.1.1 Micropollutant Analysis

The analysis of MPs was conducted by high performance liquid chromatography-tandem mass spectrometry (LC/MS-MS) at the Center for Mass Spectrometry at the University of Colorado at Boulder. The mass spectrometry analyses allowed for the separation of all the analytes in the water extracts using an HPLC system (Agilent Series 1290), consisting of vacuum degasser, autosampler, and a binary pump, equipped with a reversed phase C18 analytical column of 50 mm x 2.1 mm and 1.8 μm particle size (Zorbax Eclipse Plus). The HPLC system was connected to a triple quadrupole mass spectrometer Agilent 6460 that was equipped with electrospray Jet Stream technology, which could operate in positive and negative ion mode.

Pilot column results from the LC/MS-MS analysis were given as relative concentration (C/C_0) based on analyte area ratios of the paired effluent and influent samples. Pilot column influent concentrations (Waters A, B, C, and D) as well as influent and effluent concentrations in Water E were estimated from an internal standard (carbamazepine, 100 ng/L). The influent concentrations in Waters A, B, C, and D can be seen in Chapter 2 (Table 2.1). The relative standard deviation for all the MP analysis was less than 11% (Ferrer et al. 2010). This chapter only shows two data points for MIB because of analytical issues, but the GC/MS-MS procedure for the analysis of MIB in the aqueous-phase was developed by Yuncu (2010).

3.2.2.1.2 Dissolved Organic Carbon, Ultraviolet Absorbance, and pH

Dissolved organic carbon (DOC) was measured with a Sievers 800 TOC analyzer in accordance with Standard Method 5310C (APHA et al. 2005). Ultraviolet absorbance (UVA_{254}) was analyzed at a wavelength of 253.7 nm using a Hach DR 4000 spectrophotometer in accordance with Standard Method 5910 (APHA et al. 2005). pH was measured using a Denver Instruments Model 220 pH meter in accordance with Standard Method 4500-H^+ (APHA et al. 2005).

3.2.2.2 Pilot Column Design and Operation

Pilot columns were 2.54 cm ID glass chromatography columns with PTFE adapters operated at a hydraulic loading rate (HLR) of 5 m/h, which resulted in a flow rate of 42 mL/min. A HLR of 5 m/h is at the lower end of typical rates, but was chosen to limit the amount of water required. In this range, intraparticle mass transfer still controls MP adsorption kinetics in the presence of DOM (Corwin 2010). The aspect ratios for the columns were 27 (12x40) and 19 (8x30), which is greater than the 8 to 10 necessary to avoid wall effects on mass transfer (Knappe et al. 1999).

Water A was run at two the EBCTs of 7 and 15 minutes (Water A (7) and Water (15), respectively), which was accomplished with a 7 minute column followed by an 8 minute column. Water B was run at an EBCT of 7.5 minutes. Waters C and D were run at EBCTs of 7 minutes.

Influent water spiked with all 30 MPs at initial concentrations ranging from 3 ng/L to 3 µg/L was fed to the columns from well-mixed 200 L HDPE barrels through PVC, stainless steel and PTFE tubing using a Cole-Parmer PTFE diaphragm pump. The total MP concentration in the pilot column influent barrels averaged 8.1±2.7 µg/L (n=6, see Table 2.1), which was less than 0.5% of the any influent DOC concentration. Concentrated MP stock solutions were stored at

4°C and remade every six months. Pilot column effluent water was treated in a secondary GAC barrel before being discharged to a drain. Prior to the start of pilot testing the GAC was backwashed with dechlorinated and organics-free water to remove carbon fines.

Paired influent and effluent MP samples were collected immediately before and after the pilot column. A needle valve was used for flow control to maintain the desired EBCT during sampling. Water samples were collected in muffled 250 mL amber glass bottles, stored at 4°C, and extracted within one week before quantification. Pilot column influent and effluent DOC and UVA_{254} samples were taken biweekly at the beginning of the run. After complete DOC breakthrough, UVA_{254} was used for measurements of DOM. Strong relationships were observed between DOC and UVA_{254} ($R^2 \geq 0.95$) for all waters.

At the full-scale Water E was sampled following biological filtration and from the single adsorber with freshly reactivated GAC. The GAC adsorbers at GCWW are variable rate contactors and were designed for a HLR of 14 m/h and 15 minute EBCT but typically operate at a HLR of about 18 m/h and a 12-minute EBCT. A total of four paired influent and effluent samples were taken over the course of nine months from August 2011 to May 2012.

3.3 Results and Discussion

3.3.1 Micropollutant Breakthrough Relative to Dissolved Organic Carbon Breakthrough

GAC adsorbers can be used to control the formation of DBPs for waters with DOM levels above which coagulation is ineffective. For DBP control, typically 20 to 50% DOC removal (or 80 to 50% DOC breakthrough) is targeted for GAC adsorbers (Chowdhury et al. 2013). Depending on the initial DOC concentration, EBCT, pH, and GAC type and size (Zachman and Summers 2010), GAC bed lives can range from weeks to several months for DBP control.

The breakthrough of iopromide (C_0~3.0±1.1 µg/L, method report limit (MRL)~25 ng/L), a medical imaging contrast medium, relative to DOC breakthrough in Water A for EBCTs of 7 and 15 minutes is shown in Figure 3.1. Iopromide breakthrough was chosen as it was the most weakly adsorbing compound in this study, as well as in other studies (Westerhoff et al. 2005, Snyder et al. 2007, Rossner et al. 2009, Cardenas 2011). The breakthrough is shown as a function of pilot column operation time and the effluent concentration normalized by the influent concentration. MP breakthrough results are presented in this manner because when the background DOM concentration (as measured by DOC) is sufficiently high and the MP concentration is in the ng/L to low µg/L range, normalized MP breakthrough (C/C_0) is independent of initial MP concentration (Gillogly et al. 1998, Knappe et al. 1998, Graham et al. 2000, Matsui et al. 2003, Westerhoff et al. 2005, Rossner et al. 2009, Corwin and Summers 2012).

For an EBCT of 7 minutes, 50% DOC breakthrough (~2 mg/L) occurred within 3 weeks, while the effluent iopromide concentration remained below detection. Similarly at an EBCT of 15 minutes, 50% DOC breakthough (~2 mg/L) occurred within 8 weeks, while the effluent iopromide concentration remained below detection. At an EBCT of 7 minutes, iopromide broke through to 10% after about 6 weeks, or 70% DOC breakthrough. At an EBCT of 15 mintues iopromide broke through to 10% after about 5 months, or 80% DOC breakthrough.

For the 30 compounds investigated, even the most weakly adsorbing MP studied broke through after complete DOC breakthrough. Where iopromide exists it may be useful as a conservative tracer for complete GAC removal of other commonly found MPs. Although undesirable in drinking water, provisional drinking water guidelines presented by Schriks et al.

(2010) for iodinated contrast media were very high (>6.7 mg/L), indicating the risk would be low for using iopromide or other iodinated contrast media as tracers.

Taste and odor control represents another significant use of GAC. Although the data was limited to two data points because of analytical issues following these two samples, the taste and odor compound MIB is also shown in Figure 3.1 for comparison (C_0~105±39 ng/L, MRL~1 ng/L). MIB breaks through at the same time as iopromide and is subject to the same analysis in relation to DOC breakthrough. MIB breakthrough to 10% in Water A was predicted well by the model developed by Summers et al. (2013). For reference, the other common taste and odor causing compound geosmin would break through after MIB as it is more strongly adsorbing (Graham et al. 2000, Summers et al. 2013).

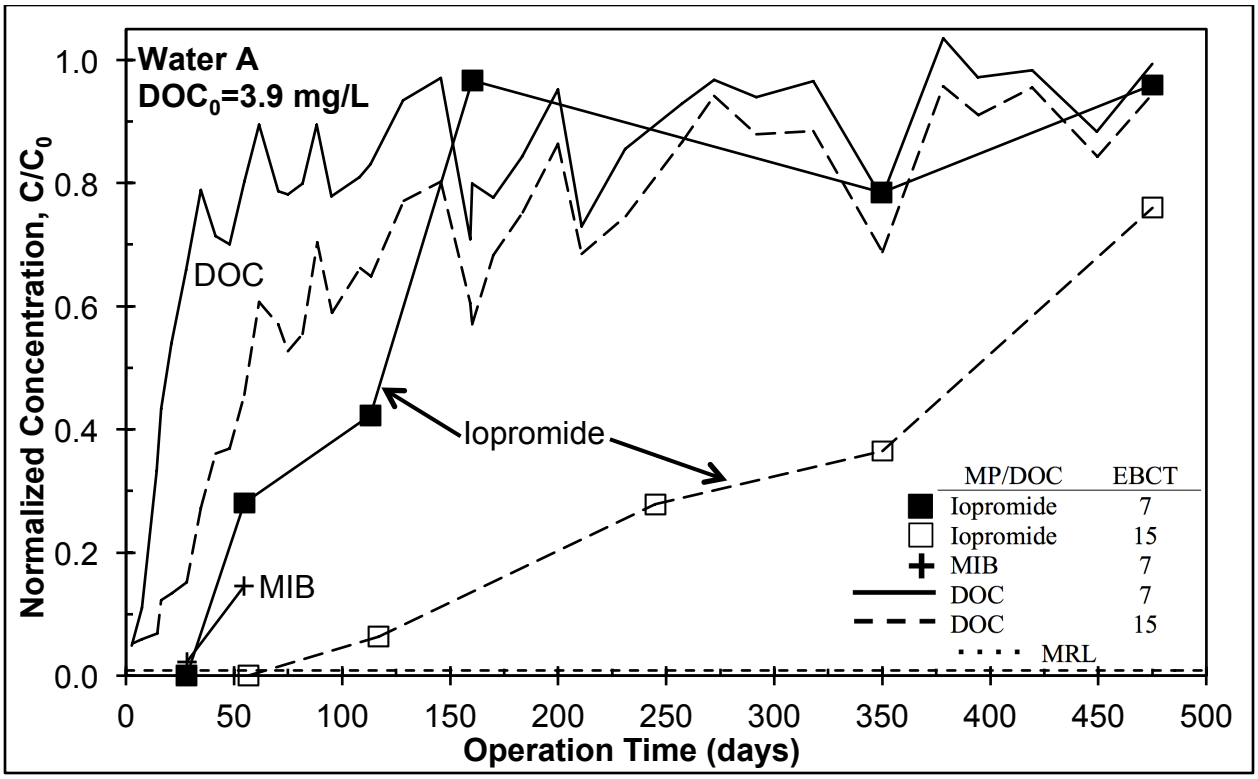

Figure 3.1. Pilot column breakthrough for DOC, the x-ray contrast media iopromide (C_0~3.0±1.1 µg/L, MRL~25 ng/L), and taste and odor compound MIB (C_0~105±39 ng/L, MRL~1 ng/L) in Water A at EBCTs of 7 and 15 minutes (DOC_0=3.9 mg/L, 12x40 bituminous GAC).

3.3.2 Effect of Empty Bed Contact Time

The effect of EBCT on DOC and iopromide breakthrough, shown in Figure 3.1, leads to longer run times at the 15 minute EBCT, compared to the EBCT of 7 minutes. In general, this was the case for all MPs with breakthrough at both EBCTs when presented on an elapsed time basis because a longer EBCT at the same hydraulic loading rate has more GAC mass. Therefore to facilitate comparisons, operation time can be expressed as throughput in bed volumes (operation time divided by the EBCT or volume of water treated divided by the GAC bed volume) or for GAC with different bed densities, as specific throughput (volume of water treated divided by the GAC mass). Throughput as bed volumes or specific throughput is useful because it is directly related to the carbon use rate (CUR), the main factor for determining GAC adsorber

capital and operation costs. An increase in throughput to a target breakthrough corresponds to a lower (better) CUR. Because the bed density of the GAC used for Waters A, B, C, and D (ρ_{bed}=450 kg/m^3) was very similar to the GAC used for Water B (ρ_{bed}=480 kg/m^3), breakthrough curves were essentially the same (<8% difference) with throughput plotted as bed volumes or specific throughput. Therefore bed volumes were used to provide a better sense of operational time.

Normalization of the time axis into throughput in bed volumes for iopromide breakthrough is shown in Figure 3.2. In Water A, the 15 minute EBCT yields longer run times, which corresponds to lower CUR values. Similar behavior is also shown in Figure 3.3 for the herbicide acetochlor (with no 15 minute EBCT breakthrough) and in Figure 3.4 for the nicotine metabolite cotinine.

However, Figure 3.5 shows approximately the same breakthrough at both EBCTs for insecticide methomyl (based on one 15 minute EBCT breakthrough data point). Other studies have shown longer EBCTs yielding the same or lower CURs at early breakthrough for atrazine (Knappe et al. 1997), clofibric acid (Ternes et al. 2002), bisphenol A (Corwin and Summers 2012), MIB (Summers et al. 2013), and several volatile organic compounds (VOCs) (Hand et al. 1989). With longer EBCTs, or increase in bed depth, a higher level of fouling from DOM adsorption is expected due to preloading. Preloading occurs because DOM adsorption is relatively slow compared to MPs due to its larger molecular size leading to a long mass transfer zone (Sontheimer et al. 1988).

In this study the number of compounds with breakthrough in the 15 minute EBCT column was limited to seven of 30 compounds, with most MPs showing no breakthrough by the end of 476 days of operation time. At equivalent bed volumes, the 15 minute EBCT pilot column

resulted in lower CURs compared to the 7 minute EBCT pilot column in Water A. Of the seven MPs with breakthrough in the 15 minute pilot column, five illustrated the benefits of a larger GAC mass in the column (methomyl and tributyl phosphate did not). Still there are other factors to consider including adsorber cost and biodegradation. When deciding on an EBCT, designers must weigh the cost of increased GAC mass and resulting adsorber size, piping, etc. versus the lower CUR, especially when most MP breakthrough occurs well after DOC breakthrough even at a 7 minute EBCT.

The apparent lack of breakthrough for most MPs in this study at the 15 minute EBCT may also be related to biodegradation. Biodegradation potentials for the MPs in this study from Zearley and Summers (2012) are shown in Table 3.2. Longer EBCTs have been shown to increase MP removal due to increased biomass available to degrade MPs (Summers et al. 2011, Zearley and Summers 2012). Biological growth was not encouraged in any of the pilot columns with nutrient or dissolved oxygen addition. However, phospholipid analysis of the media after the end of the pilot column run for Water A showed an average of 175±23 nmol PO_4 per mL of GAC bed, which represents significant biological activity (Wang et al. 1995, Zearley and Summers 2012). MPs that exhibited biodegradation behavior through (1) no breakthrough at either EBCT, (2) plateau behavior at relatively low breakthrough, or (3) erratic breakthrough behavior were acetaminophen, caffeine, diclofenac, erythromycin, gemfibrozil, ibuprofen, and trimethoprim.

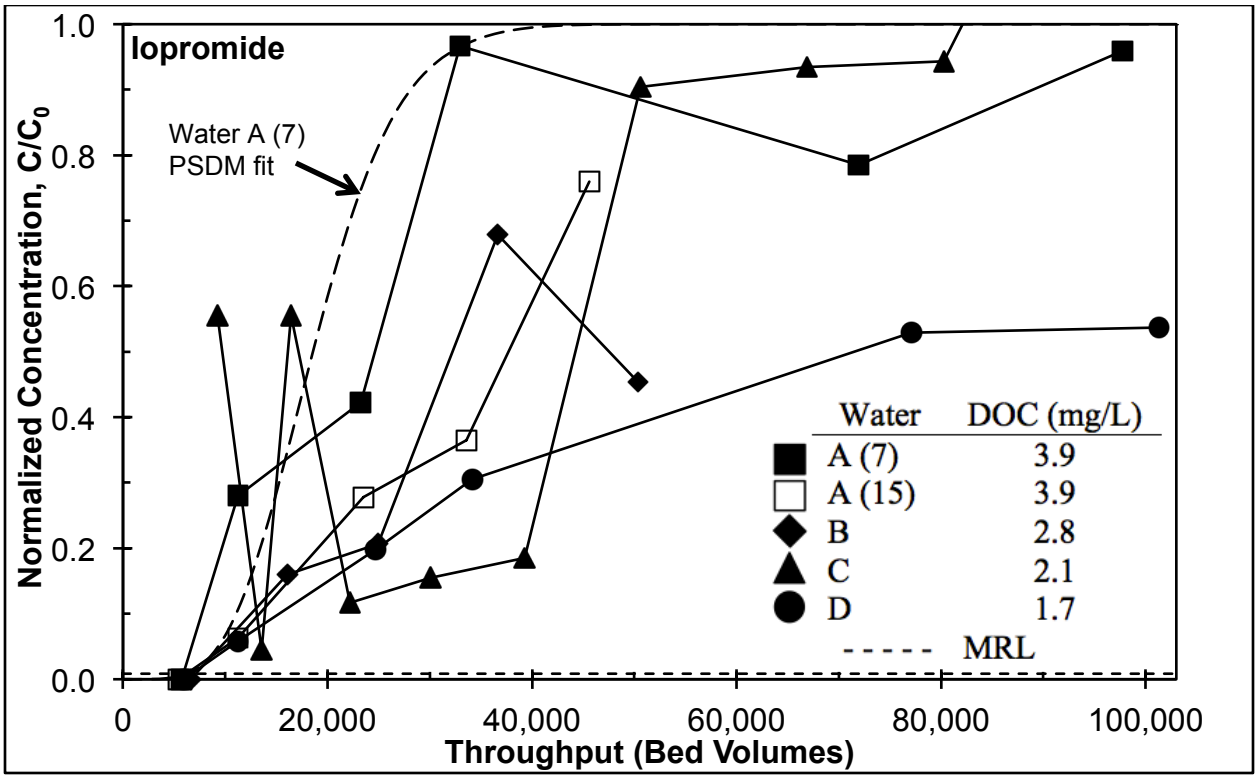

Figure 3.2. Pilot column breakthrough profiles for the x-ray contrast media iopromide (C_0~3.0±1.1 µg/L, MRL~25 ng/L, K^*=57, K_{PSDM}=43, τ=0.1) in Waters A, B, C, and D at EBCTs of 7 and 15 minutes.

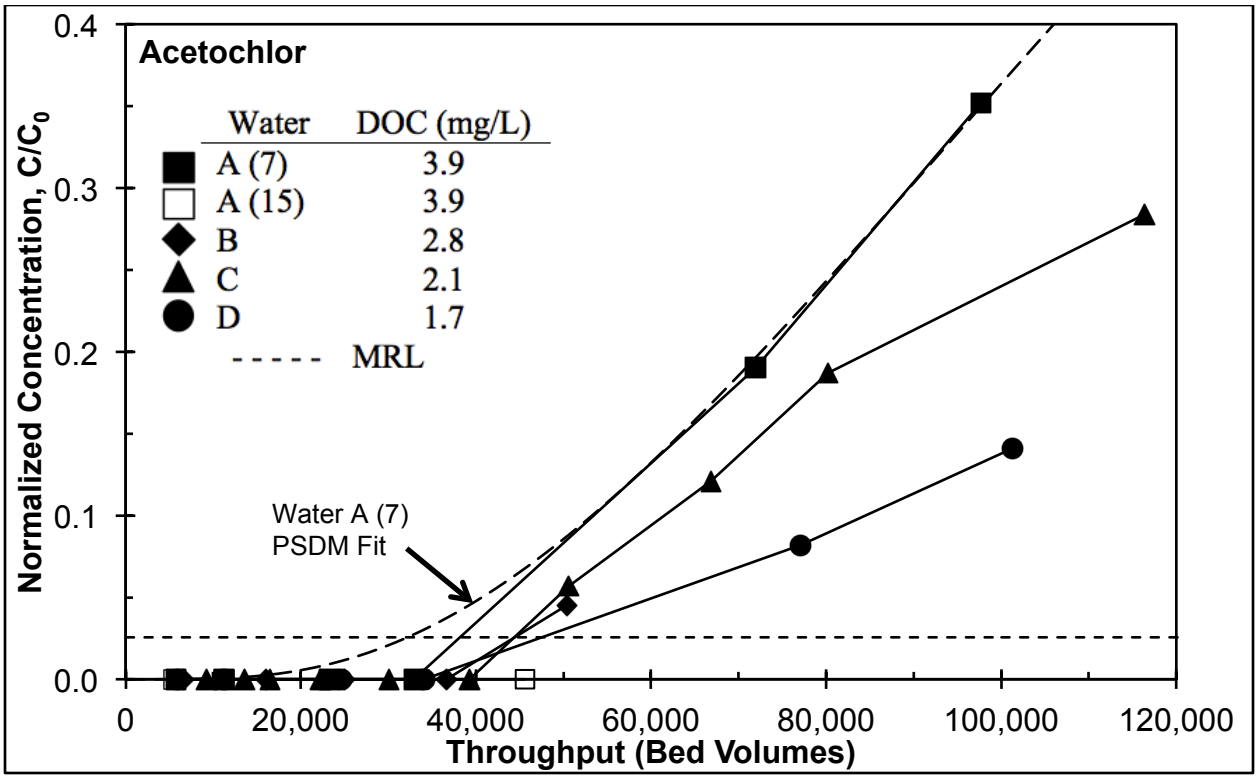

Figure 3.3. Pilot column breakthrough profiles for the herbicide acetochlor (C_0~390±160 ng/L, MRL~10 ng/L, K^*=N/A (<50%), K_{PSDM}=305, τ=0.6) in Waters A, B, C, and D at EBCTs of 7 and 15 minutes.

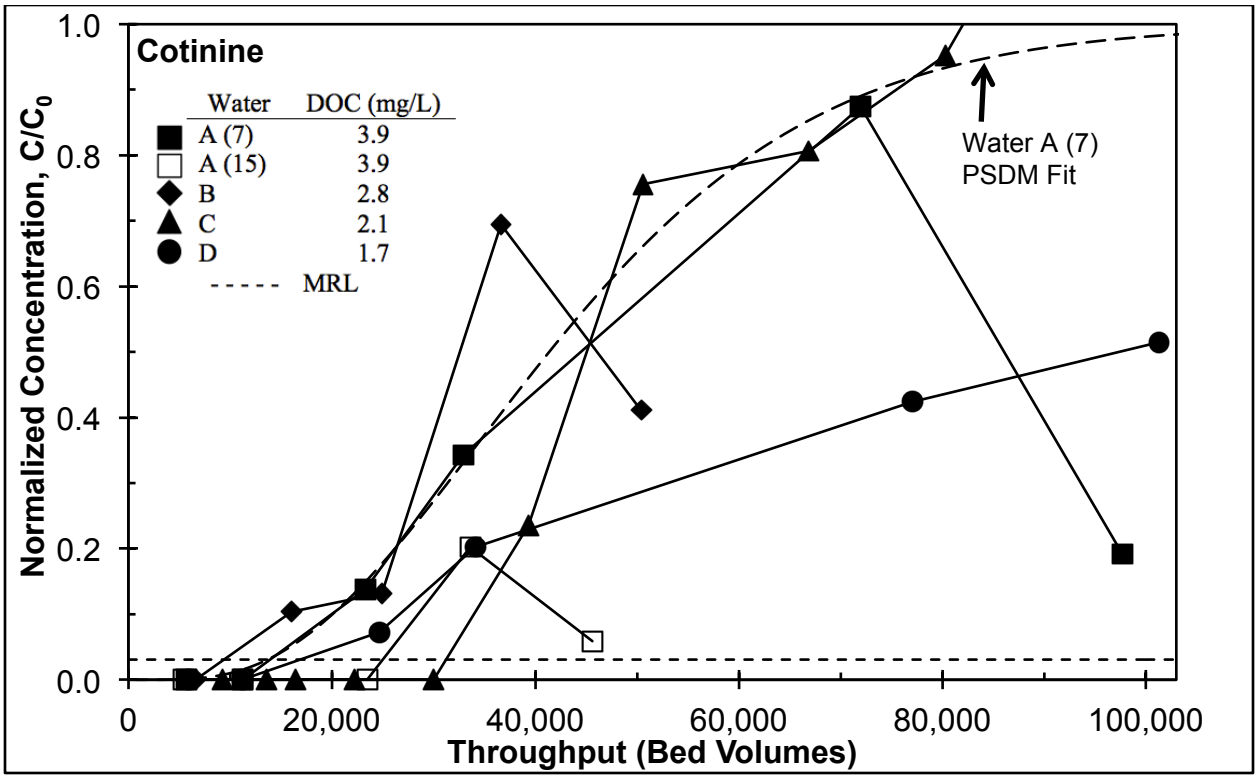

Figure 3.4. Pilot column breakthrough profiles for the nicotine metabolite cotinine (C_0~160±80 ng/L, MRL~5 ng/L, $K^*=K_{PSDM}=100$, $\tau=0.6$) in Waters A, B, C, and D at EBCTs of 7 and 15 minutes.

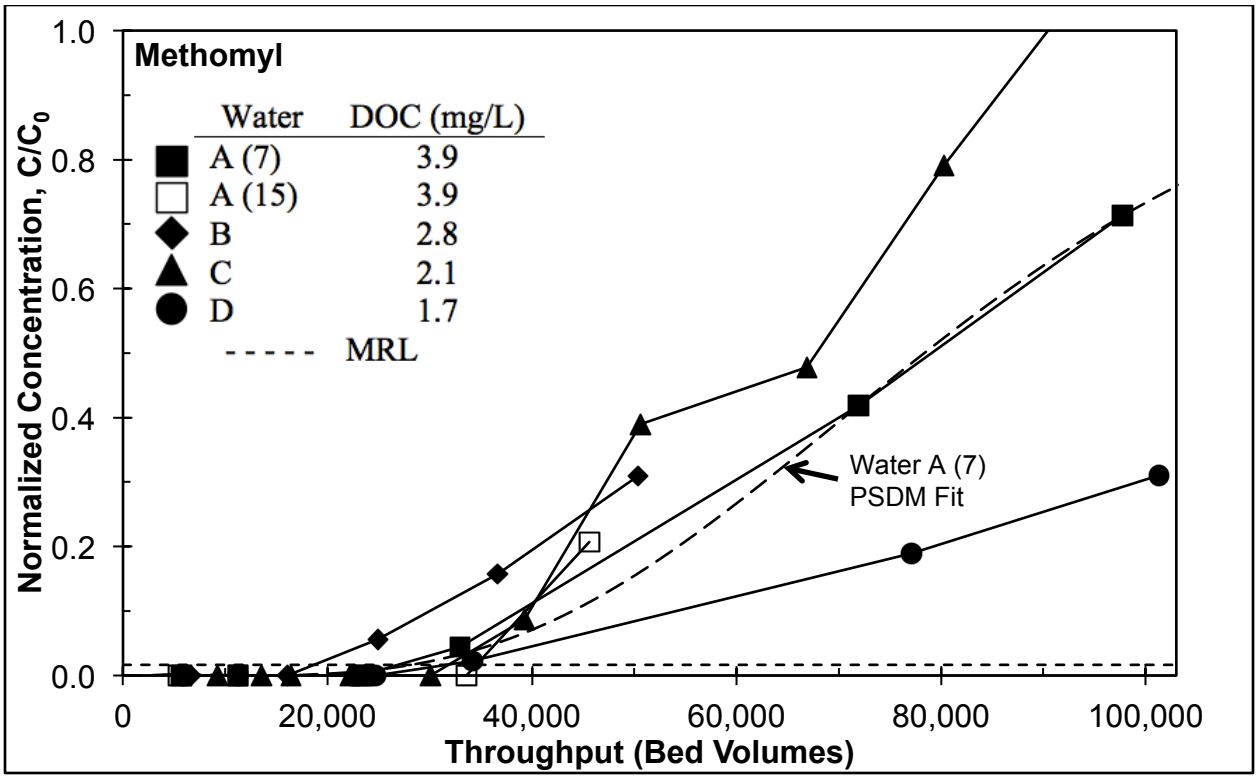

Figure 3.5. Pilot column breakthrough profiles for the insecticide methomyl (C_0~310±80 ng/L, MRL~5 ng/L, K^*=178, K_{PSDM}=185, τ=1) in Waters A, B, C, and D at EBCTs of 7 and 15 minutes.

3.3.3 Effect of Influent Dissolved Organic Carbon Concentration

The background DOM matrix, measured as the influent DOC (DOC_0) concentration, was found to impact the MP breakthrough, as illustrated by the breakthrough behavior of the four MPs shown in Figure 3.2 through Figure 3.5. Acetochlor showed later breakthrough with decreasing DOC_0 concentration, which is expected from decreased competition for a fixed number of adsorption sites. Clear separation between breakthrough curves in waters with different DOC_0 concentrations has been well established for other MPs (Sontheimer et al. 1988, Cardenas 2011, Corwin and Summers 2012, Summers et al. 2013). Summers et al. (2013) found an inverse relationship between DOC_0 concentration and the breakthrough of MIB. However upon further investigation of Figure 3.2, Figure 3.4, and Figure 3.5 a systematic trend for

iopromide, cotinine, and methomyl of later breakthrough with decreasing DOC_0 concentration is not as clear, especially at early breakthrough.

To systematically organize and quantitatively analyze breakthrough data at these low concentration ranges, the bed volumes to 10% MP breakthrough ($BV_{10\%}$) were used. Breakthrough at 10% is also relevant because high levels of removal for MPs are usually desired. $BV_{10\%}$ values are shown in Table 3.2 for Waters A (7 & 15), B, C, and D, and unless noted, all $BV_{10\%}$ values were directly interpolated from data. In some cases, the pore and surface diffusion model (PSDM using AdDesignS™ from Michigan Technological University, Houghton, MI) simulation was used to extrapolate the breakthroughs that were less than but close to 10%. Due to the presence of background DOM, initial PSDM assumptions followed those of Corwin and Summers (2011).

Since the relative standard deviation of each MP concentration sample was 11%, the relative standard deviation of each data point is ±0.011 at 10% breakthrough. In all cases MPs broke through to 10% after complete DOC breakthrough, with the exception of 10% iopromide breakthrough at 50% DOC breakthrough in Water C. DOC breakthrough to 20 and 50% ($BV_{20\%}$ and $BV_{50\%}$) for each water is also shown in Table 3.2.

For each MP, the $BV_{10\%}$ values for the different waters were normalized by the corresponding $BV_{10\%}$ value from Water A (7), as this pilot column had the highest DOC_0 concentration, which resulted in the highest number of MPs with breakthrough (n=23). The ratios are shown in the right side of Table 3.2. For each water these ratios were then averaged and compared to unity to see if their behavior was significantly different from the Water A (7) at a 95% confidence level. The stimulant caffeine $BV_{10\%}$ values are shown but were excluded from

the analysis due to erratic breakthrough behavior throughout all tests most likely related to its high biodegradation potential (Zearley and Summers 2012).

The extractant and plasticizer tributyl phosphate $BV_{10\%}$ values are also shown but were excluded from the analysis due to erratic breakthrough behavior and/or consistent breakthrough at 10 to 20% for the first sampling events when all other MPs were below detection. Although MP sampling did not occur at time equal to zero, tributyl phosphate might break through immediately similar to DOC. Tributyl phosphate is not readily biodegradable (Zearley and Summers 2012).

The statistical t-test analysis at the bottom of Table 3.2 indicates that on average MPs in Water C and Water D broke through 33% and 62% later compared to MPs in Water A (7), respectively. The DOC_0 concentrations of these waters are 46% and 56% lower than that for Water A. When the EBCT for Water A was doubled to an EBCT of 15 minutes, on average MPs broke through 52% later.

On average, MPs in Water B broke through 5% later compared to Water A (7), but this was found not to be significant. Therefore MPs in Water B yielded the same breakthrough behavior as Water A (7) despite the DOC_0 concentration being 28% lower. Earlier breakthrough to 10% than expected could be a caused by the difference in carbon size, 8x30 mesh (d_p=1.29 mm) compared to 12x40 mesh (d_p=0.92 mm). Larger GAC media yields slower adsorption kinetics because the average intraparticle diffusion path length is longer, which would result in earlier breakthrough at 10% (Sontheimer et al. 1988).

Another difference in the Water B run was that the DOM was ozonated. Ozonation as a pretreatment to GAC adsorption generally decreases DOM adsorbability by increasing the polarity of the oxidized DOM, which could result in increased MP removal from decreased

competition (Sontheimer et al. 1988). However, on average, Cardenas (2011) found no significant difference between $BV_{10\%}$ values for 12 MPs in coagulated and ozonated waters, both with DOC_0 concentrations of 2.1 mg/L. Also, for Water B, the ozonated DOM was slightly more strongly adsorbing than expected by comparing the DOC breakthrough curves of the pilot column to the model for 8x30 bituminous GAC from Zachman and Summers (2010). Although ozone oxidation can increase the fraction of hydrophilic DOM, it also reduces the overall molecular size of the DOM. Smaller DOM has greater access to micropores (d_{pore}<20 Å) where MP adsorption occurs, causing increased competition and earlier breakthrough than expected based solely on DOC_0 concentration (Sontheimer et al. 1988).

Table 3.2. Bed volumes to 10% breakthrough for pilot column runs ($x10^3$) with run times in days shown in parentheses. Biodegradation rates are from Zearley and Summers (2012). Ratios of $BV_{10\%}$ values relative to $BV_{10\%}$ values in Water A (7). Acetaminophen, carbaryl, diuron, ibuprofen, and trimethoprim not shown because there was no breakthrough in the pilot columns.

Compound	Water A	Water B	Water C	Water D	Water A	Biodegradation Rate	$BV_{10\%}/BV_{10\%,Water\ A\ (7)}$			
DOC_0 (mg/L)	3.9	2.8	2.1	1.7	3.9		Water B	Water C	Water D	Water A (15)
EBCT (min)	7	7.5	7	7	15					
DOC $BV_{20\%}$	2.1 (10)	2.2 (11)	6.8 (33)	3.0 (15)	3.0 (31)	--	--	--	--	--
DOC $BV_{50\%}$	4.0 (19)	6.5 (34)	14 (68)	11 (39)	5.5 (57)	--	--	--	--	--
2,4-D	18 (88)	36 (188)	>116 (564)	50 (243)	>46 (476)	Fast	2.00	--	2.78	
Acetochlor	55 (267)	78[b] (406)	62 (301)	85 (413)	>46 (476)	Recalcitrant	1.42	1.13	1.55	--
Aldicarb	65 (233)	53[b] (276)	>116 (564)	100 (486)	>46 (476)	Slow	0.82	--	1.54	--
Atrazine	48 (233)	36 (188)	52 (253)	90 (438)	>46 (476)	Recalcitrant	0.75	1.08	1.88	--
Caffeine[e]	6 (29)	25 (130)	48 (233)	40 (194)	13[b] (135)	Fast	4.17	8.00	6.67	2.17
Carbamazepine	80 (389)	>50 (260)	84 (408)	90[b] (438)	>46 (476)	Recalcitrant	--	1.05	1.13	--
Clofibric acid	25 (122)	16 (83)	>116 (564)	20 (97)	55[b] (573)	Slow	0.64	--	0.80	2.20
Cotinine	20 (97)	15 (78)	38 (185)	30 (146)	28 (292)	Slow	0.75	1.90	1.50	1.40
Diazinon	78 (379)	>50 (260)	>116 (564)	70 (340)	>46 (476)	Recalcitrant	--	--	0.90	--
Diclofenac	>[d]98 (476)	>50 (260)	>116 (564)	108[b] (525)	>46 (476)	Slow	--	--	--	--
Dimethoate	70 (340)	52[b] (271)	120[c] (583)	75 (365)	>46 (476)	Fast	0.74	1.71	1.07	--
Erythromycin	22 (107)	>50 (260)	>116 (564)	66 (321)	>46 (476)	Slow	--	--	3.00	--
Gemfibrozil	>98 (476)	>50 (260)	>116 (564)	75 (365)	>46 (476)	Fast	--	--	--	--
Iopromide	8 (39)	12 (63)	14 (68)	15 (73)	14 (146)	Recalcitrant	1.50	1.75	1.88	1.75
Malaoxon	55 (267)	49[b] (255)	>116 (564)	100 (486)	>46 (476)	Slow	0.89	--	1.82	--
Methomyl	40 (194)	30 (156)	44 (214)	50 (243)	40 (417)	Recalcitrant	0.75	1.10	1.25	1.00
Metolachlor	35[a] (170)	50 (260)	52 (253)	80 (389)	>46 (476)	Recalcitrant	1.43	1.49	2.29	--
Molinate	90 (438)	>50 (260)	>116 (564)	95 (462)	>46 (476)	Fast	--	--	1.06	--
Naproxen	113[b] (549)	>50 (260)	>116 (564)	>101 (491)	>46 (476)	Fast	--	--	--	--
Prometon	38 (185)	35 (182)	46 (224)	64 (311)	48[b] (500)	Recalcitrant	0.92	1.21	1.68	1.26
Simazine	75 (365)	>50 (260)	68 (331)	118[b] (574)	>46 (476)	Recalcitrant	--	0.91	1.57	--
Sulfamethoxazole	75 (365)	>50 (260)	>116 (564)	94 (457)	>46 (476)	Recalcitrant	--	--	1.25	--
Tributyl phosphate[e]	20 (97)	20[b] (104)	20 (97)	10 (49)	8 (83)	Slow	1.00	1.00	0.50	0.40
Warfarin	18 (88)	>50 (260)	120[c] (583)	35 (170)	>46 (476)	Slow	--	6.67[g]	1.94	--
						Average:	1.05	1.33	1.62	1.52
						Standard Deviation:	0.43	0.35	0.59	0.47
						Count (used is calcs):	12	10	19	5
						Different from Water A (7)[f]:	No	Yes	Yes	Yes
						t-test p-value:	0.345	0.007	0.000	0.033

[a]Value taken after averaging last two pilot data points. [b]Value taken or extrapolated from PSDM simulation. [c]Value extrapolated from data. [d]No breakthrough or could not be confidently projected to 10% using the PSDM. [e]Values not included in calculations due to erratic breakthrough behavior over all tests. [f]t-test on whether average values are significantly different than 1 (Water A, 7 min EBCT) at a 95% confidence level. [g]Statistical outlier and not included in calculations. $CUR_{10\%}= \rho_{bed}/BV_{10\%}$, Bed $Life_{10\%}=BV_{10\%}*EBCT$.

3.3.4 Micropollutant Adsorption Kinetics

As previously mentioned the PSDM was used extrapolate breakthrough curves that were less than but close to 10% while assuming intraparticle mass transfer controlled adsorption kinetics (Corwin and Summers 2011). The PSDM was used to acquire kinetic information, specifically an effective intraparticle diffusion coefficient represented by the bulk liquid diffusion coefficient (D_L) divided by the tortuosity or labyrinth factor (τ). Tortuosity represents the increased diffusion path length from pore constriction in the GAC particle due to DOM adsorption. Tortuosity values less than one imply surface diffusion is not negligible.

PSDM curve fitting revealed that a variety of combinations of the Freundlich capacity parameter K and τ worked for MPs with low breakthrough (<50%). Therefore kinetic data analysis was restricted to MPs with >50% breakthrough to establish confidence in the model fits because an apparent capacity term, K^* (equal to $BV_{50\%}/\rho_{bed}$), could be calculated (Corwin and Summers 2011). Tortuosity values ranged from 0.1 to 3 for MPs in Waters A (7 & 15), B, C, D, and E (n=19), with most values ranging from 0.1 to 1 (n=15), implying surface diffusion was needed to model breakthrough. Scatter plots for Water A (7) and Water C showed increasing τ with increasing $BV_{10\%}$ values and K^* values for some MPs, but linear and exponential relationships were found to be insignificant, most likely due to limited data. For the MPs in Figure 3.2 through Figure 3.5, PSDM fits are shown for Water A (7) with K and τ values given in the captions. K^* values were essentially the same as K values used to acquire a best fit (K_{PSDM}), except for acetochlor because breakthrough was less than 50%.

3.3.5 Micropollutant Bins

Given the water quality variability inherent in natural waters that affects MP adsorption behavior, it may be useful for preliminary analysis to bin MPs into different levels of

adsorbability. A binning approach is shown in Table 3.3 with five bins of MP adsorbability in one water, Water A (7), with adsorbability (and biodegradability) increasing from left to right. Water A (7) was again, like in Table 3.2, chosen as a base case because it had the highest DOC_0 concentration, which resulted in highest number of MPs with breakthrough, and the base EBCT of 7 minutes. Bins were defined by $BV_{10\%}$ value ranges with the corresponding $CUR_{10\%}$ also shown. The range of $BV_{10\%}$ values in any one bin is great enough, a factor of 2 to 2.8, that changes in the DOM concentration and type should not have a major impact on the bin classification. Chowdhury et al. (2013) also organized many MPs from several studies based on $BV_{10\%}$ values into the categories of weakly, moderately, and strongly adsorbing, with many similarities to Table 3.3. In this study the antibiotic sulfamethoxazole, which is negatively charged at pH 7, was more strongly adsorbing than other studies (Snyder et al. 2007, Corwin and Summers 2012). Table 3.3 also shows MP breakthrough behavior cannot be classified by MP type, i.e. herbicide, insecticide, pharmaceutical, etc., but instead gives a sense of where common MPs break through relative to other common MPs and DOC.

Distinguishing between strong adsorption potential and biodegradation, as previously discussed with regards to EBCT, can be difficult. Zearley and Summers (2012) showed many of the MPs in Table 3.3 to have fast biodegradation rates. However, the insecticide carbaryl and herbicide diuron most likely never broke through in any pilot column due to strong adsorption as opposed to biodegradation.

Table 3.3. MP removal binning by $BV_{10\%}$ values (and $CUR_{10\%}$) ranges in Water A (DOC_0=3.9 mg/L, EBCT=7 minutes).

<9,000 (>50 mg/L)	9,000 – 25,000 (50 – 18 mg/L)	25,000 – 50,000 (18 – 9 mg/L)	50,000 – 100,000 (9 – 4.5 mg/L)	>100,000 (<4.5 mg/L)
DOC	2,4-D*	Atrazine	Acetochlor	Acetaminophen*
MIB*	Clofibric acid	Methomyl	Aldicarb	Carbaryl
Iopromide	Cotinine	Metolachlor	Carbamazepine	Diclofenac
	Erythromycin	Prometon	Diazinon	Diuron
	Warfarin		Dimethoate*	Gemfibrozil*
			Malaoxon	Ibuprofen*
			Molinate*	Naproxen*
			Simazine	Trimethoprim*
			Sulfamethoxazole	
Increasing Adsorbability/Biodegradability →				

*Fast or very fast biodegradation potential following Zearley and Summers (2012).

3.3.6 Predicting Bed Volumes to 10% Micropollutant Breakthrough

From Table 3.2 it can be seen for most of the MPs in this study, bed lives to 10% breakthrough are well beyond typical bed lives of GAC adsorbers for DOM removal. The design and operation of GAC adsorbers for the removal of the most strongly adsorbing MPs is relatively straightforward as the GAC run times are very long and the CURs are very low. In most cases where these strongly adsorbing compounds occur there are other more weakly adsorbing compounds present. Thus, targeting more weakly adsorbing MPs is more relevant for adsorber design and operation. Based on the breakthrough data in Water A (7), about 8 months of operation time (~50,000 bed volumes) was established to capture weakly to moderately adsorbing MPs for regression analysis, or the first three bins in Table 3.3. The CUR at eight months is only 9 mg/L. Increasing the run time by 50% to one year only decreases the CUR to 6 mg/L. Choosing a shorter time would also significantly limit the number of data points and MP types.

The following MPs with $BV_{10\%}$ values within the first eight months of operation in Water A (7) were chosen as a base case: 2,4-D, atrazine, clofibric acid, cotinine, erythromycin,

iopromide, methomyl, metolachlor, prometon, and warfarin. Of these 10 MPs, only 2,4-D is relatively biodegradable. In addition to this MP base case, the MP counterpart in the other coagulated waters at an EBCT of 7 minutes were included if applicable. Warfarin had the largest $BV_{10\%}$ value of MPs with 10% breakthrough in Water C, whereas in the other waters warfarin was one of the first MPs to breakthrough. Statistical analysis of the $BV_{10\%}$ values within the chosen constraints confirmed warfarin in Water C was the only outlier in the group and was therefore excluded. The detection limits for the chosen 10 MPs were all less than 10% of the average influent concentrations.

In total, 26 MPs were chosen from Waters A (7), C, and D to form a predictive relationship. These three waters represent common themes among surface water adsorber installations: (1) EBCT of 7 minutes, (2) influent DOC concentrations ranging from 1.7 to 3.9 mg/L, (3) coagulated feed water, and (4) bituminous 12x40 mesh GAC. MIB was not included in the regression as breakthrough was available in only one water and the predictive relationship from Summers et al. (2013) accurately predicts $BV_{10\%}$ for MIB in Water A (7).

$BV_{10\%}$ values from the chosen 26 MPs in this study were compared to DOC_0 concentrations and easily obtainable compound properties relevant to adsorption including aqueous solubility, pH-dependent octanol-water partition coefficient (log D), molecular weight, Abraham solvation parameters (A, B, E, S, V), liquid diffusivity, and polar surface area. Singularly only DOC_0 concentration, log D, S, and V showed any systematic trend with $BV_{10\%}$ values. The Abraham parameter S represents MP polarity/polarizability and V represents MP McGowan molecular volume ($cm^3/mol/100$). Specifically, $BV_{10\%}$ for iopromide showed a very strong linear trend with initial DOC for Waters A (7), B, C, and D. The relationship is shown in

Equation 3.1 ($p<0.01$, $R^2=0.99$, $R^2_{adj}=0.99$, $R^2_{pred}=0.95$, n=4) and may be useful for conservative estimates of MP breakthrough within the constraints previously listed.

$$BV_{10\%}^{iopromide} = (20{,}582 \pm 513) + (-3{,}155 \pm 185) DOC_0 \quad (3.1)$$

Several other researchers have related activated carbon removal or breakthrough to DOC_0 concentration, log D (K_{ow}), polarizability, and molecular volume (Magnuson and Speth 2005, Westerhoff et al. 2005, Snyder et al. 2007, Ridder et al. 2009, Shih and Gschwend 2009, Ridder et al. 2010, Summers et al. 2013). Abraham solvation parameters are typically used to predict partition coefficients in linear free energy relationships (Schwarzenbach et al. 2003, Clarke 2009) but have been used for GAC breakthrough analysis (Reinert 2013). Abraham solvation parameters for all the MPs are shown in the Appendix (Table A.7). Initial MP concentration was not included because it is assumed MPs are in the concentration range where normalized breakthrough (C/C_0) is independent of initial concentration (Gillogly et al. 1998, Knappe et al. 1998, Graham et al. 2000, Matsui et al. 2003, Westerhoff et al. 2005, Rossner et al. 2009, Corwin and Summers 2012). Therefore DOC_0 concentration, log D, S, and V were chosen for a multiple linear regression of the initial first-order model form in Equation 3.2,

$$y = \beta_0 + \beta_1 x_1 + \beta_2 x_2 + \beta_3 x_3 + \beta_4 x_4 + \beta_{12} x_1 x_2 + \beta_{13} x_1 x_3 + \beta_{14} x_1 x_4 + \beta_{23} x_2 x_3 + \beta_{24} x_2 x_4 + \beta_{34} x_3 x_4 \quad (3.2)$$

where y is $BV_{10\%}$, β is the regression coefficient, x_1 is DOC_0 concentration, x_2 is log D, x_3 is S, and x_4 is V. Log D values in the range of -2.66 to 3.03 were obtained from SciFinder® (Chemical Abstracts Service) at the appropriate pH for MPs that are ionic at pH values 6 to 8 (2,4-D (-), clofibric acid (-), erythromycin (+), and warfarin (-)). Abraham parameters were obtained from Advanced Chemistry Development, Inc./Labs with S values ranging from 0.91 to 4.87 and V

values ranging from 1.21 to 5.77. In order to best stabilize the variance, the response (y) was transformed to the natural logarithm of $BV_{10\%}$. Regressions were then run in a stepwise fashion, where in each step the coefficient, β, with the highest p-value above 0.05 was eliminated until all the coefficients were significant at a 95% confidence level. The final regression is shown in Equation 3.3 ($p<0.01$, $R^2=0.83$, $R^2_{adj}=0.80$, $R^2_{pred}=0.67$, n=26).

$$\ln BV_{10\%} = (11.2 \pm 0.2) + (-0.242 \pm 0.052)DOC_0 + (0.138 \pm 0.041)\log D + (-0.305 \pm 0.093)S + (0.157 \pm 0.069)V \quad (3.3)$$

Because the Abraham parameters S and V may not be readily available, the regression in Equation 3.4 was also found to be significant ($p<0.01$, $R^2=0.74$, $R^2_{adj}=0.72$, $R^2_{pred}=0.67$, n=26).

$$\ln BV_{10\%} = (10.9 \pm 0.2) + (-0.227 \pm 0.061)DOC_0 + (0.234 \pm 0.034)\log D \quad (3.4)$$

The residuals versus fitted values plots for Equations 3.3 and 3.4 in Figure 3.6 show random equal variance and normal probability plots confirmed the residuals were normally distributed. β values were all found to be significant with p-values less than 0.05. Equations 3.3 and 3.4 also makes physical sense with respect to MP adsorption: (1) decreased $BV_{10\%}$ with increasing competition from the background matrix measured as DOC concentration, and (2) increased $BV_{10\%}$ with increasing hydrophobicity measured by log D, while S and V are strongly related to the van der Waals forces that define physical adsorption (Crittenden et al. 2012). A sensitivity analysis showing the effect of each parameter while all other parameters are held constant (at their median values) in both regression equations is shown in Table 3.4.

Table 3.4. Sensitivity analysis for predicting $BV_{10\%,full\text{-}scale}$ values from Equation 3.3 and Equation 3.4.

Parameter[a] ($\beta_{Eqn\ 3.3}$, $\beta_{Eqn\ 3.4}$)	Range (median)	$BV_{10\%,full\text{-}scale}$ Range[b]	
		Equation 3.3	Equation 3.4
DOC_0 (-0.242, -0.227)	1.7 to 3.9 (2.1)	44,000 to 25,800	42,400 to 25,700
log D (0.138, 0.234)	-2.66 to 3.03 (0.6)	25,500 to 55,800	18,000 to 68,300
S (-0.305, N/A)	0.91 to 4.87 (1.48)	47,500 to 14,200	N/A
V (0.157, N/A)	1.21 to 5.77 (1.73)	36,800 to 75,300	N/A
Median $BV_{10\%,full\text{-}scale}$:		39,900	38,700

[a]Units: DOC_0 (mg/L), log D (unitless), S (unitless), V (cm^3/mol/100). [b]Bed volume change over variable range while all other parameters are held constant at their median value.

A plot ($p<0.01$, $R^2=0.75$, $R^2_{adj}=0.74$, $R^2_{pred}=0.71$, n=26) of the fitted or predicted $BV_{10\%}$ values versus the observed $BV_{10\%}$ values for Equation 3.3 is shown in Figure 3.7. The same plot ($p<0.01$, $R^2=0.66$, $R^2_{adj}=0.65$, $R^2_{pred}=0.60$, n=26) for Equation 3.4 is shown in Figure 3.8. For visual clarity, the dashed lines represent ±1 month of operation time at a 7 minute EBCT and ±2 months of operation time at a 15 minute EBCT. The 26 values used to create the regression are shown with solids symbols while corresponding MPs in Water B are shown as open symbols for comparison. On average, MPs in Water B (n=7) were predicted within 26% of their observed $BV_{10\%}$ values using Equation 3.3 (29% for Equation 3.4). It would be expected that by using Equation 3.3 and 3.4, all of the MPs in Water B would fall above the 1:1 line in Figure 3.7 (over predicted) because the MPs broke through earlier than expected based on DOC_0 concentration. For Equation 3.4, six of seven fell above the 1:1 line in Figure 3.8. However, for Equation 3.3, only four fell above the 1:1 line in Figure 3.7, indicating the benefits of having S and V in the regression model to reduce the influence of DOC_0 concentration on predictions.

An attempt was made to use Equations 3.3 and 3.4 for predicting all 79 $BV_{10\%}$ values from Table 3.2, but results were unsatisfactory with about a third not predicted within 50%. On

average, several MPs (n=14) from the 4th and 5th bin in Table 3.3 in Waters A (7), B, C, and D were predicted within 21% using Equation 3.3 (20%, n=18 for Equation 3.4). However, beyond about 80,000 bed volumes (13 months for 7 minute EBCT) the relationship strongly deviates towards early predictions. Biodegradation is a likely cause for later than expected breakthrough as many of the MPs that broke through in this range have slow to fast biodegradation rates. The 14 or 18 values predicted within 21 and 20%, respectively, are also shown in Figure 3.7 or Figure 3.8, respectively.

EBCT was not included in the regression development due to limited data, although Table 3.2 shows doubling the EBCT resulted in approximately 52% later breakthrough on average on a normalized basis. Therefore predicted $BV_{10\%}$ values for Water A (15) using Equations 3.3 and 3.4 were multiplied by a factor of 1.52 according to Table 3.2. MPs in Water A (15) are shown in Figure 3.7 and Figure 3.8 with open symbols for comparison. On average MPs in Water A (15) were predicted within 1% of their observed $BV_{10\%}$ using Equation 3.3 (8% for Equation 3.4).

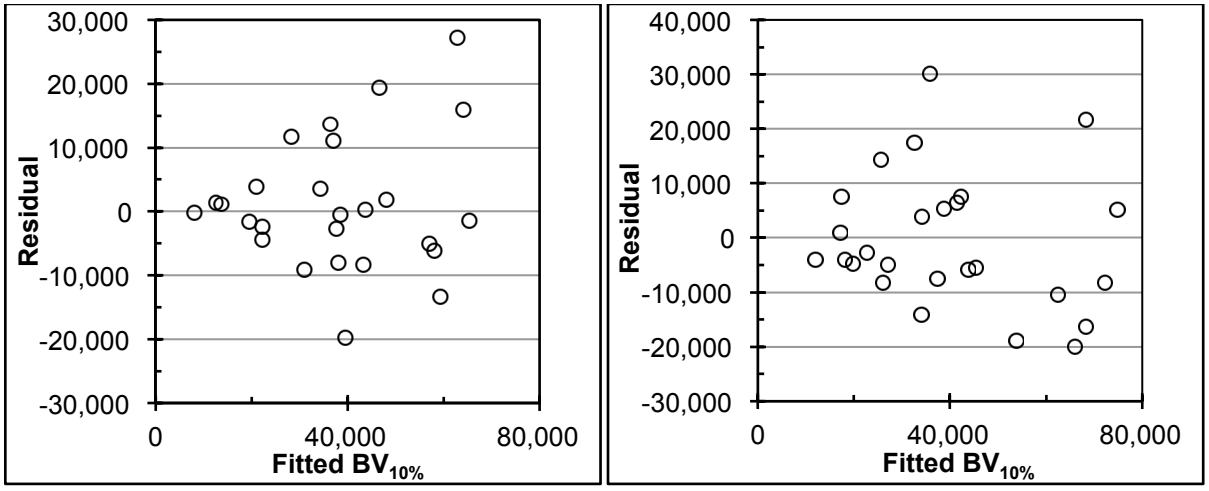

Figure 3.6. Residuals versus fitted values plot for Equation 3.3 (left) and Equation 3.4 (right) after transforming back to an arithmetic scale (n=26 for both equations).

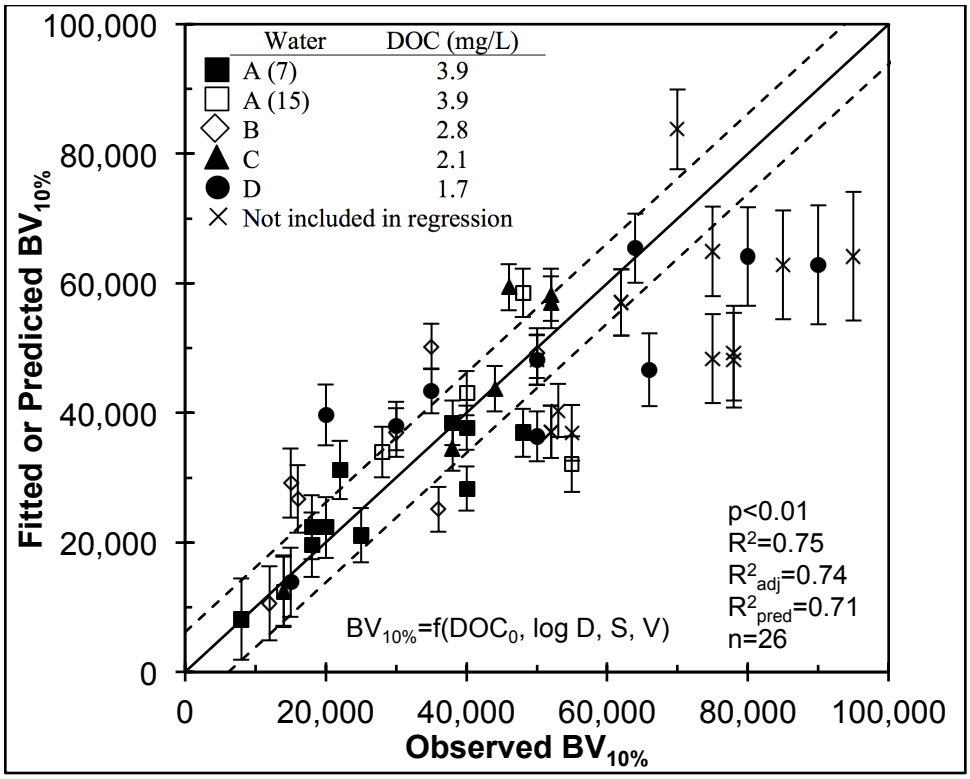

Figure 3.7. Fitted or predicted $BV_{10\%}$ values versus observed $BV_{10\%}$ values with 95% confidence intervals (based on the regression standard error of 8,423 bed volumes) for all waters and EBCTs using Equation 3.3. Solid line is 1:1 line. Dashed line is ±1 month of operation time at a 7 minute EBCT and ±2 months of operation time at a 15 minute EBCT. Solids symbols were used to create the regression (n=26) and open symbols are shown for comparison: Water B (n=7), Water A (15) (n=5). X's (n=14) are MPs from all waters that were also not included in the regression but predicted within 21% on average.

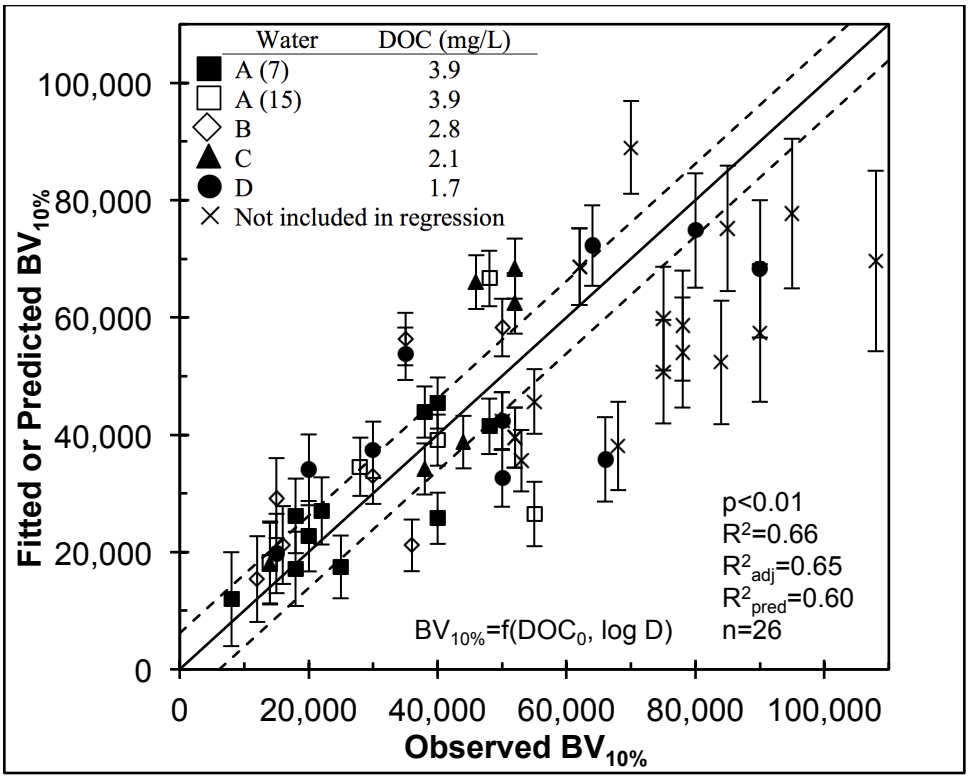

Figure 3.8. Fitted or predicted $BV_{10\%}$ values versus observed $BV_{10\%}$ values with 95% confidence intervals (based on the regression standard error of 10,782 bed volumes) for all waters and EBCTs using Equation 3.4. Solid line is 1:1 line. Dashed line is ±1 month of operation time at a 7 minute EBCT and ±2 months of operation time at a 15 minute EBCT. Solids symbols were used to create the regression (n=26) and open symbols are shown for comparison: Water B (n=7), Water A (15) (n=5). X's (n=18) are MPs from all waters that were also not included in the regression but predicted within 20% on average.

3.3.7 Effect of Impacted Waters

Influent and effluent samples from one of 10 full-scale GAC adsorbers at GCWW (Water E) designed for a 15 minute EBCT were analyzed for 18 MPs over a period of nine months. Fourteen of these 18 MPs were from the list in Table 3.2 and four (bupropion, lamotrigine, metoprolol, and sucralose) were compounds not evaluated in the spiked pilot studies of Waters A, B, C and D. The total estimated MP concentration in the full-scale adsorber influent for Water E averaged 980±50 ng/L (n=4, see Appendix Table A.6). Only six of the MPs regularly appeared

in the GAC effluent over the nine-month study and their breakthrough curves are shown in Figure 3.9.

GCWW normally replaces the GAC after 15,000 bed volumes or complete DOC breakthrough, so these compounds do not normally appear in the finished water. The other GAC adsorbers were regularly replaced during the study. Effluent concentrations were normalized to the average influent concentration over the course of the year to better illustrate the attenuation properties of GAC and provide more meaningful breakthrough curves from limited data.

Sucralose is found in high concentrations (μg/L) in wastewater streams and has been shown to be resistant to treatment via biodegradation, ultraviolet light, ozone, and chlorine but amenable to removal by activated carbon (Scheurer et al. 2010, Torres et al. 2011). Similar to iopromide or related MPs (i.e. iopamidol), sucralose may be useful as a conservative tracer for GAC removal of other common MPs beyond the breakthrough of DOC. Based on the work by Scheurer et al. (2010), the artificial sweetener cyclamate may also be useful as a conservative tracer as it is less adsorbable than sucralose. However the same study shows cyclamate to be relatively biodegradable as well.

Further inspection of Figure 3.9 compared to the $BV_{10\%}$ values for Water A (15) in Table 3.2 shows faster MP breakthrough in Water E. MPs in the Water E appear in the GAC effluent in the throughput range of Water A (7). The $BV_{10\%}$ value for cotinine in Water A (15) is 28,000 while the $BV_{10\%}$ value for cotinine in Water E is 12,500, a factor of about two in faster breakthrough. Similarly, a factor of about three was found for the herbicide prometon. This does not follow the general trend found in Table 3.2, considering the DOC_0 concentration in Water E is about half that of Water A (15). Integration of the DOC breakthrough curves to 70% breakthrough found 24 mg DOC/g GAC and 46 mg DOC/g GAC for Water E and Water A (15),

respectively. Thus, even at a lower overall DOM loading, the MPs in Water E broke through much earlier than expected based on MP breakthrough in Water A (15).

The relatively large over prediction of $BV_{10\%}$ values is not thought to originate solely from the reactivated GAC. Fotta (2012) recently showed similar performance between reactivated and virgin bituminous GAC for the adsorption of several VOCs. However, thermal reactivation of GAC has been shown to reduce micropore (d_{pore}<20 Å) volume and increase mesopore volume (20 Å<d_{pore}<500 Å), which would decrease capacity for MPs and increase capacity for DOC removal (Sontheimer et al. 1988, Moore et al. 2003).

Mainly, the discrepancy is thought to originate from the source water quality, as the Ohio River is impacted by agricultural, industrial, and wastewater inputs. From an adsorption perspective, these inputs are very different from naturally occurring DOM and represent a very competitive component to target MP adsorption that can cause earlier breakthrough for all MPs (Graham et al. 2000). These compounds, many of which are most likely small microbial by-products from wastewater, would have access to the same micropores as target MPs (similar to previous discussion concerning ozone oxidation in Section 3.3.3). Conversely, Waters A, B, C, and D used for the pilot columns in this study all originated from minimally (not wastewater) impacted sources, and all the MPs were artificially spiked in the lab to a total concentration of 8.1±2.7 μg/L (<0.5% of all influent DOC concentrations).

Predicted and observed $BV_{10\%}$ values for MPs in Water E using Equation 3.3 are shown in Table 3.5. Estimates for Water E (multiplied by a factor 1.52 for 15 minute EBCT based on Table 3.2) consistently predicted later breakthrough, which was expected as the regression was created with data from non-wastewater impacted waters. On average, Equation 3.3 over predicted MP breakthrough by a factor of 3.7±1.7 (n=6, 4.0±1.9 for Equation 3.4). With

additional full-scale data, this approach of lowering $BV_{10\%}$ values may be appropriate for use in wastewater-impacted waters using virgin and reactivated 12x40 bituminous-based GAC. Since the MP breakthrough for Water E was in the range of Water A (7), the $BV_{10\%}$ prediction using Equation 3.1 (from iopromide in Waters A (7), B, C, D) is also shown in Figure 3.9 and provides a good estimate for early breakthrough of common MPs.

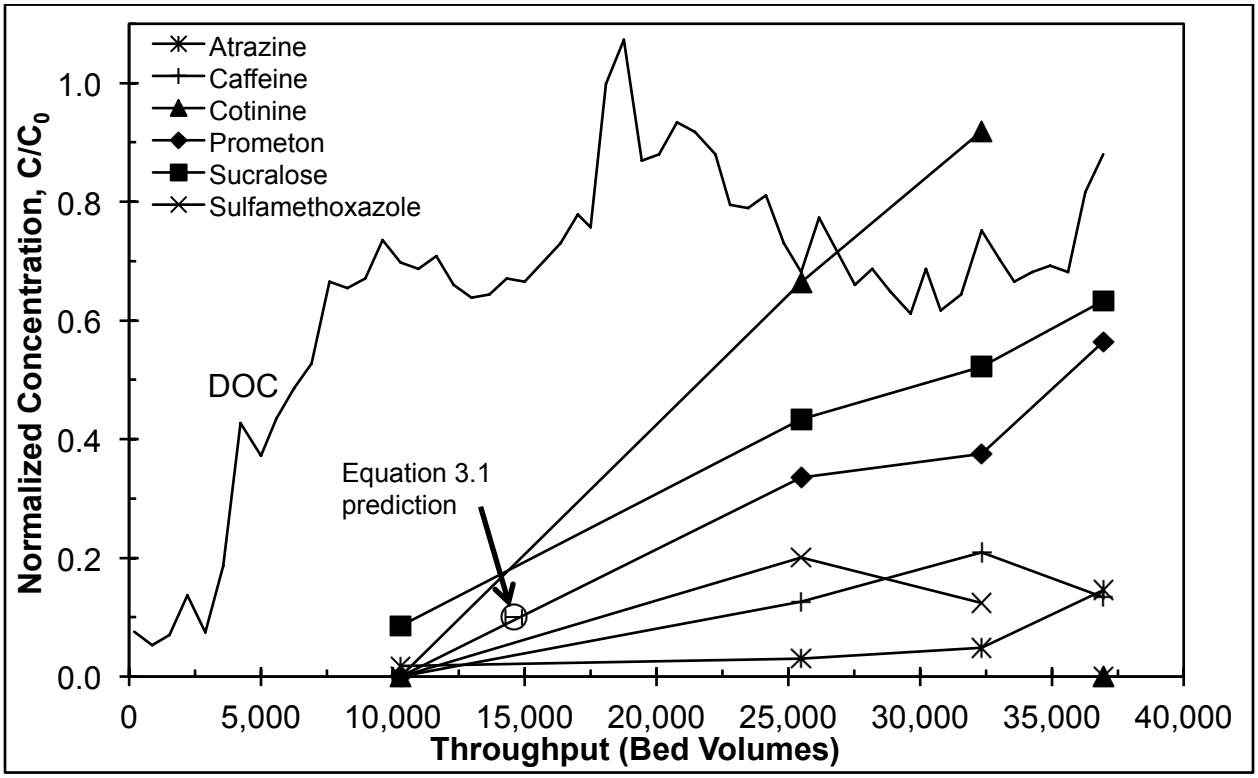

Figure 3.9. Full-scale breakthrough for caffeine (C_0~41±21 ng/L, MRL~5 ng/L), cotinine (C_0~7.1±0.7 ng/L, MRL~5 ng/L), prometon (C_0~7.5±5.1 ng/L, MRL~1 ng/L), sucralose (C_0~420±250 ng/L, MRL~15 ng/L), and sulfamethoxazole (C_0~39±11 ng/L, MRL~5 ng/L) in Water E (DOC_0=1.9 mg/L, reactivated 12x40 mesh GAC, EBCT=15 minutes). The last data point for cotinine and sulfamethoxazole were below detection.

Table 3.5. Comparison of observed and predicted (using Equation 3.3) $BV_{10\%}$ values from MPs in two surface water sources using bituminous-based GAC: Water E and water from Chowdhury et al. (2010). For Equation 3.3, $BV_{10\%}$=f(DOC_0, log D, S, and V).

System Description	Micropollutant	Observed	Predicted[a]	Pred/Obs
Water E (Ohio River) DOC_0=1.9 mg/L EBCT=15 minutes pH=7.8 12x40 mesh (d_p=0.92 mm) Postfilter adsorber 980±50 ng/L MPs	Atrazine	35,000	91,192	2.6
	Caffeine	22,000	47,141	2.1
	Cotinine	12,500	55,111	4.4
	Prometon	15,000	94,933	6.3
	Sulfamethoxazole	18,000	38,381	2.1
	Sucralose	11,000	52,527	4.8
			Over Prediction Average:	3.7
			Over Prediction Standard Deviation:	1.7
Cahaba River (AL) DOC_0=2.1 mg/L EBCT=7 minutes pH=7.3 8x20 mesh (d_p=1.47 mm) Filter adsorber 800±722 ng/L MPs	Atrazine	22,000	57,160	2.6
	DEET	22,000	51,081	2.3
	Deethylatrazine	40,000	43,367	1.1
	Deisopropylatrazine	38,000	41,140	1.1
	Prometon	20,000	59,505	3.0
	Simazine	25,000	52,723	2.1
			Over Prediction Average:	2.0
			Over Prediction Standard Deviation:	0.8

[a]Standard error=8,423 bed volumes.

3.3.8 Effect of GAC Particle Size

Breakthrough data with water from the Cahaba River was also obtained for six MPs, mainly herbicides and triazine metabolites, from Chowdhury et al. (2010) at a 7 minute EBCT. The filter adsorber used a bituminous-based 8x20 mesh (d_p=1.47 mm) GAC. Comparisons between predicted and observed $BV_{10\%}$ values using Equation 3.3 are also shown in Table 3.5. Again, the predictions overestimated $BV_{10\%}$ values by a factor of 2.0±0.8 (n=6, 2.2±0.9 for Equation 3.4). Here the difference is thought to originate from both GAC particle size and agricultural impacts (pesticides). Total measured MP concentrations from the influent of the adsorber in Chowdhury et al. (2010) averaged 800±722 ng/L.

As mentioned previously larger GAC particles result in slower adsorption kinetics, which would cause earlier MP breakthrough at 10%. In general, adsorption kinetics are inversely proportional to GAC particle size (Sontheimer et al. 1988). Assuming 8x20 and 12x40 have the same equilibrium adsorption capacity (Kim 2006) and with all other parameters held constant, the PSDM was used to model breakthrough for five MPs in Water A (7) (with >50% breakthrough, same as for Section 3.3.4) at the GAC particle sizes of 0.92 and 1.47 mm. On average, the 8x20 GAC resulted in earlier breakthrough at 10% compared to 12x40 GAC by a factor of 1.8±0.4 (n=5), suggesting the over predictions using Equations 3.3 and 3.4 are more related to differences in particle size than the presence of pesticides. The difference also increased with increasing adsorbability (factor of 1.5 for iopromide and 2.4 for prometon). Hence, reducing predictions using Equations 3.3 and 3.4 by a factor of 1.8±0.4 for 8x20 GAC may be appropriate in the absence of full-scale data.

The same approach was applied to Water B (8x30 GAC) because the predictions overestimated $BV_{10\%}$ values by an average factor of 1.3±0.4 (n=7) using both equations. On average, the 8x30 GAC resulted in earlier breakthrough at 10% compared to 12x40 GAC by a factor of 1.5±0.2 (n=5), suggesting the over predictions using Equations 3.3 and 3.4 and the earlier-than-expected breakthrough are more related to differences in particle size than the ozonated DOM discussion in Section 3.3.3. Again, reducing predictions using Equations 3.3 and 3.4 by a factor of 1.5±0.2 for 8x30 GAC may be appropriate in the absence of full-scale data.

In general, for cases with highly impacted waters and/or different GAC particle sizes, careful attention should be paid to the limits of Equations 3.2 and 3.3 because they were created using a narrow range of parameters previously listed (see Section 3.3.6).

3.4 Conclusions

Iopromide, the most weakly adsorbing compound of those studied, broke through after at least 50% DOC breakthrough at EBCTs of 7 and 15 minutes. For the majority of the MPs, the longer EBCT yielded lower CURs at high levels of removal. However, it can be difficult to distinguish between the removal mechanisms of adsorption from biodegradation.

For the tests with coagulated DOM and the same GAC, more MPs broke through as the influent DOC concentration increased and on average a higher DOC concentration caused earlier MP breakthrough. Ozonated DOM resulted in earlier breakthrough than expected; possibly due to increased competition from an overall smaller molecular size DOM, but most likely because the run utilized a larger GAC particle size.

A significant predictive relationship for $BV_{10\%}$ values for MPs that exhibited breakthrough within reasonable adsorber operation times was presented based on compound and system properties. When compared to MP breakthrough in a highly impacted water, the regression over predicted $BV_{10\%}$ values by a factor of 3.7±1.7. Comparison to MP breakthrough in another impacted water showed an over prediction of 2.0±0.8, most likely caused by the difference in GAC particle size.

Chapter 4
Using the Proportional Diffusivity Design of the Rapid Small-Scale Column Test to Predict Full-Scale GAC Adsorption of Organic Micropollutants

4.1 Introduction

Recent advances in analytical techniques have led to a large number of trace organic contaminants or micropollutants (MPs) being detected in drinking water sources as well as finished drinking waters worldwide (Kolpin et al. 2002, Stackelberg et al. 2004, Batt et al. 2007, Donald et al. 2007, Kim et al. 2007, Barnes et al. 2008, Focazio et al. 2008, Benotti et al. 2009, Loos et al. 2009). MPs are typically present below low parts per billion (μg/L) levels, well below the maximum contaminant level (MCL), if one exists. Some of these compounds are known or suspected endocrine disrupting compounds (Snyder et al. 2003, Benotti et al. 2009) and pose potential risks to public health even at these trace levels (Pomati et al. 2006, Schwarzenbach et al. 2006). Thus, they are commonly referred to as contaminants of emerging concern.

Granular activated carbon (GAC) has potential for the control of MPs, as conventional water treatment does not effectively reduce the concentrations of many common MPs (Ternes et al. 2002, Westerhoff et al. 2005, Stackelberg et al. 2007), but predicting their removal in full-scale adsorbers has been difficult using models and bench-scale techniques. From a design perspective, GAC adsorption predictions are a valuable tool over running full-scale pilot studies, which can be expensive, time consuming, and require large amounts of water. A bench-scale test known as the rapid small-scale column test (RSSCT) was developed for predicting full-scale adsorber breakthrough without the need for numerical models and extensive isotherm or kinetic studies (Crittenden et al. 1986a, Crittenden et al. 1987). A full-scale adsorber is scaled down to the RSSCT by utilizing a smaller GAC particle size (typically 5 to 10 times smaller) and key relationships developed from dimensional analysis of the dispersed-flow pore and surface

diffusion model (Crittenden et al. 1986b). These relationships assume GAC characteristics (particle porosity, bed porosity, bed density, etc.) remain constant from the large GAC particle to the crushed GAC particle and the target organic and any competing compounds can be modeled by the same scaling equations (Crittenden et al. 1991). GAC adsorber design parameters such as bed life, carbon type, filter residence time or empty bed contact time (EBCT), and operation in parallel or series can be tested directly using the RSSCT.

However, in the presence of background dissolved organic matter (DOM), predicting MP removal using the RSSCT has been inconsistent and unreliable (Speth and Miltner 1989, Summers et al. 1989, Crittenden et al. 1991, Knappe et al. 1997, Corwin and Summers 2010). DOM fouls the surface of the carbon because it is irreversibly adsorbed (Summers and Roberts 1988a), permanently reducing its capacity for MPs through direct competition and pore blockage. The reduction in adsorption capacity and kinetics is termed fouling. Capacity reductions from fouling are magnified when there is a large disparity between the respective concentrations of the MP and DOM because of the inability for the MP to compete for a limited number of adsorption sites (Sontheimer et al. 1988, Najm et al. 1991, Corwin and Summers 2010). Fouling has been shown to be particle size dependent, where larger GAC particles experience more fouling because they are more subject to capacity reductions from pore blockage (Corwin and Summers 2010). Fouling is also is not scalable using the current RSSCT design equations resulting in RSSCT predictions that consistently exhibit more adsorption capacity than the full-scale (Summers et al. 1989, Crittenden et al. 1991, Corwin and Summers 2010). Additionally, fouling affects adsorption kinetics (Hand et al. 1989, Li 2003, Li et al. 2003), complicating scale-up because of mass transfer assumptions made in the RSSCT design equations.

Currently there are two common RSSCT designs, each making a different assumption

about intraparticle mass transfer or adsorbate diffusivity within the activated carbon pores. The base design is termed constant diffusivity (CD-RSSCT) and assumes intraparticle diffusivity is independent of GAC particle size. The other design, termed proportional diffusivity (PD-RSSCT), assumes intraparticle diffusivity decreases linearly with particle size. There has been some success in using both designs for target organics in the presence of DOM (Crittenden et al. 1987, Vidic et al. 1992, Cerminara et al. 1995, Knappe et al. 1997), but in general the CD-RSSCT was accepted because of its consistent predictions of early breakthrough (Summers et al. 1989, Crittenden et al. 1991, Knappe et al. 1997).

An RSSCT is designed using Equation 4.1, where SC and LC denote small column and large column, respectively, EBCT is the empty bed contact time, d_p is the diameter of the GAC particle, and X is the diffusivity factor. X is defined in Equation 4.2, where D is the diffusion coefficient describing intraparticle diffusivity, either surface or pore. For the CD-RSSCT X=0 and for the PD-RSSCT X=1.

$$\frac{EBCT_{SC}}{EBCT_{LC}} = \left(\frac{d_{p,SC}}{d_{p,LC}} \right)^{2-X} \tag{4.1}$$

$$\frac{D_{SC}}{D_{LC}} = \left(\frac{d_{p,SC}}{d_{p,LC}} \right)^{X} \tag{4.2}$$

Recent work by Corwin and Summers (2010) has made the RSSCT more useful by developing a method for adjusting RSSCT breakthrough data to match full-scale data using the scaling factor (SF). The SF is the ratio of the $d_{p,LC}$ to $d_{p,SC}$ and was used by Corwin and Summers (2010) to establish the fouling index (FI), shown in Equation 4.3.

$$FI = SF^{Y} = \left(\frac{d_{p,LC}}{d_{p,SC}} \right)^{Y} \tag{4.3}$$

In this way a fouling term can be defined as a function of GAC particle size and varies with different values of the fouling factor, Y, similar to the way X allows variability in the relationship shown in Equation 4.2. The FI is also independent of the RSSCT scaling Equation 4.1. RSSCT breakthrough profiles typically occur after the full-scale; therefore the RSSCT throughput (i.e. bed volumes) can be normalized by the FI to match full-scale performance for adsorption capacity, shown in Equation 4.4. An example of this procedure is shown in Figure 4.1 for the nicotine metabolite cotinine in Water A from this study at a full-scale EBCT of 7 minutes.

$$\text{Throughput}_{LC} = \frac{\text{Throughput}_{SC}}{FI} \tag{4.4}$$

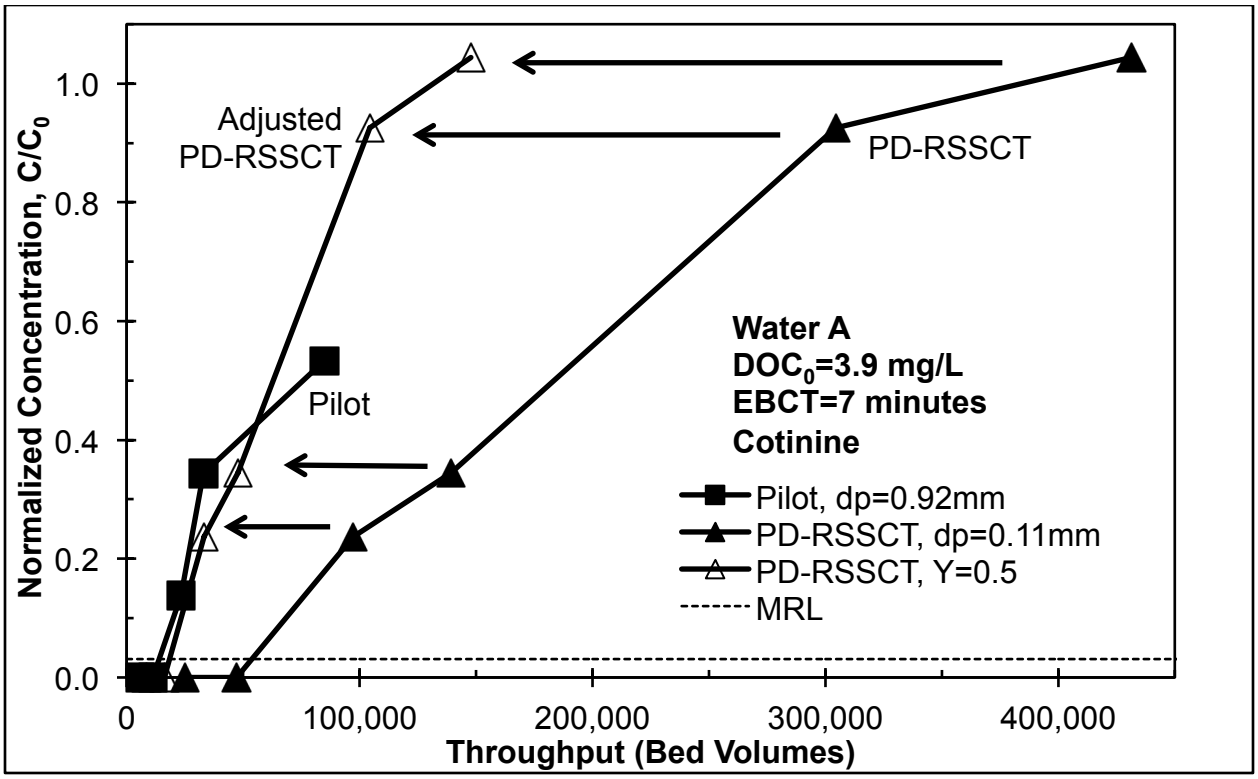

Figure 4.1. Example of visual Y-fitting for cotinine breakthrough profiles in Water A (7) ($DOC_{0,pilot}$= $DOC_{0,PD\text{-}RSSCT}$=3.9 mg/L, EBCT=7 minutes, 12x40 bituminous GAC). For Y=0.5 and SF=8.5 ($d_{p,LC}$=0.92mm, $d_{p,SC}$=0.11mm), FI=2.9. MRL: method reporting limit. The last two data points in the pilot column were averaged.

Using the PD-RSSCT and equilibrium studies, Corwin and Summers (2010) found a range for Y between 0.6 to 0.8 for six MPs. A higher value of Y represents more fouling and a lower value of Y represents less fouling. If an RSSCT were to match full-scale adsorption capacity perfectly, Y would be equal to zero. Their work also suggested an inverse relationship between Y and the influent concentration of the MP (C_0) relative to the influent background DOM concentration measured by dissolved organic carbon (DOC_0).

The primary goal of this chapter was to make the RSSCT, specifically the PD-RSSCT, a more useful design tool for engineers and utilities with savings in cost, time, and water. Using many MPs, the objectives of this study were to extend the FI based scale-up approach and develop predictive relationships for Y and other factors related to scale-up.

4.2 Materials and Methods

4.2.1 Materials

4.2.1.1 Waters

The influent water quality for the five surface waters (Waters A, B, C, and D) used to run GAC pilot columns (from Chapter 3) and a full-scale site (Water E from Chapter 3) and corresponding PD-RSSCTs are shown in Table 4.1. Waters A and B were made by spiking reverse osmosis (RO) membrane isolated DOM into pretreated tap water. City of Boulder, CO tap water was first passed through a 200 L barrel of bituminous-based GAC (Norit 1240) to remove chlorine, DOM, and disinfection by-products (DBPs) that may have interfered with MP adsorption. Periodic DBP samples taken throughout the entirety of the study confirmed no detectable DBPs in the effluent of the pretreatment GAC system. DBPs were analyzed using an Agilent 6890 Series gas chromatography (GC) system in accordance with USEPA Methods 551.1 and 552.2 (USEPA 1995b).

The DOM was isolated using a low-pressure RO system (Dow FILMTEC LE-4040) from a high organic content and low alkalinity surface water source at Big Elk Meadows (BEM), CO. Alum coagulation (~100 mg/L) of the BEM-DOM extract removed 10 to 20% of the dissolved organic carbon (DOC) followed by filtration through a 0.45 μm cartridge filter (Memtrex MNY941CGS). Water A utilized this coagulated DOM extract, while Water B utilized ozonated BEM-DOM at a ratio of 1:1 mg O_3/mg DOC.

Water C was coagulated, settled, and filtered (5 μm filter cartridge, Whirlpool WHCF-GD05) water from the Orange Water and Sewer Authority (OWASA, Carrboro, NC) and was derived from two North Carolina reservoir sources (Cane Creek Reservoir and University Lake). Water D was conventionally treated combined filter effluent water from the City of Longmont (LM), CO, derived from the St. Vrain Creek and Colorado-Big Thompson Project sources.

In addition, data was also gathered from the full-scale GAC system at the Greater Cincinnati Water Works (GCWW) Richard Miller drinking water treatment plant. GCWW uses full-scale GAC adsorbers to treat water from the Ohio River following alum coagulation, sedimentation, and filtration (biologically active). Water from GCWW was termed Water E and used solely for scale-up verification.

The water quality between the pilot columns and PD-RSSCTs was slightly different as all the water needed for the PD-RSSCTs was collected (or made) in small batches, representing a snapshot in time. The pilot columns used significantly more water (~39 times more) and were therefore subject to seasonal fluctuation in water quality or differences from feed batch preparations.

Table 4.1. Average influent water quality parameters for pilot columns/full-scale and corresponding PD-RSSCTs.

Water	Source	Scale	pH	DOC (mg/L)	UVA_{254} (cm^{-1})	$SUVA_{254}$ (L/mg/m)
A	Coagulated BEM	Pilot	7.0	3.9±0.4	0.098±0.012	2.5
		PD-RSSCT	7.0	3.9±0.4	0.097±0.012	2.5
B	Ozonated BEM	Pilot	7.7	2.8±0.3	0.044±0.007	1.6
		PD-RSSCT	7.0	2.4±0.3	0.040±0.005	1.7
C	OWASA	Pilot	6.0	2.1±0.4	0.027±0.005	1.3
		PD-RSSCT	6.0	1.6±0.4	0.025±0.006	1.5
D	LM	Pilot	6.2	1.7±0.3	0.024±0.006	1.4
		PD-RSSCT	7.0	1.4±0.1	0.018±0.001	1.3
E	GCWW	Full	7.8	1.9±0.3	0.043±0.012	2.3
		PD-RSSCT	7.8	2.0±0.2	0.043±0.001	2.2

4.2.1.2 Adsorbents

All of the pilot columns and PD-RSSCTs were run with virgin bituminous-based GAC, which is common in drinking water treatment for controlling DOM and MPs (Summers et al. 2011). GAC in the pilot columns with Waters A, C, and D was Norit 1240 with a log-mean

particle diameter of 0.92 mm (12x40 US standard mesh) and bed density of 450 kg/m^3. GAC in the pilot column run with Water B was Calgon F300 with a log-mean particle diameter of 1.29 mm (8x30 US standard mesh) and bed density of 480 kg/m^3. GAC in the full-scale system (Water E) was freshly reactivated bituminous-based GAC with a log-mean particle diameter of 0.92 mm (12x40 US standard mesh) and bed density of 490 kg/m^3. All PD-RSSCTs were run with the corresponding ground GAC with a log-mean particle diameter of 0.11 mm (100x200 US standard mesh).

4.2.1.3 Adsorbates

A total of 29 environmentally relevant MPs including pharmaceuticals, personal care products, herbicides, insecticides, and a manufacturing additive were chosen from occurrence studies of surface drinking water sources (Kolpin et al. 2002, Focazio et al. 2008). These 29 MPs were also spiked into Water E PD-RSSCT influent, but four additional MPs were already present in the water (bupropion, lamotrigine, metoprolol, and sucralose). MPs covered a wide range of sources, hydrophobicities, ionic states, and molecular weights. Target MP influent concentrations were based on the median concentrations from the same studies, detection limits, and a goal to be able to detect the onset of breakthrough at effluent concentrations that corresponded to 2.5 to 10% of the influent concentration. All MPs were purchased from Sigma-Aldrich (St. Louis, MO), with three exceptions. 2,4-D was purchased from Acros Organics (New Jersey, US), iopromide was purchased from US Pharmacopa (Rockvill, MD), and simazine was purchased from Alfa Aesar (Ward Hill, MA).

The total MP concentration in the pilot columns and PD-RSSCT influents for Waters A, B, C, and D averaged 8.1±2.7 µg/L (n=6, see Table 2.1), which is less than 0.5% of the any influent DOC concentration. The total MP concentration in the PD-RSSCT influent for Water E

averaged 4.6±2.1 µg/L (see n=6, see Appendix Table A.14) because the water was also spiked with same MPs of Water A, B, C, and D tests. The total MP concentration in the full-scale adsorber influent for Water E averaged 980±50 ng/L (n=4, see Appendix Table A.6). Both of these total MP concentrations for Water E were less than 0.3% of the influent DOC concentrations, although there were likely more MPs present that were not analyzed for by high performance liquid chromatography-tandem mass spectrometry (LC/MS-MS).

4.2.2 Methods

4.2.2.1 Analytical Methods

4.2.2.1.1 Micropollutant Analysis

The analysis of MPs was conducted using LC/MS-MS at the Center for Mass Spectrometry at the University of Colorado at Boulder. The mass spectrometry analyses allowed for the separation of all the analytes in the water extracts using an HPLC system (Agilent Series 1290), consisting of vacuum degasser, autosampler, and a binary pump, equipped with a reversed phase C18 analytical column of 50 mm x 2.1 mm and 1.8 µm particle size (Zorbax Eclipse Plus). The HPLC system was connected to a triple quadrupole mass spectrometer Agilent 6460 that was equipped with electrospray Jet Stream technology, which could operate in positive and negative ion mode.

MP results from the LC/MS-MS analysis were given as relative concentration (C/C_0) based on analyte area ratios of the paired effluent and influent samples. Pilot column and PD-RSSCT influent concentrations (Waters A, B, C, and D) as well as influent and effluent concentrations in Water E were estimated from an internal standard (carbamazepine, 100 ng/L). Water samples were collected in muffled 250 mL amber glass bottles, stored at 4°C, and extracted within one week before quantification. The relative standard deviation for all the MP

analysis was less than 11% (Ferrer et al. 2010).

Results in this chapter are shown as the effluent concentration normalized by the influent concentration versus throughput as bed volumes (volume of water treated divided by the volume of the bed or operating time divided by the EBCT). MP breakthrough results are presented in this manner because when the background DOM concentration (measured as DOC) is sufficiently high and the MP concentration is in the ng/L to low μg/L range, normalized MP breakthrough (C/C_0) is independent of initial concentration (Gillogly et al. 1998, Graham et al. 2000, Knappe et al. 1998, Matsui et al. 2003, Westerhoff et al. 2005, Rossner et al. 2009, Corwin and Summers 2012). Normalized throughput is also useful because it is directly related to carbon use rate (CUR), the main factor for determining GAC adsorber capital and operation costs. An increase in throughput to a target breakthrough corresponds to a lower (better) CUR.

4.2.2.1.2 Dissolved Organic Carbon, Ultraviolet Absorbance, and pH

Dissolved organic carbon (DOC) was measured with a Sievers 800 TOC analyzer in accordance with Standard Method 5310C (APHA et al. 2005). Ultraviolet absorbance (UVA_{254}) was analyzed at a wavelength of 253.7 nm using a Hach DR 4000 spectrophotometer in accordance with Standard Method 5910 (APHA et al. 2005). pH was measured using a Denver Instruments Model 220 pH meter in accordance with Standard Method 4500-H^+ (APHA et al. 2005).

4.2.2.2 Pilot Column Design and Operation

Operational parameters for the pilot columns and full-scale adsorber (from Chapter 3) are shown in Table 4.2. Pilot columns were 2.54 cm ID glass chromatography columns with PTFE adapters operated at a hydraulic loading rate (HLR) of 5 m/h, which resulted in a flow rate of 42 mL/min. A HLR of 5 m/h is at the lower end of typical rates, but was chosen to limit the amount

of water required. In this range, intraparticle mass transfer still controls adsorption kinetics (Corwin 2010). The aspect ratios for the columns were 27 (12x40 mesh) and 19 (8x30 mesh), which is greater than the 8 to 10 necessary to avoid wall effects on mass transfer (Knappe et al. 1999). Prior to the start of pilot testing the GAC was backwashed with dechlorinated and organics-free water to remove carbon fines.

Water A was run at two the EBCTs of 7 and 15 minutes (Water A (7) and Water A (15) respectively), which was accomplished with a 7 minute column followed by an 8 minute column. Water B was run at an EBCT of 7.5 minutes. Pilot studies for Waters A and B were run in the lab at the University of Colorado where the influent batches were prepared approximately every three days. Waters C and D were run at EBCTs of 7 minutes at their respective treatment plants where influent batches were prepared weekly.

Influent water was spiked with all 29 MPs at initial concentrations ranging from 3 ng/L to 3 μg/L. Water was fed to the columns from well-mixed 200 L HDPE barrels through PVC, stainless steel, and PTFE tubing using a Cole-Parmer PTFE diaphragm pump. Concentrated MP stock solutions (0.1 to 5 mg/L) were stored at 4°C and remade every 6 months. Pilot column effluent water was treated in a secondary GAC barrel before being discharged to a drain.

Paired influent and effluent MP samples were collected immediately before and after the pilot columns. A needle valve was used for flow control to maintain the desired EBCT during sampling. Pilot column influent and effluent DOC and UVA_{254} samples were taken biweekly at the beginning of the run. After complete DOC breakthrough, UVA_{254} was used for measurements of DOM. Strong relationships were observed between DOC and UVA_{254} ($R^2 \geq 0.95$) for all waters.

At the full-scale Water E was sampled following biological filtration and from the effluent of the single adsorber with freshly reactivated GAC. The GAC adsorbers at GCWW are variable rate contactors and were designed for a HLR of 14 m/h and 15 minute EBCT but typically operate at a HLR of about 18 m/h and a 12 minute EBCT. A total of four paired influent and effluent samples were taken over the course of nine months from August 2011 to May 2012.

4.2.2.3 Rapid Small-Scale Column Test Design and Operation

Operational parameters for the PD-RSSCTs are shown in Table 4.2. All RSSCTs were designed according the PD approach to simulate full-scale EBCTs of 7, 7.5, and 15 minutes. The PD-RSSCT design was selected for several reasons. PD-RSSCTs have been shown to result in more accurate simulations of full-scale DOC breakthrough (Crittenden et al. 1991, Summers et al. 1995, USEPA 1996). The findings of Corwin and Summers (2010) also showed that MP removal kinetics matched well for the PD-RSSCT design after adjustments using the FI. In the presence of DOM, MP adsorption under typical GAC adsorber operating conditions results in pore diffusion Biot numbers greater than 30 (Hand et al. 1984, Corwin 2010). If MP diffusivities are nonconstant with changing GAC particle size and intraparticle mass transfer controls adsorption kinetics, the constant diffusivity design cannot be expected to yield good simulations of full-scale MP breakthrough (Crittenden et al. 1991).

Fresh bituminous GAC was carefully ground using a mortar and pestle while minimizing the production of fines. The 100x200 mesh size fraction was obtained using US standard sieves and a sieve shaker. Prior to use the carbon was rinsed with deionized water (Barnstead Nanopure) to remove fines, dried at 105°C, and stored in amber glass vials in a desiccator. Crushed GAC was then placed in 4.76 mm ID PTFE columns based on a small-scale HLR of 6.7

m/h and flow rate of 2 mL/min. The aspect ratios for the columns were 43 (100x200 mesh), which is greater than the 8 to 10 necessary to avoid wall effects on mass transfer (Knappe et al. 1999). Spiked influent water was fed to the columns from well-mixed 20 L glass carboys through the same setup as the pilot columns. Sampling and column discharge followed the same procedure as the pilot columns.

PD-RSSCTs were performed in the laboratories at the University of Colorado at Boulder and North Carolina State University. Except for Waters A and B, which were made in batches, all water for the PD-RSSCTs was collected in 200 L HDPE barrels and stored at 4°C until use.

Table 4.2. Operational parameters for the pilot columns/full-scale and PD-RSSCTs for all waters.

	Pilot/Full-Scale[a]			PD-RSSCT		
Parameter	Waters A, C, D, E		Water B	Waters A, C, D, E		Water B
EBCT (min)	7	15[b]	7.5	0.82	1.8[b]	0.63
GAC Mesh Size	12x40	12x40	8x30	100x200	100x200	100x200
d_p[c] (mm)	0.92	0.92	1.29	0.11	0.11	0.11
d_{column}[d] (mm)	25.4	25.4	25.4	4.76	4.76	4.76
l_{bed}[e] (cm)	58	125	63	9.3	19.8	7.1
HLR (m/h)	5	5	5	6.7	6.7	6.7
M_{GAC}[f] (g)	132	285	152	0.74	1.6[g]	0.61

[a]Water E at the full-scale: A_{bed}=181 m^2, l_{bed}=3.5 m, HLR=14 m/h, M_{GAC}=3.1x10^5 kg. [b]Water A was evaluated at EBCTs of 7 and 15 minutes and Water E was evaluated at an EBCT of 15 minutes. [c]Log-mean GAC particle diameter. [d]Pilot column diameter. [e]Pilot column bed length. [f]Mass of GAC in pilot column. [g]1.7 g for Water E PD-RSSCT.

4.3 Results and Discussion

4.3.1 Dissolved Organic Carbon Breakthrough

DOM solids loading was evaluated at 60 to 70% DOC breakthrough because this is near exhaustion and represents the majority of adsorbed DOM (Zachman and Summers 2010). In addition Summers et al. (2013) found that the onset of taste and odor compound 2-methylisoborneol breakthrough to occur at about 70% DOC breakthrough. Integration of the area

above the DOC breakthrough curves showed good agreement, within 14%, between the pilot columns and PD-RSSCTs for Waters A (7), A (15), and B. Large differences in DOM loading were found for Waters C, D, and E; -43%, 37%, and 79%, respectively. These differences are attributed to large seasonal fluctuations in initial DOC concentration at the pilot/full-scale whereas the PD-RSSCT represented a snapshot in time of water quality. The average influent DOC concentrations from Table 4.1 were used to calculate DOM loadings. Visually, there were better agreements between the large- and small-scale for UVA_{254} breakthroughs in Waters C and E.

The throughput in bed volumes to DOC breakthrough of 20 and 50% ($BV_{20\%}$ and $BV_{50\%}$) is shown in the top of Table 4.3 for Waters A (7 & 15), B, C, and D. In addition the throughput or bed volumes to 10% breakthrough ($BV_{10\%}$) for the MPs is also shown. DOC breakthrough occurred well before any MP breakthrough for all tests, so although undesirable, imperfect matches for DOC removal should have little effect on scaling MP removal. DOM surface loading (measured using DOC) is also not a good indicator of fouling related to MP adsorption, as fouling mechanisms are a function of particle size (Carter and Weber 1994, Corwin and Summers 2010, Matsui et al. 2012).

Table 4.3. Bed volumes to 10% PD-RSSCT breakthrough (x10^3), Water A (7) Y values, Y value comparisons to Water A (7), and average Y values in all waters.

Compound	Water A	Water B	Water C	Water D	Water A	Water A (7)		B	C	D	A (15)	Waters A, B, C, D
$DOC_{0,PD\text{-}RSSCT}$ (mg/L)	3.9	2.4	1.6	1.4	3.9	PSDM Y	Visual Y	$Y/Y_{Water\ A\ (7)}$				Y
EBCT (min)[a]	7	7.5	7	7	15							Avg±SD (N)[h]
DOC $BV_{20\%}$	2.5	4.5	4.8	13	4.2	--	--	--	--	--	--	--
DOC $BV_{50\%}$	4.9	8.2	10	21	6.6	--	--	--	--	--	--	--
2,4-D	140	145	155	250[c]	>199	0.53	0.55	0.97	--	1.04	--	0.53±0.02 (3)
Acetochlor	105	140	180	210	240[b]	0.43	0.45	0.38	1.11	0.81	--	0.35±0.14 (4)
Aldicarb	120	115	170	340	260[b]	0.40	0.40	0.76	--	1.34	--	0.41±0.11 (3)
Atrazine	220	>204	230	215[c]	>199	0.70	0.70	--	0.60	0.64	--	0.52±0.15 (3)
Caffeine[f]	40	25	160	160	70	0.56	0.55	0.66	1.24	1.06	1.67	0.63±0.21 (5)
Carbamazepine	310	>204	260	330	>199	0.58	0.65	--	0.80	0.93	--	0.53±0.06 (3)
Clofibric Acid	40	40	40	55	75	0.17	0.20	1.24	--	2.36	1.27	0.24±0.10 (4)
Cotinine	70	85	60	70	105	0.49	0.50	1.39	0.48	0.67	0.96	0.44±0.17 (5)
Diazinon	280	>204	275	230	>199	0.58	0.60	--	--	0.81	--	0.52±0.08 (2)
Diclofenac	90	140	200	334[c]	>199	0.45	0.50	--	--	0.86	--	0.42±0.05 (2)
Dimethoate	180	120	190	340	>199	0.43	0.45	0.75	--	1.56	--	0.47±0.18 (3)
Erythromycin	80	100	290	>499	>199	0.46	0.50	--	--	--	--	0.46±0.00 (1)
Gemfibrozil	260	135	210	280[c]	>199	N/A[e]	N/A	--	--	--	--	0.46±0.00 (1)
Ibuprofen	>[d]431	120	310	>499	>199	N/A	N/A	--	--	--	--	N/A
Iopromide	8[b]	28[b]	30	60	22[b]	0.18	0.20	1.25	1.68	1.80	1.20	0.26±0.06 (5)
Malaoxon	160	135	170	350	>199	0.52	0.55	0.78	--	0.97	--	0.48±0.06 (3)
Methomyl	150	190	150	170	150	0.55	0.55	1.25	1.08	0.76	1.15	0.58±0.10 (5)
Metolachlor	85	120	180	170	100	0.44	0.45	0.63	1.16	0.82	--	0.40±0.10 (4)
Molinate	230	>204	190	350	>199	0.37	0.40	--	--	1.46	--	0.46±0.12 (2)
Naproxen	430	>204	230	410	>199	0.43	0.50	--	--	1.17	--	0.46±0.05 (2)
Prometon	105	115	170	160	180	0.55	0.60	0.78	1.11	0.67	1.08	0.51±0.11 (5)
Simazine	260	>204	260	210	>199	0.58	0.65	--	1.10	0.56	--	0.51±0.17 (3)
Sulfamethoxazole	110	110	190	267[c]	>199	0.29	0.30	--	--	0.92	--	0.28±0.02 (2)
Tributyl phosphate[f]	30	25	20	24	20	0.71	0.70	--	1.01	--	--	0.71±0.00 (2)
Warfarin	40	55	100	90	85	0.30	0.35	0.86	--	0.82	--	0.27±0.03 (3)
					Avg±SD (21):	0.45±0.13	0.48±0.14	$Y/Y_{Water\ A\ (7)}$ t-test				
					Average:			0.92	1.01	1.05	1.13	Across all waters Y Avg±SD (68): 0.43±0.10
					Standard Deviation:			0.30	0.35	0.45	0.12	
					Count (used in calcs):			12	9	20	5	
					Different from Water A (7)[g]:			No	No	No	Yes	
					t-test p-value:			0.195	0.453	0.320	0.034	

[a]Actual EBCT values are 0.82, 0.63, 0.82, 0.82, and 1.8 minutes. [b]Value taken from PSDM simulation. [c]Value taken as average of data and PSDM simulation. [d]>: No breakthrough or could not be confidently projected to 10% using the PSDM. [e]No pilot breakthrough, therefore no Y value could be obtained. [f]Values not included in calculations due to erratic breakthrough behavior over all tests. [g]Testing whether average values are significantly different than unity (Water A, 7 min EBCT) at a 95% confidence level, i.e. larger or smaller average Y values. [h]Average±standard deviation (count).

4.3.2 Obtaining Fouling Factor Values

The pore and surface diffusion model (PSDM using AdDesignS™ from Michigan Technological University, Houghton, MI) was the main tool used to obtain fouling factors (Y) for scaling the PD-RSSCT to match the pilot column data. Procedures for the PSDM fitting methods are given in the Appendix (pg. 168) and follow the initial assumptions of Corwin and Summers (2011), Fotta (2012), and Reinert (2013). The method essentially involved fitting the PSDM to the PD-RSSCT curve then adjusting the fit by the FI to predict the full-scale data. As mentioned in Section 3.3.4, different combinations of Freundlich K and tortuosity (τ) values could be interpreted as adequate fits of the MPs with limited (<50%) breakthrough curves. However, best fits were chosen to obtain Y values by limiting $\tau<20$ (Sontheimer et al. 1988, Hand et al. 1989) and using visual judgment to minimize the differences between the limited number of PD-RSSCT breakthrough points and the fitted PSDM curve.

Y values were also visually obtained following Corwin and Summers (2010), which involves adjusting Y values by increments of 0.05 to visually collapse the pilot/full-scale and PD-RSSCT breakthrough data. A statistical t-test confirmed the Y values from the two methods were not statistically different at a 95% confidence level for Water A (7). Y values using both methods are shown in Table 4.3 for Water A (7).

If the PSDM is available, curve fitting provides cleaner breakthrough profiles, Freundlich K values, and kinetic data such as tortuosity or surface to pore diffusion flux ratio (SPDFR). The graphical results of both approaches are shown in Figure 4.2 for the insecticide methomyl in Water A (7). With a SF of 8.5 and Y of 0.55, the FI, or difference in capacity between the pilot column and PD-RSSCT was about 3.2 for methomyl in Water A (7).

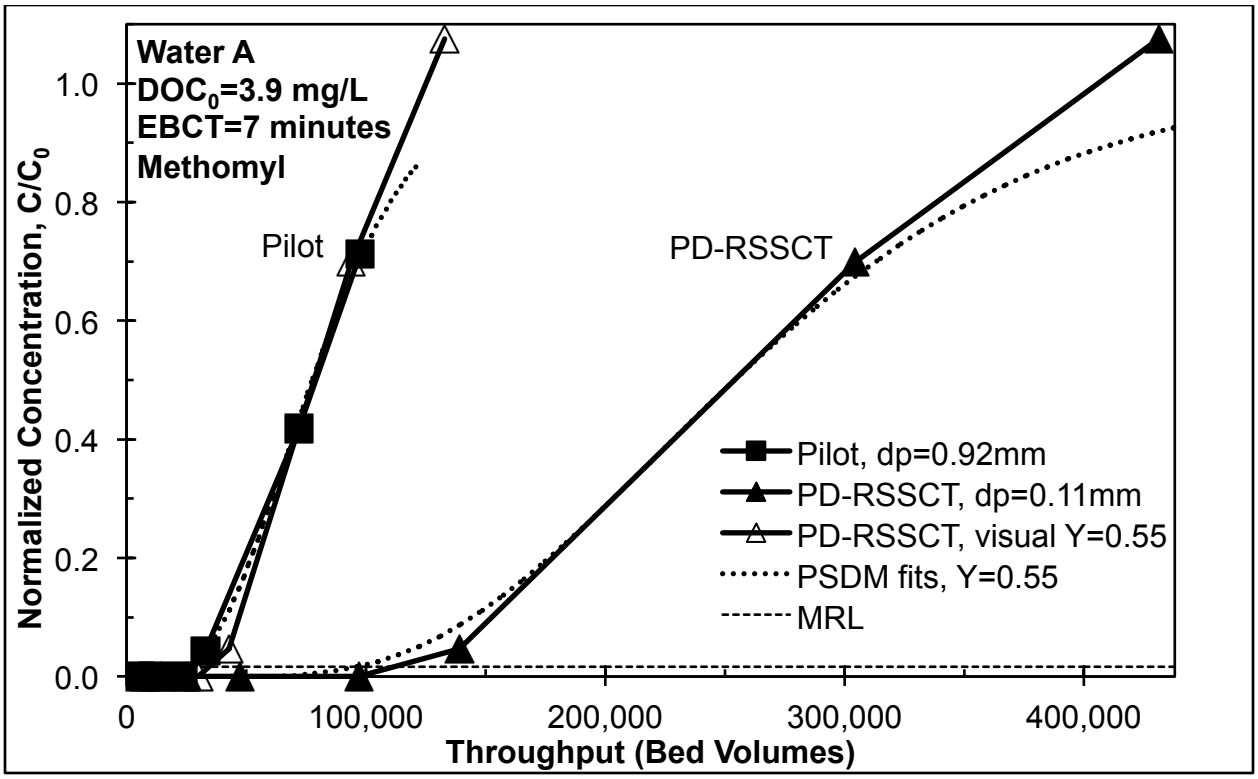

Figure 4.2. Example of (1) visual Y-fitting and (2) PSDM Y-fitting, for methomyl breakthrough profiles in Water A (7) ($DOC_{0,pilot}$= $DOC_{0,PD\text{-}RSSCT}$=3.9 mg/L, EBCT=7 mintues,12x40 bituminous GAC).

4.3.3 Predicting Full-Scale Micropollutant Adsorption Kinetics using the PD-RSSCT

Using Y and the FI to collapse the PD-RSSCT breakthrough curves onto the pilot column breakthrough curves essentially corrected for differences in adsorption capacity, but it was also found the adsorption kinetics matched as well. Since the FI is a constant value, using it to normalize PD-RSSCT throughput will inherently create a steeper breakthrough curve for the adjusted PD-RSSCT prediction.

Even so, adsorption kinetics were further investigated by curve fitting using the PSDM (Corwin and Summers 2011, Fotta 2012, Reinert 2013). Initially surface diffusion was set equal to zero due to the presence of DOM (Hand et al. 1989, Carter and Weber 1994, Jarvie et al. 2005, Corwin and Summers 2011). For all the PD-RSSCTs with Waters A (7 & 15), B, and D surface

diffusion was not required. Surface diffusion was invoked for 24 of 66 cases in the pilot columns with Waters A (7 & 15), B, and D. PD-RSSCT and pilot column MP breakthrough curves with Water C were steeper than the other waters, requiring surface diffusion for good fits. Surface diffusion was invoked for 3 of 11 cases in the PD-RSSCT and all cases (n=11) in the pilot column with Water C (Reinert 2013). Surface and pore diffusion Biot numbers were high (>30) in the pilot columns and PD-RSSCTs, so film diffusion was considered negligible to mass transfer resistance. Therefore it was assumed intraparticle mass transfer controlled adsorption kinetics (Sontheimer et al. 1988).

All PD-RSSCT breakthrough curves were less steep compared to the pilot column breakthrough curves. Using the PSDM, it was found that on average pore diffusion was about 7 times slower and surface diffusion was much slower (most SPDFRs≈0) in the PD-RSSCT compared to the pilot columns. According to the PD-RSSCT design, the amount of spreading of the mass transfer zone in the large- and small-scale columns due to intraparticle diffusion resistances should be identical. However, it cannot be expected kinetics would match because fouling does not scale using the RSSCT design equations, hence the creation of the FI method by Corwin and Summers (2010).

A probable cause for slower than expected intraparticle diffusion is that when GAC particles are ground, the micropore domain dominates mass transfer resistance by slowing diffusion (Summers et al. 2011). It is thought grinding exposes more micro- and mesopores to the bulk flow (Corwin and Summers 2010), reducing the occurrence of a two-domain transport theory of diffusion through the macropores followed by diffusion through the micropores (Summers 1986). Adsorbed DOM would therefore increase pore tortuosity to a greater extent in

the smaller GAC particle, causing slower kinetics through pore constriction and elimination of surface diffusion, increasing the spread of the mass transfer zone.

Alternatively, intraparticle diffusion would be mostly compound dependent, which would result in the same shape and length of the MP mass transfer zones in the small- and large-scale columns relative to the column size. However, because of the increased capacity (and therefore less direct competition with DOM) with smaller GAC particles from increased access to micro- and mesopores, the velocities of the MP mass transfer zones were slower, causing the breakthrough curves to spread out and appear more flat. Increased external mass transfer resistance in the small column is not a suspected cause for the shallower breakthrough curves because the amount of spreading due to film mass transfer is reduced in the PD-RSSCT design (Crittenden et al. 1986a, Crittenden et al. 1991). Regardless, if slowed intraparticle adsorption kinetics or mass transfer zone velocities caused shallower MP breakthrough curves in the PD-RSSCT, then the FI would sharpen the curve and give a valuable prediction of adsorption kinetics as well. Similar breakthrough curve slopes between the pilot- and small-scale can be seen in Figure 4.1 for cotinine and Figure 4.2 for methomyl.

The slope of most adjusted PD-RSSCT breakthrough curves matched the pilot column well with some steeper and some shallower (although this can also be a function of limited data points causing straight lines where there is curvature). Although the kinetics were not perfectly matched, alternative methods for kinetic adjustments using the diffusivity factor, X, and Equation 4.1 outlined by Corwin (2010) can be cumbersome, especially with uncertain outcomes. The method also requires the PSDM to generate breakthrough curves and the differential column batch reactor using at least three different GAC particle sizes. Therefore, the assumption that MP intraparticle diffusion effectively decreases linearly with GAC particle size is valid and the PD-

RSSCT should provide useful predictions of MP adsorption kinetics in natural waters after adjustment using the FI.

4.3.4 Effect of Influent Dissolved Organic Carbon Concentration, Empty Bed Contact Time, and GAC Particle Size on the Fouling Factor

The $BV_{10\%}$ values in Table 4.3 show that the poorest removed compound to be iopromide and the best removed compounds to be carbamazepine and naproxen. $BV_{10\%}$ values for acetaminophen, carbaryl, diuron, and trimethoprim are not shown in Table 4.3 because they exhibited no breakthrough in any water. Although the RSSCT typically underestimates MP removal from biodegradation, run times were long because of the increased capacity and low MP concentrations. Therefore some biodegradation of MPs was expected in the pilot columns and PD-RSSCTs despite the frequent replacement of the glass wool pre-filter (Zearley and Summers 2012). In these cases pilot column and PD-RSSCT data were matched only at early breakthrough.

Also shown in Table 4.3, the $BV_{10\%}$ values for a given MP are different for each water, indicating breakthrough is a function of the background matrix. In order to investigate the effects of the background matrix on scale-up, Y values (using PSDM fitting) from each water were compared to each other. Comparisons were made by normalizing Y values in each water by the corresponding Y value from Water A (7). Therefore each ratio is relative to unity. Water A (7) was chosen as the base case because it had the highest DOC_0 concentration and highest number of MPs with enough breakthrough to obtain Y values (n=23). The ratios are shown in the right side of Table 4.3. For each test these ratios were then averaged and compared to unity to see if their behavior was significantly different from the Water A (7) at a 95% confidence level using a statistical t-test.

The simulant caffeine Y values are shown but were excluded from the t-test analysis due to erratic breakthrough behavior throughout all tests most likely related to its high

biodegradation potential (Zearley and Summers 2012). The extractant and plasticizer tributyl phosphate Y values are also shown but excluded from the analysis due to erratic breakthrough behavior and/or consistent breakthrough at 10 to 20% for the first sampling events when all other MPs were below detection. Although MP sampling did not occur at time equal to zero, tributyl phosphate might break through immediately similar to DOC. Tributyl phosphate is not readily biodegradable (Zearley and Summers 2012).

The statistical t-test analysis in the bottom right of Table 4.3 indicates that on average, Y values from all the waters were not significantly different than those from Water A (7). However, Y values for Water A (15) were significantly larger on average by 13% compared to Water A (7). These differences are small though, and the data set for Water A (15) is limited (n=5). Therefore on average the fouling factor is more a function of the MP at these low concentrations than the background matrix, contrary to the findings of Corwin and Summers (2010). However this was on average, thus the background matrix cannot be ignored and is still thought to have an effect that can be seen across the rows in Table 4.3. As long as the full-scale and PD-RSSCT are run under similar conditions, the value for Y should remain relatively constant. Average Y values from Waters A (7 & 15), B, C, and D for each MP are also shown in the far right of Table 4.3. A total average of all the Y value averages at the bottom far right of Table 4.3 shows overall standard deviations are reasonable at ±0.10.

On average Y values were not significantly different for the ozonated Water B pilot and PD-RSSCT pair, despite having a SF of 11.9. All other pilot column and PD-RSSCT pairs had a SF of 8.5. The SF is the ratio of GAC particle sizes in the pilot column to the PD-RSSCT, and relates Y to FI, shown in Equation 4.3. Therefore the FI, developed by Corwin and Summers (2010), establishes the FI depends particle size but Y does not. Therefore to expedite the process

for acquiring Y values, a pilot run may not be necessary. If only two significantly different particle sizes are required (suggested SF≥3), essentially two different PD-RSSCTs can be run to yield Y values. Once the Y value is obtained, breakthrough from either PD-RSSCT can be scaled to the full-scale.

4.3.5 Predicting the Fouling Factor

Theoretical relationships for DOM fouling are difficult considering the vast number of variables that can exist between waters, GAC type, loading scenarios, etc. Therefore an empirical relationship was desired based on obtainable and adsorption-relevant parameters. A total of 47 Y values were chosen from Waters A (7 & 15), B, C, and D as well as Y values from Crittenden et al. (1989), Summers et al. (1989), Mastropole (2011), and Fotta et al (2012). The latter Y values are all from PD-RSSCTs representing 13 different volatile organic compounds and were included to obtain a breadth of Y values, MPs, GAC types, SFs, and adsorption conditions. In all, 73 Y values were used for a multiple linear regression using the least squares method.

Y values were compared to many physical parameters relevant to adsorption, including the background DOC_0 concentrations, initial MP concentrations (C_0), aqueous solubility, pH dependent octanol-water partition coefficient (log D), molecular weight, Abraham solvation parameters (A, B, E, S, V), liquid diffusivity, and polar surface area. Bed volumes to 10% MP breakthrough ($BV_{10\%}$) were also considered as a system property that incorporates the GAC type, particle size, adsorber operating conditions, and background DOM matrix. Using bed volumes to any percent breakthrough is essentially a surrogate measure of the system-specific adsorption capacity.

Singularly only the ratio of the C_0/DOC_0, $BV_{10\%,PD\text{-}RSSCT}$, and log D showed any systematic trend with Y values. These parameters represent both the specific MP and background

DOM matrix. Several other researchers have related activated carbon removal or breakthrough to these parameters (Magnuson and Speth 2005, Westerhoff et al. 2005, Snyder et al. 2007, Ridder et al. 2009, Corwin 2010, Ridder et al. 2010, Mastropole 2011, Fotta 2012, Reinert 2013). Therefore these three parameters were chosen for a multiple linear regression of the initial surface response model form in Equation 4.5,

$$y = \beta_0 + \beta_1 x_1 + \beta_2 x_2 + \beta_3 x_3 + \beta_{12} x_1 x_2 + \beta_{13} x_1 x_3 + \beta_{23} x_2 x_3 + \beta_{11} x_1^2 + \beta_{22} x_2^2 + \beta_{33} x_3^2 \quad (4.5)$$

where y is the fouling factor Y, β is the regression coefficient, x_1 is C_0/DOC_0, x_2 is $BV_{10\%,PD\text{-}RSSCT}$, and x_3 is log D. Log D values in the range of -2.66 to 3.03 were obtained from SciFinder® (Chemical Abstracts Service) at the appropriate pH for MPs that are ionic at pH values 6 to 8. C_0/DOC_0 values ranged from 4.7×10^{-6} to 0.48 and $BV_{10\%,PD\text{-}RSSCT}$ values ranged from 850 to 310,000.

In order to best stabilize the variance, the response (Y) was transformed to the reciprocal of Y. Regressions were then run in a stepwise fashion, where in each step the coefficient (β) with the highest p-value above 0.05 was eliminated until all the coefficients were significant at a 95% confidence level. Final results from the stepwise regression ($p<0.01$, $R^2=0.77$, $R^2_{adj}=0.76$, $R^2_{pred}=0.71$, n=73) showed nonlinear behavior that could not be accounted for by the linear equation, even with significant interaction terms. Therefore the model was transformed using a significant power function ($p<0.01$, $R^2=0.68$, $R^2_{adj}=0.68$, $R^2_{pred}=0.66$, n=73), yielding the final regression shown in Equation 4.6.

$$Y = \left[\begin{array}{l} (2.59 \pm 0.11) + (3.94 \pm 1.48)\dfrac{C_0^{MP}}{DOC_0} + (-7.87 \times 10^{-6} \pm 1.29 \times 10^{-6}) BV_{10\%}^{PD-RSSCT} \\ +(-0.402 \pm 0.054)\log D + (4.20 \times 10^{-4} \pm 1.73 \times 10^{-4})\dfrac{C_0^{MP} \cdot BV_{10\%}^{PD-RSSCT}}{DOC_0} \\ +(2.86 \times 10^{-6} \pm 5.87 \times 10^{-7}) BV_{10\%}^{PD-RSSCT} \cdot \log D \end{array} \right]^{(-1.47 \pm 0.06)} \quad (4.6)$$

The residuals versus fitted values plot for all steps in the regression process, including Equation 4.6, showed random equal variance and normal probability plots confirmed the residuals were normally distributed. The residual versus fitted values plot for Equation 4.6 is shown in Figure 4.3. β_0, β_1, β_2, β_3, β_{12}, and β_{23} were all found to be significant with p-values less than 0.05. With these three parameters, Equation 4.6 follows expected trends as Y values increase with: (1) increasing bed volumes to 10% MP breakthrough, i.e., more strongly adsorbing MP and more subject to fouling, (2) decreasing C_0/DOC_0, either decreasing influent MP concentration or increasing DOC_0 concentration, i.e., less ability to compete and more subject to fouling, and (3) increasing log D or MP hydrophobicity, i.e., prefer GAC surface and more subject to fouling. A sensitivity analysis showing the effect of each parameter while all other parameters are held constant (at their median values) in Equation 4.6 is shown in Table 4.4.

Table 4.4. Sensitivity analysis for predicting Y values from Equation 4.6.

Parameter[a] (β)	Range (median)	Y Range[b]
$C_{0,MP}/DOC_0$ (3.94)	4.7×10^{-6} to 0.48 (1.5×10^{-4})	0.48 to 0.015
$BV_{10\%,PD-RSSCT}$ (-7.87×10^{-6})	850 to 310,000 (70,000)	0.41 to 0.88
log D (-0.402)	-2.66 to 3.03 (1.9)	0.25 to 0.59
	Median Y:	0.47

[a]All parameters are unitless. [b]Y value change over variable range while all other parameters were held constant at their median value.

Additionally, if the PSDM is available or breakthrough to only 10% is desired, the PD-RSSCT only needs to be run to 10% MP breakthrough to obtain a Y value from Equation 4.6 and subsequent full-scale prediction. Though the PD-RSSCT already saves time, money, and water this would result in further reductions in effort and analytical costs. For most MPs, termination of a PD-RSSCT at 10% MP breakthrough should still capture complete DOC breakthrough.

A plot ($p<0.01$, $R^2=0.56$, $R^2_{adj}=0.56$, $R^2_{pred}=0.53$, $n=73$) of the fitted or predicted Y values versus the observed Y values is shown in Figure 3.7. For visual clarity, the dashed lines represent ±0.1Y. This was thought to be an acceptable Y value range considering the amount of experimental and analytical variability at these low concentrations. It was also the average standard deviation of all the Y values in Table 4.3. The 73 values used to create the regression are shown with solids symbols. Nineteen Y values from Waters A (7 & 15), B, C, and D were not used to create the regression because either (1) breakthrough was below detection, (2) only one breakthrough point could be used to obtain a Y value, (3) the MP was caffeine or tributyl phosphate for reasons previously discussed (see Section 4.3.4), or (4) the Y value experienced high (>3σ) standardized residuals during regression analysis. These Y values are shown as gray circles. Four external Y values from Corwin and Summers (2010) are also shown for comparison as gray squares.

Of the MPs used to create the regression, 75% fell within ±0.1Y. For the MPs not used to create the regression, 74% fell within ±0.1Y. All of the MPs from Corwin and Summers (2010) fell within ±0.1Y. Y values for three of these four MPs (atrazine, prometon, simazine) also fall within one standard deviation of the corresponding average Y values in Table 4.3 (DEET was not in this study).

Eight MPs, with log D values less than about two, not used to create the regression were not predicted well. These MPs broke through late in their respective PD-RSSCT (>250,000 bed volumes) possibly due to biodegradation, resulting in very large $BV_{10\%,PD\text{-}RSSCT}$ values and consequently large Y values (>1). MPs with such late breakthrough in the PD-RSSCT should not be a concern as they would also breakthrough late at the full-scale, well beyond normal adsorber run times. For additional comparison Y values were also predicted for 21 MPs from other studies using the CD-RSSCT design (Speth and Miltner 1989, Summers et al. 1989, Crittenden et al. 1989, Knappe et al. 1997, Reinert 2013). Only 33% were predicted within ±0.1Y and 62% within ±0.15Y. $BV_{10\%}$ values for the CD-RSSCT are much lower than the PD-RSSCT while C_0/DOC_0 and log D values would be the same. Although no CD-RSSCT data was used to create Equation 4.6, using it for scaling may still provide a better prediction than the raw CD-RSSCT breakthrough. CD-RSSCT-specific Y value predictions based on Abraham solvation parameters can be found in Reinert (2013).

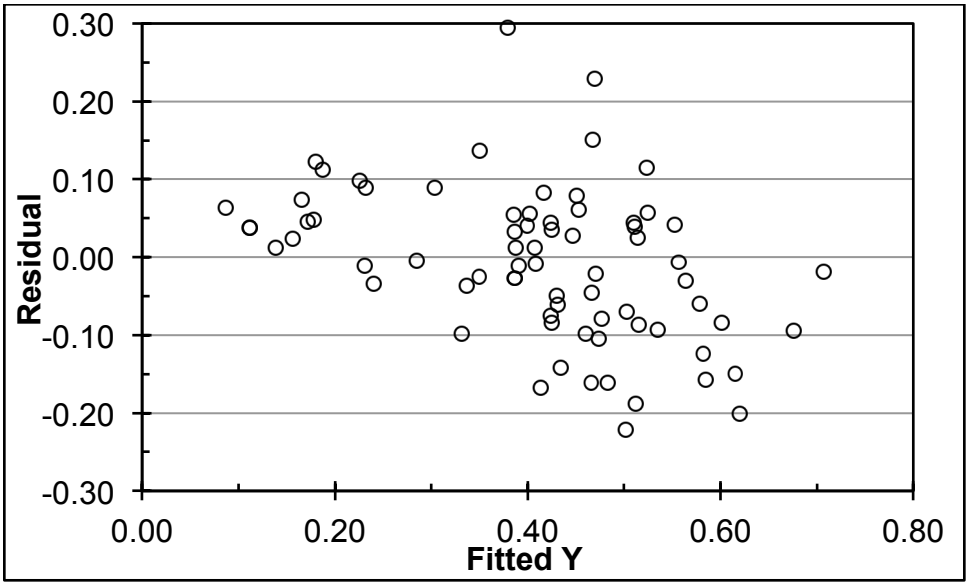

Figure 4.3. Residuals versus fitted value plot for Equation 4.6 (n=73).

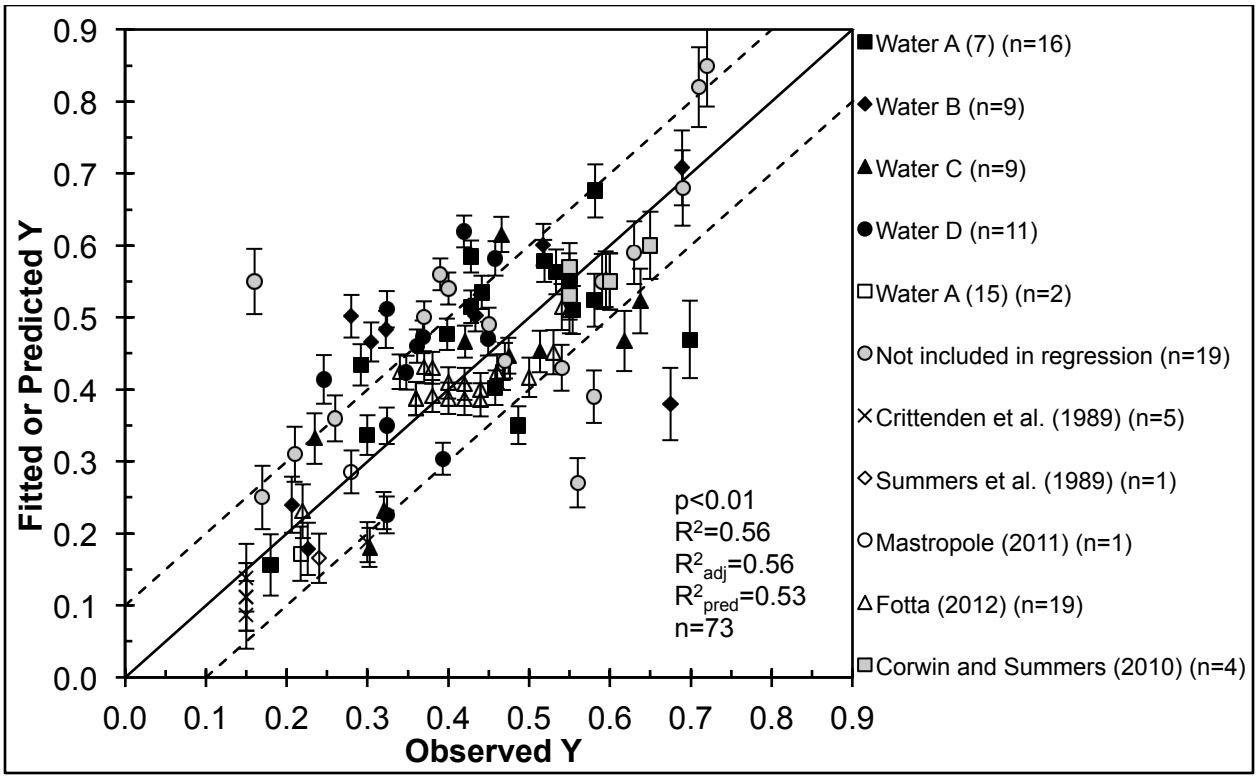

Figure 4.4. Fitted or predicted Y values using Equation 4.6 versus observed Y values with 95% confidence intervals (based on the regression standard error of 0.09). Solid line is 1:1 line. Dashed lines are ±0.1Y. All symbols but gray (n=23) were used to create the regression (n=73).

4.3.6 Predicting Full-Scale Bed Volumes to 10% Micropollutant Breakthrough

Alternatively and independent of the fouling factor, an empirical relationship related the bed volumes to 10% breakthrough ($BV_{10\%}$) in the pilot columns from Chapter 3 (Table 3.2) and PD-RSSCTs (Table 4.3) was developed. Breakthrough at this level allowed more MPs to be incorporated into the regression and is relevant because high levels of removal are usually desired. Pilot column and PD-RSSCT $BV_{10\%}$ values were chosen or not included following the same guidelines as previously discussed (see Section 4.3.5). In all, 73 $BV_{10\%}$ pair values were used for a simple linear regression using the least squares method. The 73 pairs represented SF values of 4.3, 5.3, and 8.5. In order to best stabilize the variance, the response ($BV_{10\%,full\text{-}scale}$) and

predictor ($BV_{10\%,PD\text{-}RSSCT}$) were both transformed using the natural logarithm. The final regression is shown in Equation 4.7 ($p<0.01$, $R^2=0.92$, $R^2_{adj}=0.92$, $R^2_{pred}=0.92$, n=73).

$$\ln BV_{10\%}^{full-scale} = (0.57 \pm 0.32) + (0.855 \pm 0.029) \ln BV_{10\%}^{PD-RSSCT} \quad (4.7)$$

The residuals versus fitted values plot, Figure 4.5, shows random equal variance and normal probability plots confirmed the residuals were normally distributed. β_0 and β_1 were found to be significant with p-values less than 0.1. A plot ($p<0.01$, $R^2=0.80$, $R^2_{adj}=0.80$, $R^2_{pred}=0.79$, n=73) of the fitted or predicted $BV_{10\%,full\text{-}scale}$ values versus the observed $BV_{10\%,full\text{-}scale}$ values is shown in Figure 4.6. The 73 values used to create the regression are shown with solids symbols. Of the MPs used to create the regression, 48% fell within 20% of the observed $BV_{10\%,full\text{-}scale}$. For the MPs not used to create the regression, 54% fell within 20% of the observed $BV_{10\%,full\text{-}scale}$. Three of the four MPs from Corwin and Summers (2010, SF=13.6) fell within 53% of the observed $BV_{10\%,full\text{-}scale}$. On average the PD-RSSCT predicts $BV_{10\%}$ later than the pilot/full-scale by a factor of 3.0±1.2 (n=101, SF range: 4.3 to 13.6), typically less than three for weakly adsorbing MPs and greater than three for strongly adsorbing MPs. Therefore a factor of three may be a good approximation for full-scale breakthrough of MPs using the PD-RSSCT. Equation 4.7 may also serve as a check on Equation 4.6 if a larger Y value (>1) is predicted.

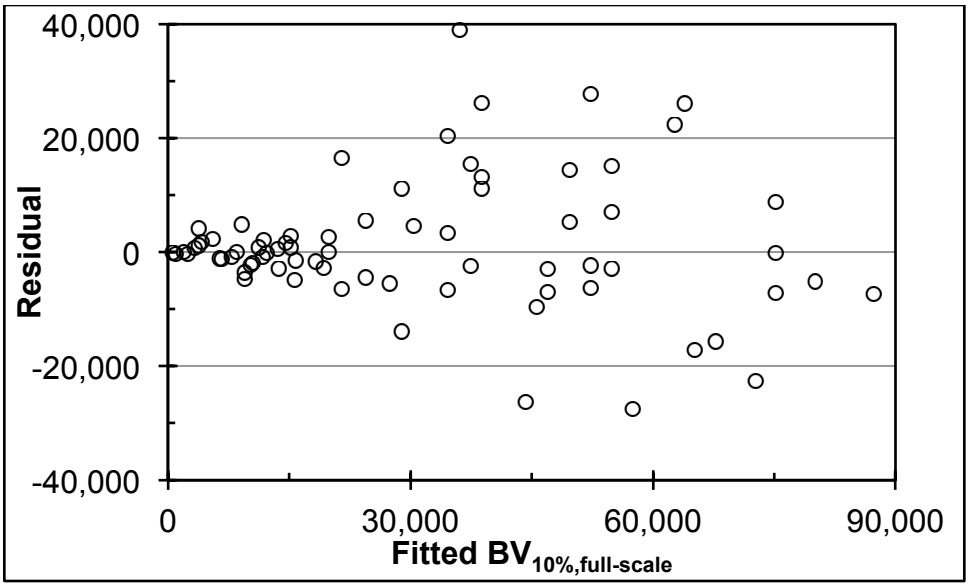

Figure 4.5. Residuals versus fitted values plot for Equation 4.7 (n=73).

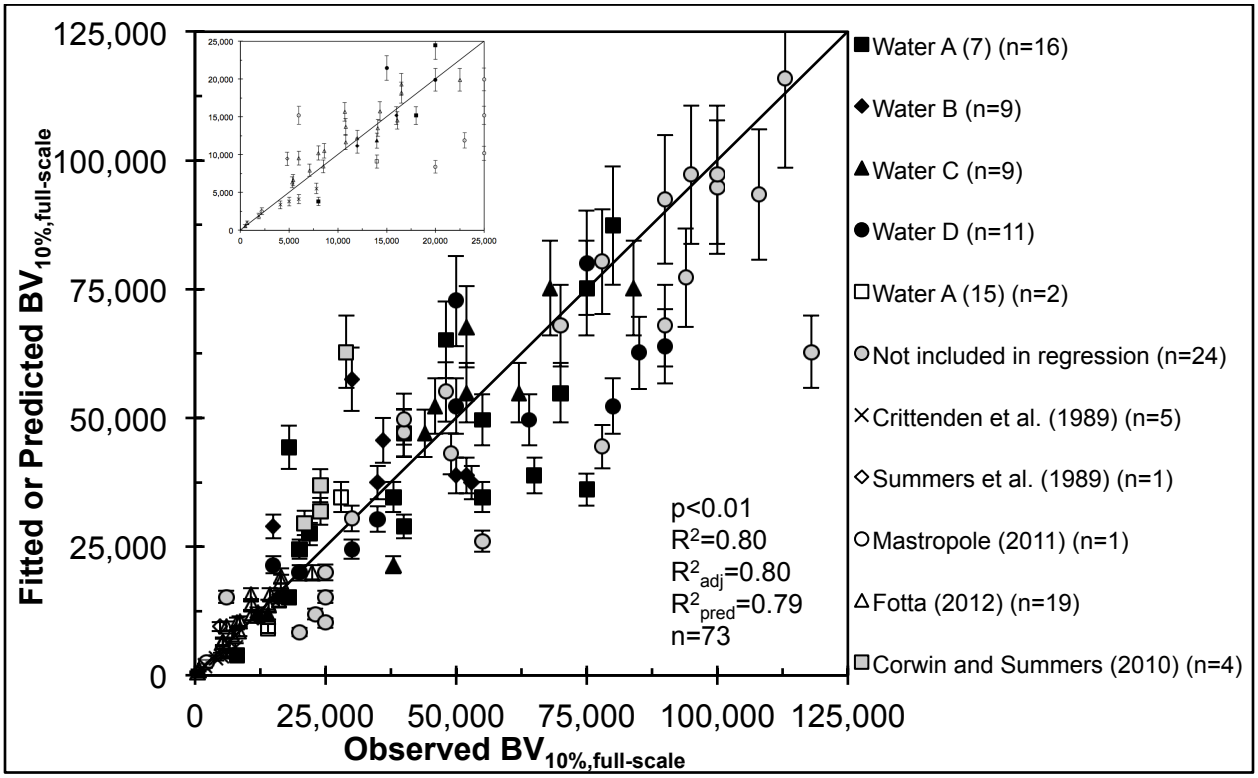

Figure 4.6. Fitted or predicted $BV_{10\%,pilot}$ values using Equation 4.7 versus observed $BV_{10\%,pilot}$ values with 95% confidence intervals (based on the regression standard error of 10,457 bed volumes). Solid line is 1:1 line. All symbols but gray (n=28) were used to create the regression (n=73). Inset is zoom in of 25,000 bed volumes.

An attempt was made to use the PD-RSSCT $BV_{10\%}$ data to create an equation similar to Equations 3.3 and 3.4 from Chapter 3, which related $BV_{10\%,full\text{-}scale}$ to DOC_0 concentration, log D, polarizability (S), and molecular volume (V). Because there was more PD-RSSCT breakthrough data it was expected to yield a robust relationship to be used in conjunction with Equation 4.7. Surprisingly, using $BV_{10\%,PD\text{-}RSSCT}$ for MPs in the coagulated Water A (7), C, and D, regression results were unsatisfactory even after limiting it to MPs with breakthrough less than 300,000 bed volumes. Regardless, the regression is shown in Equation 4.8 ($p<0.01$, $R^2=0.52$, $R^2_{adj}=0.49$, $R^2_{pred}=0.40$, n=56). McGowan molecular volume, V, was not found to be significant.

$$\ln BV_{10\%}^{PD-RSSCT} = (12.4 \pm 0.2) + (-0.151 \pm 0.058) DOC_0 + (0.178 \pm 0.049) \log D + (-0.248 \pm 0.090) S \quad (4.8)$$

The residuals versus fitted values plots showed random equal variance and normal probability plots confirmed the residuals were normally distributed. β_0, β_1, β_2, and β_3 were all found to be significant with p-values less than 0.05. After transforming back to arithmetic units the goodness of fit dropped significantly ($p<0.01$, $R^2=0.34$, $R^2_{adj}=0.33$, $R^2_{pred}=0.29$, n=56). Therefore there would be no reason to use Equation 4.8 instead of Equations 3.3 and 3.4 from Chapter 3.

There was some success in creating a regression similar to Equation 4.7 for CD-RSSCT and pilot/full-scale data from Crittenden et al. (1989), Speth and Miltner (1989), Summers et al. (1989), Knappe et al. (1997) and Reinert (2013). The final regression is shown in Equation 4.9 ($p<0.01$, $R^2=0.85$, $R^2_{adj}=0.85$, $R^2_{pred}=0.83$, n=20).

$$\ln BV_{10\%}^{full-scale} = (2.08 \pm 0.77) + (0.798 \pm 0.078) \ln BV_{10\%}^{CD-RSSCT} \quad (4.9)$$

The residuals versus fitted values plot showed random equal variance and normal probability plots confirmed the residuals were normally distributed. β_0 and β_1 were found to be significant with p-values less than 0.05. After transforming back to arithmetic units the fit was relatively good ($p<0.01$, $R^2=0.77$, $R^2_{adj}=0.75$, $R^2_{pred}=0.71$, $n=20$). However, only 12 of the 20 MPs used to create the regression showed closer predictions of $BV_{10\%,full\text{-}scale}$ compared to the raw CD-RSSCT data prediction of $BV_{10\%,full\text{-}scale}$. These results were not surprising as the CD-RSSCT was the accepted design approach for target organics because of consistent predictions of early breakthrough that led to subsequent standard method for GAC testing (ASTM 2008).

4.3.7 Full-Scale Verification

Influent and effluent samples from one of 10 full-scale GAC adsorbers at the GCWW (Water E) operated at 15 minute EBCT were analyzed for 18 MPs over a period of nine months. Fourteen of these 18 MPs were from the list in Table 4.3 and four (bupropion, lamotrigine, metoprolol, and sucralose) were compounds not evaluated in the spiked pilot studies of Waters A, B, C and D. Only six of the MPs regularly appeared in the GAC effluent: atrazine, caffeine, cotinine, prometon, sucralose, and sulfamethoxazole. Breakthrough data from these six MPs was used to verify the predictive relationships presented in this study. GCWW normally replaces the GAC after 15,000 bed volumes or complete DOC breakthrough, so these compounds do not normally appear in the finished water. The other GAC adsorbers were regularly replaced during the study.

Full-scale and PD-RSSCT breakthrough profiles are shown in Figure 4.7 through Figure 4.12 for the six MPs. Normalized full-scale breakthrough (C/C_0) in the following figures is

shown in two ways. The first is the effluent concentrations normalized to the average influent concentration over the course of the year. Breakthrough presented in this way better illustrates the attenuation properties of GAC and provides more useful breakthrough curves from limited data. The second way is termed instantaneous breakthrough, and represents the effluent concentration divided by the influent concentration from the same sampling event. If the influent concentration varies significantly with season, instantaneous C/C_0 may not convey a useful effluent profile. When the influent concentration drops higher fractional breakthroughs can be interpreted as high concentrations, when in fact the effluent concentration is much lower. If the influent MP concentration is relatively constant, there is little difference between the two methods.

Figure 4.7 and Figure 4.8 show the breakthrough profiles for the herbicide prometon and artificial sweetener sucralose, respectively. After predicting the Y value and adjusting the PD-RSSCT using the FI the scaled PD-RSSCT fits the full-scale breakthrough data well. Data was limited though so the PSDM was also used to first fit the PD-RSSCT curve then scale it using the FI to predict the full-scale data. The PSDM provides a more complete breakthrough curve prediction of full-scale data.

The PSDM was also used to demonstrate the sensitivity of Y in Figure 4.7 and Figure 4.8. As previously mentioned, ±0.1Y has been established as an adequate prediction. Figure 4.7 and Figure 4.8 show the predicted PSDM curve as well as two other cases representing if Y had been predicted 0.1 higher or lower. These ±0.1 values of Y are shown next to the PSDM simulations. Modeling with high and low Y values still provided adequate predictions of the full-scale data, confirming the use of the interval in Figure 4.4.

Figure 4.9 through Figure 4.12 also show good predictions of the full-scale data using Equation 4.6 to predict Y for the herbicide atrazine, stimulant caffeine, nicotine metabolite cotinine, and antibiotic sulfamethoxazole. For caffeine and sulfamethoxazole, PD-RSSCT PSDM fits were difficult, but attempted to represent an average of all the breakthrough points. $BV_{10\%,full-scale}$ values were also predicted using Equation 4.7, and are shown in Figure 4.7 through Figure 4.12 as an open circle. Atrazine, caffeine, cotinine, and sucralose $BV_{10\%,full-scale}$ values were predicted within 5, 9, 1, and 8%, respectively. $BV_{10\%,full-scale}$ values for prometon and sulfamethoxazole were both over predicted by a factor of 2, but match well with the adjusted PD-RSSCT curves and PSDM predictions. A comparison between the observed and predicted $BV_{10\%,full-scale}$ values is shown in Table 4.5, and shows over prediction using Equation 4.7 by an average of 1.4±0.6 (n=6). The better agreement of $BV_{10\%,full-scale}$ values in Table 4.5 demonstrates the increased predictive ability of Equation 4.7 over Equation 3.3 and Equation 3.4 (Chapter 3) because the PD-RSSCT was able to capture the competitive effects of the impacted Water E.

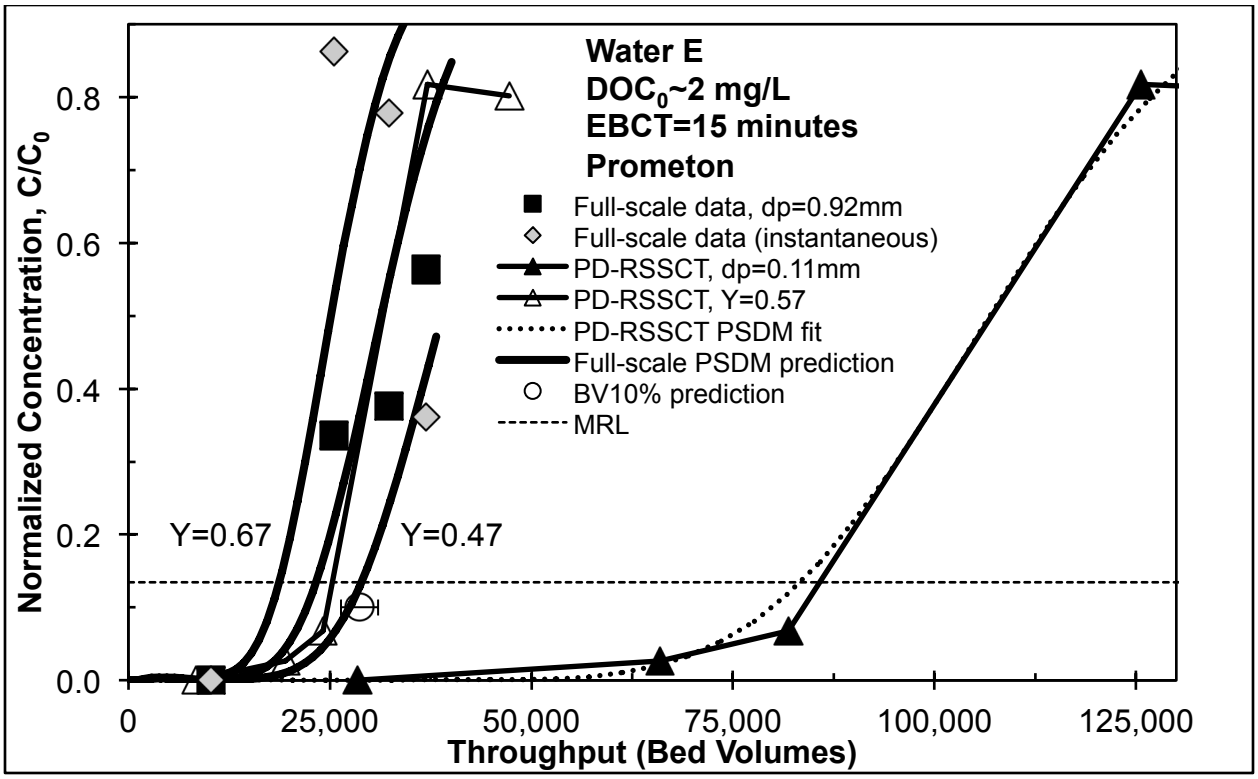

Figure 4.7. Full-scale breakthrough predictions for the herbicide prometon in Water E ($DOC_{0,full-scale}$=1.9 mg/L, $DOC_{0,PD-RSSCT}$=2.0 mg/L, EBCT=15 minutes, reactivated 12x40 bituminous GAC). PD-RSSCT and PSDM predictions used Equation 4.6 to calculate Y. PSDM predictions also show sensitivity for ±0.1Y. Black squares show full-scale breakthrough relative to the average influent prometon concentration ($C_{0,full-scale}$~7.5±5.1 ng/L, MRL~1 ng/L) over the entire run. Gray diamonds show full-scale breakthrough relative to each pair of influent and effluent samples (instantaneous). Open circle shows $BV_{10\%,full-scale}$ prediction from Equation 4.7.

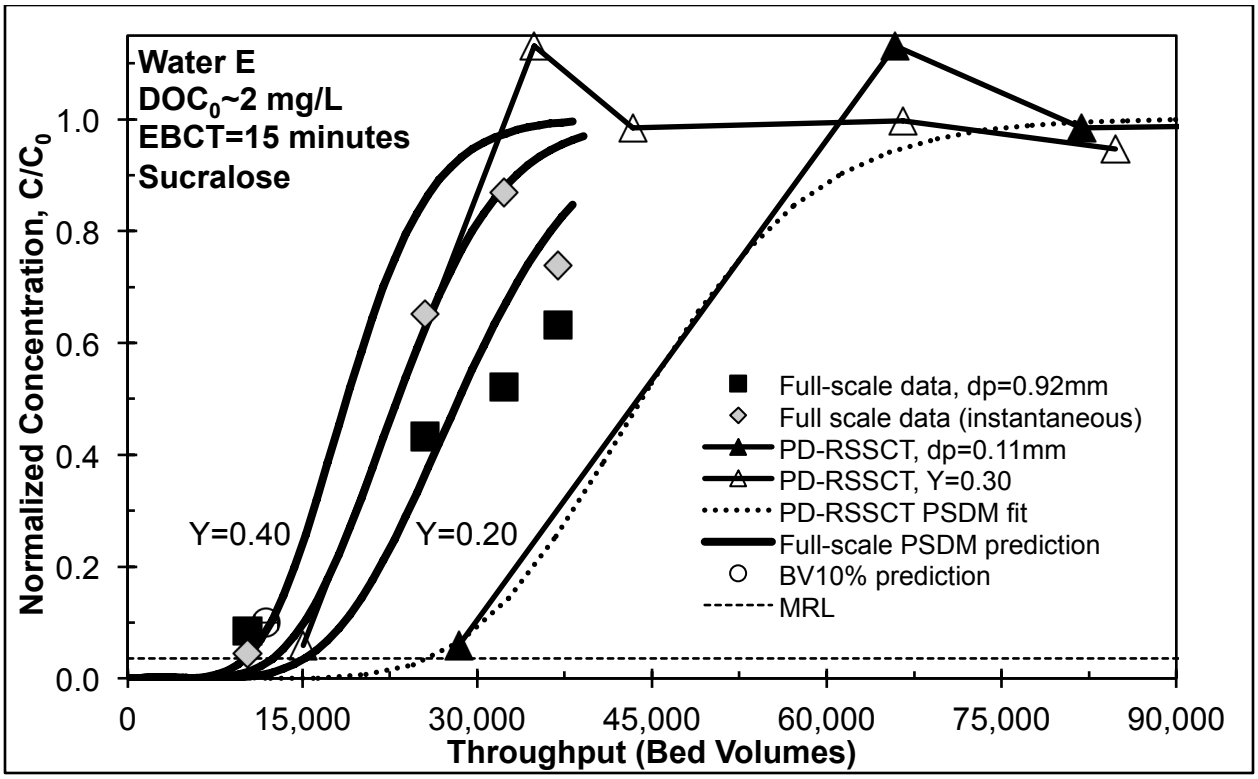

Figure 4.8. Full-scale breakthrough predictions for the artificial sweetener sucralose in Water E ($DOC_{0,full\text{-}scale}$=1.9 mg/L, $DOC_{0,PD\text{-}RSSCT}$=2.0 mg/L, EBCT=15 minutes, reactivated 12x40 bituminous GAC). PD-RSSCT and PSDM predictions used Equation 4.6 to calculate Y. PSDM predictions also show sensitivity for ±0.1Y. Black squares show full-scale breakthrough relative to the average influent sucralose concentration ($C_{0,full\text{-}scale}$~423±252 ng/L, MRL~15 ng/L) over the entire run. Gray diamonds show full-scale breakthrough relative to each pair of influent and effluent samples (instantaneous). Open circle shows $BV_{10\%,full\text{-}scale}$ prediction from Equation 4.7.

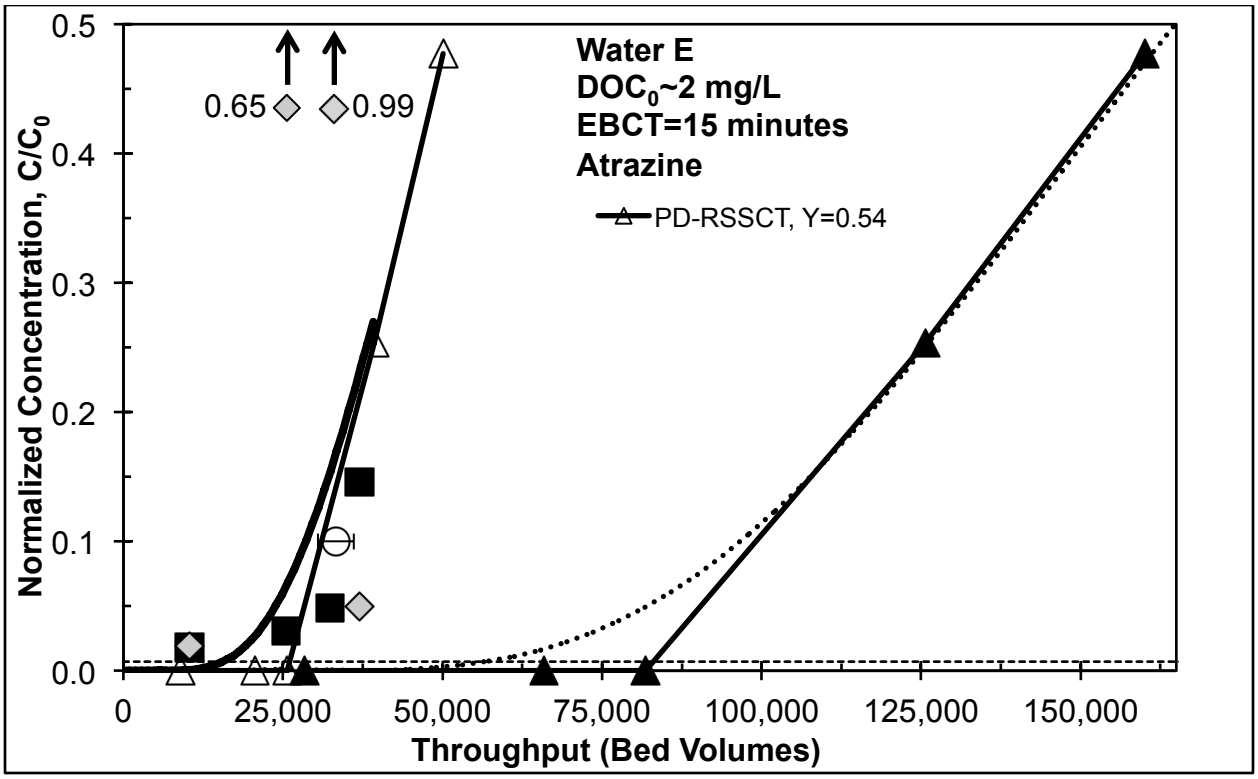

Figure 4.9. Full-scale breakthrough predictions for the herbicide atrazine in Water E ($DOC_{0,full-scale}$=1.9 mg/L, $DOC_{0,PD-RSSCT}$=2.0 mg/L, EBCT=15 minutes, reactivated 12x40 bituminous GAC). PD-RSSCT and PSDM predictions used Equation 4.6 to calculate Y. Black squares show full-scale breakthrough relative to the average influent concentrations ($C_{0,full-scale}$~284±388 ng/L, MRL~2 ng/L) over the entire run. Gray diamonds show full-scale breakthrough relative to each pair of influent and effluent samples (instantaneous). Open circle shows $BV_{10\%,full-scale}$ prediction from Equation 4.7.

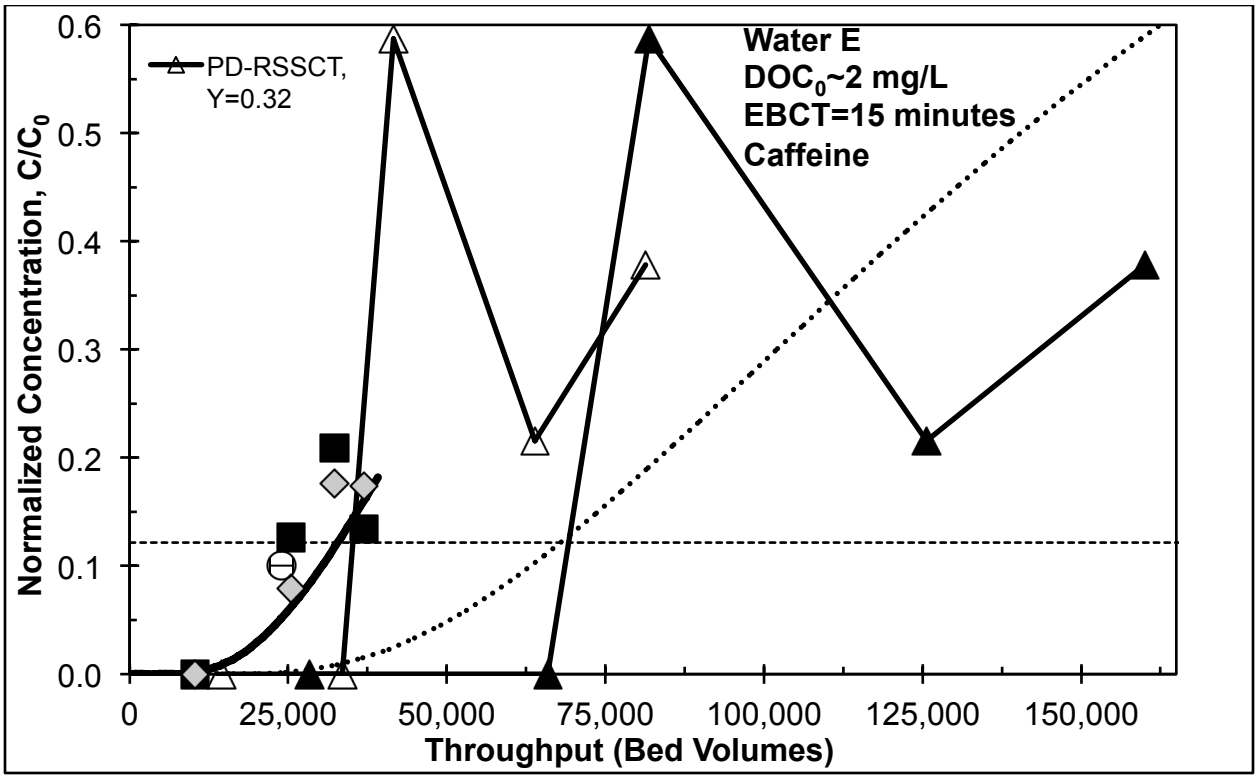

Figure 4.10. Full-scale breakthrough predictions for the simulant caffeine in Water E ($DOC_{0,full-scale}$=1.9 mg/L, $DOC_{0,PD-RSSCT}$=2.0 mg/L, EBCT=15 minutes, reactivated 12x40 bituminous GAC). PD-RSSCT and PSDM predictions used Equation 4.6 to calculate Y. Black squares show full-scale breakthrough relative to the average influent concentrations ($C_{0,full-scale}$~41±21 ng/L, MRL~5 ng/L) over the entire run. Gray diamonds show full-scale breakthrough relative to each pair of influent and effluent samples (instantaneous). Open circle shows $BV_{10\%,full-scale}$ prediction from Equation 4.7.

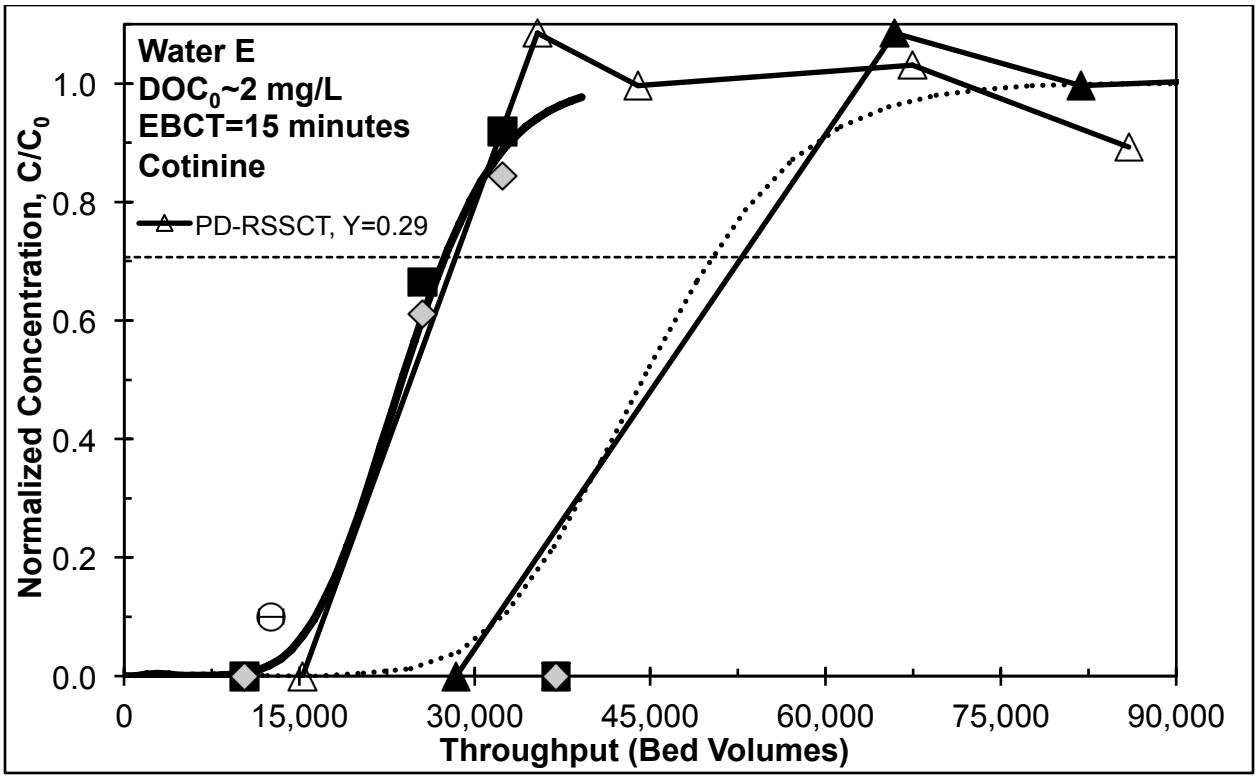

Figure 4.11. Full-scale breakthrough predictions for the nicotine metabolite cotinine in Water E ($DOC_{0,full\text{-}scale}$=1.9 mg/L, $DOC_{0,PD\text{-}RSSCT}$=2.0 mg/L, EBCT=15 minutes, reactivated 12x40 bituminous GAC). PD-RSSCT and PSDM predictions used Equation 4.6 to calculate Y. Black squares show full-scale breakthrough relative to the average influent concentrations ($C_{0,full\text{-}scale}$~7.1±0.7 ng/L, MRL~5 ng/L) over the entire run. Gray diamonds show full-scale breakthrough relative to each pair of influent and effluent samples (instantaneous). Open circle shows $BV_{10\%,full\text{-}scale}$ prediction from Equation 4.7. The last full-scale data point for cotinine was below detection.

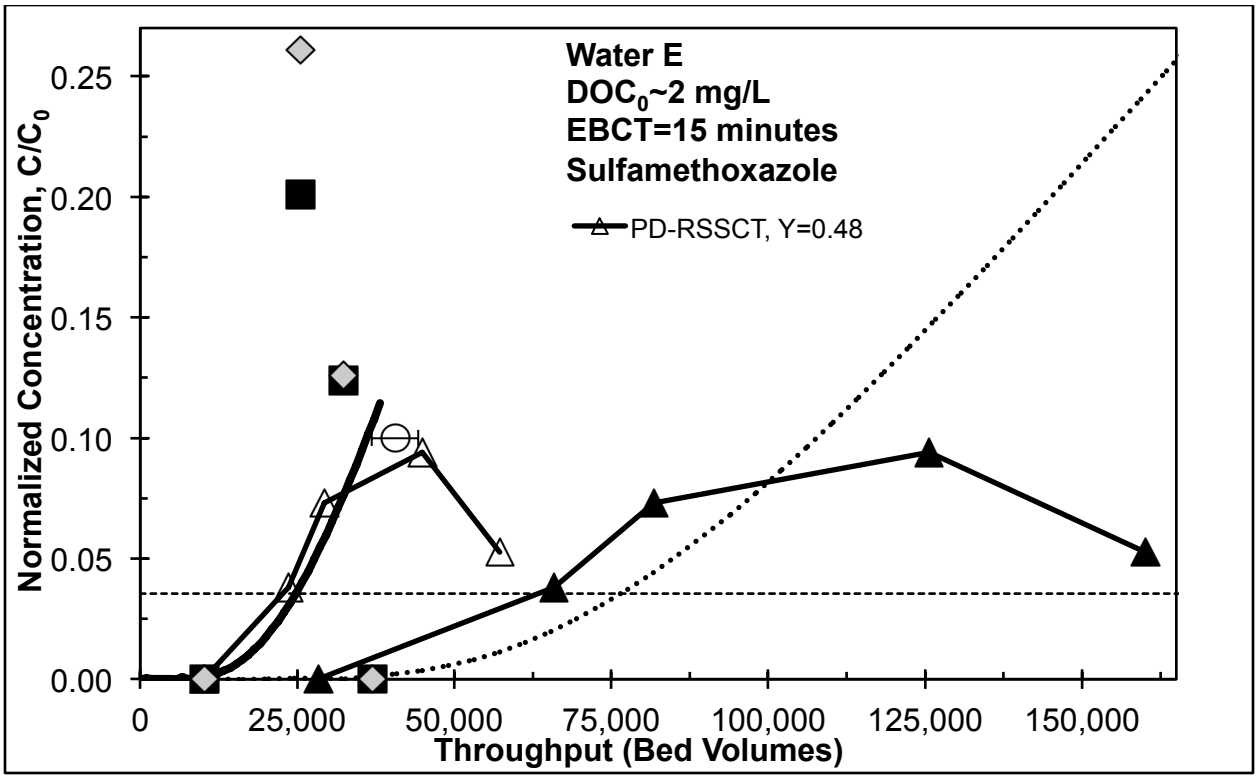

Figure 4.12. Full-scale breakthrough predictions for the antibiotic sulfamethoxazole in Water E ($DOC_{0,full\text{-}scale}$=1.9 mg/L, $DOC_{0,PD\text{-}RSSCT}$=2.0 mg/L, EBCT=15 minutes, reactivated 12x40 bituminous GAC). PD-RSSCT and PSDM predictions used Equation 4.6 to calculate Y. Black squares show full-scale breakthrough relative to the average influent concentrations ($C_{0,full\text{-}scale}$~39±11 ng/L, MRL~5 ng/L) over the entire run. Gray diamonds show full-scale breakthrough relative to each pair of influent and effluent samples (instantaneous). Open circle shows $BV_{10\%,full\text{-}scale}$ prediction from Equation 4.7. The last full-scale data point for sulfamethoxazole was below detection.

Comparisons between the predicted Y values for MPs in Water E and the average Y values from Table 4.3 are shown in Table 4.5. The Y values for atrazine, cotinine, and prometon in Water E are within one standard deviation of the corresponding Y value from Table 4.3. The Y values for caffeine do not agree well, but as stated previously caffeine exhibits erratic breakthrough behavior most likely related to its biodegradability. The Y value for sulfamethoxazole was higher than expected from Table 4.3 because of the plateau behavior it exhibited in PD-RSSCT breakthrough in Figure 4.12. However, a Y value of 0.48 provides a much better prediction of the full-scale than a Y value of 0.28 (from Table 4.3), confirming the

inclusion of the $BV_{10\%,PD\text{-}RSSCT}$ term in Equation 4.6 to represent the background matrix effects. Overall, the predicted Y values for MPs in Water E are the same as those from Table 4.3, seen by an average of 1.0±0.5.

Table 4.5. Predicted Y value and $BV_{10\%,full\text{-}scale}$ comparisons for Water E.

Micropollutant	Y-Value		$BV_{10\%,full\text{-}scale}$	
	Observed Avg±SD (N)[a]	Predicted[b] (Water E)	Observed	Predicted[c]
Atrazine	0.52±0.15 (3)	0.54	35,000	33,308
Caffeine	0.63±0.21 (5)	0.32	22,000	23,952
Cotinine	0.44±0.17 (5)	0.29	12,500	12,573
Prometon	0.51±0.11 (5)	0.57	15,000	28,695
Sucralose	N/A[d]	0.30	11,000	11,898
Sulfamethoxazole	0.28±0.02 (2)	0.48	18,000	40,585
Overall Comparison[e]	Avg±SD:	1.0±0.5	Avg±SD:	1.4±0.6

[a]Average±standard deviation (count) from Table 4.3. [b]Standard error=0.09. [c]Standard error=10,457 bed volumes. [d]Sucralose was not in Water A, B, C, or D. [e]Predicted divided by observed.

4.4 Conclusions

Statistical t-test analysis showed Y values depend more on the specific MP at these low concentrations than the background DOM matrix, probably because the same conditions existed within each pilot column and PD-RSSCT pair. Averaged across all tests, the standard deviation for 68 Y values was about ±0.1. Y is also independent of GAC particle size as long as the pilot and PD-RSSCT are run with the same GAC. Therefore Y values can be obtained using only two PD-RSSCTs at different particle sizes, further expediting the process of GAC adsorption predictions.

Two predictive relationships for were presented for Y and $BV_{10\%,full\text{-}scale}$. The predictive relationship for Y was based on the ratio of the initial MP concentration to the DOC_0 concentration, bed volumes to 10% MP breakthrough in the PD-RSSCT, and MP pH-dependent

octanol-water partition coefficient. These parameters represent both the specific MP and background DOM matrix. The relationship was verified by adequately predicting full-scale GAC breakthrough for six MPs from a utility on the Ohio River. The predictive relationship for $BV_{10\%,full\text{-}scale}$ was based directly on the corresponding $BV_{10\%,PD\text{-}RSSCT}$ values. The relationship closely predicted $BV_{10\%,full\text{-}scale}$ values for four of the six MPs from a Ohio River utility. This relationship also establishes that MPs in the PD-RSSCT break through later by an average factor of 3.0±1.2 compared to the full-scale.

Chapter 5
Effect of Background DOM Matrix on Organic Micropollutant Adsorption

5.1 Introduction

Granular activated carbon (GAC) has potential for the control of organic micropollutants (MPs) in drinking water treatment settings (Westerhoff et al. 2005, Snyder et al. 2007, Stackelberg et al. 2007, Rossner et al. 2009, Chowdhury et al. 2010, Cardenas 2011, Corwin and Summers 2012, Reinert 2013). However, adsorption by GAC is not selective for MPs as background dissolved organic matter (DOM), which is ubiquitous in all waters from either natural or anthropogenic sources, is also removed.

DOM covers a large range of molecular weights (MW), as it is comprised of humic substances (humic and fulvic acids), non-humic substances, wastewater effluent organic matter, and synthetic organic compounds. Along with MPs, DOM adsorbs in GAC micropores (d_{pore}<20 Å) but due to size exclusion (Summers and Roberts 1988b) some portions of DOM are limited to adsorption in the mesopores (20 Å<d_{pore}<500 Å) and macropores (d_{pore}>500 Å). Typical radii of gyration for humic and fulvic acids range from 4.7 Å to 33 Å (Thurman et al. 1982). Humic substances have been shown to be effectively irreversibly adsorbed due to both multi-segment attachment to the GAC surface and the constant presence of DOM in bulk solution which reduces the driving force for desorption (Summers and Roberts 1988a). Therefore background DOM permanently reduces both adsorption capacity and kinetics for MPs through the mechanisms of direct site competition and pore blockage, collectively termed fouling.

Fouling mechanisms are still not completely understood for GAC adsorbers. Several researchers have attempted to elucidate the competitive effects of DOM size fractions using isotherms, powdered activated carbon (PAC), and PAC/membrane flow-through systems (Carter et al. 1992, Newcombe et al. 1997, Kilduff et al. 1998, Li 2003, Li et al. 2003). Using the

constant diffusivity design of the rapid small-scale column test (RSSCT), Matsui et al. (2002) looked at the effects of preloaded DOM that was coagulated and ultrafiltered on intermittent herbicide exposure at μg/L concentrations. To-date no published work, to our knowledge, has studied DOM size fractions in flow-through GAC systems on the simultaneous MP and DOM loading, where MPs are at ng/L concentrations. Compared to batch systems, GAC is subject to time-dependent DOM preloading deeper in the bed and different driving forces for MP and DOM adsorption. In a batch system the carbon is exposed to higher liquid phase MP and DOM concentrations that decrease with time due to adsorption. In flow-through systems GAC is exposed to lower liquid phase MP and DOM concentrations that increase with time as the mass transfer zones travel through the bed.

There is a consensus among several studies that lower MW DOM or model compounds reduce adsorption capacity through direct site competition (Newcombe et al. 1997, Matsui et al. 2002, Li et al. 2003). It could also be expected that if total background MP concentrations were high enough; target MP adsorption capacity would also decrease from direct site competition. Competition between MPs is closely related to linear isotherm behavior where adsorption capacity is proportional to the initial MP concentration (Knappe et al. 1998, Graham et al. 2000).

Li (2003) and Li et al. (2003) attributed slowed adsorption kinetics, but not reductions in adsorption capacity, to pore blockage. Successful adsorption modeling studies have continued with the assumption that pore blockage, internal or external, only affects adsorption kinetics (Ding et al. 2006, Schideman et al. 2006). Other studies have suggested pore blockage causes significant reductions in adsorption capacity (Carter et al. 1992, Kilduff et al. 1998a, Corwin and Summers 2010). Pore blockage is expected to have a greater effect on adsorption capacity for GAC relative to PAC because a blocked pore in a GAC particle (d_p~1 mm) would have relatively

more surface area behind it compared to a PAC particle (d_p~0.01 mm). Kilduff et al. (1998b) suggested the mechanism of fouling depends on the target contaminant concentration, where direct site competition dominates at low contaminant concentrations and pore blockage dominates at high contaminant concentrations. MPs are defined by their low liquid phase concentrations, thus direct site competition is expected to be the dominant fouling mechanism.

The objectives of this research were to investigate the impact of DOM MW and type on MP adsorption capacity and kinetics. The RSSCT was used to simulate full-scale EBCTs of 4, 7, and 10 minutes with the target MPs 2-methylisoborneol (MIB) and warfarin (WFN).

5.2 Materials and Methods

5.2.1 Materials

5.2.1.1 Waters

The influent water quality for the five surface waters is shown in Table 5.1. To eliminate the effect of the background DOM matrix concentration, the influent dissolved organic carbon (DOC_0) was held constant across all tests at 4 mg/L. Ionic strength, measured as conductivity, and pH were also held constant across all tests to eliminate the effects these parameters on DOM charge and size (Cornel et al. 1986, Summers and Roberts 1988b). For all waters conductivity and pH values ranged from 117 to 121 μS/cm and 7.1 to 7.5, respectively. Ionic strength was adjusted using sodium chloride (Mallinckrodt Chemicals, St Louis, MO). Sufficient alkalinity, 8 to 35 mg/L as $CaCO_3$, was measured in each water to ensure stable pH.

All waters were made by spiking reverse osmosis (RO) membrane isolated DOM into RO-treated tap water. The DOM was isolated using a RO system (Dow FILMTEC LE-4040) from a high organic content and low alkalinity surface water source from Big Elk Meadows (BEM), CO after filtration through a 25 μm cartridge filter (Pentek DGD-7525-20). Tap water

was treated using a two-stage RO system (Merlin TLC-350 IND) following pretreatment using sediment (Pentek P5), carbon (Pentek RFC-BB), and RO pre-filters (Merlin 1237460). The DOM extract had a DOC concentration of 76 mg/L. The extract was spiked into RO-treated tap water to target DOC_0 of 4 mg/L and was designated as BEM.

The same extract was used to create two DOM size fractions using an ultrafiltration (UF) membrane with a 1,000 Da nominal molecular weight cutoff. Nominal is emphasized here because the nature of DOM is complex. The value of 1,000 Da is calibrated with proteins and cannot be taken as a true MW cutoff for DOM (Newcombe et al. 1997, Matsui et al. 2002). Two DOM size fractions were made using the UF membrane, <1,000 Da and >1,000 Da, and were spiked separately into RO-treated tap water to target DOC_0 concentrations of 4 mg/L. These two waters were designated as <1K and >1K.

The same extract was also used to create a coagulated water. Coagulation (~100 mg/L) of the DOM extract using aluminum sulfate (Macron Fine Chemicals) removed 10 to 20% of the DOC followed by filtration through a 0.45 μm cartridge filter (Memtrex MNY941CGS). The coagulated extract was spiked into RO-treated tap water to target a DOC_0 concentration of 4 mg/L. The coagulated water had two versions, one with only two MPs and one with 30 MPs, designated as CB and CBMP respectively.

Table 5.1. Average influent water quality parameters with weight average and number average molecular weights (MW_w and MW_n, respectively).

Water	Treatment of DOM Extract	DOC (mg/L)	$SUVA_{254}$ (L/mg/m)	MW_w (Da)	MW_n (Da)
<1K	Ultrafiltration permeate	4.0±0.1	2.2	940	310
BEM	Dilution only	4.0±0.2	2.5	1,200	380
>1K	Ultrafiltration retentate	4.1±0.1	2.7	1,600	1,700
CB	Coagulation	4.1±0.2	2.1	1,000	360
CBMP	Coagulation w/ MPs added	4.1±0.2	2.0	1,000	360

5.2.1.2 Adsorbents

All of the RSSCTs were run with virgin Norit 1240, a 12x40 US standard mesh bituminous-based GAC. Bituminous GAC is common in drinking water treatment for controlling DOM and MPs (Summers et al. 2011). GAC was ground to a log-mean particle diameter of 0.11 mm (100x200 US Standard mesh). Approximately, Norit 1240 has a total surface area of 902 m^2/g, micropore (d_{pore}<20 Å) volume of 0.323 cm^3/g, and mesopore (20 Å<d_{pore}<500 Å) volume of 0.164 cm^3/g (Mezzari 2006).

5.2.1.3 Adsorbates

The relevant properties and influent concentrations of the target MPs MIB and WFN are shown in Table 5.2. MIB is a common algal metabolite that causes taste and odor issues for many water utilities and WFN is the most commonly used oral anticoagulant in North America (Holbrook et al. 2005). At pH 7 MIB is neutral and WFN is negatively charged. Target MPs were radiolabeled (^{14}C-methyl MIB and ^{3}H-ring WFN) from American Radiolabeled Chemicals, Inc. Separate stock solutions in deionized water (Barnstead Nanopure) were pure radiolabeled MIB and 0.8% radiolabeled WFN that was diluted with cold WFN (Sigma-Aldrich). Specific activities for MIB and WFN were 55 and 150 mCi/mmol, respectively.

Table 5.2. Relevant properties and influent concentrations for MIB and WFN.

Parameter[a]	2-Methylisoborneol (MIB)	Warfarin (WFN)
Type	Taste and odor	Blood anticoagulant
Radiolabeled	^{14}C-methyl	^{3}H-ring
C_0 (ng/L)[b]	107±3	100±6
MW (Da)	168	308
pK_a	15.43	4.50
log D (pH 7)	2.93	0.67

[a]pK_a and log D (log K_{ow} at pH 7) from SciFinder® (American Chemical Society). [b]Averaged over all tests (n=5).

In addition to spiking radiolabeled MIB and WFN into CBMP, a total of 27 environmentally relevant MPs were also spiked (see Appendix Table A.20). These non-radiolabeled MPs included pharmaceuticals, personal care products, herbicides, insecticides, and a manufacturing additive chosen from occurrence studies of surface drinking water sources (Kolpin et al. 2002, Focazio et al. 2008). These MP influent concentrations were based on the median concentrations from the same studies, detection limits, and a goal to be able to detect the onset of breakthrough at effluent concentrations that correspond to 2.5 to 10% of the influent concentration. All MPs were purchased from Sigma-Aldrich, with three exceptions. 2,4-D was purchased from Acros Organics (New Jersey, US), iopromide was purchased from U.S. Pharmacopa (Rockvill, MD), and simazine was purchased from Alfa Aesar (Ward Hill, MA). These MP concentrations were estimated from a RSSCT that was run for the City of Aurora with the Chapter 3 and Chapter 4 MP cocktail. The analysis of these MPs was conducted by high performance liquid chromatography-tandem mass spectrometry (LC/MS-MS) at the Center for Mass Spectrometry at the University of Colorado at Boulder (Ferrer et al. 2010). The total MP concentration in CBMP was estimated to average 3.0±0.9 µg/L, less than 0.1% of any influent DOC concentration.

5.2.2 Methods

5.2.2.1 Analytical Methods

5.2.2.1.1 Micropollutant Analysis

Radiolabeled ^{14}C MIB and ^{3}H WFN allowed for simultaneous quantification on a Packard Tri Carb 2300 liquid scintillation analyzer with a 20 minute counting time. Samples consisted of 4 mL of the water sample and 16 mL of Ultima Gold scintillation cocktail in 20 mL polyethylene vials. Standard curves ($R^2 \geq 0.94$, see Appendix Figure A.2) were run with concentrations of MIB and WFN ranging from 0 to 200 ng/L to obtain scintillation counting efficiencies. Method detection limits for MIB and WFN were 19 and 8 ng/L, respectively. Average standard deviations were ±1 ng/L based on duplicate analyses.

5.2.2.1.2 Dissolved Organic Carbon, Ultraviolet Absorbance, Conductivity, pH, and Alkalinity

Dissolved organic carbon (DOC) was measured with a Shimadzu TOC-V CSH analyzer in accordance with Standard Method 5310B (APHA et al. 2005). Ultraviolet absorbance (UVA_{254}) was analyzed at a wavelength of 253.7 nm using a Hach DR 4000 spectrophotometer in accordance with Standard Method 5910 (APHA et al. 2005). pH was measured using a Denver Instruments Model 220 pH meter in accordance with Standard Method 4500-H^+ (APHA et al. 2005). Conductivity was measured using a Hanna portable conductivity meter (HI 991300) in accordance with Standard Method 2510B (APHA et al. 2005). Alkalinity was measured using a Hach Digital Titrator (16900-01) in accordance with Standard Method 2320 (APHA et al. 2005).

5.2.2.2 Rapid Small-Scale Column Test Design and Operation

All RSSCTs were designed according the proportional diffusivity (PD) design approach, as it has been successful for simulating full-scale DOM removal (Crittenden et al. 1991,

Summers et al. 1995, USEPA 1996). PD-RSSCTs were designed to simulate full-scale EBCTs of 4, 7, and 10 minutes.

Fresh bituminous GAC was carefully ground using a mortar and pestle while minimizing the production of fines. The 100x200 mesh size fraction was obtained using US standard sieves and a sieve shaker. Prior to use the carbon was rinsed with deionized water to remove fines, dried at 105°C, and stored in amber glass vials in a desiccator. Crushed GAC was then placed in 4.76 mm ID PTFE columns based on a hydraulic loading rate of 6.7 m/h (2 mL/min). The aspect ratios for the columns were 43, which is greater than the 8 to 10 necessary to avoid wall effects on mass transfer (Knappe et al. 1999).

Spiked influent water was fed to the columns from well-mixed 20 L glass carboys through stainless steel and PTFE tubing using a Cole-Parmer PTFE diaphragm pump. Paired influent and effluent MP samples were collected before and after the columns. A needle valve was used for flow control to maintain the desired EBCT during sampling. Influent and effluent DOC and UVA_{254} samples were taken daily at the beginning of the run. After complete DOC breakthrough, UVA_{254} was used for measurements of DOM. Strong relationships were observed between DOC and UVA_{254} ($R^2 \geq 0.95$) for all waters.

5.2.2.3 Adsorption Modeling

Adsorption capacity and kinetic information in the form of Freundlich adsorption capacity parameters (K) and diffusion coefficients (D) was obtained by curve fitting using the pore and surface diffusion model (PSDM using AdDesignS™ from Michigan Technological University, Houghton, MI). Due to the presence of significant background DOM in all waters, the PSDM modeling approach followed that of Corwin and Summers (2011) where the following initial assumptions were made: (1) surface diffusion was negligible, (2) pore diffusion controlled

mass transfer, (3) pore diffusion Biot numbers for MIB and WFN were high (>30), indicating film diffusion was negligible, and (4) isotherm behavior was linear, or the Freundlich adsorption intensity parameter, 1/n, was effectively equal to one. Freundlich K ((μmol/g)*(L/μmol)$^{1/n}$) values from the PSDM were essentially the same as K^* (L/g) values. K^* is defined by Corwin and Summers (2011) and is shown in Equation 5.1, where $BV_{50\%}$ is the bed volumes to 50% MP breakthrough and ρ_{bed} is the GAC bed density.

$$K^* = \frac{BV_{50\%}}{\rho_{bed}} \tag{5.1}$$

5.2.2.4 Fractionation and Size Exclusion Chromatography

The <1,000 Da DOM extract size fraction (<1K concentrate) was obtained after running approximately 100 L of the DOM extract through a 1,000 Da nominal molecular weight cutoff UF membrane (0.1 m^2 Pellicon 2 Mini Ultrafiltration Module P2PLACC01). Prior to use the membrane was cleaned according to the manufacturer's specifications. DOM extract was fed to the UF membrane in a tangential flow membrane holder (Pellicon 2 Mini filter holder XX42 PMI NI) using an external gear pump at a feed pressure of 60 psi. The UF system was operated in batch mode, where the retentate was also the feed. Permeate flow was about 2% of the retentate flow. After filtration the <1K concentrate had a DOC concentration of 22 mg/L and the retentate had a concentration of 220 mg/L. There was about 10% mass loss in the UF membrane.

The >1,000 Da DOM size fraction (>1K concentrate) was obtained by cleaning the retentate (DOC of 220 mg/L). This was accomplished by using deionized water to dilute 10 L of the retentate up to a total volume of 40 L. The diluted 40 L was then recirculated through the UF membrane system to remove any remaining <1,000 Da DOM through the permeate until the feed/retentate was the original volume of 10 L. The final retentate (>1K concentrate) had a DOC

concentration of 147 mg/L, indicating significant DOM had passed through the membrane during cleaning. However, a portion of DOM that could have potentially passed through the filter was likely retained in the >1K fraction.

Although small, differences in MW distributions (MWD) for <1K, BEM, >1K, and CB were confirmed using size exclusion chromatography (SEC). The SEC chromatograph is shown in the Appendix (Figure A.1), and confirmed the UF membrane and coagulation preferentially removed larger MW DOM. CBMP was assumed to have the same MWD as CB. SEC was performed using an Agilent 1200 series high performance liquid chromatograph with a Protein-Pak™ 125 7.8 x 300 mm column (Waters Corporation). The detector was an Agilent diode array that monitored UVA_{254}. The mobile phase buffer consisted of 0.0024 M NaH_2PO_4, 0.0016 M Na_2HPO_4, and 0.025 M $NaSO_4$ at a flow rate of 0.7 mL/min. A calibration curve was generated using polystyrene sulfonates with MWs ranging from 210 to 17,000 Da and a linear relationship between the logarithm of MW and the retention time was found (R^2=0.92, see Appendix Figure A.3). Weight (MW_w) and number averaged (MW_n) MWs were determined using the absorbance and MW estimated from the calibration curve at the corresponding elution time. These values are shown in Table 5.1.

5.3 Results and Discussion

5.3.1 Dissolved Organic Carbon Breakthrough

The breakthrough curves for DOC in waters <1K, BEM, >1K, and CB are shown in Figure 5.1 at a full-scale EBCT of 4 minutes. DOC breakthrough for CBMP was visually the same as CB, but a large difference in absorbability was found between the two size fractions with >1K being the least adsorbable and <1K being the most adsorbable. Solid phase concentrations of DOM typically increase with decreasing molecular size, a result of size

exclusion because smaller DOM has access to more surface area in smaller pores (Summers and Roberts 1988b). Aiken et al. (1979) also witnessed size exclusion of fulvic acid using five different XAD resins with pore diameters ranging from 50 to 250 Å. Size exclusion of larger DOM in >1K also implies increased potential for blocked pores. In addition to DOM size, charge most likely contributed to the adsorbability of the DOM size fractions. At neutral pH DOM is mostly negatively charged mainly from deprotonated carboxylic functional groups (Thurman et al. 1982). Therefore during ultrafiltration both the negative charge of the cellulose UF membrane and attached DOM would have repelled DOM in the feed flow, resulting in a permeate DOM with relatively less charge (hydrophobic, more absorbable) and a retentate DOM with relatively more charge (hydrophilic, less adsorbable). Solid phase DOM loadings based on DOC breakthrough are shown in Table 5.3 for all waters and EBCTs at 50 and 70% breakthrough.

The adsorbability of BEM fell in between the two BEM size fractions. The DOC of the <1K DOM concentrate was about 22 mg/L while the DOC of the BEM concentrate was about 76 mg/L, or 29% of the original BEM-DOM extract water was nominally smaller than 1,000 Da and 71% was nominally larger than 1,000 Da. Despite the majority of BEM being nominally larger than 1,000 Da, the breakthrough more closely matches that of <1K. For comparison a composite DOC curve was generated from the <1K and >1K breakthrough curves. The calculated composite curve represents the expected breakthrough of BEM based on the assumption that 33% of the DOM in BEM was less than 1000 Da and 67% of the DOM in BEM was greater than 1,000 Da. The estimates were adjusted from 29 and 71% due to the fact that the cleaning procedure did not remove all the DOM less than 1,000 Da in the >1K concentrate. The composite breakthrough curve confirms the BEM DOC breakthrough curve showed stronger adsorbability than would be expected from the size fractions present in BEM.

One explanation may be that the greater than 1,000 Da DOM size fraction in BEM is smaller than the greater than 1,000 Da DOM size fraction in >1K. During ultrafiltration the ionic strength of the retentate, which was used to create the >1K concentrate, decreased with time because small ions could have passed through the UF membrane. Decreasing ionic strength would have increased the average size of the retentate DOM that much more (Cornel et al. 1986), and may not have returned to the expected average size when the ionic strengths were adjusted in RO-treated tap water before testing.

Using isotherms, Summers and Roberts (1988b) also found unfractionated humic acid to behave like smaller humic acid fractions at liquid phase DOC concentrations similar to this study (>4 mg/L). Conversely, using peat fulvic acid, Lee et al. (1981) found the unfractionated and >50K fraction to have similar isotherm adsorption capacity, while the <1K fraction exhibited the most adsorption capacity. However, as previously discussed, extending isotherm behavior to flow-through GAC adsorbers can be difficult because of the different driving forces and loading conditions.

The adsorbability of CB also fell in between the two size fractions. Coagulation is known to preferentially remove large molecular weight and hydrophobic (humic) DOM (Semmens et al. 1986, Hooper et al. 1996). Removal of the hydrophobic DOM would result in overall less adsorbable DOM, however CB adsorbability seems to have characteristics of both <1K and BEM, probably due to the smaller MWD following coagulation.

Breakthrough trends in Figure 5.1 were also true for UVA_{254} breakthrough and at the longer EBCTs of 7 and 10 minutes. DOC breakthrough at the longer EBCTs is shown in the Appendix (Figure A.4 through Figure A.6). Although small, as shown in Table 5.3, most waters

showed systematically later breakthrough or larger DOM loading with increasing EBCT, which was expected for coagulated waters (Zachman and Summers 2010).

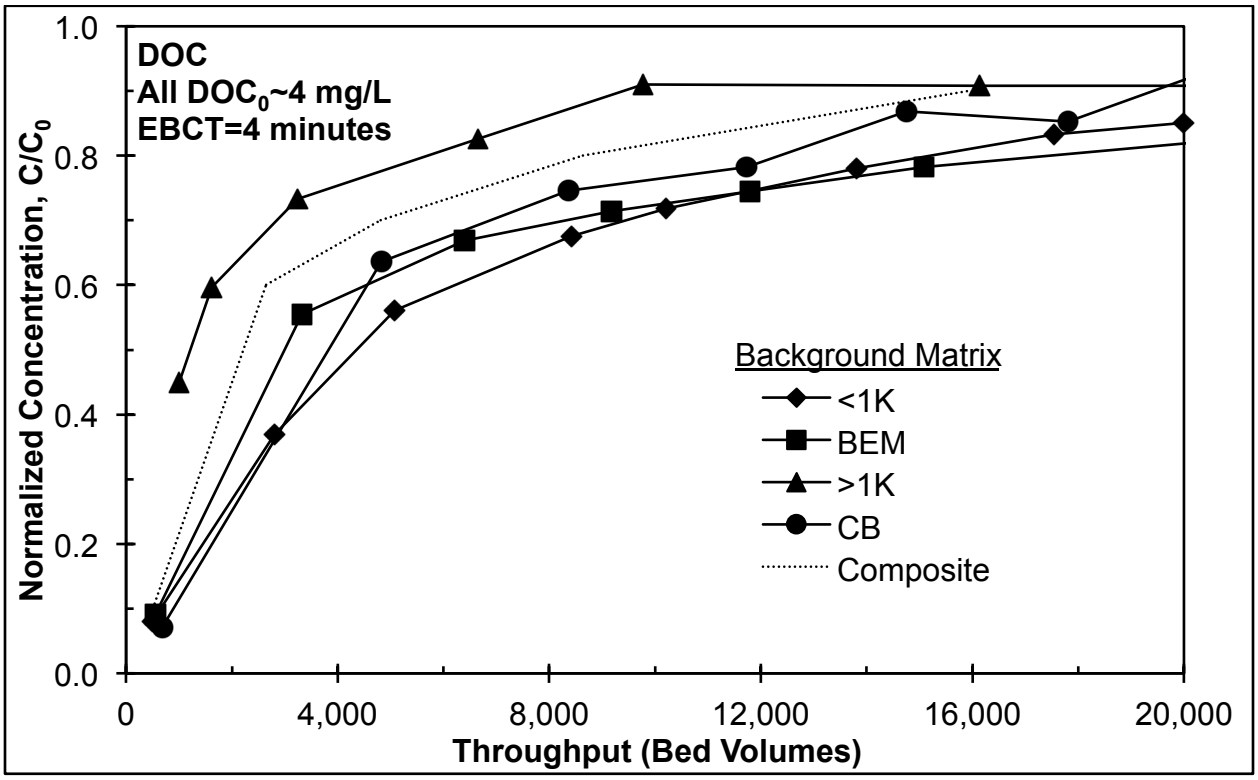

Figure 5.1. DOC breakthrough curves for waters <1K, BEM, >1K, and CB at a full-scale EBCT of 4 minutes. Calculated composite curve based on a BEM water with 33% of the DOM less than 1,000 Da and 67% greater than 1,000 Da.

Table 5.3. Solid phase DOM loadings based on DOC breakthrough for all waters and EBCTs.

Water	EBCT	$BV_{50\%}$[a]	$q_{50\%}$ (μg DOC/mg GAC)	$BV_{70\%}$[a]	$q_{70\%}$ (μg DOC/mg GAC)
<1K	4	4,500	25	9,500	41
	7	5,000	29	10,000	46
	10	5,900	33	12,000	55
BEM	4	3,000	15	8,000	32
	7	4,500	25	8,400	37
	10	4,500	28	8,100	39
>1K	4	1,200	6	3,000	11
	7	1,600	9	3,500	14
	10	2,200	13	4,500	20
CB	4	3,900	20	7,000	29
	7	3,500	18	7,900	33
	10	4,000	26	6,300	33
CBMP	4	3,000	16	6,000	23
	7	4,000	25	6,000	32
	10	4,000	28	5,500	32

[a]BV – bed volumes to 50 and 70% DOC breakthrough.

5.3.2 Micropollutant Adsorption Capacity

5.3.2.1 Effect of DOM Type

If MP adsorption capacity were strongly related to DOM loading, which has been shown for unfractionated waters and MIB (Summers et al. 2013), then based on the DOC breakthrough curves shown in Figure 5.1 and the overall DOM loadings in Table 5.3 MIB and WFN would breakthrough noticeably earlier in <1K compared to >1K, and MIB and WFN would yield similar breakthrough in <1K, BEM, and CB. However, MIB breakthrough was less correlated to DOC breakthrough or DOM loading than expected, and was more pronounced than the differences in DOC breakthrough curves. The time scale (in bed volumes) is much larger for MIB breakthrough shown in Figure 5.2 at the same full-scale EBCT of 4 minutes.

In Figure 5.2, the <1K fraction reduced the GAC adsorption capacity or fouled the most and >1K fraction fouled the GAC the least. Compared to MIB breakthrough in BEM, this caused earlier breakthrough of MIB in <1K and later breakthrough of MIB in >1K. Quantitatively using

K^* values, <1K exhibited 59% less capacity for MIB compared to BEM, while >1K exhibited 67% more capacity for MIB. Although MIB breakthrough in BEM and CB are the same at early breakthrough, CB exhibited 21% less capacity for MIB compared to BEM. Similar results were seen with the more strongly adsorbing WFN, shown in the Appendix (Figure A.7). Bulk DOM loading (measured using DOC) has been established as a poor indicator of fouling mechanisms (Carter and Weber 1994, Corwin and Summers 2010, Matsui et al. 2012).

Thus, preferentially selecting for smaller MW DOM using ultrafiltration resulted in highly competitive DOM for the adsorption of MIB and WFN such that adsorption capacity was significantly reduced, consistent with the findings of others (Newcombe et al. 1997, Matsui et al. 2002; Li et al. 2003). The effect was exaggerated by the low concentrations of MIB and WFN, which significantly reduced the ability for them to compete for adsorption sites (Najm et al. 1991, Kilduff et al. 1998b). As previously mentioned charge was also responsible for DOM adsorption behavior where the smaller MW DOM (UF permeate) was most likely more hydrophobic and the larger MW DOM (UF retentate) was most likely more hydrophilic. Although hydrophobic DOM would be expected to decrease MP adsorption capacity more than hydrophilic DOM, Wigton and Kilduff (2004) showed the same effect of the two DOM types on reducing trichloroethylene adsorption capacity, and concluded small DOM size was the major cause for adsorption capacity reductions.

Interestingly, coagulation also reduced MIB and WFN adsorption capacity through the removal of larger DOM compounds, resulting in smaller and more competitive DOM, consistent with Matsui et al. (2002) for the herbicide simazine. Additionally, in agreement with Wigton and Kilduff (2004), similar competitive behavior between small hydrophobic and hydrophilic DOM is supported by MIB and WFN breakthrough in CB. Following coagulation, the DOM in CB

would have been more hydrophilic in nature, yet the background matrix still reduced the adsorption capacity for MIB and WFN relative to BEM. Deciding to run the PD-RSSCTs at equal DOC concentrations yielded higher concentrations of the smaller DOM fraction in CB. Such a scenario has little bearing on water treatment though, as coagulation selectively removes the large DOM fraction yielding a lower DOC concentration with the smaller DOM fraction remaining the same, thus overriding the negative effects of coagulated DOM's potentially competitive nature (Hooper et al. 1996).

Further illustrating the differences in adsorption capacity, the throughput in bed volumes to 10, 20, and 50% breakthrough of WFN in waters <1K, BEM, >1K, and CB at a longer full-scale EBCT of 7 minutes is shown in Figure 5.3. For <1K, BEM, and >1K, strong linear relationships ($R^2 \geq 0.97$) showed a correlation between increased bed volumes to 10, 20, and 50% MIB and WFN breakthrough with increasing DOM size (MW_w from Table 5.1). In other words, MP adsorption capacity was inversely proportional to DOM size. CB exhibited more adsorption capacity for MIB and WFN than expected from these relationships, reducing the goodness of fit (decrease in R^2 to 0.80-0.90).

DOM size alone may not be the best indicator of fouling. Not all small DOM fractions translate to increased MP competition, demonstrated by the nonadsorbable, non-UVA_{254} absorbing fraction of DOM (10-20%) in most surface waters (Summers et al. 2011). Hooper et al. (1996) observed the least adsorbable (first to breakthrough) DOM fraction after coagulation was the <0.5K Da fraction. From capacity analysis alone it is difficult to discern whether the fouling mechanism is direct site competition or pore blockage. However, such a dramatic decrease in MP adsorption capacity in <1K relative to the other waters and the fact that MIB and WFN adsorption capacity increased in >1K compared to BEM lends itself to increased direct site

competition with the <1K matrix. Alternatively, small DOM in <1K could also have caused pore blockage in the GAC micropores. Despite the clear differences in the MIB and WFN breakthrough curves in the different waters, specific competitive mechanisms are difficult to elucidate with such complex background DOM matrices and small differences in MW (Table 5.1).

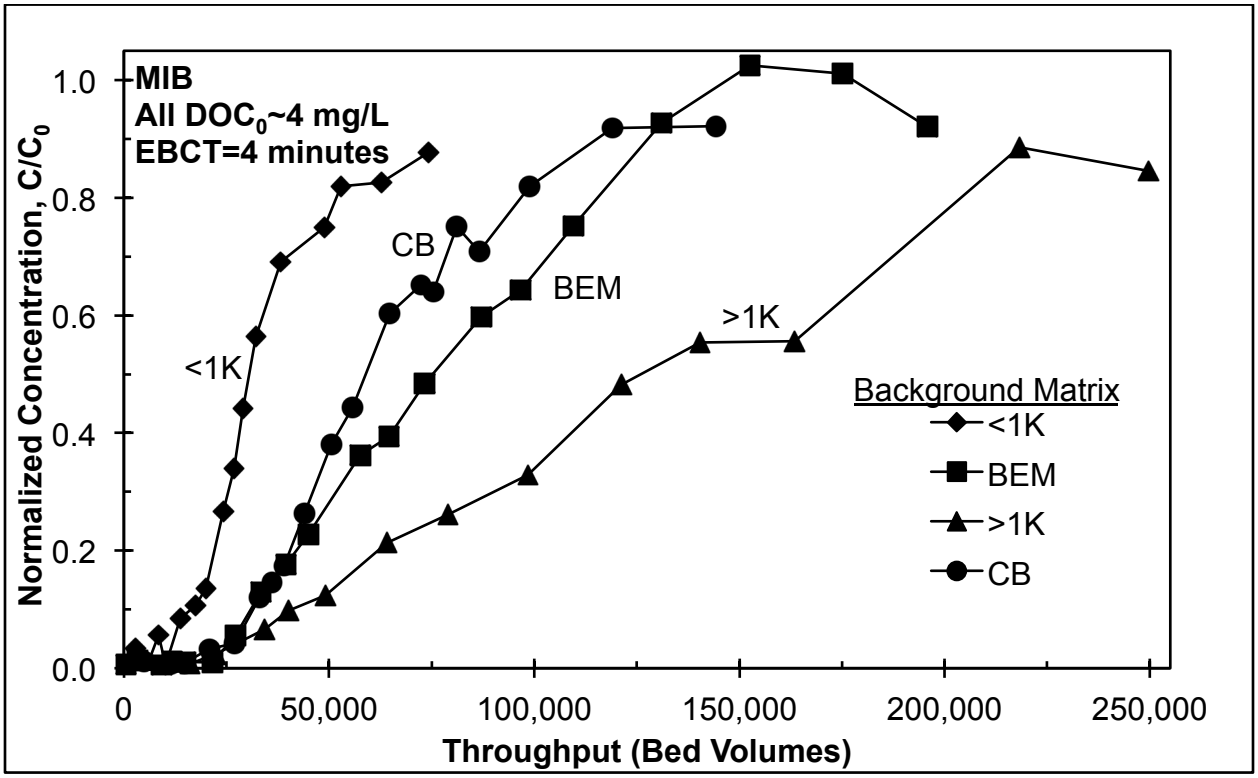

Figure 5.2. Breakthrough curves for MIB in <1K, BEM, >1K, and CB at a full-scale EBCT of 4 minutes.

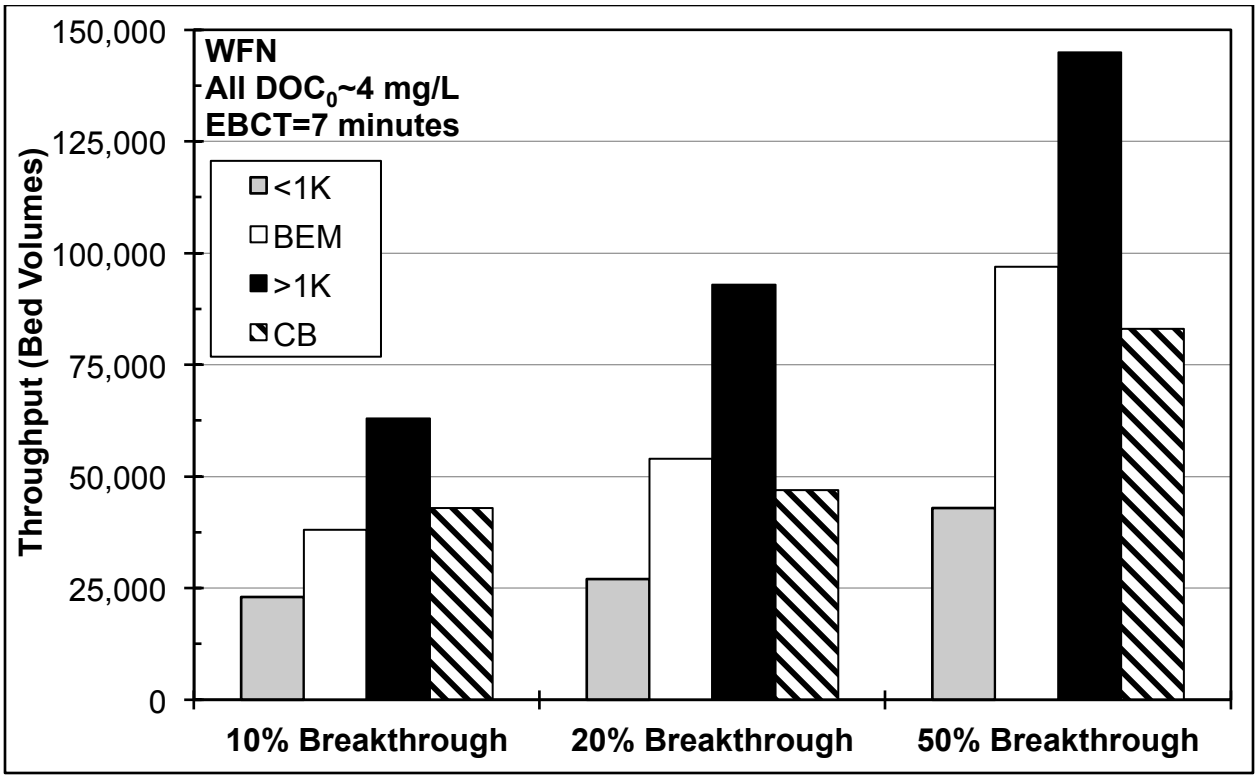

Figure 5.3. Bed volumes to 10, 20, and 50% breakthrough for WFN in <1K, BEM, >1K, and CB at a full-scale EBCT of 7 minutes.

5.3.2.2 Effect of Empty Bed Contact Time

The relationships between breakthrough curves illustrated in Figure 5.2 and Figure 5.3 were the same for MIB and WFN at EBCTs of 4, 7, and 10 minutes (see Appendix Figure A.7 through Figure A.11). The breakthrough of WFN in >1K at full-scale EBCTs of 4, 7, and 10 minutes in Figure 5.4 shows little impact of EBCT to 10% breakthrough, and a longer EBCT yields worse performance starting at about 75,000 bed volumes for this background DOM matrix. Less efficient carbon use rates with increasing EBCT has been observed on a normalized throughput basis for atrazine, bisphenol A, erythromycin, and MIB (Knappe et al. 1997, Corwin 2010, Corwin and Summers 2012, Summers et al. 2013) in unfractionated waters.

With longer EBCTs, or increase in bed depth, a higher level of fouling from DOM is expected. The adsorption of DOM is relatively slow due to its large molecular size components

leading to a long mass transfer zone. Conversely, most MP adsorption kinetics are relatively fast (1 to 2 orders of magnitude faster) leading to well-defined short mass transfer zones that slowly migrate through the GAC bed. The adsorption of DOM in the absence of MPs deeper in the bed is termed preloading and results in significant reductions in MP adsorption capacity (Summers et al. 2011).

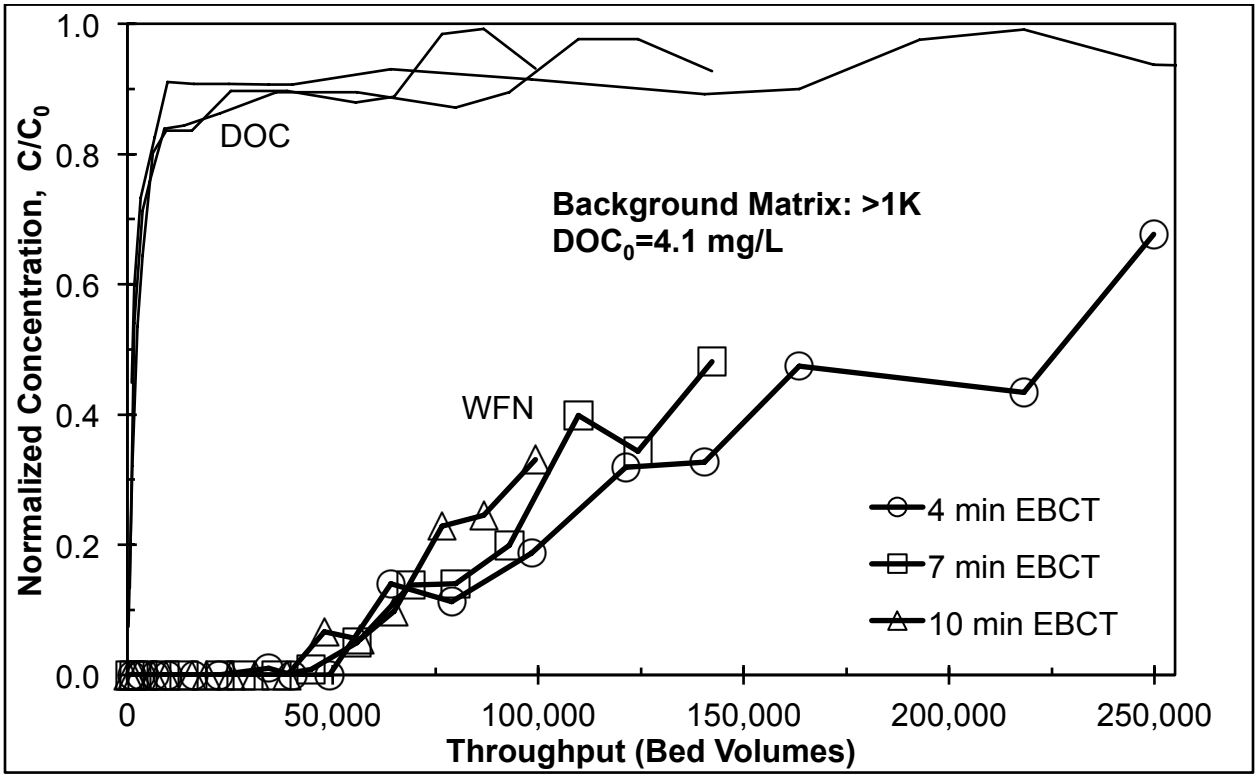

Figure 5.4. Breakthrough curves for DOC and WFN in >1K at full-scale EBCTs of 4, 7, and 10 minutes.

Similar to that shown in Figure 5.4, all waters displayed DOM preloading behavior with increasing EBCT for MIB and WFN but to different degrees. Effects of preloading with increasing EBCT can be seen in Figure 5.5 for MIB and Figure 5.6 for WFN using K^* or the apparent capacity value in each water. For breakthrough curves that were less than 50%, K^* was estimated from the PSDM model fit.

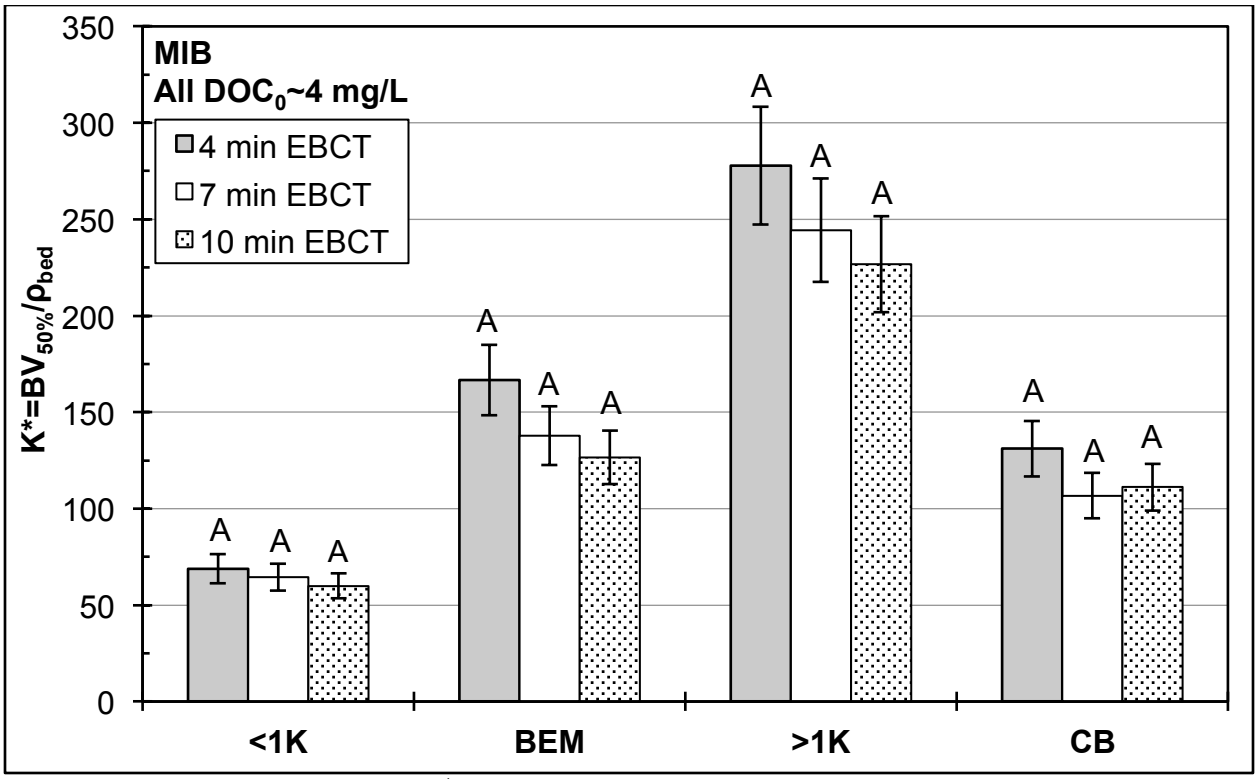

Figure 5.5. Comparison of MIB K^* values in each water at full-scale EBCTs of 4, 7, and 10 minutes. Error bars represent ±11%. K^* values that do not share a letter are significantly different at 95% confidence level. For breakthroughs <50%, K^* was estimated from the PSDM model fit.

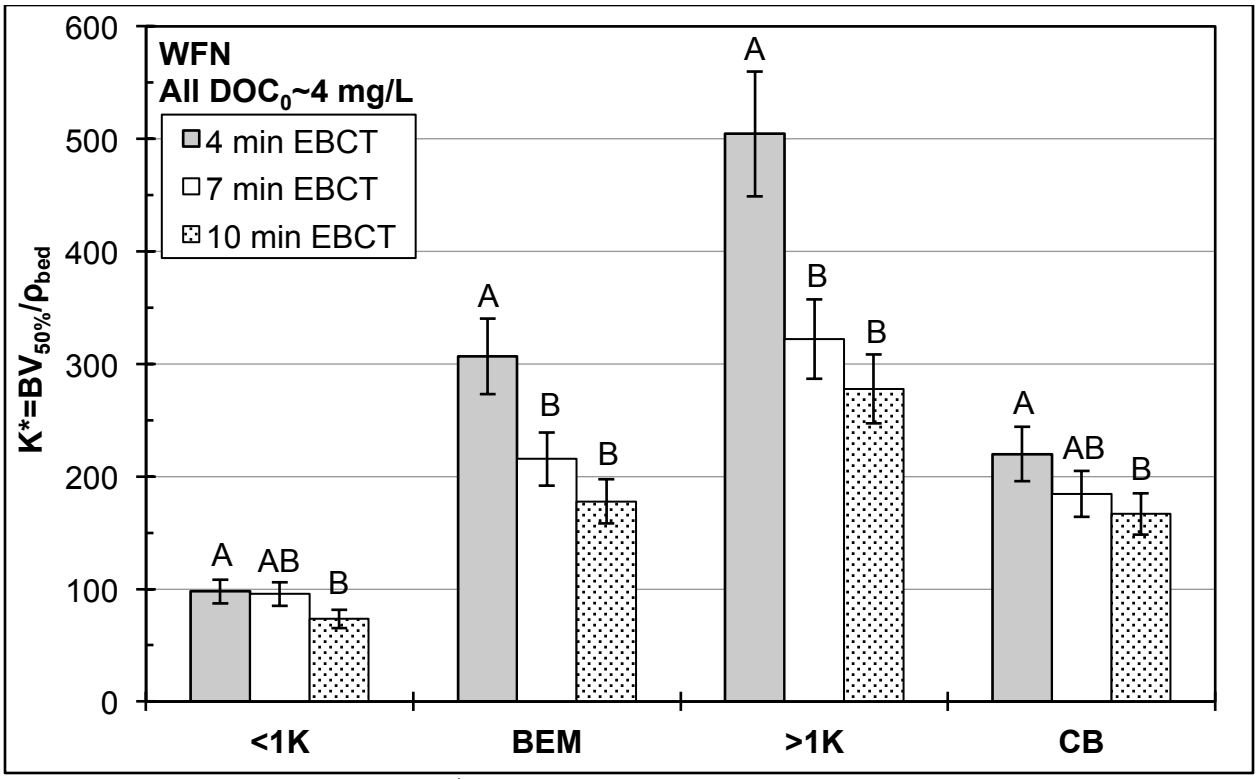

Figure 5.6. Comparison of WFN K^* values in each water at full-scale EBCTs of 4, 7, and 10 minutes. Error bars represent ±11%. K^* values that do not share a letter are significantly different at 95% confidence level. For breakthroughs <50%, K^* was estimated from the PSDM model fit.

5.3.2.2.1 Within One Water

To see if there was a significant difference between the MP breakthrough at 50% with increasing EBCT, Tukey's Test was applied to the K^* values for MIB and WFN at each EBCT in each water. However a standard deviation for K^* was required, which was difficult because K^* is not an average but a single value. To address this problem, the DOC and UVA_{254} breakthrough curves in CB and CBMP were used to establish an average percent difference. These breakthrough curves were generated using the same water and differ only by 3.0±0.9 μg/L (n=3, see Appendix Table A.20) of MPs, which is probably less than the error from spiking the DOM extract. Therefore the two sets of breakthrough curves served the purpose of representing PD-RSSCT experimental and analytical error at the midpoint of breakthrough. In fact the estimate

should be conservative because the analytical error for radiolabeled MIB and WFN was low (~1%). The average percent difference between the DOC and UVA_{254} breakthrough curves for CB and CBMP across all EBCTs was 11%. Although slightly greater, this difference agrees well with PD-RSSCT reproducibility demonstrated in Summers et al. (1995) for DOC breakthrough. The difference is most likely greater because of the limited number of data points between initial and 50% DOC breakthrough. Therefore K^* values for Tukey's Test were represented by three values at each EBCT: K^* and $K^* \pm 11\%$.

The results are shown with the letters A and B in Figure 5.5 and Figure 5.6, where K^* values that don't share a letter are significantly different at a 95% confidence level. There was no significant difference between EBCT K^* values in all waters for MIB. Therefore each EBCT exhibited approximately the same adsorption capacity for MIB in all waters. In all waters, an EBCT of 4 minutes exhibited more adsorption capacity for WFN compared to an EBCT of 10 minutes. In BEM and >1K the 4 minute EBCT exhibited more adsorption capacity for WFN compared to an EBCT of 7 minutes. In all waters, an EBCT of 7 minutes exhibited the same adsorption capacity for WFN compared to an EBCT of 10 minutes. One explanation could be WFN is more strongly adsorbing than MIB and was therefore more subject to the effects of preloading with increasing EBCT.

5.3.2.2.2 Between Waters

It is difficult to discern whether there is a difference in K^* between waters with increasing EBCT on a relative basis. The percent reductions in K^* values for EBCTs of 7 and 10 minutes relative to the 4 minute EBCT for MIB and WFN were averaged (n=2 per water). For MIB those values were 10, 21, 15, and 17% for <1K, BEM, >1K, and CB, respectively. For WFN those values were 14, 36, 41, and 20% for <1K, BEM, >1K, and CB, respectively. For example, at

EBCTs of 7 and 10 minutes, MIB exhibited 10% less capacity on average compared to an EBCT of 4 minutes in <1K. Statistical analysis using Tukey's Test revealed the percent decrease in K^* values for MIB and WFN with increasing EBCT between waters were not statistically different at a 95% confidence level.

Therefore all the waters showed similar percent reductions in adsorption capacity with increasing EBCT. Combined with the previous analysis the following general conclusions can be made: (1) MIB exhibited a single adsorption capacity in each water, independent of EBCT, and (2) WFN exhibited less adsorption capacity with increasing EBCT, but the decrease was similar across all waters. Summers et al. (2013) also observed similar adsorption capacities for MIB at EBCTs of 5, 10, and 20 minutes up to about 40% breakthrough using the PD-RSSCT in a natural water. Corwin and Summers (2011) saw larger differences in adsorption capacities for the weakly adsorbing bisphenol A at EBCTs of 5, 7.5, 10, and 17 minutes using the PD-RSSCT in a natural water.

If pore blockage reduced MP adsorption capacity more than direct site competition, it would be expected that the larger MW DOM in >1K would have an increased effect on reducing capacity with increasing EBCT. Because the decrease in adsorption capacity was not significantly different between waters, these results suggest either minimal pore blockage was occurring or pore blockage did not completely restrict MP access to the surface area behind a blocked pore.

5.3.2.3 Micropollutant Desorption

After complete or near complete breakthrough, desorption of MIB and WFN was monitored at a full-scale EBCT of 4 minutes in <1K, BEM, and >1K (see Appendix Figure A.12 and Figure A.13). At initial glance it appeared that desorption occurred much faster with

decreasing DOM size. However, when compared to the amount adsorbed, the mass desorbed over equal time intervals (~40,000 bed volumes) was about the same percent of the mass adsorbed in each water. These percentages are shown in Table 5.4 for the three waters, and match well with the amount desorbed of other MPs from GAC (Corwin and Summers 2011). Such small amounts of desorption is not likely because of irreversible adsorption but from hindered back diffusion causing slower desorption kinetics (To et al. 2008b, Corwin and Summers 2011). Less WFN desorption was observed most likely because it is more strongly adsorbed than MIB.

Table 5.4. Percent mass desorbed for MIB and WFN at an EBCT of 4 minutes. Desorbed mass was calculated over shown bed volumes.

Water	Mass Desorbed[a]		Duration of Desorption
	MIB	WFN	(Bed Volumes)
<1K	16%	7%	40,078
BEM	17%	6%	43,690
>1K	13%	4%	36,263

[a](Mass desorbed/mass adsorbed)*100%.

5.3.3 Micropollutant Adsorption Kinetics

Conclusions regarding the fouling effects of the different waters cannot be made without considering adsorption kinetics. It was assumed intraparticle mass transfer controlled adsorption kinetics and could be described by the pore diffusion coefficient, D_p (cm^2/s), shown in Equation 5.2,

$$D_p = \frac{D_L}{\tau} \tag{5.2}$$

where D_L (cm^2/s) is the diffusion coefficient for MIB or WFN in water and τ is the tortuosity or labyrinth factor. D_L was calculated using the correlation from Hayduk and Laudie (1974). In the

PSDM, tortuosity can be manually adjusted by the user to acquire a good model fit. Tortuosity accounts for pore constrictions in the GAC particle caused by adsorbed DOM, which cause a longer diffusion path length. Typical tortuosity values for GAC adsorption in natural waters range from about 1 to 20 for DOM and MPs (Sontheimer et al. 1988, Hand et al. 1989, Carter and Weber 1994, Corwin and Summers 2011). Although it was not necessary in this study, surface diffusion would theoretically be invoked for cases where $\tau \leq 1$.

Using the PSDM, a sensitivity analysis showing the effect of tortuosity on breakthrough curves is shown in Figure 5.7. Increasing tortuosity slows pore diffusion, causing increased spreading of the MTZ, which results in slower breakthrough. MIB breakthrough data in BEM at a full-scale EBCT of 7 minutes is shown to demonstrate the judgments that must be made to describe MP breakthrough kinetics using a single value for tortuosity. Over complicating the process by using more than one significant figure, varying τ with time, or using fitting algorithms (Traegner and Suidan 1989) did not seem justified considering the initial PSDM assumptions (e.g. 1/n=1, film diffusion not controlling, negligible surface diffusion). A best-fit value was chosen in each case so that comparisons could be made between waters. The MIB data in Figure 5.7 was best described using a tortuosity value of 4. Also shown in Figure 5.7, a tortuosity value of one does not provide a good fit, further confirming the absence of surface diffusion.

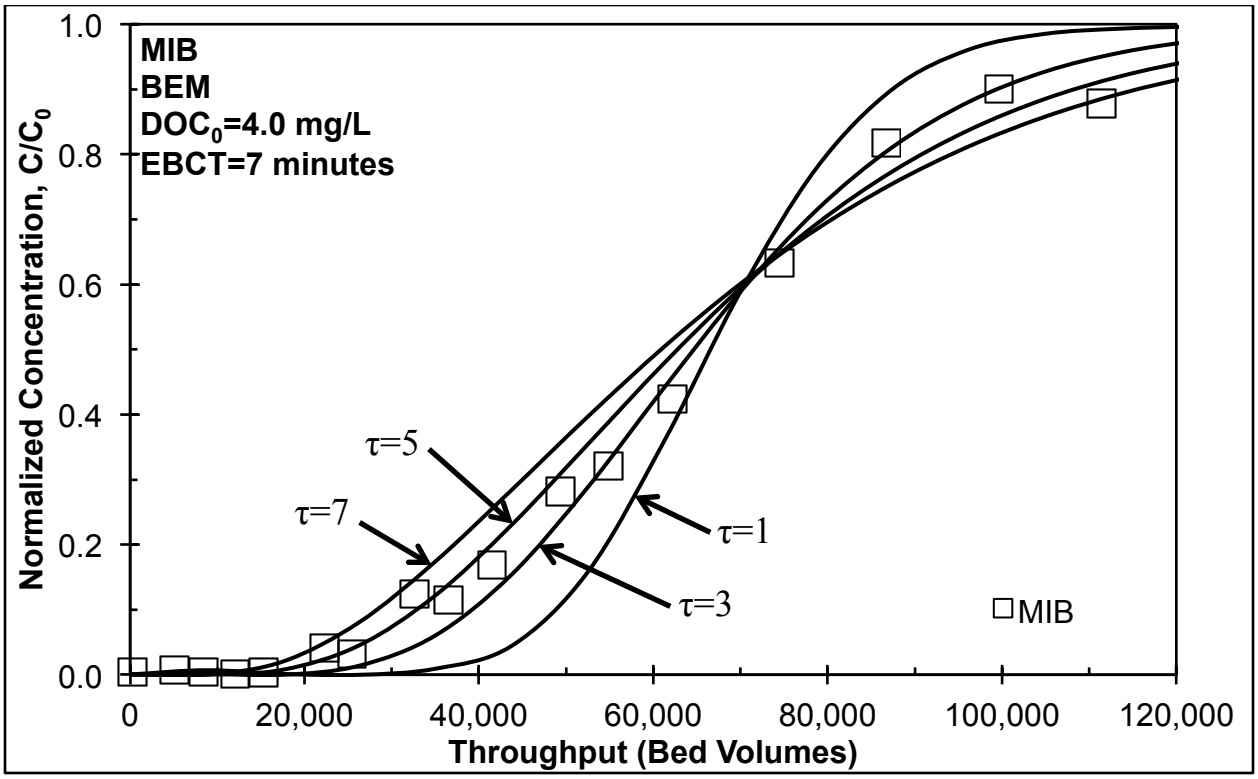

Figure 5.7. Sensitivity analysis showing the effect of tortuosity (τ) on MIB breakthrough curves using the PSDM. MIB data is in BEM at a full-scale EBCT of 7 minutes. K_{PSDM}=150 (μmol/g)*(L/μmol)$^{1/n}$ and K^*=138 L/g.

For each EBCT, tortuosity values were averaged over all four waters for MIB and WFN (n=8) to see if EBCT or preloading had an effect on tortuosity. Previous results showed longer EBCTs reduced WFN adsorption capacity. Reductions were also seen for MIB but they were deemed insignificant. Therefore it was expected tortuosity values would increase with increasing bed depth or EBCT.

Average tortuosity values were 4.8±2.4, 5.0±1.2, and 5.4±2.1 for EBCTs of 4, 7, and 10 minutes, respectively. Although this shows an increasing trend in tortuosity with EBCT, statistical analysis using Tukey's Test confirmed these differences were not significant at a 95% confidence level. The same was conclusion was made if MIB and WFN tortuosity values were analyzed separately (n=4). Knappe et al. (1999) also observed a negligible effect of preloaded

DOM on atrazine (~50 μg/L) intraparticle adsorption kinetics, attributable to the large mesopore volume of wood-based GAC and small DOM MW after advanced oxidation. Alternatively, Hand et al. (1989) saw a reduction in trichloroethylene (C_0~1,050 μg/L) surface diffusivity over a DOM preloading time of four weeks. However, the same study demonstrated a constant surface diffusivity value from four to 10 weeks of preloading. In this study the DOM must have preloaded far enough ahead of MIB and WFN to establish a relatively constant tortuous path.

Though these results were unexpected, they allowed for more robust comparisons of tortuosity between waters. Because the effect of EBCT was found to be insignificant, tortuosity values (n=6) were averaged over all EBCTs for MIB and WFN in each water. Average tortuosity values for each water are shown in Figure 5.8 and show an increase in tortuosity with increasing background DOM MW. Tukey's Test was applied again to this data set and only <1K and >1K were found to be statistically different from each other at a 95% confidence level. The average D_p was $2.5x10^{-6}\pm1.6x10^{-6}$ cm^2/s for <1K and $9.0x10^{-7}\pm1.8x10^{-7}$ cm^2/s for >1K, which shows slower adsorption kinetics on average in >1K compared to <1K by a factor of 2.8. If the same averaging is applied to the K^* values for MIB and WFN in the two waters, >1K exhibits more MP adsorption capacity on average by a factor of 3.4 compared to <1K.

An insignificant increase in tortuosity with increasing EBCT suggests that in this study tortuosity did not increase with adsorber operation time. Therefore the increased tortuosity values in >1K are more attributable to the larger MW DOM matrix than the later breakthrough of MIB and WFN, suggesting that MW DOM slows adsorption kinetics most likely through pore blockage. Even if the later breakthrough of MIB and WFN in >1K was the source of increased tortuosity values because DOM had a longer time to preload, the larger MW DOM matrix in >1K would still be the reason for the slower kinetics. Although size exclusion of large DOM

may block pores, this work suggests it is not a complete blockage, because adsorption capacity increased for MIB and WFN compared to the unfractionated background DOM matrix, BEM.

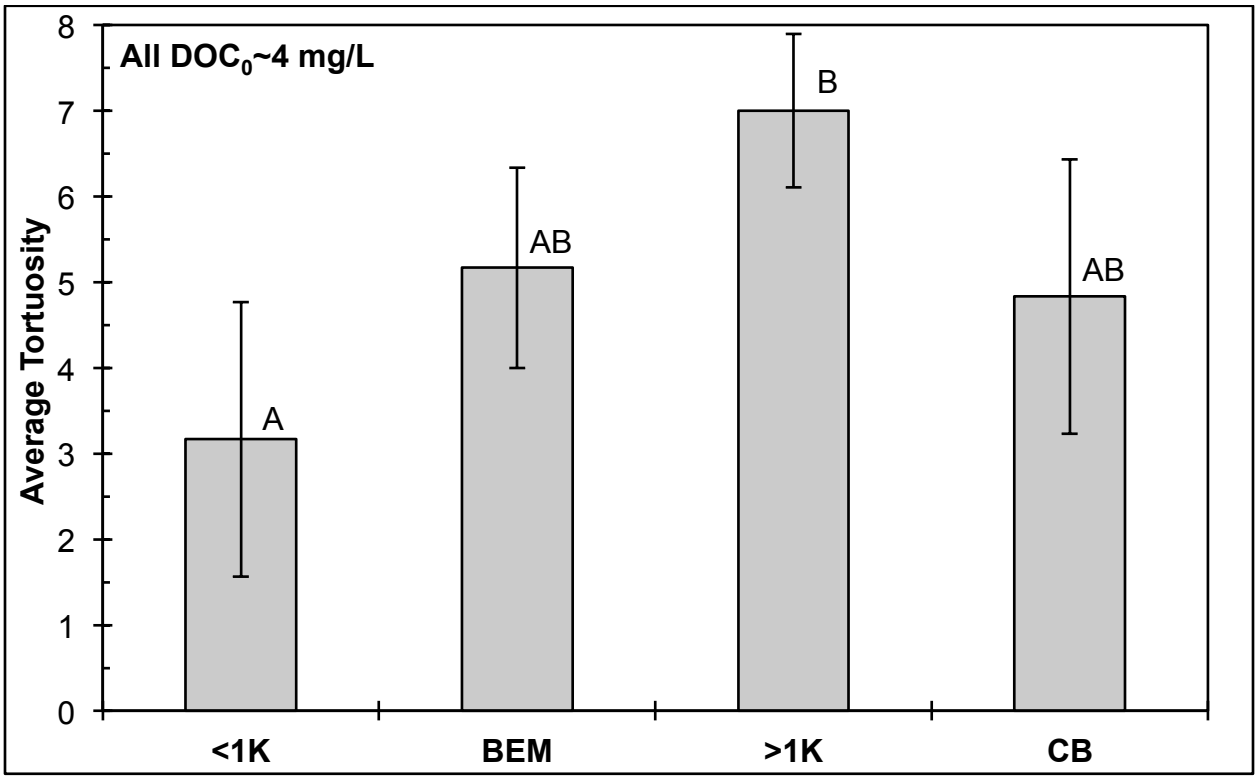

Figure 5.8. Average toruosity values (n=6) for MIB and WFN breakthrough curves in each water averaged over all EBCTs. Error bars show standard deviations. Tortuosity values that do not share a letter are significantly different at 95% confidence level.

5.3.4 Implications for Scaling Using the Rapid Small-Scale Column Test

Using a smaller GAC particle size in the PD-RSSCT, the results of this paper showed that compared to an unfractionated water (1) larger MW DOM slowed adsorption kinetics and fouled the carbon less and (2) smaller MW DOM fouled the carbon more by reducing adsorption capacity. Although crushing GAC has been shown to yield the same MP isotherm capacity, total surface area, total pore volume, and pore size volumes (Summers 1986, Crittenden et al. 1989, Patni et al. 2008), RSSCTs have consistently over predicted adsorption capacity in the presence

of background DOM (Crittenden et al. 1991, Corwin and Summers 2010). Corwin and Summers (2010) hypothesized pore blockage as the mechanism causing the differences in adsorption capacity between the small- and full-scale. When a GAC particle is ground more micro- and mesopores, or where MP adsorption occurs, are exposed to the bulk flow. At the full-scale, those same micro- and mesopores are deeper within the GAC particle and become unavailable to MP adsorption from pore blockage. Unavailable to MP adsorption could be defined as the pore is completely blocked or is blocked sufficiently to cause an apparent decrease in adsorption capacity from extremely slow adsorption kinetics. For example, a decrease in adsorption capacity is observed from large τ values in Figure 5.7 for any throughput relevant to typical desired MIB removals.

The MIB and WFN breakthrough curves in >1K showed that larger MW DOM, which would be expected to cause more pore blockage, actually showed more capacity for MPs than water with lower MW DOM background matrix. Increased MP adsorption capacity in >1K is consistent with the hypothesis that smaller GAC particles would reduce the effects of pore blockage on adsorption capacity. Therefore if >1K was run with full-scale media, the results for MIB and WFN may not be the same because a blocked pore in a large GAC particle has significantly more surface area behind the blockage compared to a small GAC particle. At the same DOC concentration, the >1K background matrix may cause earlier MP breakthrough compared to an unfractionated water.

Additionally, because MIB and WFN broke through earlier in water with lower MW compared to BEM, this should provide a closer prediction of full-scale MP breakthrough. Stated differently, if a field-scale GAC column was run with MIB and WFN in a typical surface water (BEM or CB), the PD-RSSCT with MIB and WFN in <1K would be expected to give the best

prediction of the field-scale breakthrough. Thus, this study suggests differences in small- and large-scale breakthrough are most likely related to the fouling effects of larger MW DOM, which is also consistent with the pore blockage hypothesis proposed by Corwin and Summers (2010). However, as with most GAC applications to date, it is difficult to predict what would happen at the full-scale without using full-scale GAC media. This study also only looked at bituminous-based GAC, which has different pore size distributions than other GACs.

5.3.5 Micropollutant Adsorption in the Presence of other Micropollutants

In the systems discussed thus far, MP competition came mainly from background natural DOM, because it was present at much higher concentrations than MIB and WFN. Researchers have successfully modeled systems containing a MP with background DOM using the Ideal Adsorbed Solution Theory (IAST) by representing DOM as an equivalent background compound (EBC) (Najm et al. 1991, Knappe et al. 1998, Graham et al. 2000). Both theoretical (IAST-EBC approach) and experimental findings have shown that fractional breakthrough (C/C_0) of a MP at low concentrations in the presence of much higher concentration DOM is independent of initial MP concentration (Gillogly et al. 1998, Knappe et al. 1998, Graham et al. 2000, Matsui et al. 2003, Corwin and Summers 2012). Such behavior is observed as long as the competing fraction of the background DOM surface loading is unaffected by the target MP loading ($q_{competing\ DOM} >> q_{MPs}$), which is the expected at low liquid phase MP concentrations. Breakthrough curves independent of initial MP concentration is also what would be expected from a linear isotherm, demonstrated by Corwin and Summers (2011) by equating the Freundlich isotherm equation ($q=KC^{1/n}$) to the mass balance of an ideal plug flow adsorber. Assumptions therein led to the modeling approach used in this thesis.

If high enough total MP concentrations existed in the micropores then significant competition between MPs would occur, which could have an effect on the solid phase concentration of the competing fraction of the background DOM to the point where assuming $q_{competing\ DOM} >> q_{MPs}$ is no longer valid. Therefore the assumption that fractional breakthrough is independent of initial MP concentration may not be valid, complicating GAC adsorption predictions because influent MP concentrations are rarely constant and fluctuate with seasons.

Kim (2006) investigated the adsorption of MIB in the presence and absence of disinfection by-products (DBPs) in natural water (DOC_0=1.3 mg/L) using the PD-RSSCT. The study found no effect of 15 μg/L of DBPs on MIB breakthrough, but trihalomethanes (~30% of DBPs) were poorly adsorbed by GAC. Other than the work by Kim (2006) and similar to the DOM size research, most of the work in this area has been done with batch systems, which are subject to different adsorption driving forces and DOM loading. In relation to this study, Gillogly et al. (1998) observed the same fractional removal with one PAC and MIB at 150 and 1,245 ng/L and another PAC and MIB at 175, 234, and 1,029 ng/L (DOC_0=1.8 mg/L). More recently, Rossner et al. (2009) investigated equilibrium adsorption of sulfamethoxazole (SMX) in natural water (DOC=2.5 mg/L). One test contained only SMX at an initial concentration of 100 μg/L. Another test contained SMX at an initial concentration of 426 ng/L with 24 additional MPs, for a collective concentration of about 14 μg/L. Many of the 24 MPs in Rossner et al. (2009) are the same as the MPs spiked into CBMP. Results showed SMX percent removal to be independent of both initial SMX concentration and the addition of 24 other MPs.

The effect of background MPs on MIB and WFN was investigated in CBMP compared to CB. Twenty-nine MPs in CBMP ranged from 3 to 336 ng/L for a total collective average MP concentration of 3.0±0.9 μg/L (n=3, see Appendix Table A.20). The background was meant to

represent a typical impacted water source (Kolpin et al. 2002, Focazio et al. 2008), although it did not contain soluble microbial byproducts representative of wastewater effluent. CB and CBMP results for DOC, MIB, and WFN are shown in Figure 5.9 at a full-scale EBCT of 4 minutes. In Figure 5.9, CB and CBMP K^* values were within 5% and 14% for MIB and WFN, respectively, indicating these curves are probably not statistically different based on the previous EBCT analysis that used 11% as a baseline (see Section 5.3.2.2.1). However, Figure 5.9 does show systematically earlier breakthrough behavior of MIB and WFN in CBMP compared to CB for nearly all the data points, despite similar DOM loading shown in Table 5.3 and Figure 5.9. To give a sense of solid phase concentrations, the DOM loadings in Table 5.3 (μg DOC/mg GAC) were three orders of magnitude higher than MIB and WFN loadings (ng/mg GAC). Solid phase loadings of the other 27 MPs in CBMP could not be calculated because they were not directly analyzed for by LC/MS-MS.

Proving statistically significant differences between GAC breakthrough curves is difficult and sometimes unmerited due to its unsteady state and times series nature. For this reason statistical analysis was limited to K^*, or the midpoint of breakthrough in the discussion involving the effect of EBCT (Section 5.3.2.2.1). Hooper (1996) describes two methods by which breakthrough curves can be evaluated for statistically significant differences. However, sound engineering judgment may still override the conclusions of the analysis, especially if data is limited.

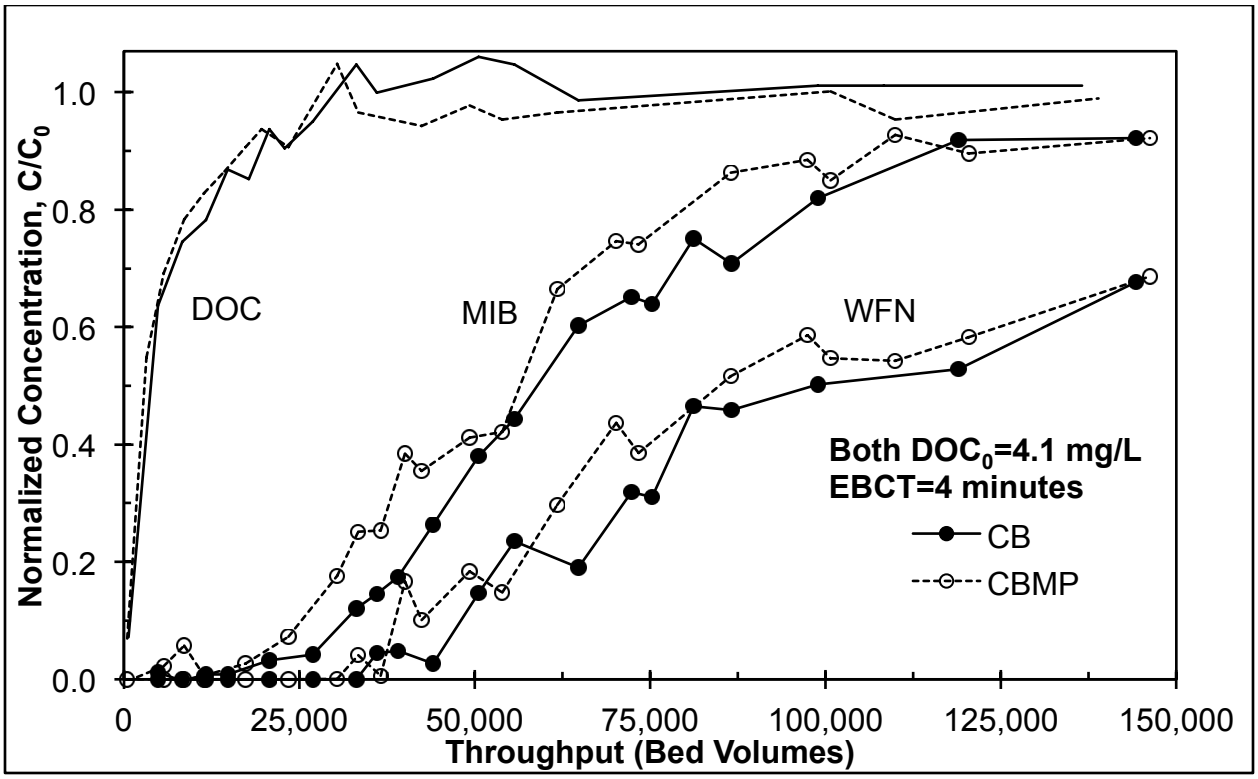

Figure 5.9. Breakthrough curves for DOC, MIB, and WFN in CB and CBMP at a full-scale EBCT of 4 minutes. The only MPs in CB are MIB and WFN, while the collective MP concentration in CBMP is 3.0±0.9 μg/L (n=3, see Appendix Table A.20).

Although the difference is small between the breakthrough curves for MIB and WFN in CB and CBMP in Figure 5.9, it suggests the background MP concentration in CBMP is near the point at which assuming $q_{competing\ DOM} >> q_{MPs}$ begins to deviate at least for MIB and WFN. In CB and CBMP, estimated MIB and WFN solid phase loadings (ng/mg) were within 12 and 5% respectively. At longer EBCTs, MIB and WFN in CBMP still appeared to systematically breakthrough ahead of CB, although it was less discernable. Estimated solid phase loadings in CB and CBMP for MIB were within 5 and 1% for EBCTs of 7 and 10 minutes, respectively, and within 2% for EBCTs of 7 and 10 minutes for WFN. Indistinguishable breakthrough behavior with increasing EBCT suggests that preloading of natural DOM dominates deeper in the bed, reestablishing the assumption of breakthrough independence from initial MP concentration.

Therefore at more typical EBCTs the presence of background MPs at relevant concentrations does not appear to significantly affect target MP breakthrough. The same graph as Figure 5.9 is shown in the Appendix for full-scale EBCTs of 7 and 10 minutes (Figure A.14 and Figure A.15, respectively).

A threshold concentration for breakthrough behavior independent of initial MP concentration would increase with decreasing adsorbability because the MP's ability to compete against the background matrix is diminished (Corwin and Summers 2011). Stated differently, a more strongly adsorbing MP would be more subject to the effects of fouling because it can compete better, lowering the threshold. If the differences in adsorbability between MIB and WFN were more exaggerated this behavior may have been observed. Regardless, a threshold would be relevant to either (1) the total background MP concentration relative to one MP or (2) a single MP in natural water as long as MPs are considered to have similar adsorbabilities and pore access relative to the background DOM matrix.

5.4 Conclusions

For the adsorption of the MPs MIB and WFN, it was found smaller MW DOM represented by ultrafiltered and coagulated waters caused the greatest reduction in adsorption capacity, or fouled the GAC the most. Compared to an unfractionated water, a larger MW DOM matrix increased the adsorption capacity for MIB and WFN, or fouled the GAC the least. However, all waters exhibited similar behavior with respect to EBCT by causing the same percent decreases in K^* values with increasing EBCT. Decreased capacity caused by preloading deeper in the GAC bed affected the more strongly adsorbing WFN more than MIB. Compared to the small MW DOM matrix, the larger MW DOM matrix resulted in slower adsorption kinetics by increasing tortuosity in the GAC pores, most likely through pore blockage. Over the same

throughput ranges the mass desorbed of MIB and WFN was similar across the small, large, and unfractionated waters. Using a coagulated water at a short EBCT, it appears a background MP concentration in the low μg/L range may be near the point at which linear isotherm behavior beings to deviate for weakly adsorbing MPs. However, the effect of background MPs decreases with increasing EBCT because deeper in the bed preloaded DOM dominates adsorption.

Chapter 6
Conclusions

6.1 Hypothesis Conclusions

Hypothesis 1: At the full-scale, the system characteristics of DOC concentration and EBCT affect GAC removal of a wide array of MPs. Increasing the DOC concentration causes earlier breakthrough of MPs on a normalized basis. Longer EBCTs yield lower carbon usage rates for high levels of MP removal. MP breakthrough can be predicted using properties of the MP and system.

Results in Chapter 3 showed earlier MP breakthrough on average with increasing DOC and 52% later breakthrough on average by doubling the EBCT based on the bed volumes to 10% breakthrough. At an EBCT of 15 minutes only seven MPs exhibited breakthrough after 46,000 bed volumes. Several predictive relationships were presented for predicting the bed volumes to 10% MP breakthrough. However these relationships required adjustments depending on the water source and GAC particle size. MPs in highly impacted water sources, most likely from wastewater, broke through much earlier than predicted from increased competition beyond natural DOM. MPs in adsorbers with larger GAC particle sizes also broke through earlier than predicted because of slower adsorption kinetics associated with the larger particle size.

Hypothesis 2: The rapid small-scale column test (RSSCT) can be used to predict full-scale removal of MPs by GAC. RSSCT results can be scaled using a fouling factor to predict full-scale GAC adsorption capacity and kinetics assuming intraparticle diffusivity decreases linearly with GAC particle size. MP molecular descriptors and system properties can be used to predict a fouling factor.

Results in Chapter 4 showed breakthrough generated using PD-RSSCT could be adjusted using the fouling factor to adequately predict full-scale breakthrough. A relationship was

presented to predict the fouling factor from the influent MP and DOC concentrations, MP pH-dependent octanol-water partition coefficient, and bed volumes to 10% MP breakthrough in the PD-RSSCT. Another relationship was presented to predict bed volumes to 10% MP breakthrough at the full-scale based solely on bed volumes to 10% MP breakthrough in the PD-RSSCT. Both relationships were verified using full-scale MP breakthrough data.

Hypothesis 3: The molecular size of DOM affects GAC adsorption of MPs. Small molecular weight fractions of DOM reduce GAC adsorption capacity for MPs. Large molecular weight fractions of DOM slow MP adsorption kinetics. At a constant DOC concentration the type of background DOM, defined only by the presence or absence of MPs, has no impact on the breakthrough behavior of target MPs.

Results in Chapter 5 showed small molecular weight DOM caused the greatest reduction in MP adsorption capacity while larger molecular weight DOM actually increased MP adsorption capacity compared to an unfractionated water. All DOM sizes resulted in similar reductions in capacity with increasing EBCT. The more strongly adsorbing WFN was more subject to the reduced capacity from preloading. Compared to small molecular weight DOM, larger molecular weight DOM slowed MP adsorption kinetics through increased tortuosity in the GAC pores. The addition of common MPs at typical concentrations to a coagulated water had little impact on the breakthrough of MIB and WFN. However their breakthrough behavior suggests the background MP concentration is near the linear isotherm threshold.

6.2 Future Research

The following research could advance the findings of this study and aid in the design and operation of GAC contactors for the control of MPs.

- Controlled pilot GAC studies could investigate the effect of impacted waters either through SEC, fluorescence, or quantification of wastewater effluent organic matter as a percentage of the total DOM present in the water. A DOM 'log K_{ow}' value could be evaluated to see if could be a good predictor of MP breakthrough behavior.
- Controlled pilot studies could also quantify the effect of GAC particle size and reactivated GAC on MP breakthrough. Both of these pilot studies would strengthen the use of the predictive relationships developed in Chapter 3, and possibly extend their use to water reuse applications.
- PD-RSSCTs could be run and compared to field-scale breakthrough data from drinking water utilities to verify or alter the predictive relationships presented in Chapter 4.
- Theoretical relationships could be developed for the fouling factor based on DOM molecular weight distributions.
- Additional attempts could be made to use equilibrium data from isotherms in conjunction with the PSDM to predict full-scale MP breakthrough without the use of the RSSCT.
- Pilot columns could be run with different DOM size fractions from concentrates or bulk waters to confirm or refute the findings in Chapter 5.
- Using the RSSCT, MP-specific linear isotherm thresholds could be identified.
- More work could be done with predicting breakthrough from intermittent loading of MPs, as there are seasonal patterns for many of the compounds, e.g., MIB, pesticides.
- Using the RSSCT, further investigate operation of GAC beds in parallel or series for the removal of MPs

References

Aiken, GR, EM Thurman, RL Malcolm, and HF Walton. 1979. "Comparison of XAD Macroporous Resins for the Concentration of Fulvic Acid From Aqueous Solution." *Analytical Chemistry* 51 (11): 1799–1803.

ASTM. 2008. D6586: Standard Practice for the Prediction of Contaminant Adsorption on GAC in Aqueous Systems Using Rapid Small-Scale Column Tests.

Barnes, KK, DW Kolpin, ET Furlong, SD Zaugg, MT Meyer, and LB Barber. 2008. "A National Reconnaissance of Pharmaceuticals and Other Organic Wastewater Contaminants in the United States - I) Groundwater." *Science of the Total Environment* 402: 192–200.

Batt, AL, S Kim, and DS Aga. 2007. "Comparison of the Occurrence of Antibiotics in Four Full-Scale Wastewater Treatment Plants with Varying Designs and Operations." *Chemosphere* 68 (3): 428–435.

Benotti, MJ, RA Trenholm, BJ Vanderford, JC Holady, BD Stanford, and SA Snyder. 2009. "Pharmaceuticals and Endocrine Disrupting Compounds in U.S. Drinking Water." *Environmental Science & Technology* 43 (3): 597–603.

Cardenas, J. 2011. "Granular Activated Carbon Adsorption of Dissolved Organic Matter and Trace Organic Contaminants: Effects of Influent Dissolved Organic Matter Concentration and Pretreatment." MS Thesis, University of Colorado.

Carter, MC, WJ Weber, and KP Olmstead. 1992. "Effects of Background Dissolved Organic Matter on TCE Adsorption by GAC." *Journal American Water Works Association* 84 (8): 81–91.

Carter, MC, and WJ Weber. 1994. "Modeling Adsorption of TCE by Activated Carbon Preloaded by Background Organic Matter." *Environmental Science & Technology* 28 (4): 614–623.

Chowdhury, ZK, RS Summers, GP Westerhoff, BJ Leto, KO Nowack, and CJ Corwin. 2013. *Activated Carbon: Solutions for Improving Water Quality*. American Water Works Association.

Chowdhury, ZK, A Traviglia, J Carter, T Brown, RS Summers, C Corwin, T Zearley, M Thurman, I Ferrer, J Olson, R Thacker, P Barron. 2010. "Cost-Effective Regulatory Compliance with GAC Biofilters." Water Research Foundation Report No. 4155.

Clarke, ED. 2009. "Beyond Physical Properties–Application of Abraham Descriptors and LFER Analysis in Agrochemical Research." *Bioorganic & Medicinal Chemistry* 17 (12): 4153–4159.

Cornel, PK, RS Summers, and PV Roberts. 1986. "Diffusion of Humic Acid in Dilute Aqueous Solution." *Journal of Colloid and Interface Science* 110 (1): 149–164.

Corwin, CJ. 2010. "Trace Organic Contaminant Removal From Drinking Waters by Granular Activated Carbon: Adsorption, Desorption, and the Effect of Background Organic Matter." PhD Dissertation, University of Colorado.

Corwin, CJ, and RS Summers. 2010. "Scaling Trace Organic Contaminant Adsorption Capacity by Granular Activated Carbon." *Environmental Science & Technology* 44 (14): 5403–5408.

Corwin, CJ, and RS Summers. 2011. "Adsorption and Desorption of Trace Organic Contaminants From Granular Activated Carbon Adsorbers After Intermittent Loading and Throughout Backwash Cycles." *Water Research* 45 (2): 417–426.

Corwin, CJ, and RS Summers. 2012. “Controlling Trace Organic Contaminants with GAC Adsorption.” *Journal American Water Works Association* 104: E36–E47.

Crittenden, JC, JK Jr Berrigan, and DW Hand. 1986a. “Design of Rapid Small-Scale Adsorption Tests for a Constant Diffusivity.” *Journal Water Pollution Control Federation* 58 (4): 312–319.

Crittenden, JC, NJ Hutzler, DG Geyer, JL Oravitz, and G Friedman. 1986b. “Transport of Organic Compounds with Saturated Groundwater Flow: Model Development and Parameter Sensitivity.” *Water Resources Research* 22 (3): 271–284.

Crittenden, JC, JK Jr Berrigan, DW Hand, and BW Lykins. 1987. “Design of Rapid Fixed-Bed Adsorption Tests for Nonconstant Diffusivities.” *Journal of Environmental Engineering* 113 (2): 243–259.

Crittenden, JC, PS Reddy, DW Hand, and H Arora. 1989. “Prediction of GAC Performance Using Rapid Small-Scale Column Tests.” American Water Works Research Foundation Report No. 90549.

Crittenden, JC, PS Reddy, H Arora, J Trynoski, DW Hand, DL Perram, and RS Summers. 1991. “Predicting GAC Performance with Rapid Small-Scale Column Tests.” *Journal American Water Works Association* 83 (1): 77–87.

Crittenden, JC, RR Trussell, DW Hand, KJ Howe, and G Tchobanoglous. 2012. "Adsorption.” In *Water Treatment: Principles and Design*, 3rd Edition, 1117–1262. John Wiley & Sons, Inc.

Ding, L, BJ Marinas, LC Schideman, and VL Snoeyink. 2006. “Competitive Effects of Natural Organic Matter: Parametrization and Verification of the Three-Component Adsorption Model COMPSORB.” *Environmental Science & Technology* 40 (1): 350–356.

Donald, DB, AJ Cessna, E Sverko, and NE Glozier. 2007. “Pesticides in Surface Drinking-Water Supplies of the Northern Great Plains.” *Environmental Health Perspectives* 115 (8): 1183–1191.

Ferrer, I, JA Zweigenbaum, and EM Thurman. 2010. “Analysis of 70 Environmental Protection Agency Priority Pharmaceuticals in Water by EPA Method 1694.” *Journal of Chromatography A* 1217 (36): 5674–5686.

Focazio, MJ, DW Kolpin, KK Barnes, ET Furlong, MT Meyer, SD Zaugg, LB Barber, and ME Thurman. 2008. “A National Reconnaissance for Pharmaceuticals and Other Organic Wastewater Contaminants in the United States - II) Untreated Drinking Water Sources.” *Science of the Total Environment* 402: 201–216.

Fotta, ME. 2012. “Effect of Granular Activated Carbon Type on Adsorber Performance and Scale-Up Approaches for Volatile Organic Compound Removal.” MS Thesis, North Carolina State University.

Gillogly, TET, VL Snoeyink, JR Elarde, CM Wilson, and EP Royal. 1998. “14C-MIB Adsorption on PAC in Natural Water.” *Journal American Water Works Association* 90 (1): 98–108.

Gnielinski, V. 1978. Gleichungen zur Berechnung des Warme- und Stoffaustausches in durchstromten ruhenden Kugelschuttungen bei mitteren und grossen Pecletzahlen. Verf. Tech. 12 (6): 363–366.

Graham, MR, RS Summers, MR Simpson, and BW MacLeod. 2000. “Modeling Equilibrium Adsorption of 2-Methylisoborneol and Geosmin in Natural Waters.” *Water Research* 34 (8): 2291–2300.

Holbrook, AM, JA Pereira, R Labiris, H McDonald, JD Douketis, M Crowther, and PS Wells. 2005. "Systematic Overview of Warfarin and Its Drug and Food Interactions." *Archives of Internal Medicine* 165 (10): 1095–1106.

Hayduk, W, and H Laudie. 1974. "Prediction of Diffusion Coefficients for Nonelecrolytes in Dilute Aqueous Solutions." *AlChE* 20 (3): 611–615.

Hooper, SM, RS Summers, G Solarik, and DM Owen. 1996. "Improving GAC Performance by Optimized Coagulation." *Journal American Water Works Association* 88 (8): 107–120.

Jones, OA, JN Lester, and N Voulvoulis. 2005. "Pharmaceuticals: a Threat to Drinking Water?" *Trends in Biotechnology* 23 (4): 163–167.

Kilduff, JE, T Karanfil, and WJ Weber. 1998a. "TCE Adsorption by GAC Preloaded with Humic Substances." *Journal American Water Works Association* 90 (5): 76–89.

Kilduff, JE, T Karanfil, and WJ Weber. 1998b. "Competitive Effects of Nondisplaceable Organic Compounds on Trichloroethylene Uptake by Activated Carbon. II. Model Verification and Applicability to Natural Organic Matter." *Journal of Colloid and Interface Science* 205 (2): 280–289.

Kim, SM. 2006. "Understanding and Predicting 2-Methylisoborneol (MIB) Adsorption by Granular Activated Carbon and Process Selection Approaches for Controlling Taste and Odor." PhD Dissertation, University of Colorado.

Kim, SD, J Cho, IS Kim, BJ Vanderford, and SA Snyder. 2007. "Occurrence and Removal of Pharmaceuticals and Endocrine Disruptors in South Korean Surface, Drinking, and Waste Waters." *Water Research* 41 (5): 1013–1021.

Knappe, DRU, VL Snoeyink, P Roche, MJ Prados, and MM Bourbigot. 1997. "The Effect of Preloading on Rapid Small-Scale Column Test Predictions of Atrazine Removal by GAC Adsorbers." *Water Research* 31 (11): 2899–2909.

Knappe, DRU, VL Snoeyink, P Roche, MJ Prados, and MM Bourbigot. 1999. "Atrazine Removal by Preloaded GAC." *Journal American Water Works Association* 91 (10): 97–109.

Knappe, DRU, Y Matsui, VL Snoeyink, P Roche, MJ Prados, and MM Bourbigot. 1998. "Predicting the Capacity of Powdered Activated Carbon for Trace Organic Compounds in Natural Waters." *Environmental Science & Technology* 32 (11): 1694–1698.

Kolpin, DW, ET Furlong, MT Meyer, EM Thurman, SD Zaugg, LB Barber, and HT Buxton. 2002. "Pharmaceuticals, Hormones, and Other Organic Wastewater Contaminants in U.S. Streams, 1999−2000: A National Reconnaissance." *Environmental Science & Technology* 36 (6): 1202–1211.

Kuehn, BM. 2008. "Traces of Drugs Found in Drinking Water." *JAMA: the Journal of the American Medical Association* 299 (17): 2011–2013.

Lee, MC, VL Snoeyink, and JC Crittenden. 1981. "Activated Carbon Adsorption of Humic Substances." *Journal American Water Works Association* 73 (8): 440–446.

Li, Q. 2003. "Pore Blockage Effect of NOM on Atrazine Adsorption Kinetics of PAC: the Roles of PAC Pore Size Distribution and NOM Molecular Weight." *Water Research* 37 (20): 4863–4872.

Li, QL, VL Snoeyink, BJ Mariaas, and C Campos. 2003. "Elucidating Competitive Adsorption Mechanisms of Atrazine and NOM Using Model Compounds." *Water Research* 37 (4): 773–784.

Loos, R, BM Gawlik, G Locoro, E Rimaviciute, S Contini, and G Bidoglio. 2009. "EU-Wide Survey of Polar Organic Persistent Pollutants in European River Waters." *Environmental Pollution* 157 (2): 561–568.

Mastropole, A. 2011. "Evaluation of Available Scale-Up Approaches for the Design of GAC Contactors." MS Thesis, North Carolina State University.

Matsui, Y, DRU Knappe, K Iwaki, and H Ohira. 2002. "Pesticide Adsorption by Granular Activated Carbon Adsorbers. 2. Effects of Pesticide and Natural Organic Matter Characteristics on Pesticide Breakthrough Curves." *Environmental Science & Technology* 36 (15): 3432–3438.

Matsui, Y, Y Fukuda, T Inoue, and T Matsushita. 2003. "Effect of Natural Organic Matter on Powdered Activated Carbon Adsorption of Trace Contaminants: Characteristics and Mechanism of Competitive Adsorption." *Water Research* 37 (18): 4413–4424.

Matsui, Y, T Yoshida, S Nakao, DRU Knappe, and T Matsushita. 2012. "Characteristics of Competitive Adsorption Between 2-Methylisoborneol and Natural Organic Matter on Superfine and Conventionally Sized Powdered Activated Carbons." *Water Research* 46 (15): 4741–4749.

Mezzari, IA. 2006. "Predicting the Adsorption Capacity of Activated Carbon for Organic Contaminants From Fundamental Adsorbent and Adsorbate Properties." MS Thesis, North Carolina State University.

Montgomery, DC. 2013. *Design and Analysis of Experiments*, 8th Edition. John Wiley & Sons, Inc.

Moore, BC, FS Cannon, DH Metz, and J DeMarco. 2003. "GAC Pore Structure in Cincinnati During Full-Scale Treatment/Reactivation." *Journal American Water Works Association* 95 (2): 103–112.

Newcombe, G, M Drikas, and R Hayes. 1997. "Influence of Characterised Natural Organic Material on Activated Carbon Adsorption: II. Effect on Pore Volume Distribution and Adsorption of 2-Methylisoborneol." *Water Research* 31 (5): 1065–1073.

Patni, AG, DK Ludlow, and CD Adams. 2008. "Characteristics of Ground Granular Activated Carbon for Rapid Small-Scale Column Tests." *Journal of Environmental Engineering* 134 (3): 216–221.

Pomati, F, S Castiglioni, E Zuccato, R Fanelli, D Vigetti, C Rossetti, and D Calamari. "Effects of a Complex Mixture of Therapeutic Drugs at Environmental Levels on Human Embryonic Cells." *Environmental Science & Technology* 40 (7): 2442–2447.

Potter, BB, and JC Wimsatt. 2012. "EPA Method 415.3: Quantifying TOC, DOC, and SUVA." *Journal American Water Works Association* 104: E358–E369.

Reinert, AM. 2013. "Granular Activated Carbon Adsorption of Micropollutants From Surface Water: Field-Scale Adsorber Performance and Scale-Up of Bench-Scale Data." MS Thesis, North Carolina State University.

Rossner, A, SA Snyder, and DRU Knappe. 2009. "Removal of Emerging Contaminants of Concern by Alternative Adsorbents." *Water Research* 43 (15): 3787–3796.

Scheurer, M, FR Storck, HJ Brauch, and FT Lange. 2010. "Performance of Conventional Multi-Barrier Drinking Water Treatment Plants for the Removal of Four Artificial Sweeteners." *Water Research* 44 (12): 3573–3584.

Schideman, LC, BJ Mariñas, VL Snoeyink, and C Campos. 2006. "Three-Component Competitive Adsorption Model for Fixed-Bed and Moving-Bed Granular Activated Carbon Adsorbers. Part II. Model Parameterization and Verification." *Environmental Science & Technology* 40 (21): 6812–6817.

Schriks, M, MB Heringa, MME van der Kooi, P de Voogt, and AP van Wezel. 2010. "Toxicological Relevance of Emerging Contaminants for Drinking Water Quality." *Water Research* 44 (2): 461–476.

Schwarzenbach, RP, PM Gschwend, and DM Imboden. 2003. *Environmental Organic Chemistry*. 2nd Edition. John Wiley & Sons, Inc.

Schwarzenbach, RP, BI Escher, K Fenner, TB Hofstetter, CA Johnson, Urs von Gunten, and B Wehrli. 2006. "The Challenge of Micropollutants in Aquatic Systems." *Science* 313 (5790): 1072–1077.

Snyder, SA, P Westerhoff, Y Yoon, and DL Sedlak. 2003. "Pharmaceuticals, Personal Care Products, and Endocrine Disruptors in Water: Implications for the Water Industry." *Environmental Engineering Science* 20 (5): 449–469.

Snyder, SA, S Adham, AM Redding, FS Cannon, J DeCarolis, J Oppenheimer, EC Wert, and Y Yoon. 2007. "Role of Membranes and Activated Carbon in the Removal of Endocrine Disruptors and Pharmaceuticals." *Desalination* 202 (1-3): 156–181.

Sontheimer, H, JC Crittenden, and RS Summers. 1988. *Activated Carbon for Water Treatment*. 2nd Edition. DVGW-Forschungsstelle, Engler-Bunte-Institut, Universitat Karlsruhe.

Speth, TF, and RJ Miltner. 1989. "Effect of Preloading on the Scale-Up of GAC Microcolumns." *Journal American Water Works Association* 81 (4): 141–148.

Stackelberg, PE, ET Furlong, MT Meyer, SD Zaugg, AK Henderson, and DB Reissman. 2004. "Persistence of Pharmaceutical Compounds and Other Organic Wastewater Contaminants in a Conventional Drinking-Water-Treatment Plant." *Science of the Total Environment* 329 (1-3): 99–113.

Stackelberg, PE, J Gibs, ET Furlong, MT Meyer, SD Zaugg, and RL Lippincott. 2007. "Efficiency of Conventional Drinking-Water-Treatment Processes in Removal of Pharmaceuticals and Other Organic Compounds." *Science of the Total Environment* 377 (2-3): 255–272.

Summers, RS. (1986) Activated Carbon Adsorption of Humic Substances: Effect of Molecular Size and Heterodispersity. PhD Dissertation, Stanford University.

Summers, RS, and PV Roberts. 1988a. "Activated Carbon Adsorption of Humic Substances: I. Heterodisperse Mixtures and Desorption." *Journal of Colloid and Interface Science* 122 (2): 367–381.

Summers, RS, and PV Roberts. 1988b. "Activated Carbon Adsorption of Humic Substances: II. Size Exclusion and Electrostatic Interactions." *Journal of Colloid and Interface Science* 122 (2): 382–397.

Summers, RS, B Haist, J Koehler, J Ritz, G Zimmer, and H Sontheimer. 1989. "The Influence of Background Organic Matter on GAC Adsorption." *Journal American Water Works Association* 81 (5): 66–74.

Summers, RS, SM Hooper, G Solarik, DM Owen, and SH Hong. 1995. "Bench-Scale Evaluation of GAC for NOM Control." *Journal American Water Works Association* 87 (8): 69–80.

Summers, RS, DRU Knappe, and VL Snoeyink. 2011. "Adsorption of Organic Compounds by Activated Carbon." In *Water Quality and Treatment: a Handbook on Drinking Water*, 6th Edition, 14.1–14.105. American Water Works Association.

Summers, RS, SM Kim, K Shimabuku, SH Chae, and CJ Corwin. 2013. "Granular Activated Carbon Adsorption of MIB in the Presence of Dissolved Organic Matter." *Water Research* 47 (10): 3507–3513.

Ternes, TA, M Meisenheimer, D McDowell, F Sacher, HJ Brauch, BH Gulde, G Preuss, U Wilme, and NZ Seibert. 2002. "Removal of Pharmaceuticals During Drinking Water Treatment." *Environmental Science & Technology* 36 (17): 3855–3863.

Thurman, EM, RL Wershaw, RL Malcolm, and DJ Pinckney. 1982. "Molecular Size of Aquatic Humic Substances." *Organic Geochemistry* 4 (1): 27–35.

To, PC, BJ Mariñas, VL Snoeyink, and WJ Ng. 2008. "Effect of Pore-Blocking Background Compounds on the Kinetics of Trace Organic Contaminant Desorption From Activated Carbon." *Environmental Science & Technology* 42 (13): 4825–4830.

Torres, CI, S Ramakrishna, CA Chiu, KG Nelson, P Westerhoff, and R Krajmalnik-Brown. 2011. "Fate of Sucralose During Wastewater Treatment." *Environmental Engineering Science* 28 (5): 325–331.

Vermeulen, T. 1958. "Separation by Adsorption Methods." *Advances in Chemical Engineerin*g 2: 147–203.

Wang, JZ, RS Summers, and RJ Miltner. 1995. "Biofiltration Performance: Part 1, Relationship to Biomass." *Journal American Water Works Association* 87 (12): 55–63.

Westerhoff, P, Y Yoon, S Snyder, and E Wert. 2005. "Fate of Endocrine-Disruptor, Pharmaceutical, and Personal Care Product Chemicals During Simulated Drinking Water Treatment Processes." *Environmental Science & Technology* 39 (17): 6649–6663.

Yuncu, B. (2010). "Removal of 2-Methylisoborneol and Geosmin by High-Silica Zeolites and Powdered Activated Carbon in the Absence and Presence of Ozone." PhD Dissertation, North Carolina State University.

Zachman, BA, and RS Summers. 2010. "Modeling TOC Breakthrough in Granular Activated Carbon Adsorbers." *Journal of Environmental Engineering* 136 (2): 204–210.

Zearley, TL, and RS Summers. 2012. "Removal of Trace Organic Micropollutants by Drinking Water Biological Filters." *Environmental Science & Technology* 46 (17): 9412–9419.

USEPA. 1995a. National Primary Drinking Water Regulations: Contaminant Specific Fact Sheets for Synthetic Organic Chemicals – Technical Version. 811-F-95-003-T.

USEPA. 1995b. Methods for the Determination of Organic Compounds in Drinking Water – Supplement III. 600-R-95-131.

USEPA. 1996. ICR Manual for Bench- and Pilot-Scale Treatment Studies. 814-B-96-003.

USEPA. 2009a. National Primary Drinking Water Regulations. 816-F-09-004.

USEPA. 2009b. Fact Sheet: Final Third Drinking Water Contaminant Candidate List (CCL3). 815-F-09-001.

Appendix

Chapter 3

Table A.1. Pilot column breakthrough data for Water A (7).

Bed Volumes	5,755	11,246	23,273	32,932	71,964	97,707
MP	C/C_0					
2,4–D	0.000	0.000	0.181	0.056	0.157	0.228
Acetaminophen	0.000	0.000	0.000	0.000	0.063	0.000
Acetochlor	0.000	0.000	0.000	0.000	0.190	0.352
Aldicarb	0.000	0.000	0.022	0.047	0.113	0.206
Atrazine	0.154	0.224	0.207	0.059	0.173	0.393
Caffeine	0.051	0.362	0.098	0.083	0.303	0.140
Carbamazepine	0.000	0.000	0.000	0.000	0.072	0.164
Carbaryl	0.000	0.000	0.000	0.000	0.000	0.000
Clofibric acid	0.000	0.025	0.104	0.167	0.330	0.313
Cotinine	0.000	0.000	0.138	0.343	0.874	0.192
Diazinon	0.000	0.000	0.000	0.000	0.053	0.237
Diclofenac	0.000	0.000	0.038	0.044	0.053	0.042
Dimethoate	0.000	0.000	0.000	0.036	0.102	0.089
Diuron	0.000	0.000	0.000	0.000	0.000	0.000
Erythromycin	0.000	0.000	0.105	0.118	0.159	0.160
Gemfibrozil	0.000	0.000	0.000	0.000	0.000	0.000
Ibuprofen	0.000	0.000	0.000	0.000	0.000	0.000
Iopromide	0.000	0.280	0.423	0.967	0.785	0.959
Malaoxon	0.000	0.000	0.000	0.042	0.143	0.286
Methomyl	0.000	0.000	0.000	0.044	0.418	0.713
Metolachlor	0.000	0.000	0.040	0.073	1.000	0.336
Molinate	0.000	0.000	0.000	0.000	0.000	0.150
Naproxen	0.000	0.000	0.000	0.000	0.041	0.053
Prometon	0.000	0.000	0.037	0.077	0.285	0.510
Simazine	0.000	0.000	0.000	0.000	0.083	0.223
Sulfamethoxazole	0.000	0.000	0.031	0.038	0.097	0.155
Tributyl phosphate	0.093	0.076	0.110	0.164	0.180	0.508
Trimethoprim	0.000	0.000	0.000	0.247	0.000	0.000
Warfarin	0.000	0.024	0.148	0.164	0.280	0.322

Table A.2. Pilot column breakthrough data for Water A (15).

Bed Volumes	5,430	11,224	23,498	33,596	45,609
MP	C/C_0				
2,4–D	0.000	0.085	0.000	0.000	0.000
Acetaminophen	0.000	0.000	0.000	0.100	0.000
Acetochlor	0.000	0.000	0.000	0.000	0.000
Aldicarb	0.000	0.000	0.000	0.000	0.000
Atrazine	0.273	0.252	0.000	0.000	0.000
Caffeine	0.279	0.142	0.165	0.664	0.103
Carbamazepine	0.000	0.000	0.000	0.000	0.000
Carbaryl	0.000	0.000	0.000	0.000	0.000
Clofibric acid	0.000	0.000	0.000	0.000	0.065
Cotinine	0.000	0.000	0.000	0.202	0.059
Diazinon	0.000	0.000	0.000	0.000	0.000
Diclofenac	0.000	0.000	0.000	0.000	0.000
Dimethoate	0.000	0.000	0.000	0.000	0.000
Diuron	0.000	0.000	0.000	0.000	0.000
Erythromycin	0.000	0.000	0.000	0.000	0.000
Gemfibrozil	0.000	0.000	0.000	0.000	0.000
Ibuprofen	0.000	0.000	0.000	0.000	0.000
Iopromide	0.000	0.063	0.278	0.365	0.760
Malaoxon	0.000	0.000	0.000	0.000	0.000
Methomyl	0.000	0.000	0.000	0.000	0.207
Metolachlor	0.000	0.000	0.000	0.305	0.000
Molinate	0.000	0.000	0.000	0.000	0.000
Naproxen	0.000	0.000	0.000	0.000	0.000
Prometon	0.000	0.000	0.000	0.000	0.083
Simazine	0.000	0.000	0.000	0.000	0.000
Sulfamethoxazole	0.000	0.000	0.000	0.000	0.000
Tributyl phosphate	0.070	0.117	0.076	0.171	0.191
Trimethoprim	0.000	0.000	0.000	0.000	0.000
Warfarin	0.000	0.000	0.000	0.000	0.000

Table A.3. Pilot column breakthrough data for Water B.

Bed Volumes	6,629	16,034	24,930	36,649	50,375
MP	C/C_0				
2,4–D	0.000	0.051	0.055	0.102	0.061
Acetaminophen	0.000	0.000	0.000	1.115	0.226
Acetochlor	0.000	0.000	0.000	0.000	0.045
Aldicarb	0.000	0.000	0.000	0.032	0.024
Atrazine	0.292	0.150	0.038	0.109	0.101
Caffeine	0.159	0.161	0.080	0.956	0.411
Carbamazepine	0.000	0.000	0.000	0.000	0.000
Carbaryl	0.000	0.000	0.000	0.000	0.000
Clofibric acid	0.000	0.099	0.096	0.275	0.078
Cotinine	0.000	0.104	0.132	0.694	0.411
Diazinon	0.000	0.000	0.000	0.000	0.000
Diclofenac	0.000	0.000	0.000	0.000	0.000
Dimethoate	0.000	0.000	0.000	0.050	0.050
Diuron	0.000	0.000	0.000	0.000	0.000
Erythromycin	0.000	0.030	0.034	0.000	0.000
Gemfibrozil	0.000	0.024	0.000	0.028	0.027
Ibuprofen	0.000	0.000	0.000	0.000	0.000
Iopromide	0.000	0.160	0.207	0.679	0.454
Malaoxon	0.000	0.000	0.000	0.037	0.042
Methomyl	0.000	0.000	0.056	0.157	0.309
Metolachlor	0.000	0.021	0.029	0.021	0.109
Molinate	0.000	0.000	0.000	0.035	0.000
Naproxen	0.000	0.000	0.000	0.000	0.000
Prometon	0.000	0.027	0.050	0.112	0.167
Simazine	0.000	0.000	0.000	0.000	0.051
Sulfamethoxazole	0.000	0.032	0.027	0.033	0.000
Tributyl phosphate	0.204	0.462	0.132	0.463	0.814
Trimethoprim	0.000	0.000	0.000	0.000	0.000
Warfarin	0.000	0.044	0.034	0.051	0.043

Table A.4. Pilot column breakthrough data for Water C (Reinert 2013).

Bed Volumes	9,258	13,579	16,459	22,219	30,047	39,304	50,618	66,870	80,253	116,429
MP	C/C_0									
2,4–D	0.000	0.000	0.000	0.000	0.000	0.000	0.000	0.000	0.077	0.000
Acetaminophen	0.000	0.000	0.000	0.000	0.000	0.000	0.000	0.000	0.000	0.000
Acetochlor	0.000	0.000	0.000	0.000	0.000	0.000	0.057	0.121	0.187	0.284
Aldicarb	0.000	0.000	0.000	0.000	0.000	0.000	0.000	0.000	0.000	0.000
Atrazine	0.391	0.029	0.063	0.000	0.000	0.000	0.061	0.657	1.484	0.291
Caffeine	0.069	0.059	0.091	0.000	0.000	0.000	0.152	0.194	0.813	1.108
Carbamazepine	0.000	0.000	0.000	0.000	0.000	0.000	0.000	0.046	0.087	0.209
Carbaryl	0.000	0.000	0.000	0.000	0.000	0.000	0.000	0.000	0.000	0.000
Clofibric acid	0.037	0.037	0.037	0.000	0.000	0.000	0.033	0.000	0.058	0.075
Cotinine	0.000	0.000	0.000	0.000	0.000	0.236	0.756	0.807	0.952	1.926
Diazinon	0.462	0.076	0.000	0.051	0.000	0.000	0.000	0.000	0.054	0.000
Diclofenac	0.000	0.000	0.000	0.000	0.000	0.000	0.000	0.000	0.000	0.000
Dimethoate	0.000	0.000	0.000	0.000	0.000	0.000	0.000	0.000	0.000	0.090
Diuron	0.000	0.000	0.000	0.000	0.000	0.000	0.000	0.000	0.000	0.000
Erythromycin	1.000	0.065	0.021	0.065	0.000	0.000	0.000	0.000	0.000	0.000
Gemfibrozil	0.037	0.000	0.000	0.000	0.000	0.000	0.000	0.000	0.000	0.000
Ibuprofen	0.000	0.000	0.000	0.000	0.000	0.000	0.000	0.000	0.000	0.000
Iopromide	0.556	0.044	0.556	0.117	0.155	0.185	0.904	0.935	0.943	2.060
Malaoxon	0.000	0.000	0.000	0.000	0.000	0.000	0.000	0.000	0.052	0.000
Methomyl	0.000	0.000	0.000	0.000	0.000	0.087	0.390	0.478	0.791	1.534
Metolachlor	0.000	0.000	0.000	0.000	0.000	0.000	0.091	0.155	0.279	0.508
Molinate	0.000	0.000	0.000	0.000	0.000	0.000	0.000	0.000	0.000	0.000
Naproxen	0.000	0.000	0.000	0.000	0.000	0.000	0.000	0.000	0.000	0.000
Prometon	0.000	0.000	0.000	0.000	0.000	0.000	0.186	0.846	1.288	2.126
Simazine	0.000	0.000	0.000	0.000	0.000	0.000	0.048	0.088	0.210	0.759
Sulfamethoxazole	0.000	0.000	0.000	0.000	0.000	0.000	0.048	0.033	0.027	0.060
Tributyl phosphate	1.673	0.264	0.000	0.123	0.093	0.114	0.266	0.335	0.447	0.353
Trimethoprim	0.038	0.038	0.091	0.000	0.000	0.000	0.000	0.000	0.000	0.000
Warfarin	0.000	0.000	0.000	0.000	0.000	0.000	0.026	0.036	0.063	0.098

Table A.5. Pilot column breakthrough data for Water D.

Bed Volumes	5,910	11,212	24,677	34,116	77,049	101,299
MP	C/C_0					
2,4–D	0.000	0.000	0.000	0.064	0.191	0.181
Acetaminophen	0.000	0.000	0.000	0.000	0.000	0.000
Acetochlor	0.000	0.000	0.000	0.000	0.082	0.141
Aldicarb	0.000	0.000	0.000	0.026	0.061	0.106
Atrazine	0.127	0.000	0.000	0.000	0.067	0.132
Caffeine	0.052	0.034	0.066	0.056	0.286	0.343
Carbamazepine	0.000	0.000	0.000	0.000	0.076	0.054
Carbaryl	0.000	0.000	0.000	0.000	0.000	0.000
Clofibric acid	0.000	0.000	0.149	0.274	0.338	0.374
Cotinine	0.000	0.000	0.073	0.202	0.424	0.515
Diazinon	0.000	0.000	0.000	0.000	0.114	0.035
Diclofenac	0.000	0.000	0.000	0.000	0.055	0.046
Dimethoate	0.000	0.000	0.000	0.032	0.102	0.180
Diuron	0.000	0.000	0.000	0.000	0.000	0.000
Erythromycin	0.330	0.402	0.000	0.000	0.135	0.097
Gemfibrozil	0.000	0.000	0.000	0.028	0.107	0.053
Ibuprofen	0.000	0.000	0.000	0.000	0.107	0.000
Iopromide	0.000	0.058	0.198	0.305	0.529	0.537
Malaoxon	0.000	0.000	0.000	0.000	0.064	0.104
Methomyl	0.000	0.000	0.000	0.023	0.189	0.310
Metolachlor	0.000	0.000	0.000	0.046	0.091	0.166
Molinate	0.000	0.000	0.000	0.000	0.045	0.122
Naproxen	0.046	0.000	0.000	0.000	0.024	0.021
Prometon	0.000	0.000	0.000	0.025	0.135	0.179
Simazine	0.509	0.000	0.000	0.000	0.030	0.086
Sulfamethoxazole	0.000	0.000	0.000	0.000	0.069	0.070
Tributyl phosphate	0.075	0.143	0.089	0.108	0.189	0.207
Trimethoprim	0.000	0.000	0.000	0.000	0.000	0.000
Warfarin	0.000	0.000	0.039	0.102	0.164	0.121

Table A.6. Full-scale adsorber breakthrough data for Water E from August 2011 to May 2012. n.d. – no detect.

Bed Volumes	10,296		25,499		32,331		36,950	
Sample Date	8/3/11		1/18/12		3/29/12		5/16/12	
MP	C_{inf} (ng/L)	C_{eff} (ng/L)	C_{inf} (ng/L)	C_{eff} (ng/L)	C_{inf} (ng/L)	C_{eff} (ng/L)	C_{inf} (ng/L)	C_{eff} (ng/L)
2,4-D	0.0	0.0	5.8	0.0	4.1	0.0	7.1	0.0
Acetaminophen	n.d.	n.d.	4.7	0.0	0.0	0.0	n.d.	n.d.
Atrazine	272.5	5.1	13.4	8.7	13.9	13.8	836.7	41.5
Bupropion	n.d.	n.d.	3.2	0.0	2.3	0.0	1.9	0.0
Caffeine	18.0	0.0	65.9	5.2	48.9	8.6	31.7	5.5
Carbamazepine	11.4	0.0	5.5	0.0	5.0	0.0	7.2	0.0
Cotinine	6.3	0.0	7.7	4.7	7.7	6.5	6.6	0.0
Diuron	42.6	0.0	n.d.	n.d.	n.d.	n.d.	17.2	0.0
Gemfibrozil	n.d.	n.d.	7.4	0.0	3.1	0.0	0.0	0.0
Ibuprofen	n.d.	n.d.	6.1	0.0	n.d.	n.d.	n.d.	n.d.
Lamotrigine	29.9	0.0	9.8	0.0	9.6	0.0	16.1	0.0
Metolachlor	67.7	0.0	6.4	0.0	4.3	0.0	167.7	2.8
Metoprolol	2.9	0.0	8.1	0.0	4.5	0.0	4.1	0.0
Prometon	13.6	0.0	2.9	2.5	3.6	2.8	9.7	3.5
Simazine	29.1	0.0	9.4	0.0	5.3	0.0	99.8	4.2
Sucralose	793.7	36.0	280.9	183.1	253.4	220.4	362.1	267.3
Sulfamethoxazole	55.1	0.0	29.9	7.8	38.1	4.8	32.1	0.0
Trimethoprim	2.1	0.0	2.7	0.0	1.7	0.0	1.6	0.0

Table A.7. Abraham solvation parameters for MPs in this study. See Clarke (2009) for complete descriptions. Obtained from http://ilab.acdlabs.com/iLab2/index.php > Phys Chem > Absolv.

Compound	S	A	B	V	E
2,4-D	1.41	0.57	0.58	1.38	1.04
Acetochlor	1.63	0.00	0.94	2.14	1.11
Aldicarb	0.91	0.21	0.87	1.49	0.78
Atrazine	1.17	0.32	0.96	1.62	1.51
Caffeine	1.72	0.05	1.28	1.36	1.51
Carbamazepine	2.06	0.39	0.92	1.81	2.12
Clofibric acid	1.29	0.57	0.69	1.54	0.92
Cotinine	1.54	0.00	1.14	1.39	1.24
Diazinon	1.10	0.00	1.38	2.31	1.31
Diclofenac	1.95	0.70	0.67	2.03	1.81
DEET	1.47	0.00	0.74	1.68	0.93
Deethylatrazine	1.42	0.46	0.91	1.34	1.34
Deisopropylatrazine	1.43	0.46	0.88	1.20	1.33
Dimethoate	1.44	0.26	1.32	1.58	1.22
Erythromycin	3.04	1.05	4.63	5.77	2.51
Gemfibrozil	1.07	0.57	0.71	2.12	0.81
Iopromide	4.87	1.65	3.36	3.82	4.33
Malaoxon	1.49	0.00	1.84	2.21	0.70
Methomyl	0.91	0.21	0.85	1.21	0.77
Metolachlor	1.62	0.00	0.98	2.28	1.12
Molinate	1.32	0.00	0.76	1.55	0.88
Naproxen	1.49	0.57	0.75	1.79	1.54
Prometon	1.26	0.26	1.19	1.84	1.20
Simazine	1.20	0.33	0.95	1.48	1.55
Sucralose	2.30	1.28	2.50	2.42	2.04
Sulfamethoxazole	2.43	0.59	1.21	1.72	1.99
Tributyl Phosphate	0.72	0.00	1.25	2.24	0.25
Warfarin	2.28	0.31	1.23	2.31	1.98

Chapter 4

Table A.8. PD-RSSCT breakthrough data for Water A (7).

Bed Volumes	25,020	47,242	97,182	139,188	304,358	431,254
MP	C/C_0					
2,4–D	0.000	0.000	0.000	0.103	0.215	0.348
Acetaminophen	0.000	0.000	0.000	0.313	0.000	0.000
Acetochlor	0.000	0.000	0.084	0.179	0.319	0.471
Aldicarb	0.000	0.000	0.075	0.116	0.229	0.347
Atrazine	0.000	0.000	0.000	0.000	0.201	0.357
Caffeine	0.022	0.161	0.108	0.101	0.445	0.360
Carbamazepine	0.000	0.000	0.000	0.000	0.099	0.181
Carbaryl	0.000	0.000	0.000	0.000	0.000	0.000
Clofibric acid	0.024	0.160	0.493	0.579	0.661	0.684
Cotinine	0.000	0.000	0.237	0.345	0.925	1.044
Diazinon	0.000	0.000	0.000	0.000	0.115	0.339
Diclofenac	0.000	0.000	0.122	0.160	0.208	0.105
Dimethoate	0.000	0.000	0.033	0.063	0.205	0.320
Diuron	0.000	0.000	0.000	0.000	0.000	0.000
Erythromycin	0.000	0.000	0.161	0.282	0.236	0.248
Gemfibrozil	0.000	0.000	0.054	0.058	0.116	0.127
Ibuprofen	0.000	0.000	0.066	0.059	0.071	0.028
Iopromide	0.416	0.574	0.818	0.968	0.955	0.976
Malaoxon	0.000	0.000	0.048	0.084	0.212	0.346
Methomyl	0.000	0.000	0.000	0.047	0.699	1.075
Metolachlor	0.000	0.000	0.129	0.243	1.000	8.505
Molinate	0.000	0.000	0.000	0.000	0.189	0.376
Naproxen	0.000	0.000	0.000	0.000	0.087	0.101
Prometon	0.000	0.000	0.087	0.153	0.389	0.626
Simazine	0.000	0.000	0.000	0.000	0.133	0.243
Sulfamethoxazole	0.000	0.000	0.084	0.125	0.318	0.350
Tributyl phosphate	0.099	0.109	0.105	0.163	0.283	0.440
Trimethoprim	0.000	0.000	0.000	0.000	0.000	0.000
Warfarin	0.024	0.133	0.363	0.491	0.565	0.541

Table A.9. PD-RSSCT breakthrough data for Water A (15).

Bed Volumes	21,720	43,565	98,070	139,839	198,952
MP	C/C_0				
2,4–D	0.000	0.000	0.000	0.000	0.000
Acetaminophen	0.000	0.000	0.000	0.208	0.000
Acetochlor	0.000	0.000	0.000	0.000	0.054
Aldicarb	0.000	0.000	0.000	0.000	0.035
Atrazine	0.000	0.000	0.000	0.000	0.000
Caffeine	0.193	0.064	0.149	0.198	0.309
Carbamazepine	0.000	0.000	0.000	0.000	0.000
Carbaryl	0.000	0.000	0.000	0.000	0.000
Clofibric acid	0.000	0.000	0.187	0.168	0.345
Cotinine	0.000	0.000	0.042	0.417	0.855
Diazinon	0.000	0.000	0.000	0.000	0.000
Diclofenac	0.000	0.000	0.000	0.000	0.000
Dimethoate	0.000	0.000	0.000	0.000	0.000
Diuron	0.000	0.000	0.000	0.000	0.000
Erythromycin	0.000	0.000	0.000	0.000	0.000
Gemfibrozil	0.000	0.000	0.000	0.000	0.000
Ibuprofen	0.000	0.000	0.000	0.000	0.000
Iopromide	0.112	0.372	0.701	0.808	1.007
Malaoxon	0.000	0.000	0.000	0.000	0.000
Methomyl	0.000	0.000	0.000	0.055	0.291
Metolachlor	0.000	0.000	0.000	0.952	3.393
Molinate	0.000	0.000	0.000	0.000	0.000
Naproxen	0.000	0.000	0.000	0.000	0.000
Prometon	0.000	0.000	0.000	0.000	0.134
Simazine	0.000	0.000	0.000	0.000	0.000
Sulfamethoxazole	0.000	0.000	0.000	0.000	0.000
Tributyl phosphate	0.116	0.105	0.162	0.117	0.150
Trimethoprim	0.000	0.000	0.000	0.000	0.000
Warfarin	0.000	0.000	0.134	0.097	0.159

Table A.10. PD-RSSCT breakthrough data for Water B.

Bed Volumes	26,989	63,492	100,395	139,266	203,756
MP	C/C_0				
2,4–D	0.000	0.000	0.000	0.095	0.156
Acetaminophen	0.000	0.000	0.000	0.000	0.000
Acetochlor	0.000	0.000	0.042	0.095	0.189
Aldicarb	0.000	0.000	0.057	0.159	0.159
Atrazine	0.031	0.000	0.000	0.000	0.000
Caffeine	0.114	0.250	1.000	0.039	0.403
Carbamazepine	0.000	0.000	0.000	0.000	0.000
Carbaryl	0.000	0.000	0.000	0.000	0.000
Clofibric acid	0.029	0.275	0.418	0.816	0.609
Cotinine	0.000	0.000	0.169	0.536	0.504
Diazinon	0.000	0.000	0.000	0.000	0.000
Diclofenac	0.000	0.000	0.064	0.106	0.158
Dimethoate	0.000	0.000	0.042	0.165	0.210
Diuron	0.000	0.000	0.000	0.000	0.000
Erythromycin	0.000	0.000	0.103	0.082	0.277
Gemfibrozil	0.000	0.000	0.000	0.116	0.090
Ibuprofen	0.000	0.069	0.072	0.133	0.042
Iopromide	0.176	0.428	0.683	1.301	0.780
Malaoxon	0.000	0.000	0.039	0.107	0.130
Methomyl	0.000	0.000	0.000	0.030	0.116
Metolachlor	0.000	0.000	0.081	0.119	0.267
Molinate	0.000	0.000	0.000	0.000	0.075
Naproxen	0.000	0.000	0.000	0.000	0.034
Prometon	0.000	0.000	0.059	0.172	0.249
Simazine	0.000	0.000	0.000	0.000	0.000
Sulfamethoxazole	0.000	0.000	0.051	0.278	0.196
Tributyl phosphate	0.155	0.132	0.128	0.246	0.189
Trimethoprim	0.000	0.000	0.000	0.000	0.000
Warfarin	0.000	0.122	0.251	0.496	0.435

Table A.11. PD-RSSCT breakthrough data for Water C (Reinert 2013).

Bed Volumes	19,554	32,651	51,301	70,665	122,812	150,000	185,222	243,073	281,707	357,220
MP	C/C_0									
2,4–D	0.000	0.000	0.000	0.000	0.058	0.089	0.196	0.610	--	--
Acetaminophen	0.000	0.000	0.000	0.000	0.000	0.000	0.000	0.000	0.000	0.000
Acetochlor	0.000	0.000	0.000	0.000	0.000	0.000	0.124	0.189	0.318	0.494
Aldicarb	0.000	0.000	0.000	0.000	0.063	0.037	0.162	0.247	0.148	0.453
Atrazine	0.116	0.107	0.195	0.134	0.025	0.000	0.041	0.116	0.243	0.397
Caffeine	0.023	0.030	0.054	0.050	0.095	0.025	0.320	0.301	0.351	0.573
Carbamazepine	0.000	0.000	0.000	0.000	0.000	0.000	0.032	0.055	0.169	0.292
Carbaryl	0.000	0.000	0.000	0.000	0.000	0.000	0.000	0.000	0.000	0.000
Chlorpyrifos	0.000	0.000	0.000	0.000	0.000	0.000	0.000	0.000	0.000	0.000
Clofibric Acid	0.025	0.070	0.285	0.377	0.412	0.209	0.157	0.176	0.159	0.625
Cotinine	0.000	0.000	0.000	0.212	0.944	0.542	0.908	0.785	0.964	0.747
Diazinon	0.000	0.000	0.000	0.000	0.000	0.000	0.000	0.000	0.115	0.228
Diclofenac	0.000	0.000	0.000	0.000	0.000	0.000	0.060	0.224	0.376	0.597
Dimethoate	0.000	0.000	0.000	0.000	0.038	0.037	0.077	0.256	0.055	0.524
Diuron	0.000	0.000	0.000	0.000	0.000	0.000	0.000	0.000	0.000	0.000
Erythromycin	0.000	0.000	0.000	0.000	0.000	0.000	0.000	0.000	0.091	0.172
Gemfibrozil	0.000	0.000	0.000	0.000	0.000	0.000	0.000	0.271	0.090	0.558
Ibuprofen	0.000	0.000	0.035	0.055	0.000	0.000	0.000	0.000	0.000	0.293
Iopromide	0.000	0.160	0.190	0.493	0.758	0.867	0.814	0.793	0.895	0.893
Malaoxon	0.000	0.000	0.000	0.000	0.000	0.075	0.114	0.365	0.092	--
Methomyl	0.000	0.000	0.000	0.000	0.045	0.065	0.477	0.606	0.644	0.821
Metolachlor	0.000	0.000	0.000	0.000	0.041	0.050	0.107	0.244	0.418	0.536
Molinate	0.000	0.000	0.000	0.000	0.000	0.000	0.094	0.197	0.071	0.344
Naproxen	0.000	0.000	0.000	0.000	0.000	0.000	0.000	0.135	0.264	0.512
Prometon	0.000	0.000	0.000	0.000	0.054	0.058	0.134	0.330	0.467	0.618
Simazine	0.000	0.000	0.000	0.000	0.000	0.000	0.000	0.059	0.145	0.253
Sulfamethoxazole	0.000	0.000	0.000	0.000	0.000	0.065	0.083	0.465	0.548	0.908
Tributyl phosphate	0.106	0.080	0.141	0.368	0.086	0.043	0.138	0.223	0.270	0.480
Trimethoprim	0.000	0.000	0.000	0.000	0.000	0.000	0.000	0.000	0.000	0.117
Warfarin	0.000	0.000	0.046	0.043	0.156	0.229	0.247	0.574	0.579	0.755

Table A.12. PD-RSSCT breakthrough data for Water D.

Bed Volumes	24,413	45,648	97,955	139,577	296,117	499,434
MP	C/C_0					
2,4–D	0.000	0.000	0.000	0.062	0.053	0.514
Acetaminophen	0.000	0.000	0.000	0.000	0.045	0.000
Acetochlor	0.000	0.000	0.000	0.000	0.228	0.456
Aldicarb	0.000	0.000	0.000	0.000	0.000	0.426
Atrazine	0.000	0.000	0.000	0.000	0.892	0.342
Caffeine	0.114	0.329	0.162	0.080	0.267	0.363
Carbamazepine	0.000	0.000	0.000	0.000	0.079	0.203
Carbaryl	0.000	0.000	0.000	0.000	0.000	0.000
Clofibric acid	0.000	0.044	0.391	0.630	0.151	0.919
Cotinine	0.000	0.000	0.198	0.652	0.546	1.016
Diazinon	0.000	0.000	0.000	0.000	0.170	0.052
Diclofenac	0.000	0.000	0.000	0.036	0.000	0.256
Dimethoate	0.000	0.000	0.000	0.000	0.000	0.432
Diuron	0.000	0.000	0.000	0.000	0.000	0.000
Erythromycin	0.000	0.000	0.000	0.000	0.000	0.000
Gemfibrozil	0.000	0.000	0.000	0.035	0.000	0.470
Ibuprofen	0.000	0.000	0.000	0.386	0.000	0.086
Iopromide	0.000	0.000	0.307	0.601	0.845	1.037
Malaoxon	0.000	0.000	0.000	0.000	0.000	0.391
Methomyl	0.000	0.000	0.000	0.000	0.548	0.954
Metolachlor	0.000	0.000	0.000	0.041	0.321	0.511
Molinate	0.000	0.000	0.000	0.000	0.000	0.400
Naproxen	0.000	0.000	0.000	0.000	0.000	0.183
Prometon	0.000	0.000	0.000	0.000	0.839	0.612
Simazine	0.000	0.000	0.000	0.000	0.211	0.237
Sulfamethoxazole	0.000	0.000	0.000	0.063	0.000	0.413
Tributyl phosphate	0.105	0.158	0.201	0.111	0.273	0.384
Trimethoprim	0.000	0.000	0.000	0.000	0.000	0.000
Warfarin	0.000	0.000	0.111	0.253	0.069	0.642

Table A.13. PD-RSSCT breakthrough data for Water E.

Bed Volumes	28,413	65,884	81,856	125,631	160,084
MP	C/C_0				
2,4–D	0.000	0.000	0.000	0.000	0.000
Acetaminophen	0.000	0.000	0.000	0.000	0.000
Acetochlor	0.000	0.000	0.000	0.000	0.000
Aldicarb	0.000	0.197	0.170	0.336	0.215
Atrazine	0.000	0.000	0.000	0.253	0.477
Caffeine	0.000	0.000	0.587	0.216	0.378
Carbamazepine	0.000	0.000	0.000	0.000	0.033
Carbaryl	0.000	0.000	0.000	0.000	0.000
Clofibric acid	0.000	0.634	0.641	0.626	0.399
Cotinine	0.000	1.085	0.997	1.031	0.892
Diazinon	0.000	0.000	0.000	0.000	0.000
Diclofenac	0.000	0.000	0.000	0.000	0.000
Dimethoate	0.000	0.000	0.171	0.440	0.315
Diuron	0.000	0.000	0.000	0.000	0.000
Erythromycin	0.000	0.000	0.000	0.000	0.000
Gemfibrozil	0.000	0.000	0.000	0.000	0.000
Ibuprofen	0.000	0.000	0.000	0.000	0.000
Iopromide	0.000	1.187	1.196	1.079	0.882
Malaoxon	0.000	0.000	0.000	0.000	0.000
Methomyl	0.000	0.000	0.203	0.943	0.998
Metolachlor	0.000	0.000	0.000	0.020	0.074
Molinate	0.000	0.000	0.000	0.174	0.130
Naproxen	0.000	0.000	0.000	0.000	0.000
Prometon	0.000	0.027	0.068	0.818	0.802
Simazine	0.000	0.000	0.000	0.048	0.133
Sulfamethoxazole	0.000	0.038	0.073	0.094	0.053
Tributyl phosphate	0.123	0.000	0.000	0.103	0.140
Trimethoprim	0.000	0.000	0.000	0.000	0.000
Warfarin	0.000	0.000	0.000	0.000	0.000
Bupropion	0.000	0.000	0.000	0.000	0.000
Lamotrigine	0.000	0.000	0.000	0.000	0.000
Metoprolol	0.000	0.000	0.000	0.000	0.000
Sucralose	0.059	1.132	0.985	0.997	0.947

Table A.14. Average MP influent concentrations for PD-RSSCT with Water E.

Micropollutant	Type[a]	C_0[b] (ng/L)	MRL[c] (ng/L)
2,4-D	Herb.	96±33	5
Acetaminophen	PPCP	124±63	5
Acetochlor	Herb.	117±15	10
Aldicarb	Insect.	123±31	10
Atrazine	Herb.	781±135	2
Bupropion[d]	PPCP	1±0	1
Caffeine	PPCP	168±57	5
Carbamazepine	PPCP	128±25	2
Carbaryl	Insect.	79±27	10
Clofibric acid	Herb.	92±41	5
Cotinine	PPCP	87±28	5
Diazinon	Insect.	1±1	1
Diclofenac	PPCP	25±11	10
Dimethoate	Insect.	41±10	5
Diuron	Herb.	75±35	5
Erythromycin	PPCP	199±94	10
Gemfibrozil	PPCP	256±177	5
Ibuprofen	PPCP	375±338	10
Iopromide	PPCP	395±574	25
Lamotrigine[d]	PPCP	11±3	5
Malaoxon	Insect.	46±16	10
Methomyl	Insect.	64±21	5
Metolachlor	Herb.	231±25	1
Metoprolol[d]	PPCP	4±1	2
Molinate	Herb.	54±29	10
Naproxen	PPCP	58±29	10
Prometon	Herb.	118±29	1
Simazine	Herb.	155±54	5
Sucralose[d]	PPCP	302±39	15
Sulfamethoxazole	PPCP	282±104	5
Tributyl phosphate	Plasticizer	57±17	5
Trimethoprim	PPCP	74±14	2
Warfarin	PPCP	11±11	5

[a]Herb-herbicide, T&O-taste and odor, PPCP-pharmaceutical/personal care product, Insect-insecticide. [b]Avg±SD, n=6 for each MP. [c]Method reporting limit by LC/MS-MS. [d]MPs were already present in Water E before spiking in other MPs.

PSDM Modeling Procedure

More detail for this PSDM modeling procedure can be found in Fotta 2012, Reinert 2013, and Corwin and Summers (2011). The procedure can be used for scaling the RSSCT or for single curve fitting (full-scale or RSSCT).

1. PSDM input for PD-RSSCT
    a. Adsorber characteristics (bed depth, diameter, mass, etc.)
    b. Adsorbent characteristics (GAC particle density, particle radius, etc.)
    c. Adsorbate characteristics (MP molecular weight, concentration, etc.)
    d. Simulation time and time step (e.g. 600 day run time with intervals of 10 days)
2. Assuming the Freundlich equilibrium relationship, the following equilibrium and kinetic parameters were used for MP adsorption in the presence of DOM, termed the K^* approach (Corwin and Summers 2011).
    a. Freundlich K and 1/n
        i. For $q=KC^{1/n}$, assume 1/n=1
        ii. If $BV_{50\%}$ is available from the data, start with Equation 1 for the Freundlich K input, otherwise use an extrapolated guess of 50% breakthrough. The units of K^* in Equation 1 are L/g, reduced from (μmol/g)*(L/μmol)$^{1/n}$ when 1/n=1.

$$K^* = \frac{BV_{50\%}}{\rho_{bed}} \tag{1}$$

    b. Adsorption Kinetics
        i. Pore diffusion with a tortuosity (τ) of 3.
        ii. No surface diffusion, with a surface to pore diffusion flux ratio (SPDFR) of 10^{-30}.
        iii. Select Gnielinski (1978) correlation for film diffusion.
3. Adjust K, τ, and SPDFR until a good fit of the PD-RSSCT data is obtained. Experimental values for τ range from about 1 to 20 depending on the molecular size and run time (Sontheimer et al. 1988, Hand et al. 1989, Corwin and Summers 2011). Alternatively only adjust K and τ with SPDFR constant at 10^{-30}. For any τ<1 surface diffusion is implied and kinetics are represented by an effective diffusion coefficient.
4. Use the normalized total intraparticle flux (NTIF) method to obtain a good fit of the pilot data (Fotta 2012, Reinert 2013).
    a. Input adsorber characteristics into the PSDM for the full-scale system following steps 1a through 1d.
    b. Determine the NTIF for the PD-RSSCT.
        i. If surface diffusion was negligible (SPDFR=10^{-30} and τ≥1) use Equation 2 to calculate $NTIF_{PD\text{-}RSSCT}$:

$$NTIF = \frac{1}{\tau} \tag{2}$$

        ii. If surface diffusion was not negligible (SPDFR>10^{-30} and τ=1) use Equation 3 to calculate $NTIF_{PD\text{-}RSSCT}$. If only τ was adjusted (i.e. τ<1), use Equation 2.

$$NTIF = 1 + SPDFR \tag{3}$$

c. Use Equation 4 to calculate $NTIF_{full\text{-}scale}$:

$$NTIF_{full-scale} = NTIF_{PD-RSSCT}\left(\frac{d_{p,full-scale}}{d_{p,PD-RSSCT}}\right) \tag{4}$$

d. Calculate τ and SPDFR for the full-scale.

i. If $NTIF_{full\text{-}scale}>1$, then τ=1 and $SPDFR=NTIF_{full\text{-}scale}-1$. If only τ was adjusted (i.e. τ<1), then τ=1/NTIF and $SPDFR=10^{-30}$.

ii. If $NTIF_{full\text{-}scale}<1$, then $\tau=1/NTIF_{full\text{-}scale}$ and $SPDFR=10^{-30}$.

5. Use the K values from the model to calculate Y using Equation 5:

$$Y = \frac{\log(FI)}{\log(SF)} = \frac{\log\left(\frac{K_{PD-RSSCT}^{PSDM}}{K_{full-scale}^{PSDM}}\right)}{\log\left(\frac{d_{p,full-scale}}{d_{p,PD-RSSCT}}\right)} \tag{5}$$

Chapter 5

Table A.15. PD-RSSCT breakthrough data for <1K.

4 min EBCT			7 min EBCT			10 min EBCT		
WFN C/C_0	MIB C/C_0	Bed Volumes	WFN C/C_0	MIB C/C_0	Bed Volumes	WFN C/C_0	MIB C/C_0	Bed Volumes
0.00	-0.01	491	0.00	0.00	242	0.00	0.00	142
0.00	0.03	2799	0.00	0.00	1522	0.00	0.00	1011
0.00	-0.01	5075	0.00	0.00	2783	0.00	-0.01	1867
0.00	0.06	8413	0.00	0.00	4652	0.00	0.00	3148
0.00	0.01	10211	0.00	0.01	5640	0.00	0.01	3812
0.00	0.08	13815	0.00	0.00	7661	0.00	0.00	5199
0.00	0.11	17548	0.00	0.01	11108	0.00	0.00	7585
0.03	0.14	19984	0.00	0.02	13554	0.00	0.00	9568
0.06	0.27	24285	0.00	0.06	16237	0.00	0.08	12404
0.18	0.34	26856	0.01	0.16	18058	0.00	0.06	14726
0.29	0.44	29023	0.07	0.26	21414	0.00	0.16	18993
0.36	0.56	32234	0.20	0.47	27524	0.13	0.27	20574
0.43	0.69	38176	0.30	0.52	29794	0.02	0.33	24492
0.57	0.75	48893	0.25	0.61	35404	0.22	0.60	29101
0.64	0.82	52888	0.47	0.75	42001	0.44	0.64	32191
0.64	0.83	62727	0.64	0.81	46427			
0.73	0.88	74292						
0.06	0.47	103437						
0.11	0.32	106380						
0.10	0.23	110970						
0.09	0.14	117791						
0.10	0.13	124187						
0.07	0.09	126812						
0.07	0.08	137277						
0.13	0.07	143514						

Table A.16. PD-RSSCT breakthrough data for BEM.

4 min EBCT			7 min EBCT			10 min EBCT		
WFN C/C_0	MIB C/C_0	Bed Volumes	WFN C/C_0	MIB C/C_0	Bed Volumes	WFN C/C_0	MIB C/C_0	Bed Volumes
0.00	0.01	555	0.00	0.00	278	0.00	0.01	167
0.00	0.01	3330	0.00	0.00	1825	0.00	-0.01	1223
0.00	0.00	6403	0.00	0.00	3542	0.00	0.00	2398
0.00	0.01	9178	0.00	0.01	5089	0.00	0.01	3454
0.00	0.01	11799	0.00	0.00	6548	0.00	0.00	4448
0.00	0.01	15084	0.00	0.00	8386	0.00	0.01	5707
0.00	0.01	21504	0.00	0.00	12016	0.00	0.00	8221
0.00	0.05	27246	0.00	0.00	15285	0.00	0.01	10500
0.03	0.13	33440	0.00	0.04	22272	0.00	0.01	15381
0.13	0.18	39520	0.00	0.03	25408	0.00	0.01	17568
0.13	0.23	45029	0.04	0.12	32607	0.00	0.03	22597
0.29	0.36	57653	0.03	0.11	36535	0.00	0.02	25322
0.25	0.39	64592	0.08	0.17	41508	0.00	0.05	28794
0.36	0.48	73315	0.14	0.28	49349	0.04	0.10	34274
0.38	0.60	87058	0.22	0.32	54868	0.09	0.14	38129
0.41	0.64	96737	0.22	0.42	62178	0.13	0.17	43237
0.42	0.75	109551	0.30	0.63	74467	0.23	0.32	51831
0.44	0.93	131077	0.44	0.82	86695	0.36	0.59	60382
0.64	1.03	152497	0.52	0.90	99621	0.40	0.74	69422
0.75	1.01	175139	0.64	0.88	111393	0.47	0.85	77654
0.76	0.92	195762						
0.20	0.48	199237						
0.25	0.44	202605						
0.24	0.34	205336						
0.23	0.37	208066						
0.16	0.27	210637						
0.14	0.28	219743						
0.15	0.20	230708						
0.10	0.17	242927						
0.12	0.15	266323						
0.07	0.12	272188						

Table A.17. PD-RSSCT breakthrough data for >1K.

4 min EBCT			7 min EBCT			10 min EBCT		
WFN C/C_0	MIB C/C_0	Bed Volumes	WFN C/C_0	MIB C/C_0	Bed Volumes	WFN C/C_0	MIB C/C_0	Bed Volumes
0.00	0.00	1001	0.00	0.02	533	0.00	-0.01	346
0.00	0.00	3234	0.00	0.01	1734	0.00	0.00	1159
0.00	0.00	6652	0.00	0.00	3648	0.00	0.00	2472
0.00	0.01	9770	0.00	0.00	8990	0.00	0.01	6159
0.00	0.01	16136	0.00	0.00	13825	0.00	0.01	9516
0.00	0.02	22304	0.00	0.01	22610	0.00	0.01	15640
0.01	0.07	34403	0.00	0.01	27765	0.00	0.01	19240
0.00	0.10	40146	0.00	0.05	36259	0.00	0.01	25177
0.00	0.12	49187	0.01	0.06	44737	0.00	0.02	31104
0.14	0.21	64073	0.05	0.07	55860	0.00	0.01	38881
0.11	0.26	78932	0.14	0.12	68908	0.07	0.03	48006
0.19	0.33	98418	0.14	0.22	79830	0.05	0.11	56727
0.32	0.48	121273	0.20	0.29	93029	0.10	0.12	64874
0.33	0.55	140408	0.40	0.51	109750	0.23	0.32	76562
0.47	0.56	163528	0.34	0.62	124224	0.25	0.37	86685
0.43	0.89	218162	0.48	0.68	142293	0.33	0.48	99325
0.68	0.85	249803						
0.20	0.50	256465						
0.19	0.45	259143						
0.23	0.44	265380						
0.15	0.33	283782						
0.15	0.31	292728						
0.13	0.27	305553						
0.14	0.27	317474						
0.11	0.26	326101						

Table A.18. PD-RSSCT breakthrough data for CB.

4 min EBCT			7 min EBCT			10 min EBCT		
WFN C/C_0	MIB C/C_0	Bed Volumes	WFN C/C_0	MIB C/C_0	Bed Volumes	WFN C/C_0	MIB C/C_0	Bed Volumes
0.00	0.01	4826	0.00	0.01	2725	0.00	0.01	1884
0.00	0.00	8362	0.00	0.01	8345	0.00	0.00	5785
0.00	0.01	11739	0.00	0.01	18755	0.00	0.01	15369
0.00	0.01	14756	0.00	0.02	22130	0.00	0.02	21927
0.00	0.03	20706	0.00	0.03	24972	0.00	0.06	25531
0.00	0.04	26975	0.02	0.10	28633	0.13	0.32	37975
0.00	0.12	33120	0.06	0.13	31553	0.12	0.32	39071
0.04	0.15	36010	0.01	0.20	36720	0.16	0.36	42781
0.05	0.17	39081	0.09	0.30	42719	0.18	0.43	47044
0.03	0.26	44085	0.15	0.42	46076	0.27	0.62	54048
0.15	0.38	50524	0.26	0.55	49136	0.25	0.62	57100
0.24	0.44	55667	0.23	0.57	54570			
0.19	0.60	64740	0.27	0.58	56155			
0.32	0.65	72369	0.33	0.65	61473			
0.31	0.64	75302	0.37	0.67	67581			
0.47	0.75	81209	0.46	0.84	77605			
0.46	0.71	86596	0.48	0.83	81983			
0.50	0.82	98942						
0.53	0.92	119002						
0.68	0.92	144258						

Table A.19. PD-RSSCT breakthrough data for CBMP.

4 min EBCT			7 min EBCT			10 min EBCT		
WFN C/C_0	MIB C/C_0	Bed Volumes	WFN C/C_0	MIB C/C_0	Bed Volumes	WFN C/C_0	MIB C/C_0	Bed Volumes
0.00	0.00	491	0.00	0.00	242	0.00	0.00	142
0.00	0.02	5684	0.00	0.01	6420	0.00	0.01	4438
0.00	0.06	8636	0.00	0.01	17194	0.00	0.00	14362
0.00	0.01	11388	0.00	0.03	20691	0.00	0.02	21238
0.00	0.03	17338	0.00	0.09	24019	0.00	0.04	24353
0.00	0.07	23447	0.00	0.11	27892	0.11	0.26	34141
0.00	0.18	30390	0.01	0.11	30570	0.14	0.36	38510
0.04	0.25	33439	0.02	0.23	35038	0.13	0.42	39777
0.01	0.25	36563	0.16	0.38	41614	0.14	0.41	43466
0.17	0.38	40090	0.26	0.60	49057	0.19	0.46	47622
0.10	0.35	42438	0.30	0.57	55317	0.24	0.64	54987
0.18	0.41	49249	0.38	0.63	57144	0.21	0.67	57911
0.15	0.42	53967	0.34	0.67	62433			
0.30	0.66	61818	0.39	0.76	68389			
0.44	0.75	70138	0.44	0.87	78929			
0.39	0.74	73389	0.48	0.88	83124			
0.52	0.86	86479						
0.59	0.88	97465						
0.55	0.85	100695						
0.54	0.93	109982						
0.58	0.90	120437						
0.69	0.92	146277						

Table A.20. Estimated MP influent concentrations for PD-RSSCT with CBMP.

Micropollutant	Type[a]	C_0[b] (ng/L)	MRL[c] (ng/L)
2,4-D	Herb.	68±22	5
Acetaminophen	PPCP	261±80	5
Acetochlor	Herb.	123±41	10
Aldicarb	Insect.	94±10	10
Atrazine	Herb.	18±3	2
Caffeine	PPCP	57±46	5
Carbamazepine	PPCP	64±7	2
Carbaryl	Insect.	49±24	10
Clofibric acid	Herb.	64±32	5
Cotinine	PPCP	162±79	5
Diazinon	Insect.	3±2	1
Diclofenac	PPCP	71±27	10
Dimethoate	Insect.	39±25	5
Diuron	Herb.	179±59	5
Erythromycin	PPCP	163±21	10
Gemfibrozil	PPCP	66±24	5
Iopromide	PPCP	336±130	25
Malaoxon	Insect.	26±21	10
Methomyl	Insect.	69±6	5
Metolachlor	Herb.	117±63	1
^{14}C-MIB[d]	T&O	107±3	19
Molinate	Herb.	46±22	10
Naproxen	PPCP	40±32	10
Prometon	Herb.	171±23	1
Simazine	Herb.	83±20	5
Sulfamethoxazole	PPCP	270±35	5
Tributyl phosphate	Plasticizer	73±11	5
Trimethoprim	PPCP	144±43	2
^{3}H-Warfarin[d]	PPCP	100±6	8

[a]Herb-herbicide, T&O-taste and odor, PPCP-pharmaceutical/personal care product, Insect-insecticide. [b]Avg±SD, n=3 for each MP. [c]Method reporting limit by LC/MS-MS. [d]Radiolabeled.

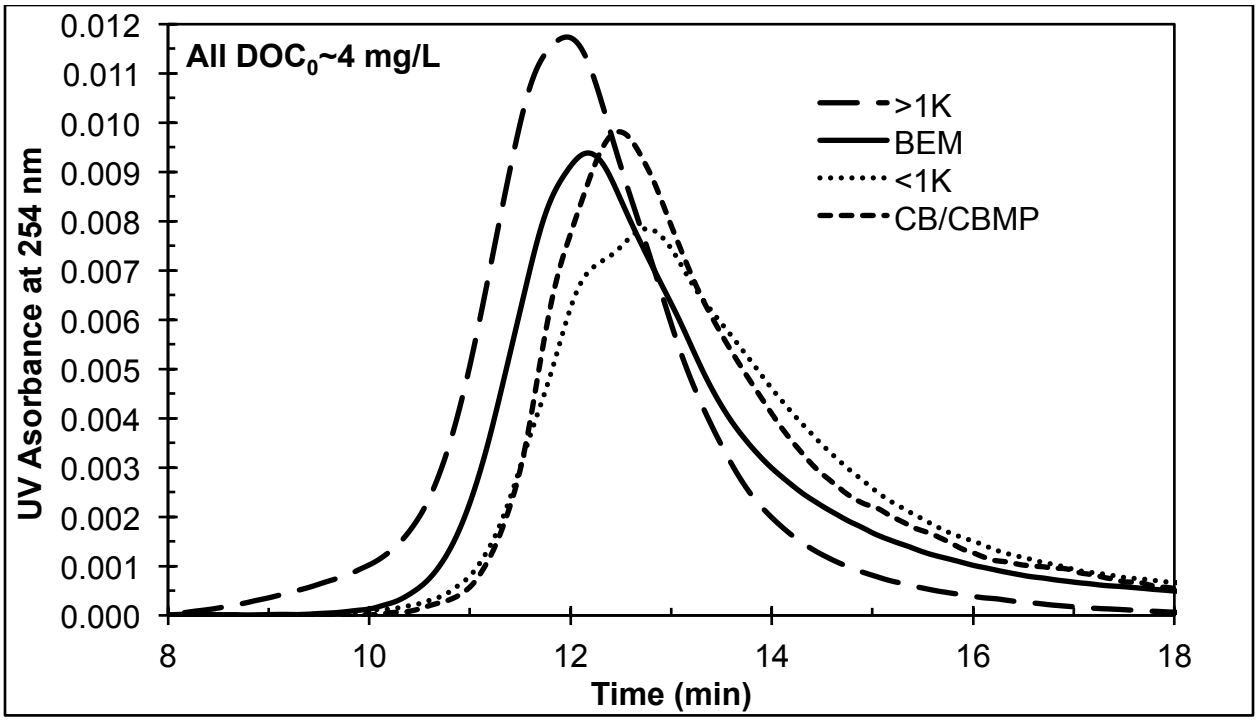

Figure A.1. SEC chromatograph for the five waters normalized for area. UVA absorbance is arbitrary and only defines the signal strength or response.

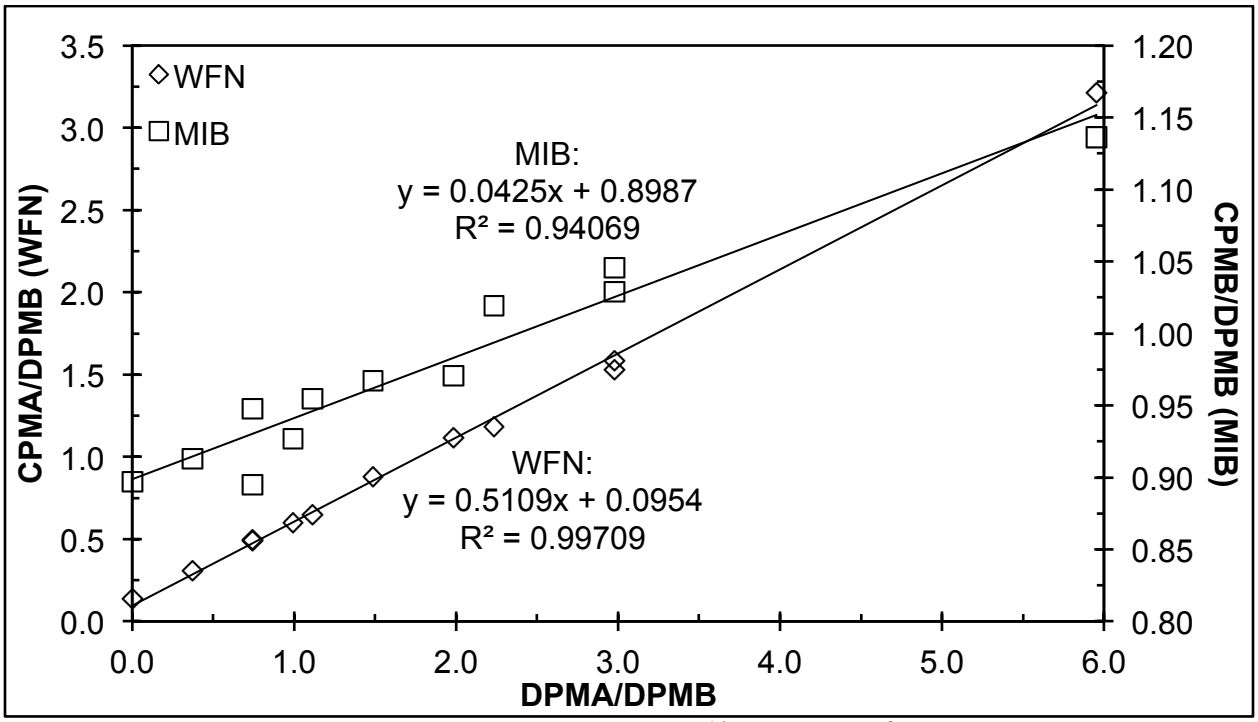

Figure A.2. Liquid scintillation calibration curves for ^{14}C-MIB and ^{3}H-WFN. Efficiency values: EHB=0.8987, EHA=0.0954, ELB=0.0425, ELA=0.5109. The letter A refers to ^{3}H and the letter B refers to ^{14}C.

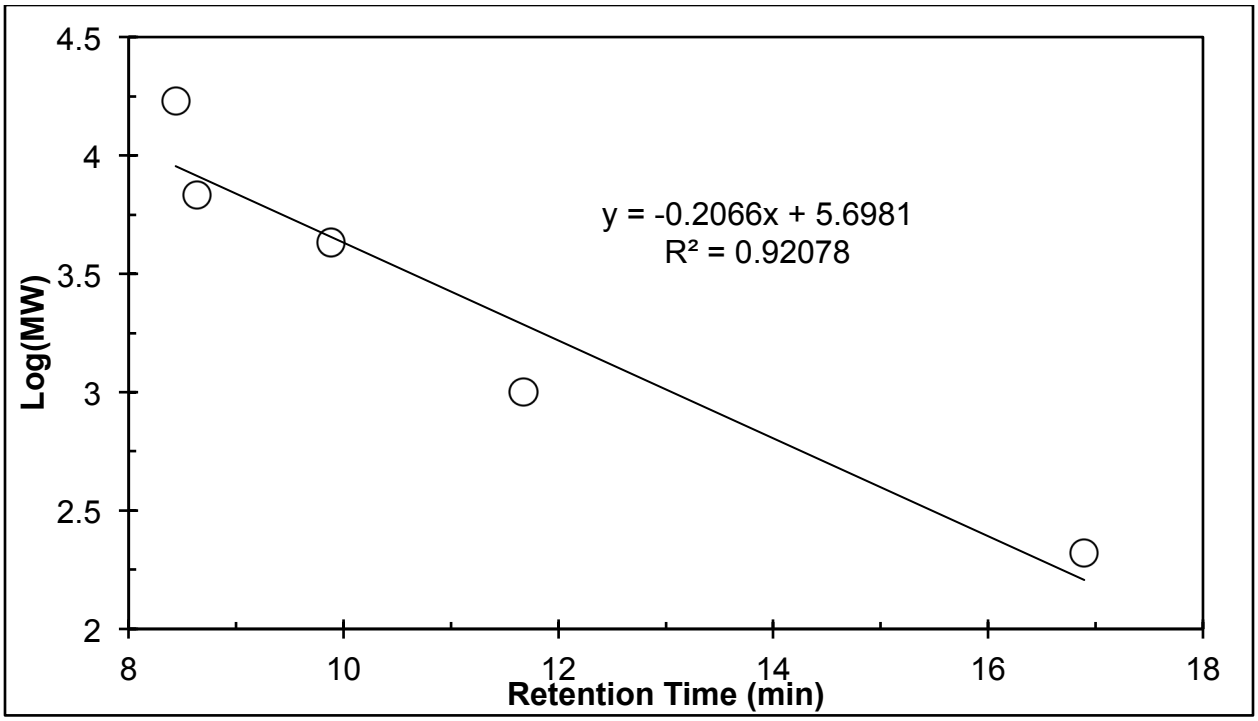

Figure A.3. SEC calibration curve for molecular weight (MW). Polystyrene sulfonate MWs were 210, 1K, 4.3K, 6.8K, and 17K Da.

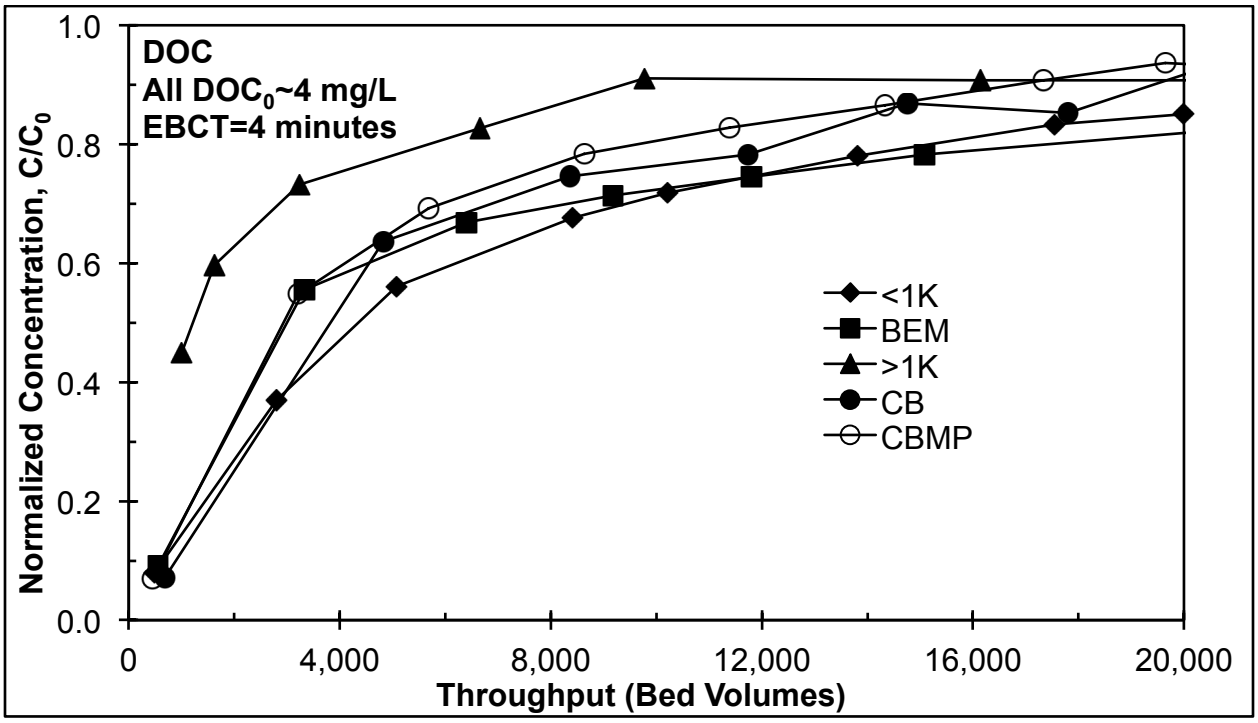

Figure A.4. DOC breakthrough curves for waters <1K, BEM, >1K, CB, and CBMP at a full-scale EBCT of 4 minutes.

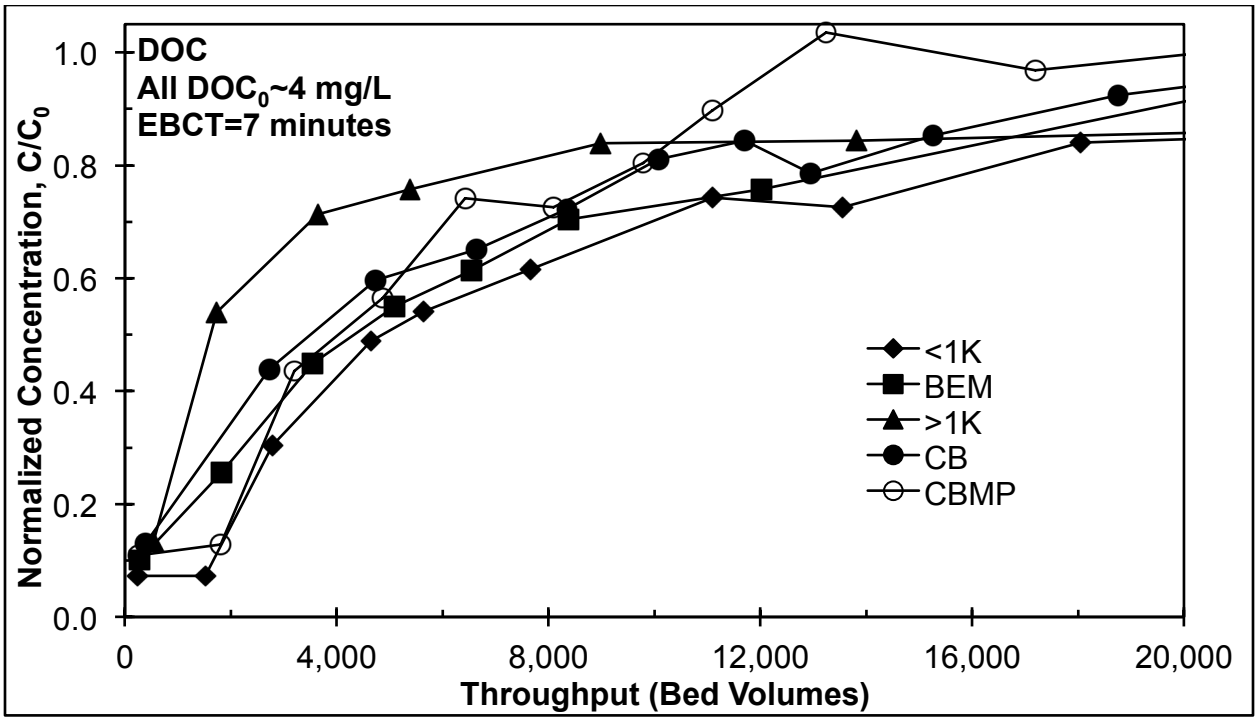

Figure A.5. DOC breakthrough curves for waters <1K, BEM, >1K, CB, and CBMP at a full-scale EBCT of 7 minutes.

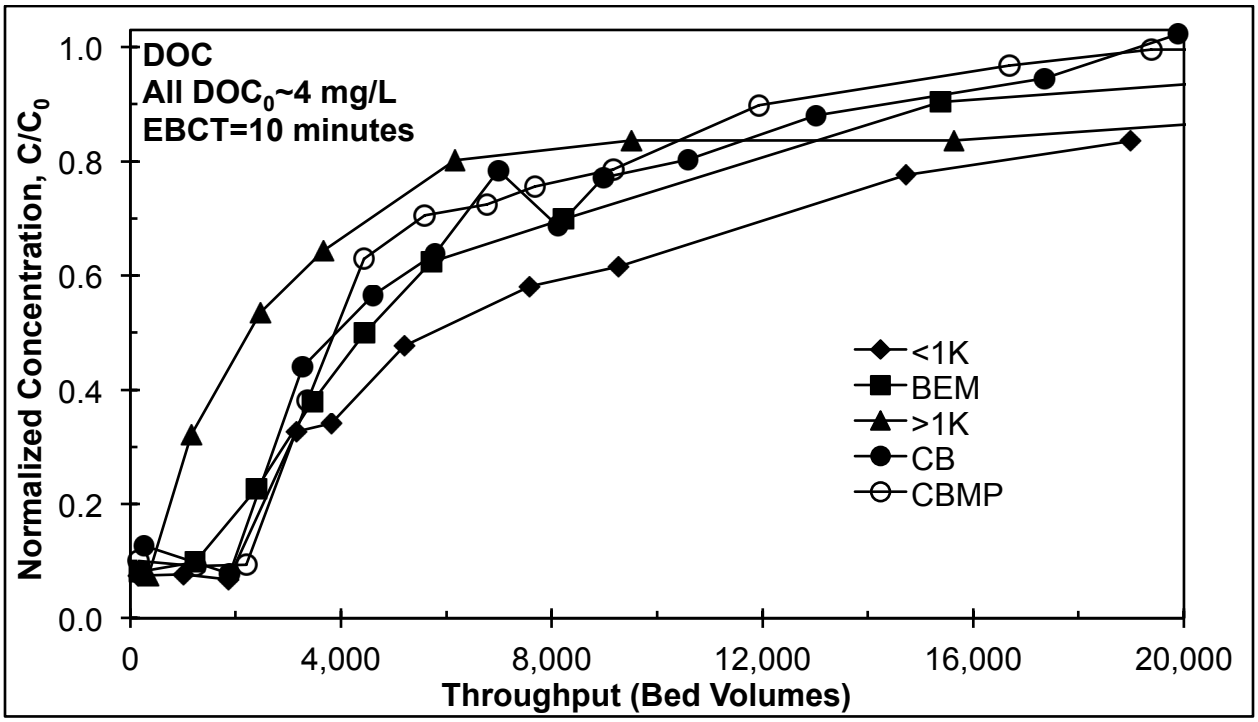

Figure A.6. DOC breakthrough curves for waters <1K, BEM, >1K, CB, and CBMP at a full-scale EBCT of 10 minutes.

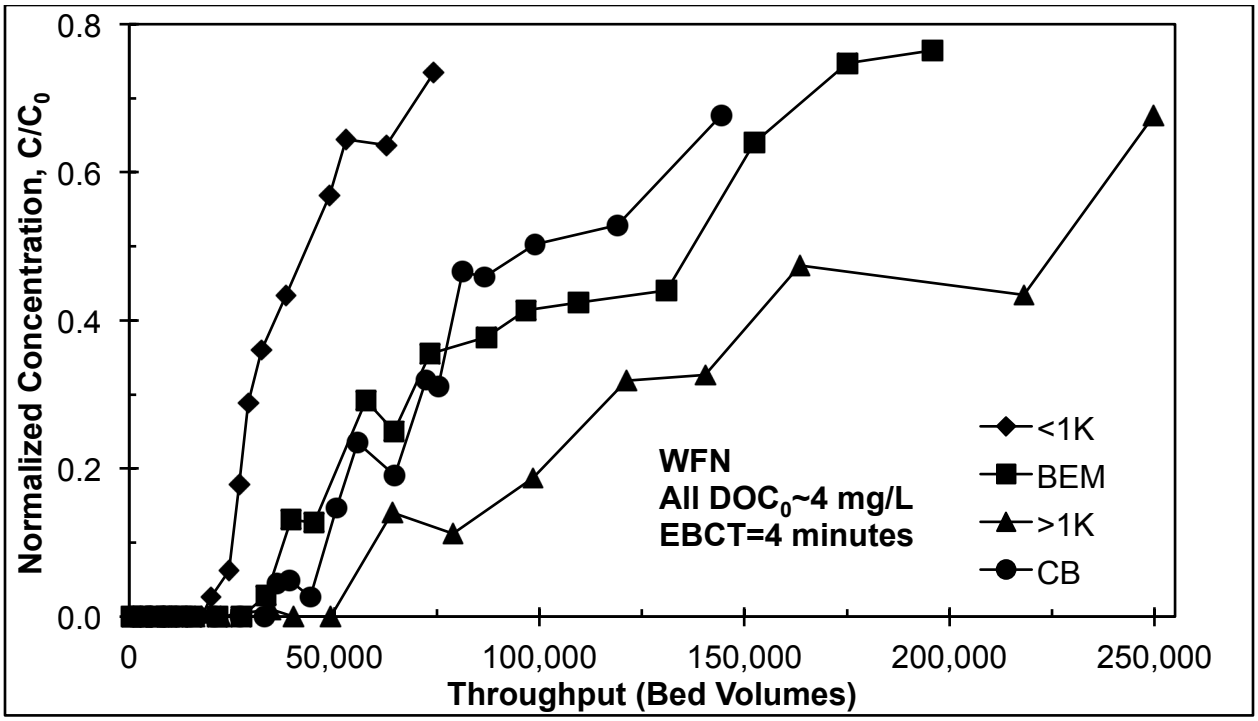

Figure A.7. Breakthrough curves for WFN in <1K, BEM, >1K, and CB at a full-scale EBCT of 4 minutes.

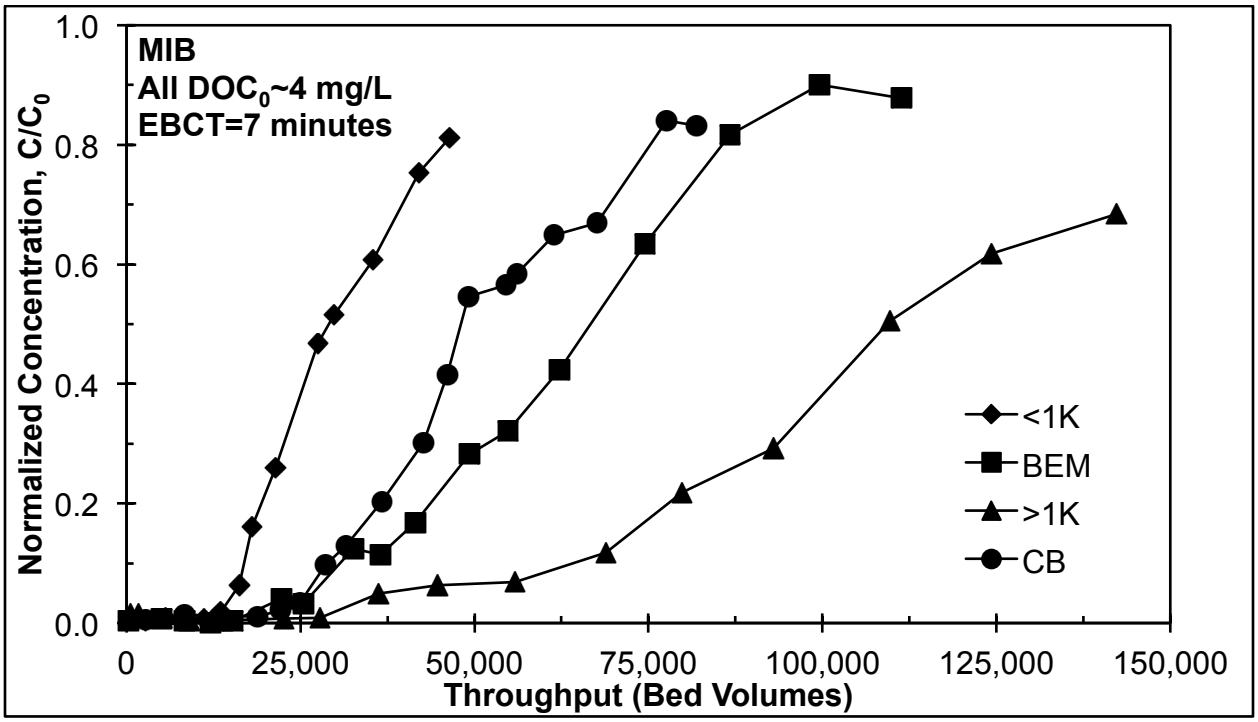

Figure A.8. Breakthrough curves for MIB in <1K, BEM, >1K, and CB at a full-scale EBCT of 7 minutes.

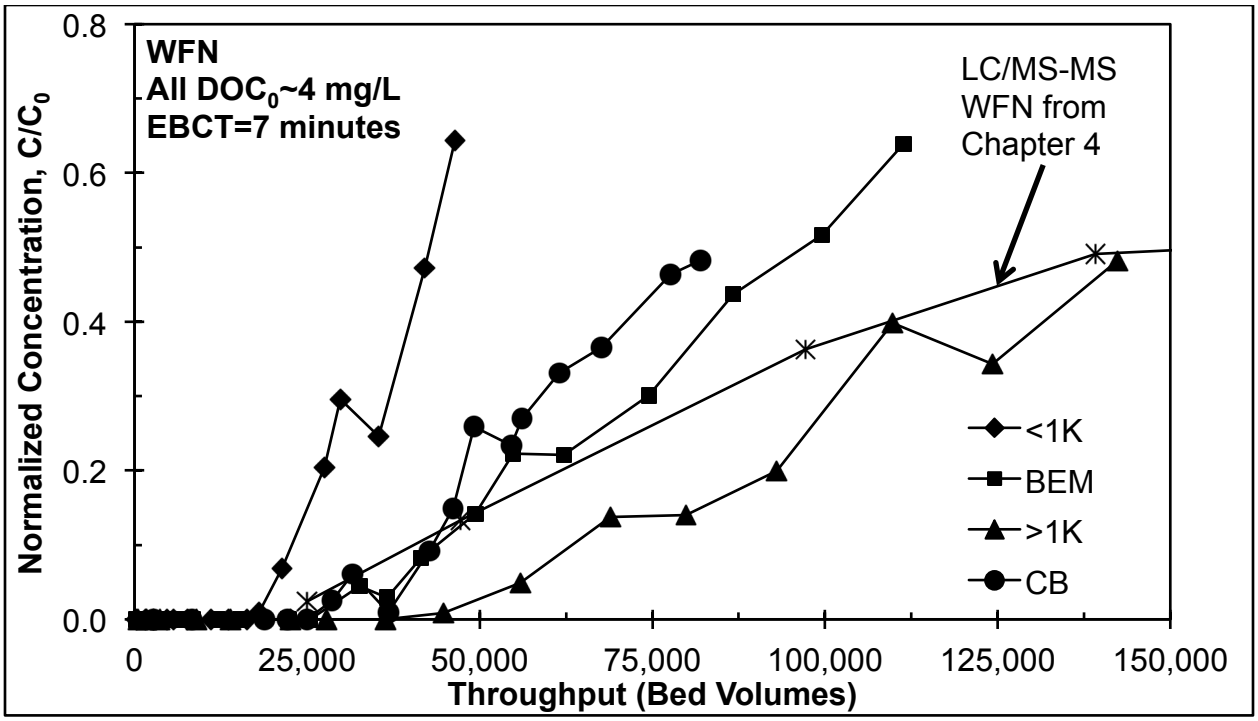

Figure A.9. Breakthrough curves for WFN in <1K, BEM, >1K, and CB at a full-scale EBCT of 7 minutes. WFN breakthrough from Chapter 4 using LC/MS-MS analysis shown for comparison.

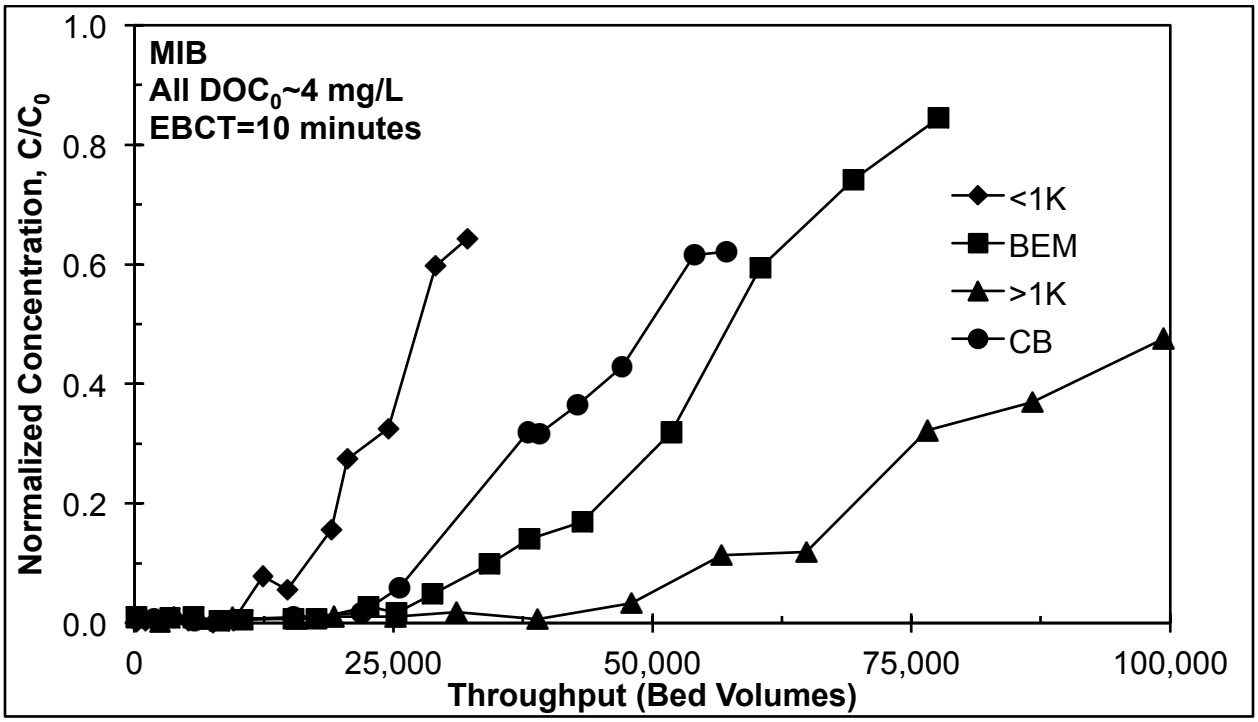

Figure A.10. Breakthrough curves for MIB in <1K, BEM, >1K, and CB at a full-scale EBCT of 10 minutes.

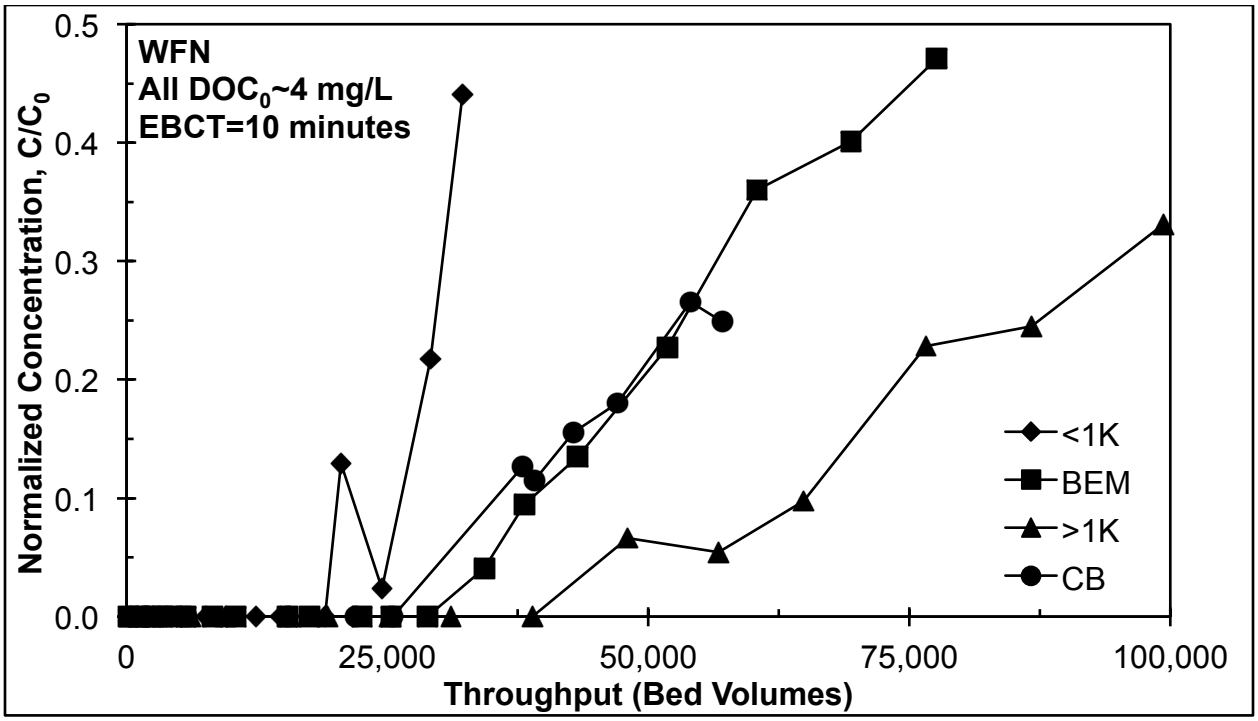

Figure A.11. Breakthrough curves for WFN in <1K, BEM, >1K, and CB at a full-scale EBCT of 10 minutes.

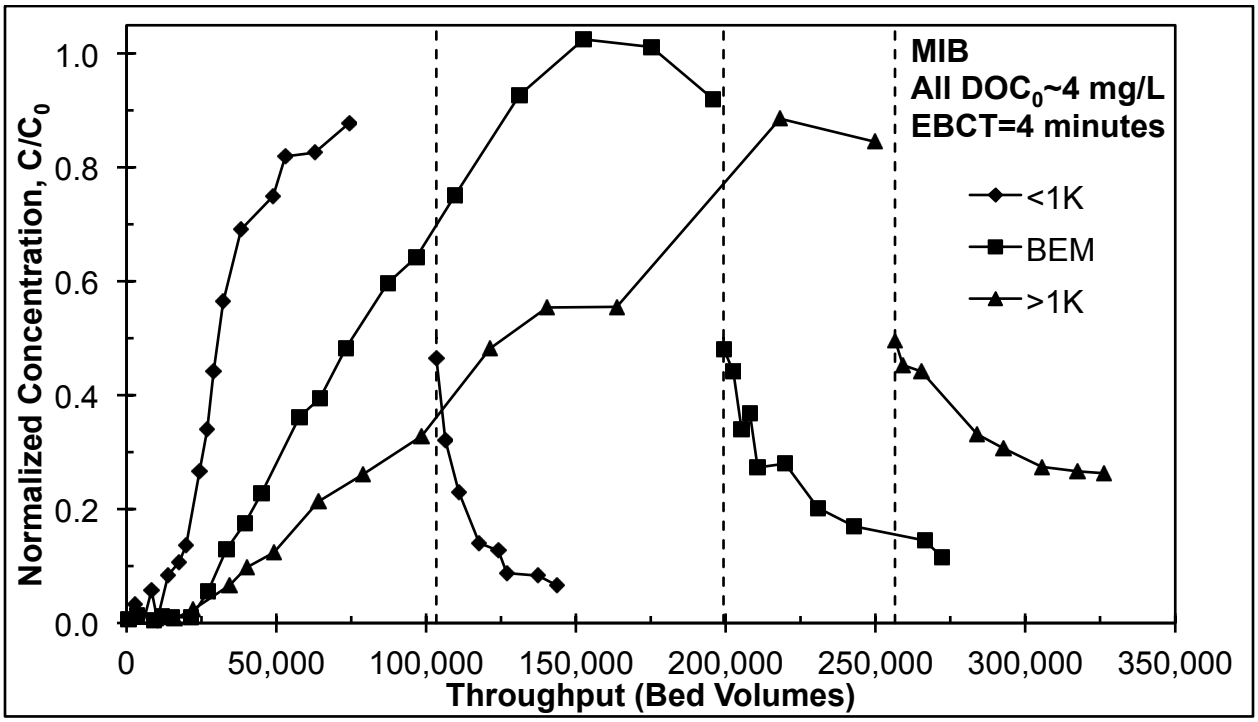

Figure A.12. Desorption of MIB in <1K, BEM, and >1K at a full-scale EBCT of 4 minutes.

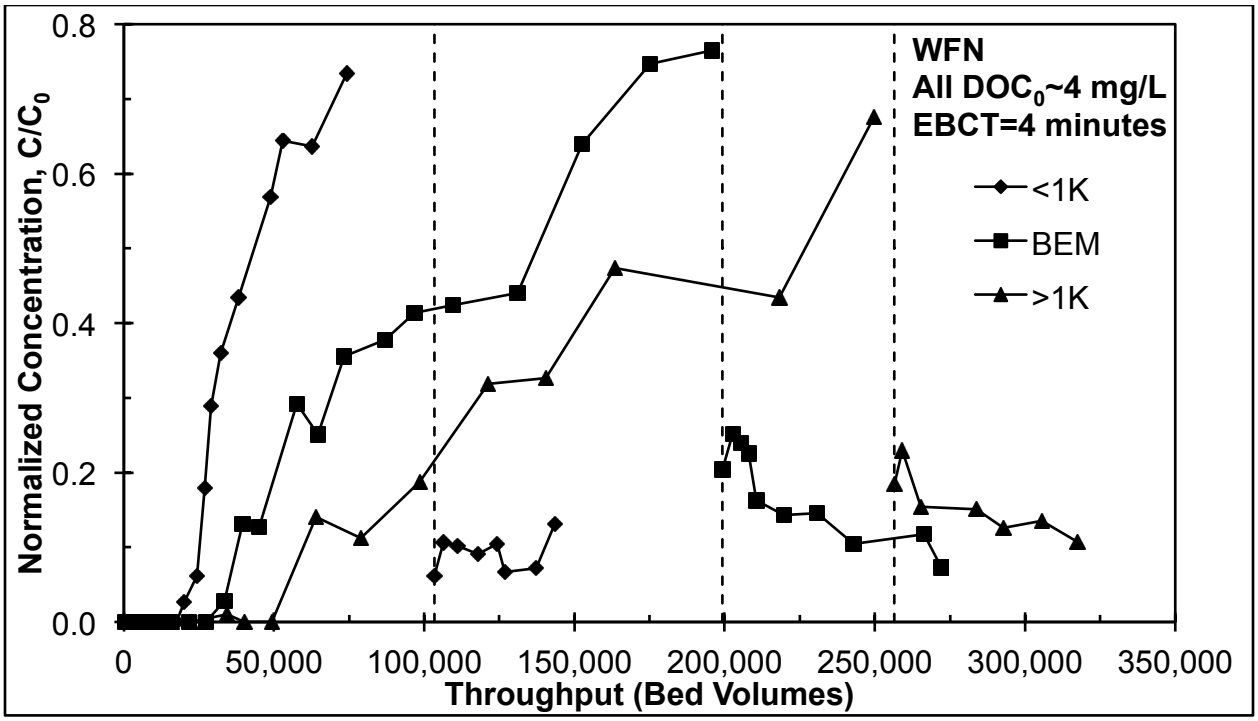

Figure A.13. Desorption of WFN in <1K, BEM, and >1K at a full-scale EBCT of 4 minutes.

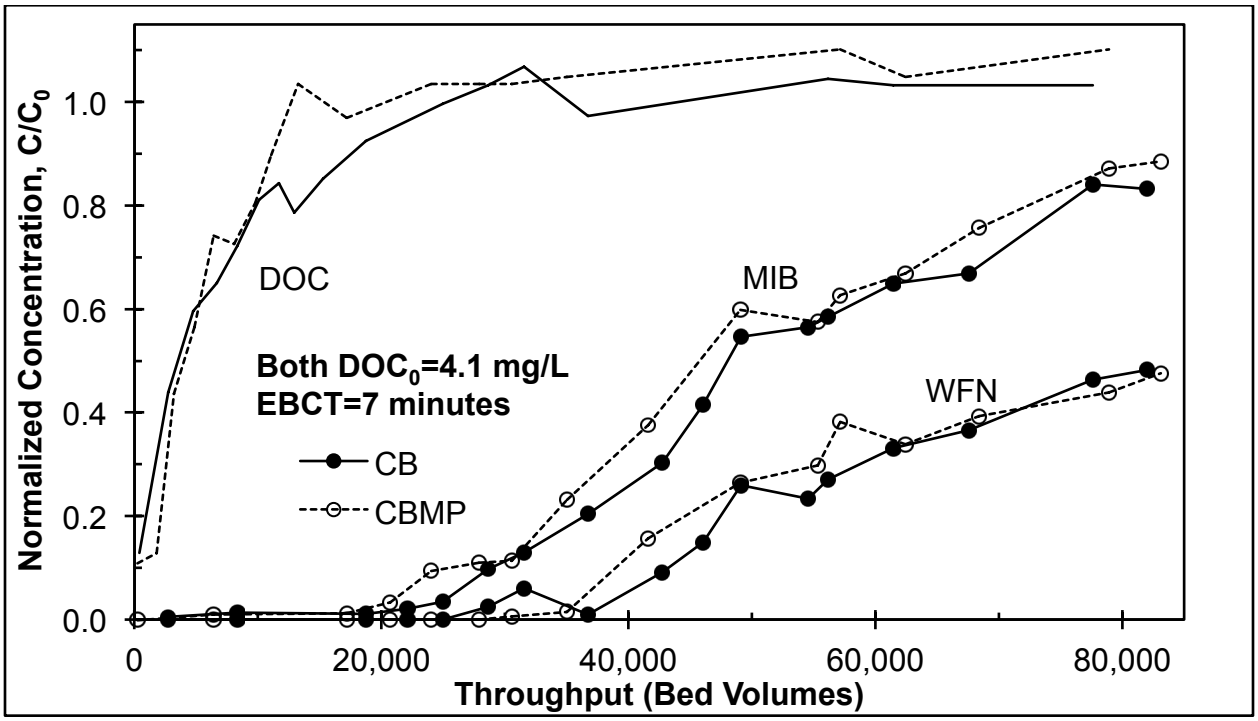

Figure A.14. Breakthrough curves for DOC, MIB, and WFN in CB and CBMP at a full-scale EBCT of 7 minutes. The only MPs in CB are MIB and WFN, while the collective MP concentration in CBMP was approximately 3.0±0.9 µg/L (n=3, see Appendix Table A.20).

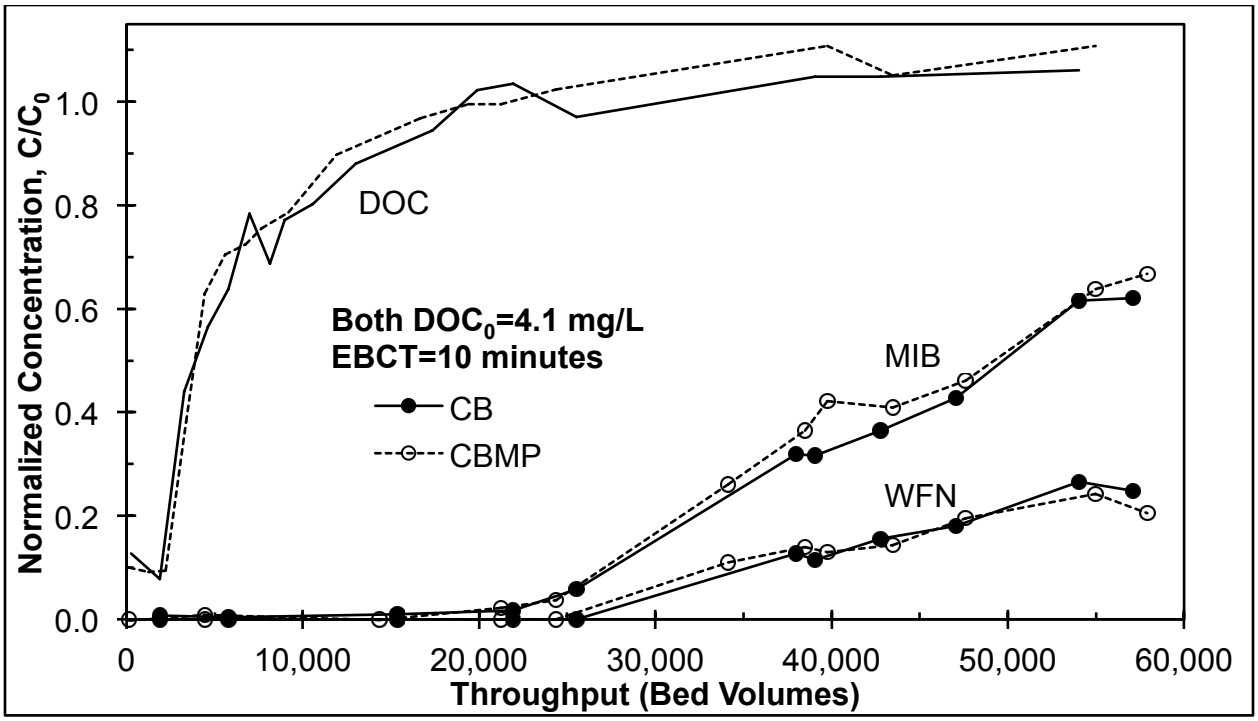

Figure A.15. Breakthrough curves for DOC, MIB, and WFN in CB and CBMP at a full-scale EBCT of 10 minutes. The only MPs in CB are MIB and WFN, while the collective MP concentration in CBMP was approximately 3.0±0.9 µg/L (n=3, see Appendix Table A.20).